Hybrid Time Domain Simulation: Application to Fault Induced Delayed Voltage Recovery

Final Project Report

S-58

Power Systems Engineering Research Center

Empowering Minds to Engineer
the Future Electric Energy System

Hybrid Time Domain Simulation: Application to Fault Induced Delayed Voltage Recovery

Final Project Report

Project Team
Vijay Vittal, Project Leader
Arizona State University

Sakis Meliopoulos
Georgia Institute of Technology

Graduate Students
Qiuhua Huang
Arizona State University

Rohit Atul Jinsiwale
Georgia Institute of Technology

PSERC Publication 17-04

October 2017

For information about this project, contact

Vijay Vittal
Arizona State University
School of Electrical, Computer, and Energy Engineering
P.O. BOX 875706
Tempe, AZ 85287-5706
Phone: 480-965-1879
Fax: 480-727-2052
Email: Vijay.Vittal@asu.edu

Power Systems Engineering Research Center

The Power Systems Engineering Research Center (PSERC) is a multi-university Center conducting research on challenges facing the electric power industry and educating the next generation of power engineers. More information about PSERC can be found at the Center's website: http://www.pserc.org.

For additional information, contact:

Power Systems Engineering Research Center
Arizona State University
527 Engineering Research Center
Tempe, Arizona 85287-5706
Phone: 480-965-1643
Fax: 480-727-2052

Notice Concerning Copyright Material

Acknowledgements

The work described in this report was sponsored by the Power Systems Engineering Research Center (PSERC).

We express our appreciation for the support provided by PSERC's industry members:

Brian Keel – Salt River Project

Juan Castaneda – Southern California Edison

Bajrang Agrawal – Arizona Public Service

Patrick Panciatici – Réseau de Transport d'Électricité (RTE)

Evangelos Farantatos – Electric Power Research Institute

Anish Gaikwad – Electric Power Research Institute

Eduard Muljadi – National Renewable Energy Laboratory

Bruce Fardanesh – New York Power Authority

Mahendra Patel – Electric Power Research Institute

Alan Engelmann – ComEd

Executive Summary

This project develops two complementary hybrid simulation approaches that electromechanical transient stability analysis and electromagnetic transient analysis (time domain analysis). One approach is electromagnetic transient (EMT)-transient stability (TS) hybrid simulation, the other is quadratic integration method based quasi-dynamic domain and time-domain hybrid simulation. The developed capabilities provide the ability to represent desired portions of the system in greater detail, while the rest of the system is adequately modeled in phasor modeling detail and the dynamic responses are well-represented without simplification. Such an ability is of great importance to better understand the dynamics of increasing number of power electronic devices and single-phase induction motors, such as residential air conditioner motors, and their impacts on power systems.

The project consists of two parts. Part 1 deals with the development of a new EMT-TS hybrid simulation tool, named OpenHybridSim, and its applications to fault-induced delayed voltage recovery (FIVDR) studies on the Western Electricity Coordinating Council (WECC) system as well as dynamic simulation of power systems interfaced with high voltage direct current (HVDC) systems. Part 2 develops an approach for hybrid time domain simulation that combines electromechanical transient stability analysis (quasi-dynamic domain) and electromagnetic transient analysis (time domain analysis). Some details of each part are provided below.

Part 1: Electromagnetic Transient and Electromechanical Transient Stability Hybrid Simulation: Design, Development and its Applications

Two significant trends of recent power system evolution are: (1) increasing installation of dynamic loads and distributed generation resources in distribution systems; (2) large-scale renewable energy integration at the transmission system level. A majority of these devices interface with power systems through power electronic converters. However, existing TS simulators are inadequate to represent the dynamic behavior of these devices accurately. On the other hand, simulating a large system using an EMT simulator is computationally impractical. EMT-TS hybrid simulation approach is an alternative to address these challenges. Furthermore, to thoroughly analyze the increased interactions among the transmission and distribution systems, an integrated modeling and simulation approach is essential.

Firstly, an improved hybrid simulation approach is proposed and a tool named OpenHybridSim is developed based on the proposed approach. Compared to the previous work, the proposed approach has three salient features: three-sequence TS simulation algorithm, three-phase/three-sequence network equivalencing and flexible switching of the serial and parallel interaction protocols.

The second part of the work concentrates on the applications of the hybrid simulation tool. The developed platform is first applied to conduct a detailed fault-induced delayed voltage recovery (FIDVR) study on the Western Electricity Coordinating Council (WECC) system. This study uncovers that after a normally cleared single line to ground fault at the transmission system could cause air conditioner motors to stall in the distribution systems, and the motor stalling could further propagate to an unfaulted phase under certain conditions. The developed tool is also applied to

simulate power systems interfaced with HVDC systems, including classical HVDC and the new generation voltage source converter (VSC)-HVDC system.

The third part centers on the development of integrated transmission and distribution system simulation and an advanced hybrid simulation algorithm with a capability of switching from hybrid simulation mode to TS simulation. Firstly, a modeling framework suitable for integrated transmission and distribution systems is proposed. Secondly, a power flow algorithm and a diakoptics based dynamic simulation algorithm for the integrated transmission and distribution system are developed. Lastly, the EMT-TS hybrid simulation algorithm is combined with the diakoptics based dynamic simulation algorithm to realize flexible simulation mode switching to increase the simulation efficiency.

Part 2: Hybrid Time Domain Simulation: Quadratic Integration Approach

This project develops an approach for hybrid time domain simulation that combines electromechanical transient stability analysis (quasi-dynamic domain) and electromagnetic transient analysis (time domain analysis). This capability makes it possible to represent desired portions of the system in greater detail and enable the analysis of phenomena associated with switching of power electronic systems, unbalance in phases, unsymmetrical faults, single phase devices and many more detailed analysis for large power systems in an efficient manner. While the project was initially conceived to demonstrate the hybrid method for the study of Fault Induced Delayed Voltage Recovery phenomena, the proposed method is general and applicable to several problems that require variable detail at different parts of the system such as Geomagnetically Induced Currents, HV ACDC systems, and inverter interfaced generation. It enables electromagnetic transient analysis at selected parts of the system, while utilizing the entire model of the systems and therefore the effect of the entire system in this studies.

The advantage of the hybrid approach is that it can combine two different systems discretized over two different scales in time. The quasi-dynamic domain uses ms resolution while the time-domain uses microsecond resolution. The hybrid system achieves a simultaneous solution with reduced computational burden while preserving the ability to observe nonlinearities and fast switching transients. The Georgia Tech work resulted in a hybrid simulation method that allows arbitrary placement of an interface boundary to separate the system into two subsystems, one to be modeled and simulated with the quasi-dynamic method and the other subsystem to be modeled and simulated in the time domain while obtaining simultaneous solution at the interface.

An example of this method is presented in the report.

Project Publications:

[1] Q. Huang, V. Vittal, – Arizona State University – "OpenHybridSim: an open source tool for EMT and phasor domain hybrid simulation," IEEE PES General Meeting, Boston, MA, United States, July. 2016.

[2] Q. Huang, V. Vittal, – Arizona State University – "Application of Electromagnetic Transient-Transient Stability Hybrid Simulation to FIDVR Study," *IEEE Transactions on Power Systems*, Vol. 31, No. 4, PP. 2634-2646, July 2016.

[3] Q. Huang, V. Vittal, – Arizona State University – "Integrated Transmission and Distribution Modeling and Simulation with three-sequence/three-phase mixed modeling," *IEEE Transactions on Power Systems*, under review.

Student Theses:

[1] Qiuhua Huang. *Electromagnetic Transient and Electromechanical Transient Stability Hybrid Simulation: Design, Development and its Applications*. PhD Dissertation, Arizona State University, May2016.

Part I

Electromagnetic Transient and Electromechanical Transient Stability Hybrid Simulation: Design, Development and its Applications

Vijay Vittal
Qiuhua Huang

Arizona State University

For information about this project, contact:

Vijay Vittal
Arizona State University
School of Electrical, Computer, and Energy Engineering
P.O. BOX 875706
Tempe, AZ 85287-5706
Phone: 480-965-1879
Fax: 480-727-2052
Email: Vijay.Vittal@asu.edu

Power Systems Engineering Research Center

The Power Systems Engineering Research Center (PSERC) is a multi-university Center conducting research on challenges facing the electric power industry and educating the next generation of power engineers. More information about PSERC can be found at the Center's website: http://www.pserc.org.

For additional information, contact:

Power Systems Engineering Research Center
Arizona State University
527 Engineering Research Center
Tempe, Arizona 85287-5706
Phone: 480-965-1643
Fax: 480-727-2052

Notice Concerning Copyright Material

Table of Contents

List of Figures

List of Tables

1. Electromagnetic Transient and Electromechanical Transient Stability Hybrid Simulation: Design, Development and its Applications

1.1 Introduction

1.1.1 Problem Statement

With the proliferation of converter based power electronic devices and small single-phase induction motors in power systems, the interaction of such fast responding elements with the power systems over time spans as long as 20 seconds has become a subject of significant interest [1]-[2]. The fault-induced delayed voltage recovery (FIDVR) phenomenon [3]-[5] falls into this category of events. Detailed modeling and sim ulation of single-phase compressor motors of air conditioners (A/Cs) and the distribution network is critical for the accuracy of FIDVR simulation results, especially under asymmetric fault conditions [5]-[7]. However, positive sequence transient stability (TS) simulators are unable to accurately model the A/C response to unbalanced faults. Simulation of large power systems with associated detailed modeling of large numbers of fast responding elements is too computationally burdensome for existing electromagnetic transient (EMT) simulators. While the scale of the system can be reduced by modeling a large portion of the system with a Norton or Thévenin equivalent, the drawback is that the nonlinear, dynamic response of the equivalenced portion of the system cannot be represented in the EMT simulation.

It has been recognized that combining the EMT and the TS simulations into one simulation process provides a feasible solution to address the issues above where neither EMT nor TS itself is not adequate, but some features from both EMT and TS are required. Within the framework of hybrid simulation, a part of the study system, which requires detailed representation, is modeled and simulated in an EMT program. This portion is usually referred to as the detailed system While the rest of the system is represented and simulated by a traditional TS program, which is referred to as the external system.

1.1.2 Literature Review

Hybrid simulation was first proposed for analyzing the dynamics of power systems interfaced with HVDC system by combining the TS simulation and a transient converter simulation algorithm [3]. Previous research on EMT-TS hybrid simulation mainly focused on interfacing techniques [11], including network equivalents on both sides [1],[12],[18] and interaction protocols [9],[13],[18]-[21] as well as the development of hybrid simulation programs [1]-[2], [10], [14]-[15]. The external net-work equivalents used in previous research, with the exception of [12], were developed based on positive-sequence network models. Consequently, if the resulting network equivalents were used in study cases with unbalanced conditions, the internal network would have to be extended substantially in the cases with a mesh network topology, in order to comply with the three-phase balanced assumption, which would under-mine the merits of hybrid simulation. For the interaction protocol, either the serial or the parallel protocol was used in previous research. The serial protocol has been found to be a limiting factor of simulation speed, whereas the parallel proto-col could lead to accuracy issues. Moreover, these programs, with the exception of [2] and [10] are designed to run all simulations on only one computer, thus they are potentially limited by

the local computing resources. References [2] and [10], however, did not provide implementation details of the commercial solution.

1.1.3 Project Objectives

From the background description and the literature overview above, hybrid simulation has been proven to be an effective method to simulate a large-scale power system of which a small portion of special concern can be modeled in three-phase, point-on-wave detail. This research is primarily motivated by the demand of a better simulation tool for phenomena like FIDVR in large power systems, especially under unbalanced fault conditions. For this purpose, a new hybrid simulation tool is developed, with a special focus on the following areas:

1. Simulating unsymmetrical faults within the detailed system without extensive-ly extending the boundary and the extent of the detailed system

2. Improving the interaction protocol for hybrid simulation

3. Development of a new simulation tool with the objective of making hybrid simulation flexible and accessible to other researchers

4. Application to some critical issues that require the capability provided by the hybrid simulation, including detailed FIDVR study and dynamic simulation of power systems interfaced with power electronic converter based devices

5. Further enhancing the simulation efficiency of hybrid simulation for 20-30 s simulations, by switching back to dynamic simulation when appropriate

In addition, to address the demand of a simulation tool for analyzing the impacts of more “active” distribution systems on bulk power systems and for transmission and distribution system integrated planning and operation, development of power flow and dynamic simulation algorithms for integrated transmission and distribution systems is an important objective in this project.

1.1.4 Research Organization

The organization of research in Part 1 is shown in Fig. 1.1. In Section 1.1, the background of this research is descripted. Then, an introduction to FIDVR and an overview of EMT-TS hybrid simulation are presented. The objectives of this research are also outlined.

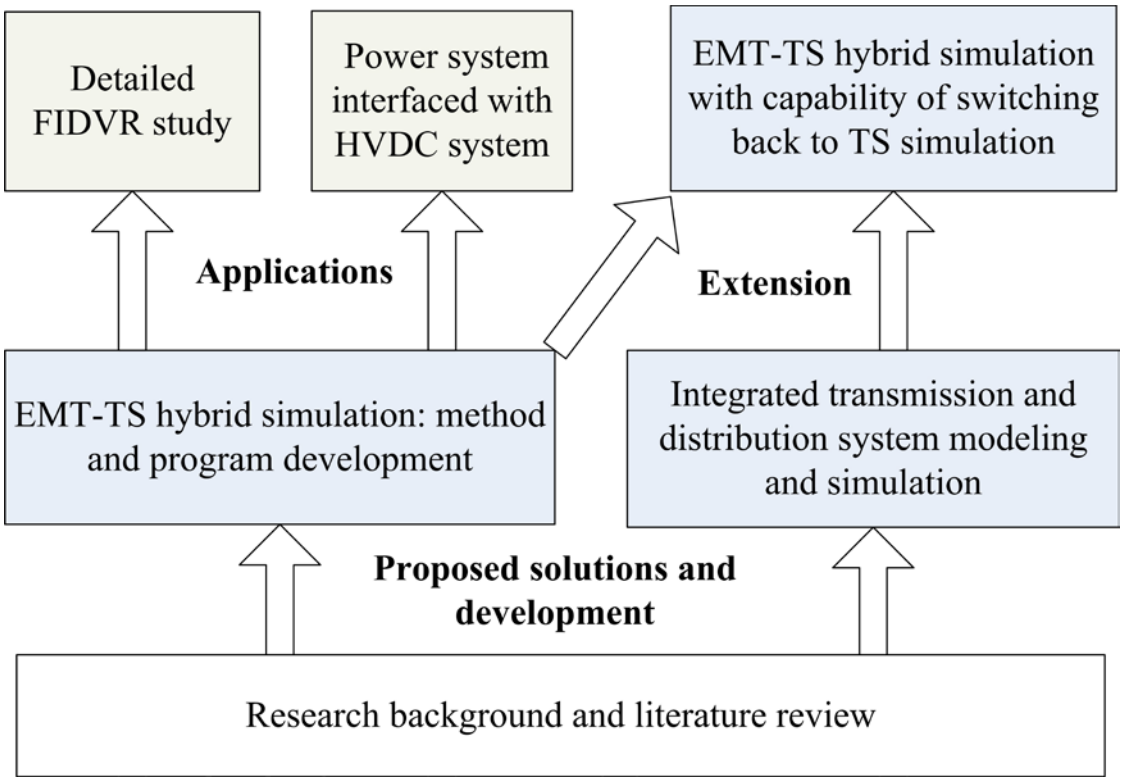

Figure 1.1: Organization of the research

In Section 1.2, two techniques to improve the hybrid simulation method, which are also two key features of the proposed hybrid simulation approach, are proposed. They are 1) three-phase and three-sequence oriented network equivalents and 2) the improved interaction protocol between the two simulators.

The development of a hybrid simulation tool, including a three-sequence TS simulation algorithm and a socket-based communication framework for hybrid simulation, is presented in Section 1.3.

In Section 1.4, the hybrid simulation platform developed in Section 1.3 is applied to conduct a detailed simulation of the FIDVR phenomenon in a region within the WECC system. Special techniques to determine the boundary of the detailed system and initialize the detailed system with a large percentage of induction motor loads are discussed. Detailed simulation results confirm that a normally cleared single-line-to-ground fault could lead to a FIDVR event affecting all three phases. Specifically, the phenomenon of A/C motor stalling propagating to other A/C units on unfaulted phase is also uncovered for the first time. The effects of the load composition and the point-on-wave of fault inception on the occurrence and evolution of the FIDVR event are also analyzed.

In Section 1.5, the hybrid simulation tool is utilized to simulate power systems interfaced with power electronic devices. Two types of HVDC system, including the classical HVDC and the relatively new VSC-HVDC are used for testing in this research. Results show that the both the fast switching behaviors of the converters of the HVDC systems and the slow dynamics of the external system can be adequately captured by the proposed hybrid simulation. In addition, the results

confirm that the hybrid simulation has a significant advantage over the full EMT simulation in terms of simulation speed.

In Section 1.6, a modeling framework for integrated transmission and distribution systems is developed, which provides a common system modeling for both power flow and dynamic simulation applications. Both power flow and dynamic simulation algorithms for integrated transmission and distribution systems are developed. In the dynamic simulation, the multi-area Thévenin equivalent approach is employed in the network solution step to address the challenge associated with different network representations of the transmission system and the distribution systems.

In Section 1.7, an advanced hybrid simulation algorithm is developed by integrating the EMT-TS hybrid simulation developed in Section 1.5 and the multi-area dynamic simulation algorithm developed in Section 1.6. The new algorithm allows the hybrid simulation to be switched back to TS simulation when appropriate, to achieve better simulation efficiency for a relatively long (e.g., 20-30 s) simulation.

Conclusions and future research plans are presented in Section 1.8.

1.2 Hybrid Simulation with Three-Phase/Three-Sequence Net-Work Equivalents and A Combined Interaction Protocol

1.2.1 Three-Phase Thévenin Equivalent of the External System

A three-phase (multi-port) Thévenin equivalent is used to represent the external system in the EMT simulation, as shown in Fig. 1.2. The equivalent includes two parts, the open circuit voltages and the equivalent impedances viewed at the terminals. The equivalent is updated at each interaction step based on the conditions of the external system at that instant. If the faults of concern occur within the detailed system, the topology of the external system does not change, thus, the equivalent impedance part can be assumed constant during the simulation. The process of building the three-phase Thévenin equivalent is carried out in five steps as shown in Fig. 1.3.

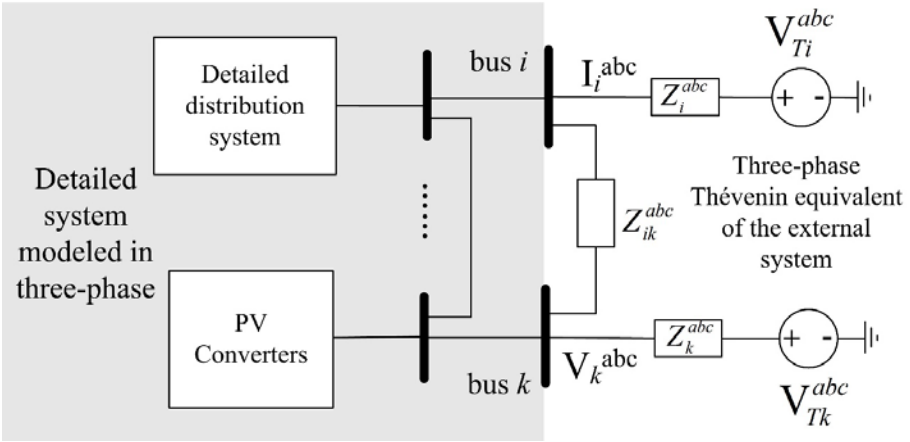

Figure 1.2: Detailed system interfaced with a three-phase Thévenin equivalent of the external system

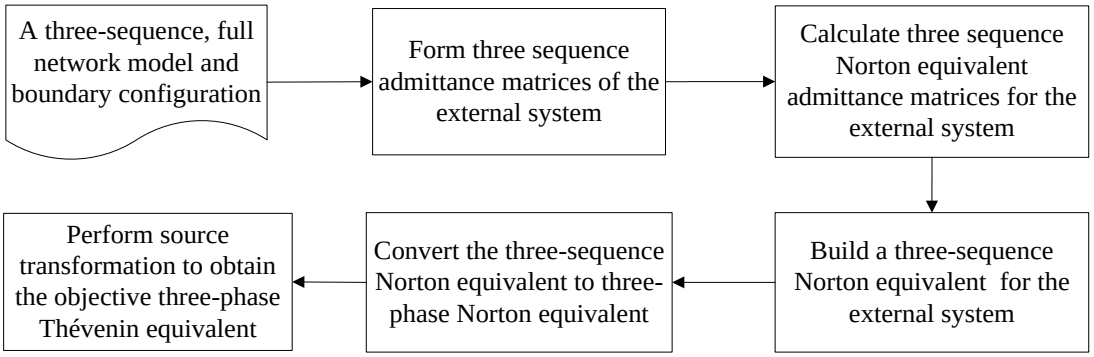

Figure 1.3: The procedure of building a three-phase Thévenin equivalent

1.2.2 Three-Sequence Equivalent of the Detailed System

There are several approaches for representing detailed systems in TS simulation, including current sources, constant PQ loads and Norton or Thévenin equivalents. It should be noted that it is difficult to derive the Norton admittance or Thévenin impedance matrix of the detailed system, because there may be power electronic devices in the detailed system and such matrix data is not accessible from most existing EMT simulators. Three-sequence current sources, as shown in Fig. 1.4, are used for the following reasons:

1. The current source representation seamlessly integrates into the network solution step of the TS simulation.

2. In some existing EMT simulators such as PSCAD [21], an FFT component is available and can be directly used to extract the *fundamental frequency*, three-sequence current magnitude and phase values, as shown in Fig. 1.5.

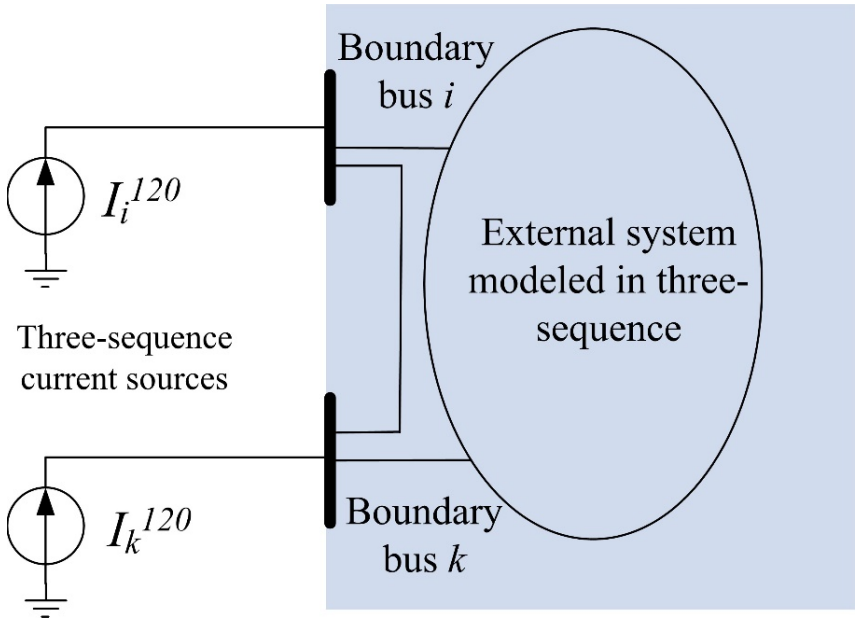

Figure 1.4: The detailed system is represented by three-sequence current sources in TS simulation

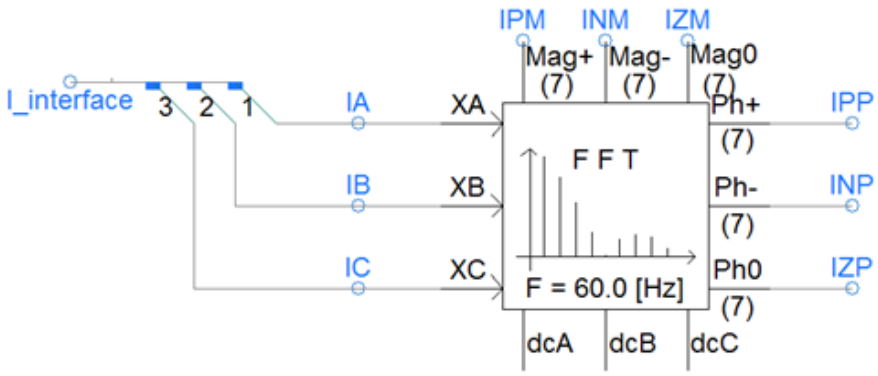

Figure 1.5: Extracting fundamental frequency, three-sequence current injections using the FFT component in PSCAD

1.2.3 A Combined Interaction Protocol

The interaction protocol relates to how the two simulators interact with each other in exchanging the necessary network equivalent parameters. There are mainly two types of interaction protocols used in previous research, i.e., the serial and parallel protocol [11]. With the serial protocol, one simulator must wait until the other completes the simulation of one interaction time step and transfers the equivalent data. To overcome this performance issue, several types of parallel protocols have been proposed [11]. The parallel protocol proposed in [9] requires data exchange for each iteration within one TS simulation time step. This requirement not only makes the data exchange process complicated, but is also impractical for most existing commercial EMT simulators as the iteration times required are unknown a priori. The parallel protocol proposed in [10] is relatively easy to implement. However, it could cause significant errors when the internal system experiences large disturbances, as the equivalents of the external network are not updated in a timely fashion to reflect the disturbances within the internal network.

In an effort to combine the advantages of both types of protocols, a combined interaction protocol is proposed based on the following observation: fast dynamics and significant system changes usually occur during the faulted period and last for up to tens of cycles after the fault is cleared; in order to reflect the fast dynamic response of the internal network in the external network, or vice versa, in a timely manner, the serial protocol should be used. For the rest of the simulation period, the parallel protocol can be used to achieve good efficiency, as the system mainly experiences slow dynamics. A schematic diagram of the combined protocol is shown in Fig. 1.6

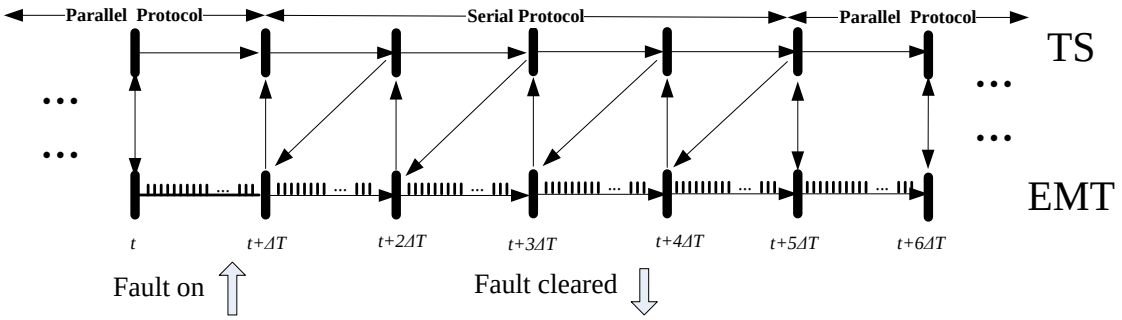

Figure 1.6: A combined interaction protocol

First, both serial and parallel interaction protocols are implemented as shown in Fig. 1.7 and Fig. 1.8 respectively. In both figures, t denotes the start time for the processing step, ΔT is TS simulation time step as well as the EMT-TS interaction time step, $I_{EMT(t)}^{120}$and $I_{EMT(t-\Delta T)}^{120}$ are the three-sequence current injection vectors sent from the PSCAD side at the present and previous interaction time step, respectively.

If a fast transient phenomenon within the internal network is detected, the serial protocol is used for this time step. As shown in Fig. 1.7, the operation involved is divided into 5 steps. The first step is data transfer via a socket and pre-processing. Then, in step (2), $I_{EMT(t)}^{120}$ is used as the input for the three-sequence TS simulation and the three-sequence voltages of the boundary buses $V_{TS(t+\Delta T)}^{120}$ are updated. Subsequently, the three- phase Thévenin equivalent voltages $V_{T(t+\Delta T)}^{ab}$ are derived by the network equivalent helper in step (3) and sent back to PSCAD in step (4). On receiving $V_{T(t+\Delta T)}^{120}$, PSCAD continues to step (5), which usually consists of hundreds of EMT simulation steps. Considering the computational complexity of each step, it is obvious that step (2) and step (5) are the two most time-consuming steps.

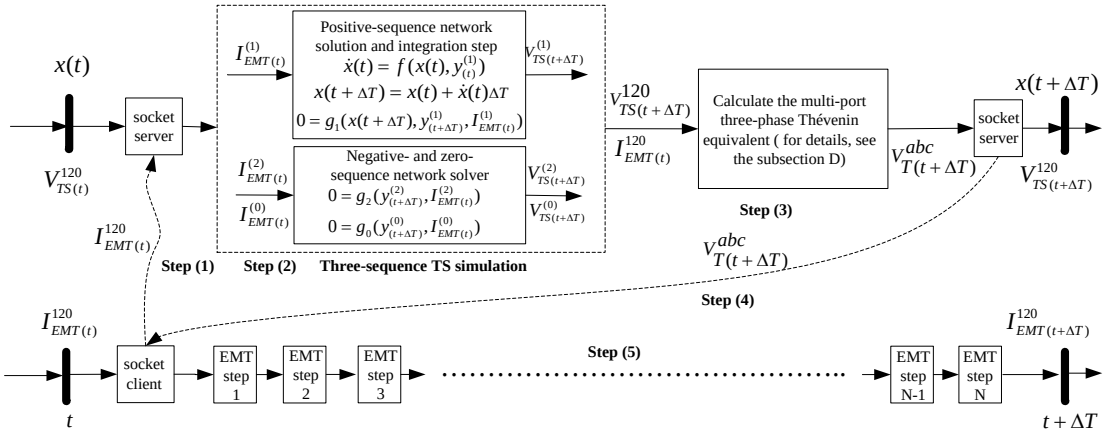

Figure 1.7: The implementation of EMT-TS hybrid simulation with the serial type of interaction protocol

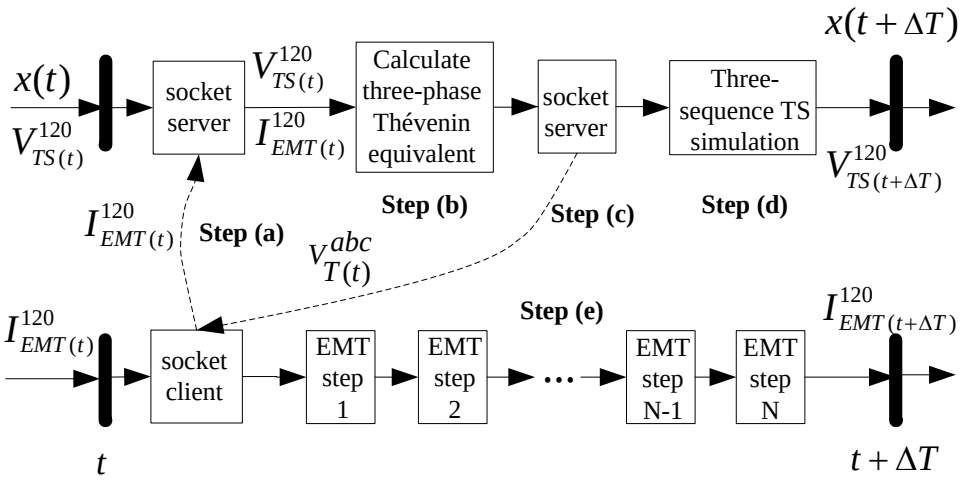

Figure 1.8: One interaction step of the developed EMT-TS hybrid simulation with the parallel type protocol.

Otherwise, the parallel protocol shown in Fig. 1.8 is used. The step for calculating the Thévenin equivalent (step (b)) is executed right after step (a), while the time-consuming step (d) is the last step on the TS simulation side. With this execution sequence, the Thévenin equivalent is calculated using the voltages obtained from the previous step and sent back to PSCAD immediately, such that step (d) and step (e) can be run simultaneously.

One of the challenges in this combined protocol design is to identify an appropriate protocol switching time for general applications. To address this challenge, a protocol switching control scheme is proposed for selecting the processing step interaction protocol based on the last step protocol and detection of any large transient event within the internal network. The details of the design of the scheme are as follows:

1) Detection of Fast Dynamics within the Internal Network

There are basically two options for detecting disturbances: one is the rate of change, the other is the change of magnitude. The change of magnitude fails to provide the information for determining whether the system is undergoing a fast transient or a slow dynamic condition. In contrast, the rate of change, or the maximum rate of change for multiple monitored variables, can provide the necessary information. Thus the rate of change is adopted for controlling the protocol switching.

2) Variable Selection for Detecting Fast Dynamics

In principle, current, voltage and power are good candidates for detecting transient events within the internal network. Considering that the sequence current injections at the boundary have been used as the interfacing variables, reusing them for protocol switching control can reduce the communication overhead and simplify the interfacing design. Therefore, the three-sequence current injections are adopted for detecting fast dynamics.

3) Implementation

The detection is based on the maximum rate of change of the three-sequence current injections at the boundary, which is denoted by $RI^{120}_{EMT(t)}$ and defined by (1.1).

$$RI^{120}_{EMT(t)} = \max_{i}\left(\max_{s\in(1,2,0)}\left(\left|\frac{I^{(s)}_{EMT(i,t)} - I^{(s)}_{EMT(i,t-\Delta T)}}{I^{(1)}_{EMT(i,t-\Delta T)}}\right|\right)\right) / \Delta T \tag{1.1}$$

where *i* denotes one of the boundary buses, *s* represents one of the three sequences; $I^{(s)}_{EMT(i,t)}$ is the current injection of sequence *s* at the boundary bus *i* at time *t*.

It is observed that $RI^{120}_{EMT(t)}$ generally becomes smaller or settles down after reaching the peak. If only $RI^{120}_{EMT(t)}$ were used for decision-making, the scheme would sometimes switch the protocol back to the parallel type even during the fault period. To address the issue, a delay function is introduced. With this delay function, $RI^{120}_{EMT(t)}$ must be consecutively less than the threshold for at least a period defined by the delay setting before switching from the serial protocol to the parallel protocol, otherwise the serial protocol is used.

The logic of the final protocol switching control scheme is illustrated by Fig. 1.9. When $RI^{120}_{EMT(t)}$ is larger than the threshold ε, the serial protocol is used; otherwise, the decision is made based on the protocol used in the last interaction step. When the protocol is switched from the serial type to the parallel type, the delay function becomes active.

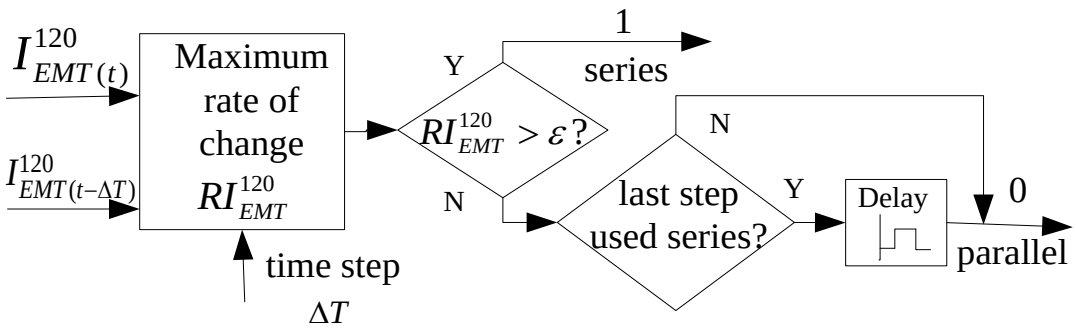

Figure 1.9: The logic of protocol switching control algorithm.

4) A Guide for Parameter Selection

The choice of the threshold is based on the characteristic of the power system transient, specifically the characteristic of $RI^{120}_{EMT(t)}$. Typically, $RI^{120}_{EMT(t)}$ is very small under a steady state or a slow dynamic condition, while it becomes notably larger under the fast-transient condition of a fault. Thus, the threshold here, to a large extent, is analogous to the threshold setting for over-current protection. But the threshold selection in this scheme is much simpler, as the reference value is

almost irrelevant to the operating conditions. Thus, a 2-10% step change for each interaction time step is recommended as the threshold. The interaction time step ΔT is usually the same as the TS time step, thus 1-10 *ms* can used depending on the integration method of the TS simulation and the phenomenon studied. For the delay time setting, based on the characteristics of power system transients and simulation experience, the delay time should be at least half of the fault period.

1.3 Development of A Hybrid Simulation Tool: Openhybridsim

The two key improvements discussed in last section will be applied to the development of an open source hybrid simulation tool—OpenHybridSim. Details of the development, including the overall design, main components of the tool and interfacing with an EMT simulator, will be presented in this section.

1.3.1 Overall design of OpenHybridSim

OpenHybridSim is designed with a decoupled architecture that enables flexibility. Its architecture is shown in Fig. 1.10. This tool includes four modules: the hybrid simulation manager, the core engine of the open source power system simulator InterPSS [22], the network equivalent helper, and the socket communication framework.

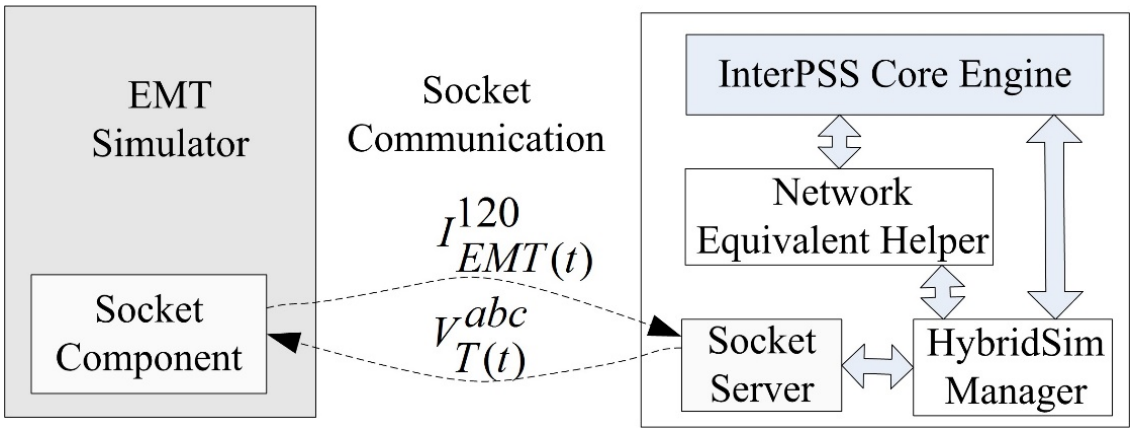

Figure 1.10: The architecture of OpenHybridSim

InterPSS is an open source software for power system analysis and simulation. This software has an open and flexibly coupled system architecture. It is developed using object-oriented programming (OOP). The models and algorithms within InterPSS can be flexibly modified and extended. Moreover, the software itself can be easily integrated into other systems [22]. Network models and algorithms for power flow, short circuit analysis and transient stability simulation have been developed in InterPSS. In view of these available features, InterPSS is used as a TS program for the proposed hybrid simulation tool.

The core functions of the hybrid simulation manager include determining the processing step interaction protocol, managing data conversion and interchange among modules on the TS side. A three-sequence TS simulation algorithm has been developed based on the InterPSS core engine. The primary objective of the network equivalent helper is to prepare a Thévenin equivalent for the

detailed system modeling at the modeling preparation stage and update the equivalent for the EMT simulation during hybrid simulation.

For each interaction between the two simulators, sequence current injection data is first sent from the EMT simulator to OpenHybridSim. Upon receiving the data, the hybrid simulation manager determines a proper protocol for this interaction, based on the algorithm proposed in Section 1.2. If the serial protocol is selected, the equivalent data from the EMT simulator is input into the InterPSS core engine to perform one time step TS simulation, and then the external system Thévenin equivalent is updated and sent back to the EMT simulator via the socket server. Otherwise, the Thévenin equivalent is updated first by the network equivalent helper, and the TS simulation step is postponed to the last step.

1.3.2 Development of OpenHybridSim

1.3.2.1 A Three-Sequence TS simulation

In accordance with the use of the three-phase Thévenin equivalent for representing the external system, all components in the external system, including the generators, transmission elements and loads, are represented using their three-sequence components. Correspondingly, a three-sequence based TS simulation algorithm is developed, as depicted in Fig. 1.11. The algorithm is composed of the conventional positive sequence TS algorithm and a sequence network solver. The sequence network solver is developed based on the existing short circuit analysis module of InterPSS. It calculates the negative- and zero-sequence voltages with the sequence current injections at the boundary buses and other buses inside the external system, if any. The algebraic equations shown in Fig. 1.11 can be described by (1.2) and (1.3), respectively.

$$\boldsymbol{Y}_{ext}^{(2)}\boldsymbol{V}_{ext}^{(2)} = \boldsymbol{I}_{ext}^{(2)} \tag{1.2}$$

$$\boldsymbol{Y}_{ext}^{(0)}\boldsymbol{V}_{ext}^{(0)} = I_{ext}^{(0)} \tag{1.3}$$

where the subscript ext denotes external system, $\boldsymbol{V}_{ext}^{(2)}$and $\boldsymbol{V}_{ext}^{(0)}$ are the vectors of negative- and zero-sequence voltages, respectively; $\boldsymbol{Y}_{ext}^{(2)}$ and $\boldsymbol{Y}_{ext}^{(0)}$ are the negative- and zero-sequence admittance matrices of the external system, respectively; $\boldsymbol{I}_{ext}^{(2)}\ and\ \boldsymbol{I}_{ext}^{(0)}$ are vectors of the negative- and zero-sequence bus current injections, respectively. $\boldsymbol{I}_{ext}^{(2)}\ and\ \boldsymbol{I}_{ext}^{(0)}$ include the sequence current injections at the boundary buses obtained from the EMT simulation and sequence current injections at the buses inside the external system, if any.

It should be noted that when the fault is applied within the detailed system and the topology of the external system is unchanged during the simulation, factorization of the three sequence admittance matrices is required for only once. In addition, these sequence networks are decoupled and can be solved independently. To further improve the computational efficiency, the sequence network solver could be disabled when there are negligible negative- and zero-sequence current injections at the boundary, and it could be enabled on detecting non-negligible negative and zero sequence current injections.

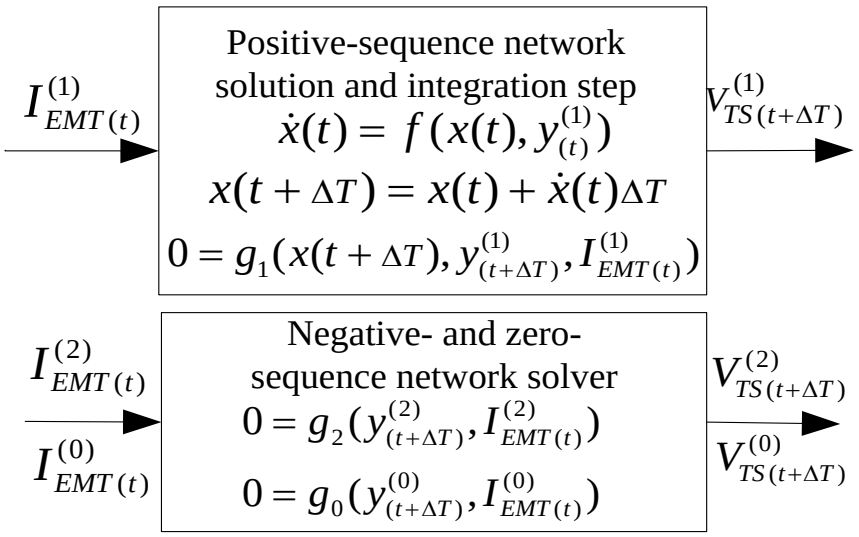

Figure 1.11: A three-sequence based TS simulation algorithm

1.3.2.2 Creation and Initialization of External System

To ease the burden of data preparation and facilitate the application of hybrid simulation, the external system is automatically created and initialized from a given base case. The creation and initialization process is as follows:

Run power flow with the whole system, then calculate the positive sequence current injections from the detailed system into the external system based on the boundary configuration information

With the boundary information, apply the depth first search (DFS) algorithm to the base case to identify all buses and branches within the detailed system and set them out of service

Initialize the positive sequence part of the external system using the existing initialization function of the TS program, with the detailed system represented by the current injections calculated in step 1). Both the negative- and zero- sequence current injections are assumed to be zero at the initialization stage. The negative- and zero-sequence admittance matrices of the external system are factorized and ready for use during hybrid simulation.

1.3.2.3 Procedures of Conducting Hybrid Simulation

Some screenshots of the GUI of the developed tool are shown in Figs. 1.12 and 1.13. The procedure for conducting hybrid simulation using the tool is shown in Fig. 1.14.

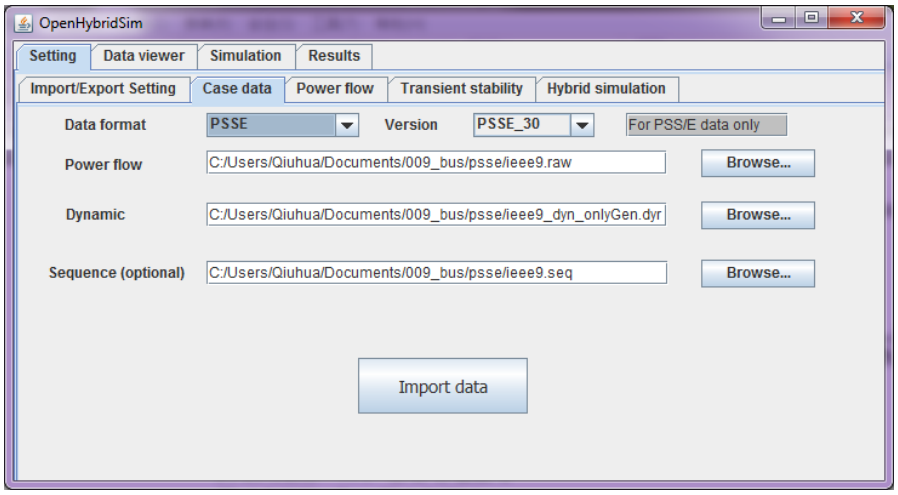

Figure 1.12: Importing data through the GUI of OpenHybridSim

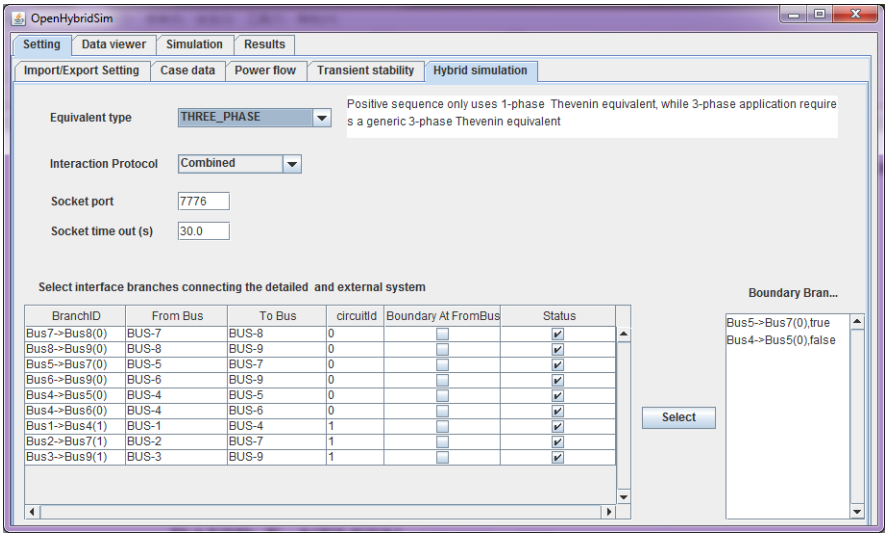

Figure 1.13: Configuration for hybrid simulation in the GUI of OpenHybridSim

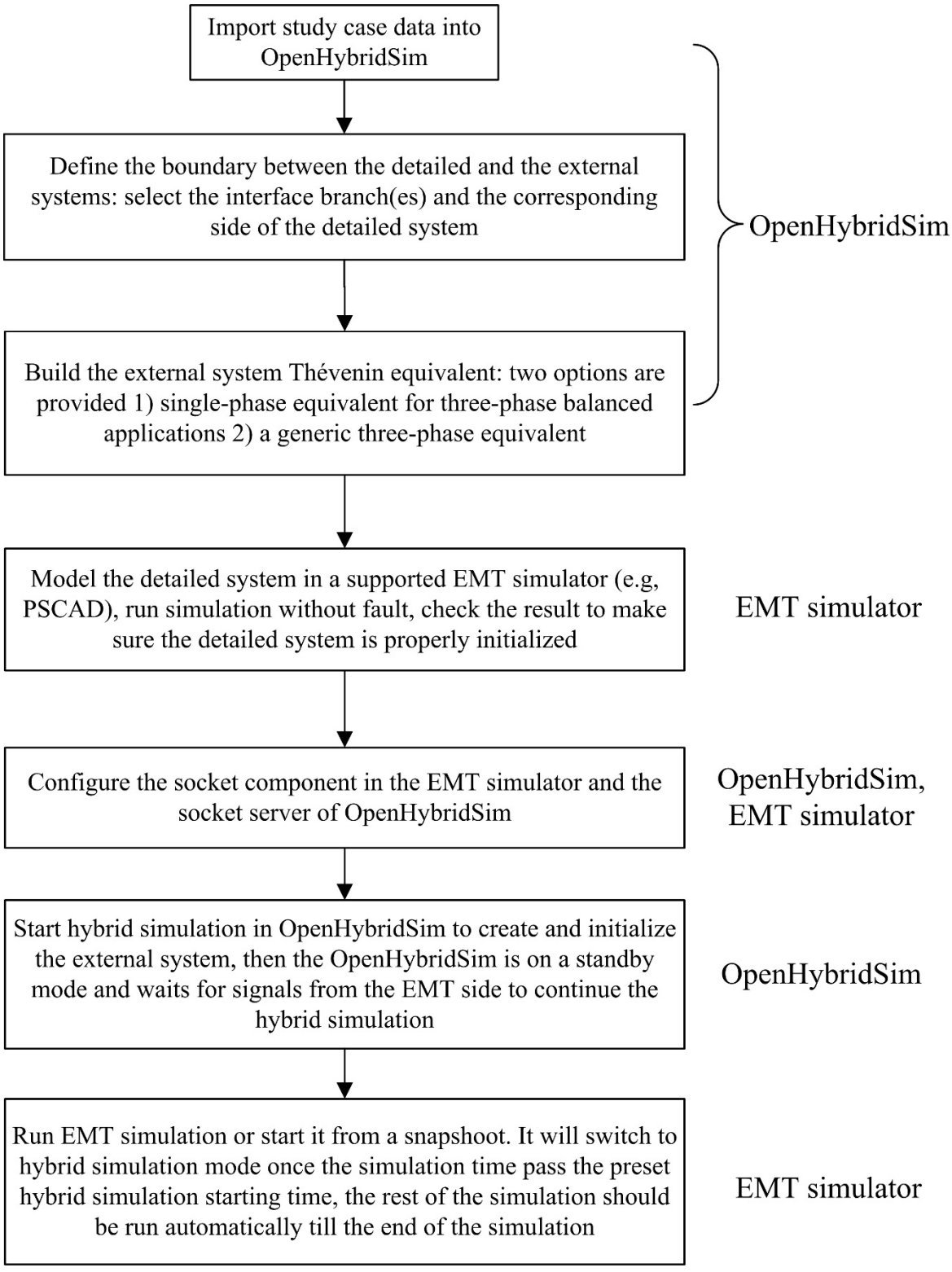

Figure 1.14: The flow chart of running hybrid simulation with OpenHyridSim

1.3.3 Interfacing with an EMT Simulator

1.3.3.1 A Socket-based Communication Framework Protocol

The socket technology is widely used for inter-process communication (IPC) between two programs, and the socket programing interface is supported by all modern operating systems. In addition, socket APIs are standard in almost all mainstream programming languages. Thus, the socket technology is chosen as the communication "bridge" between the EMT simulator and OpenHybridSim, with a socket client on the EMT side and a socket server in OpenHybridSim.

When the socket technology is combined with transmission control protocol/Internet protocol (TCP/IP) communication, a socket can not only integrate two programs on the same computer, but also connect simulation programs running on different computers through the Internet. Thus, the communication framework enables OpenHybridSim to have a good potential of running hybrid simulation in a distributed manner, as illustrated in Fig. 1. 15. The architecture of the parallel hybrid simulation is a typical client-server model. The server is built on the TS simulation side and can create several (up to tens or even hundreds, depending on the capability of the server machine) sockets to communicate with multiple EMT simulation clients concurrently.

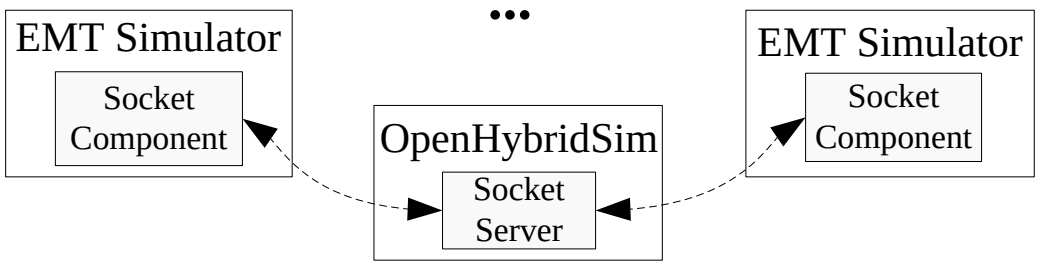

Figure 1.15: A perspective distributed hybrid simulation with OpenHybridSim

1.3.3.2 An Interface between OpenHybridSim and PSCAD

PSCAD is one of the widely used, comprehensive EMT simulators. An interface between OpenHybridSim and PSCAD has been developed and this interface is introduced here as an interfacing example. The interface mainly involves a socket client developed as a component in PSCAD, as shown in Fig. 1.16. The basic socket communication function is based on [23], and modifications and enhancements have been made for hybrid simulation applications. The logic of the socket component shown in Fig. 1.16 is implemented in the "script" section of the component definition in PSCAD. Features of the socket component include:

- Two ends: a sending end for passing data from PSCAD side to the TS side and a receiving end for catching and saving the data from TS side.
- The number of data at both ends must be explicitly specified.
- IP address and port must be set properly beforehand. The combination of both forms a socket address

- Time delay: an initialization process is required for EMT type simulations, therefore, a time delay must be properly set to make sure the detailed system in PSCAD has been successfully initialized before starting hybrid simulation

- Time step: the interaction time step for hybrid simulation. It is usually set to be the same as TS simulation time step.

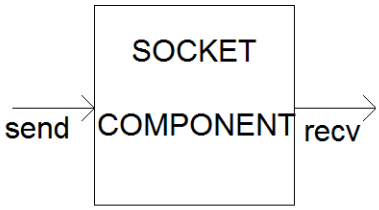

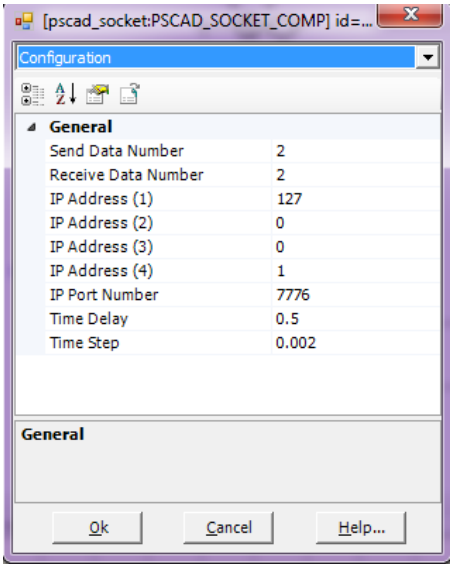

(a) (b)

Figure 1.16: Socket component developed in PSCAD

1.4 Application of Hybrid Simulation to A Detailed FIDVR Study On The WECC System

With A/C compressor motor models developed for planning studies and detailed simulation, in-depth knowledge of the FIDVR problem at the load component level is obtained. However, a better understanding of the FIDVR events from a system perspective is urgently needed. To develop such an understanding, dynamic responses of single-phase A/C compressor motors to unsymmetrical faults at the transmission system and the interaction between the transmission system and the distribution systems during a FIDVR event need to be examined. Detailed simulation of FIDVR events on power systems, which are subjected to this problem, is one feasible approach to fulfill this objective. A detailed FIDVR study of a region within the WECC system is conducted in this chapter, based on the developed hybrid simulation platform.

1.4.1 Overview of the WECC system

FIDVR events have been observed in several areas within the WECC system, e.g., Southern California and Arizona. In this study, a region within the WECC which is known to have experienced FIDVR events in recent years is chosen for this study. A summer peak case of the system is used, and its basic information is summarized in Table 1.1. The one-line diagram of this region and the surrounding area is depicted in Fig. 1.17 The buses 24138 and 24151 in Fig. 1.17 correspond to two 500 kV substations, where a large percentage of the loads are induction motors,

and a majority of them are single-phase A/Cs, particularly, for the bus 24151. Thus, both substations are of primary interest in this study.

Table 1.1 Case summary of the WECC system

Buses	Transmission lines	Generators	Loads
15750	13715	3074	7787

For the sake of simplicity, the details of the sub-systems below 500 kV are not presented in Fig. 1.17, although some buses within these sub-systems are also connected to the northern and eastern parts of the system.

The first step in a detailed FIDVR study is to build an appropriate simulation model for hybrid simulation, based on the existing system planning model. The simulation model includes two parts, the external system and the detailed system. For the detailed system modeled in PSCAD, a specific modeling process is required as outlined in Fig. 1.18. The details of each step in the process will be discussed in the following three sections.

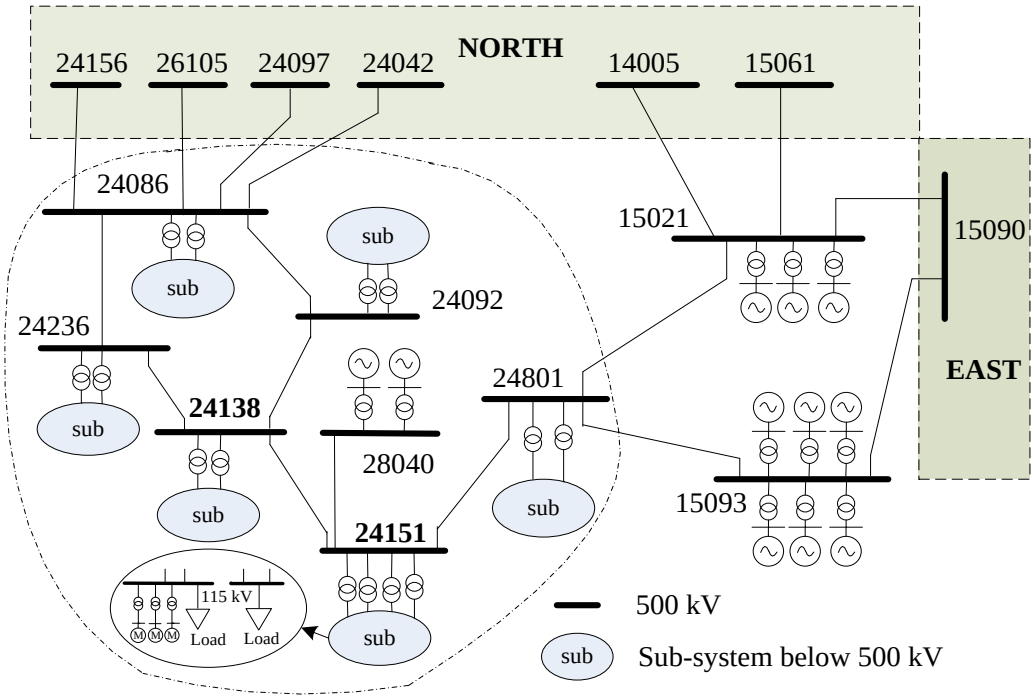

Figure 1.17: One-line diagram of the study region

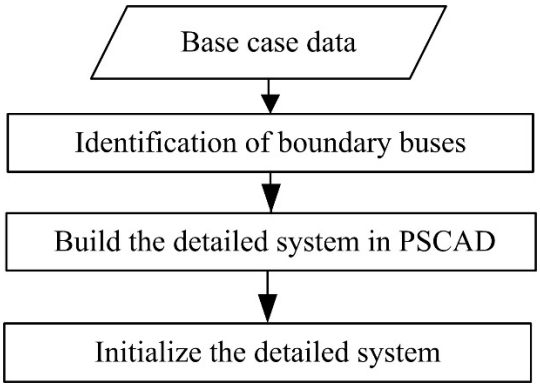

Figure 1.18: Procedure of the detailed system modeling in PSCAD

1.4.2 Determining the Boundary of the Detailed System

1.4.2.1 Guide Regarding Transmission Bus Voltage Dip

To develop a guide to determine what transmission bus voltage dip will cause A/C motors in the underlying systems to stall, a generic subtransmission and distribution model as shown in Fig. 1.19 is considered. The total load is 20 + *j*10 MVA. The 115/12.47 kV transformer reactance and the equivalent feeder impedance are specified on a 30 MVA base. A wide range of impedances between the source and end-use points, different A/C loading percentages (based on the ratio of the real power consumption of A/Cs to the real power of the total load) and typical A/C power levels have been considered. Voltage dips of different magnitudes, lasting 4 cycles were applied at Bus 1 and those that caused the A/C motors connected to Bus 3 to stall were recorded. It can be observed from Fig. 1.20 that the smallest voltage dip magnitude causing A/C stall is larger than 0.25 pu. Thus, 0.75 pu can be adopted as the A/C stalling voltage threshold at a transmission bus. Accordingly, a voltage threshold of 0.75 pu was set as the voltage criterion in selecting buffer buses.

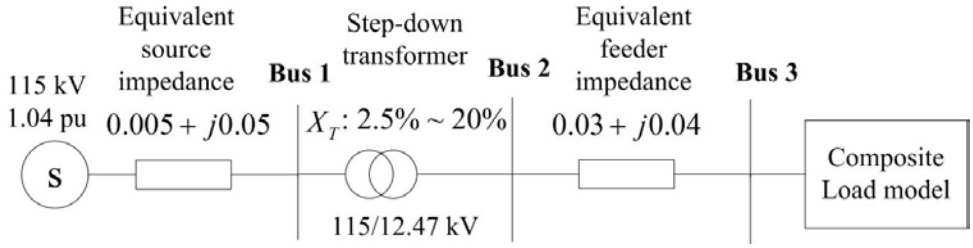

Figure 1.19: One-line diagram of a test system for determining the A/C motor stalling voltage tip at a transmission bus

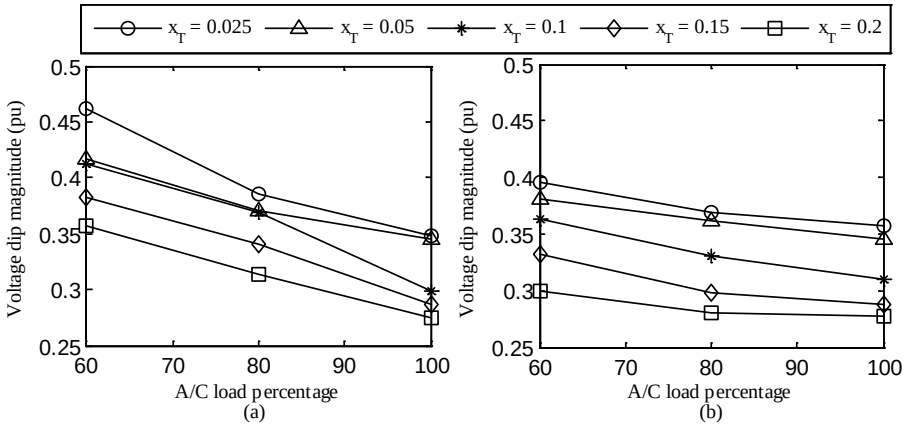

Figure 1.20: Voltage dip magnitude with respect to the A/C load percentage and the transformer impedance: (a) A/C power = 4.9 kW (b) A/C power = 6.0 kW

1.4.2.2 Boundary Identification

The study area includes the buses 24138 and 24151, together with the subtransmission and distribution systems that are supplied from them. A bus is included in the detailed system if a single-phase or three-phase fault at that bus cause a phase-to-neutral voltage at buses 24151 and 24138 to fall below 0.75 pu.

Single-line-to-ground and three-phase faults at the 500 kV buses in this region are analyzed and the fault voltages at bus 24138 and bus 24151 are recorded and summarized in Table 1.2. Based on the short circuit voltages and the threshold of 0.75 pu, the area encircled by the dashed-dot line in Fig. 1.17 is chosen as the detailed system. It should be noted that a three-phase fault at bus 26105 causes the voltage of bus 24138 to fall below 0.75, nonetheless it is excluded from the detaield system, since it is relatively far from the load center of interest at bus 24151 and including it will significantly complicate the interface. A summary of the detailed system is provided in Table 1.3.

Table 1.2 The lowest phase voltage magnitude of the buses 24138 and 24151

Faulted bus	bus 24151		bus 24138	
	3-phase fault	1-phase fault	3-phase fault	1-phase fault
24801	0.49	0.60	0.80	0.87
24092	0.60	0.71	0.34	0.40
24086	0.65	0.77	0.42	0.53
24236	0.69	0.78	0.47	0.53
15021	0.82	0.87	0.92	0.95
26105	0.83	0.91	0.70	0.79
24156	0.87	0.93	0.76	0.83
15093	0.87	0.92	0.96	0.99
24042	0.90	0.95	0.84	0.89
24097	0.99	1.00	0.96	0.97

Table 1.3 Statistics of the detailed system model including subtransmission buses not shown in Fig. 1.17

Total number of buses	238	
Number of buses shown in Fig. 1.17	500 kV	7
Number of buses of different voltage levels (not shown in Fig. 5.1)	230 kV	37
	161 kV	3
	115 kV	68
	92 kV	18
	<= 66 kV	105
Total Load	11.9 GW	

1.4.3 Initialization of the Detailed System

The first phase of the EMT simulation is to obtain a steady state initial condition. PSCAD initializes a system by ramping up the system from a zero initial condition to a steady state. In this study, the induction motor loads in the distribution systems served by buses 24151 and 24138 account for more than 60% of the total load in terms of real power. At the induction motor starting stage, the induction motors draw a large amount of reactive power from the system. The bus voltages in the distribution system are significantly depressed to an extent that these induction motors, including the single-phase A/C induction motors, cannot be properly initialized. Consequently, with the default initialization procedure, PSCAD fails to properly initialize the detailed system.

To address this issue, a two-step initialization method is proposed, which is illustrated by the Fig. 1.21. A fixed voltage source whose magnitude and phase angle are set based on the power flow result of the reference planning model is used in the first step. For the first step, the switch *K* for each load bus where a CLM is connected is turned to the position 0. The distribution systems and the CLMs are energized by the fixed voltage source and initialized independently. At the same time, the static equivalent load representing the distribution system is connected to the transmission bus and the transmission elements in the detailed system are initialized. After the CLMs are successfully initialized, the initialization process moves to the second step where the switch *K* is turned to the position 1 such that the detailed distribution system model is connected to the transmission system and replace the corresponding equivalent static load. Then the whole detailed system goes through a short-term adjustment process before finally reaching a steady state.

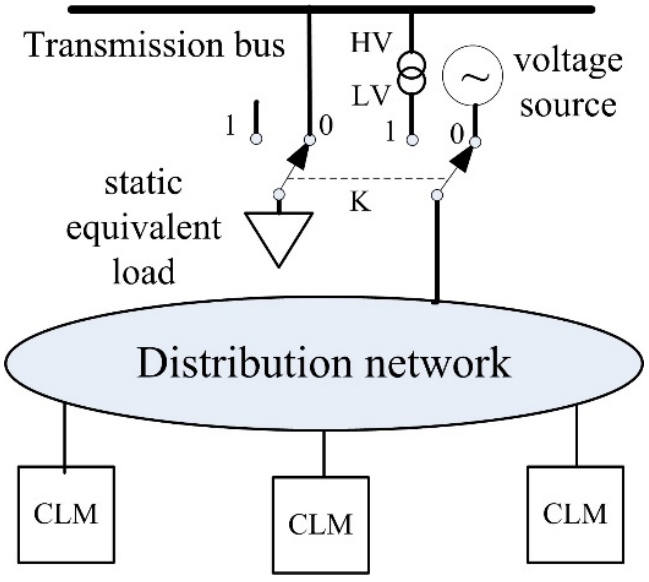

Figure 1.21: A schematic for illustrating the two-stage detailed system initialization process

1.4.4 Benchmarking Hybrid Simulation against Transient Stability

The study case includes a detailed system consisting of 238 buses, 8 interface buses and an external system consisting of more than 15000 buses. To check whether the detailed system is correctly

built in PSCAD and to test the accuracy and applicability of the hybrid simulation for a realistic large power system, the proposed hybrid simulation approach has been benchmarked against the positive sequence based TS simulation on the WECC system with all the loads represented by constant impedances.

The hybrid simulation starts at t = 0 s. A single line to ground (SLG) fault is applied on the phase A of bus 24151 at t = 0.2 s. Figs. 5.6-5.8 show the benchmark results. The positive sequence voltages of buses 24151 and 24806 (one of the interface buses) are monitored and depicted in Figs. 1.22 and 1.23. The reactive power output of a machine at a large power plant at bus 15021 is also shown in Fig. 1.24. The results of the EMT-TS hybrid simulation and the TS simulation matched except for a small discrepancy in the post-fault voltage recovery level at bus 24806 and a small time delay by the hybrid simulation. The delay is introduced by the positive sequence value extraction component of PSCAD.

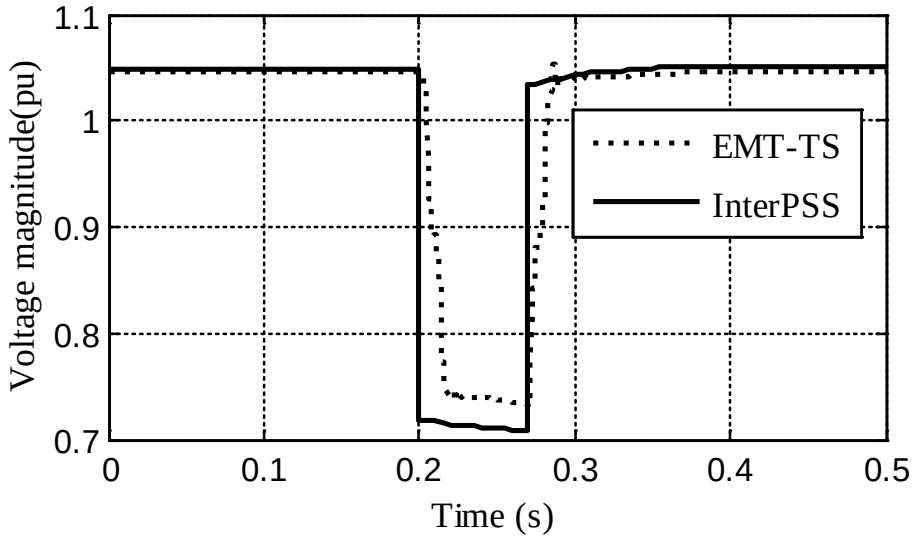

Figure 1.22: The positive sequence voltage at bus 24151

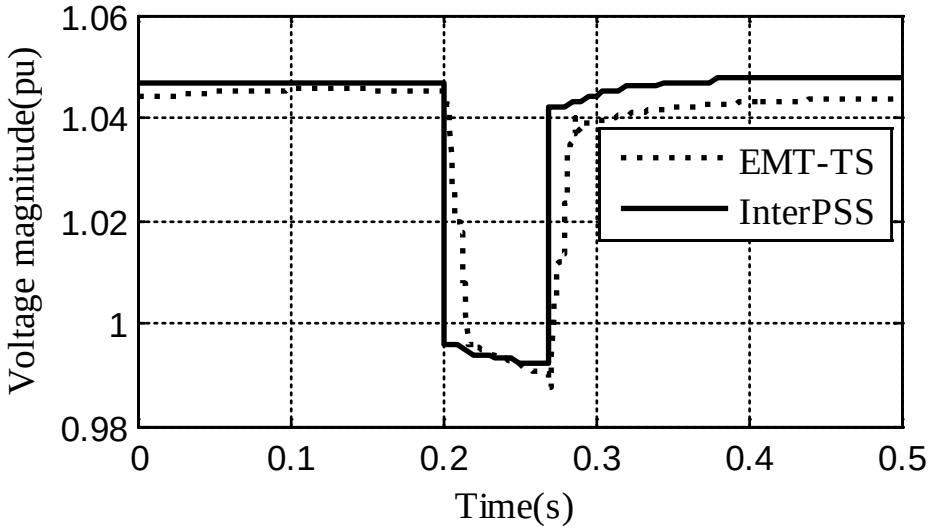

Figure 1.23: The positive sequence voltage at bus 24806

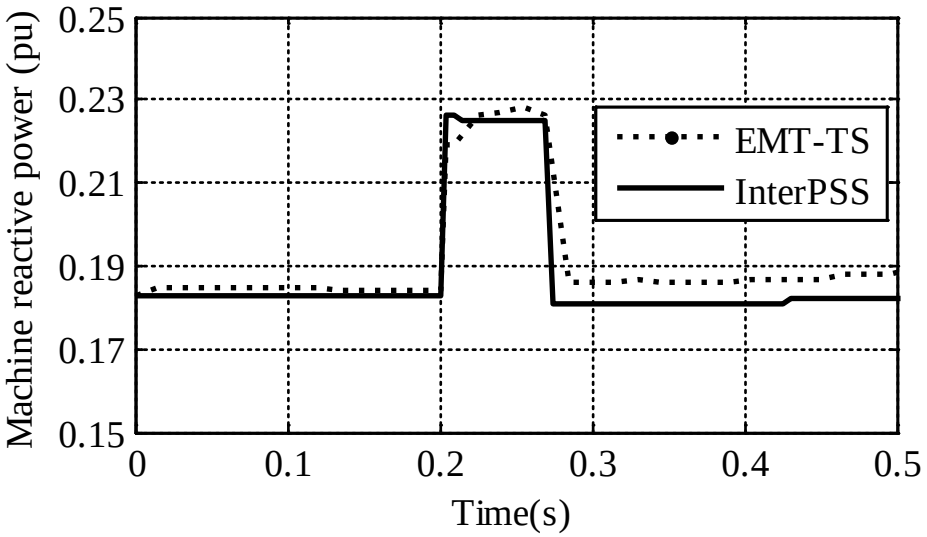

Figure 1.24: Reactive power output of the generator at bus 15021

1.4.5 Application of Hybrid Simulation to FIDVR Study on the WECC System

1.4.5.1 Distribution Network and Load Modeling

Equivalent models for the distribution networks and feeders are used to represent the distribution networks within the substation of bus 24151. The equivalent impedances of subtransmission systems are included in the models of the 115/12.5 kV transformers. The distribution feeders are modeled in two sections, i.e., the total load is divided into two portions. Two thirds of the total loads are connected at a quarter point along the feeder, with the rest one third of the load connected at the end of the feeder [25], as shown in Fig. 1.25. The parameters of the detailed A/C models [12] have been appropriately chosen to match the target percentage of total load. To model three-phase induction motors, a 20 horsepower, 380 V three-phase squirrel-cage induction motor has been used. The parameters of the motor are chosen to represent a typical NEMA type B induction motor. The driven mechanical torque is proportional to the square of its speed. Under-voltage motor protection is not modeled. A one-line diagram and data of the substation of bus 24151 are provided in the Fig. 1.26. Buses 24160 and 24229 are two 115 kV load-serving buses connected to bus 24151. The parameters and load models for all the equivalent feeders are assumed to be identical. Thus, the responses of A/Cs on one feeder will be used to illustrate the results in the following case studies.

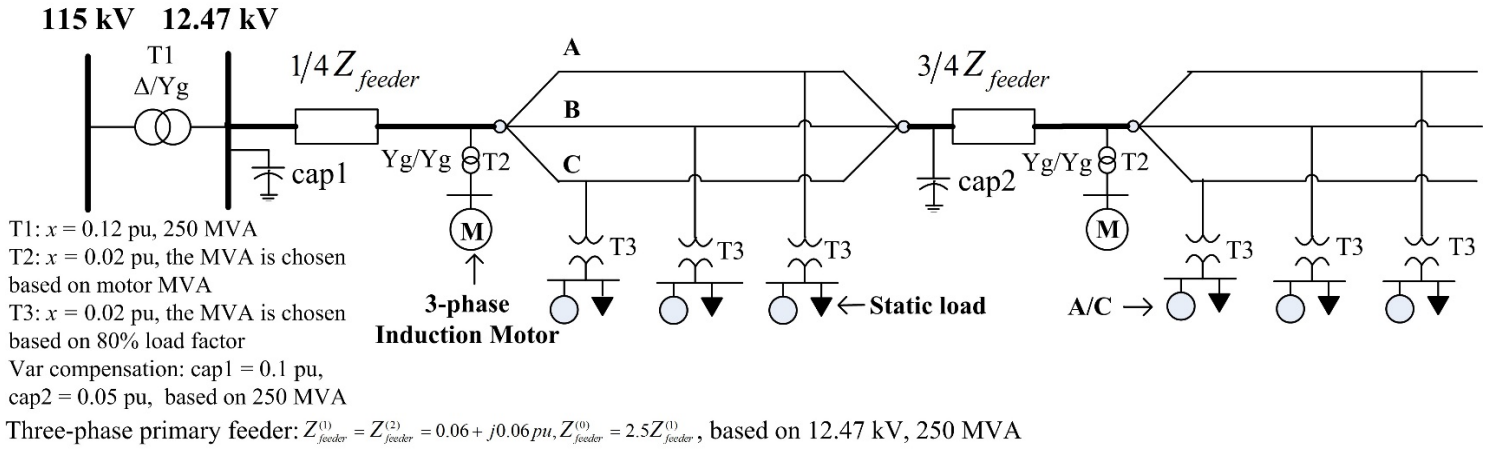

Fig. 1.25 A two-section equivalent feeder model

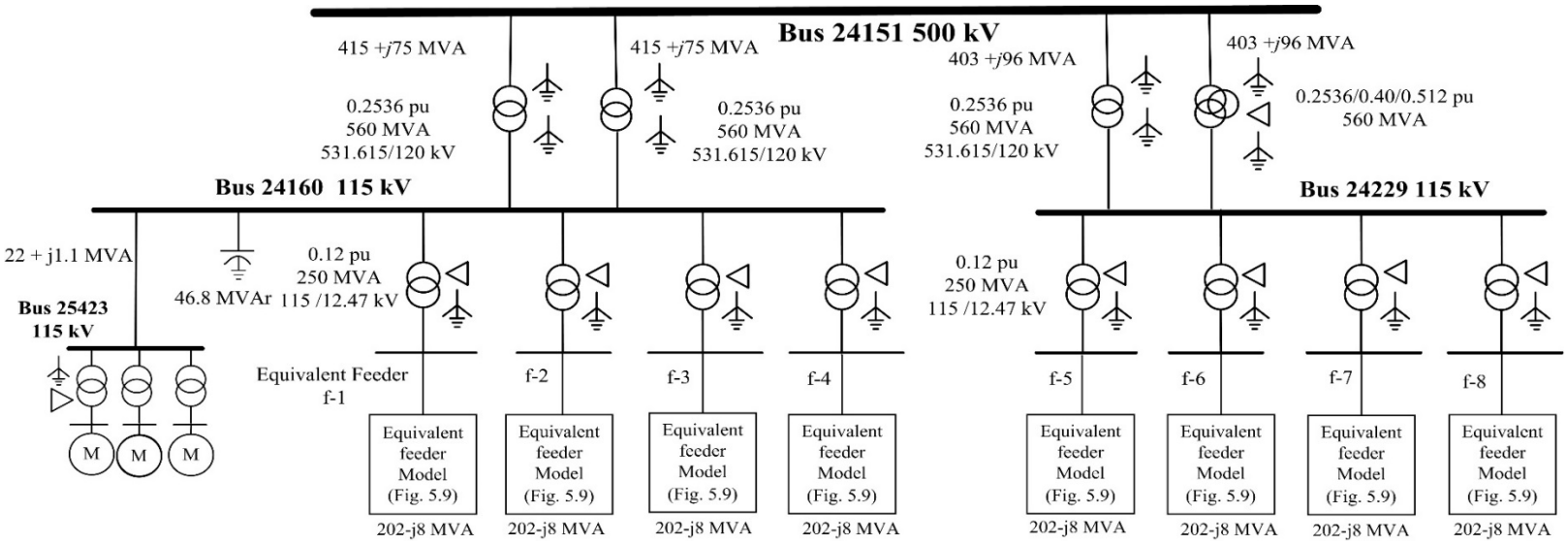

Figure 1.26: A detailed modeling of the substation of bus 2415

1.4.5.2 Propagation of A/C motor stalling to unfaulted phases

In this case, 75% of total load of the bus 24151 is assumed to be A/C load with the remaining load modeled by constant impedance loads. This case is referred to as case 1 hereafter. A single line to ground (SLG) fault is applied on the phase A of bus 24151 at 0.7 s (the corresponding fault point-on-wave is 0 degree), and cleared after 4 cycles.

The three phase voltages of the buses served by 500 kV bus 24151 are shown in Fig. 1.27. It can be observed that the SLG fault at bus 24151 depressed the phase voltage of both phases A and C at the distribution system level, due to the delta-wye connection of the 115 kV/12.47 kV step-down transformers.

The responses of the A/C motors connected at the quarter length point of a feeder are shown in Fig. 1.28. The terminal voltages of the A/C motors on all three phases drop when the fault is in effect, with the voltages on phases *A* and *C* being depressed down to around 0.4 pu. The terminal voltages of these two phases recover partially upon clearance of the fault. Consequently, the speeds of the A/C compressor motors on both phases *A* and *C* also recover. However, the level to which the voltages recover is lower than 0.6 pu. The speed recovery of A/C motors on both phases is not sustained under such a low voltage condition, and these motors start to stall at about 0.75 s. A/Cs on phase *C* stall at 0.9 s and A/Cs on phase *A* stall at 1.0 s. Subsequently, the terminal voltages of A/Cs on both phases are further depressed to about 0.4 pu.

The speeds of the A/C motors on phase *B* fully recover after the fault is cleared and sustain for 0.6 s. However, the voltage of phase *B* is also depressed due to the interaction with phases *A* and *C* through those 115/12.5 kV transformers. Further, reactive power consumption by the A/C motors on phase *B* increases as the terminal voltages decrease, as depicted in the Fig. 1.28, which, in turn, depresses the voltages further. These combined effects eventually lead to stalling of the A/C motors on phase *B* after 1.5 s.

As a result of the A/C stalling on all three-phases, three phase line-to-ground voltages of all the buses served by the substation of bus 24151 are significantly depressed, as shown in Fig. 1.29. Because the A/C motors on three phases stall at the different times, the three-phase voltages become significantly unbalanced after fault clearance until all A/Cs on three phases stall. The unbalance is clearly shown in both Fig. 1.29 and Fig. 1.30. After A/Cs on all three phases are stalled, the positive sequence voltage of the 115 kV bus 24160 is depressed down to 0.6 pu and the positive sequence voltage of the 500 kV bus 24151 is depressed down to 0.9 pu. During the simulation period, A/C motors remain in the stalled state, thus the voltages remain depressed. It can be expected that the transmission system voltage will only recover after the stalled A/Cs are tripped off.

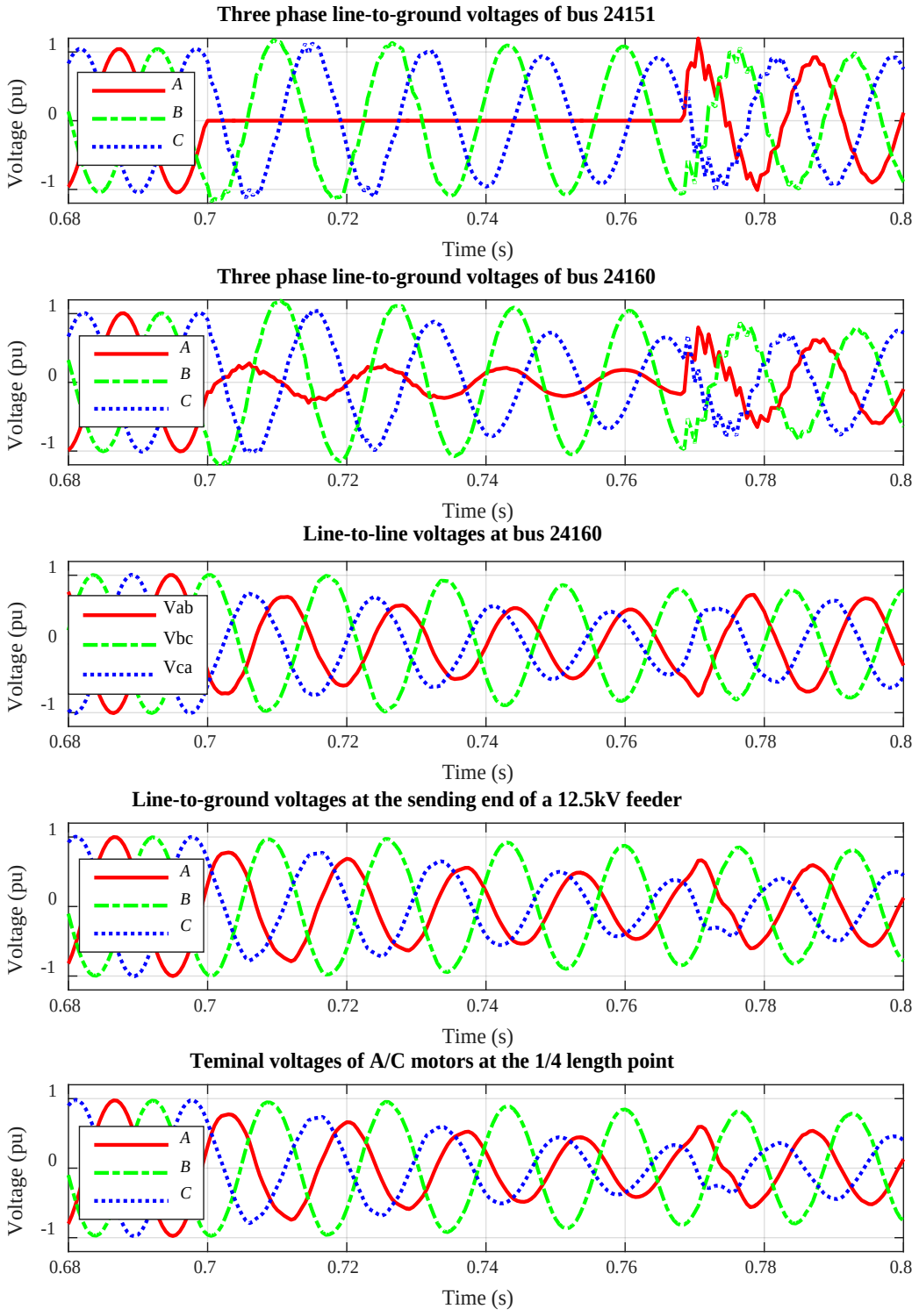

Figure 1.27: Three phase voltages at different locations served by the substation of bus

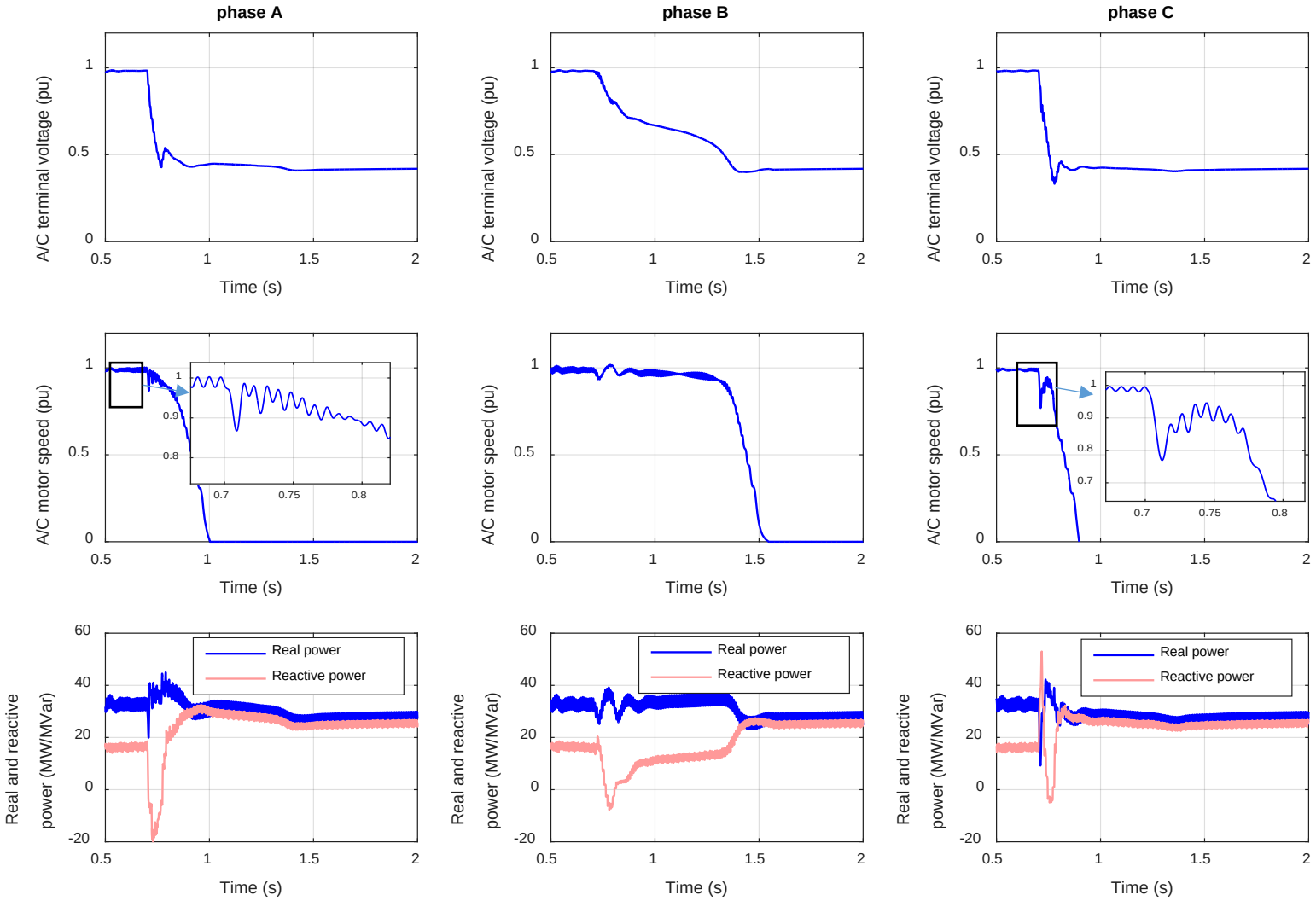

Fig. 1.1 The responses of the A/C motors at the quarter length point of a feeder

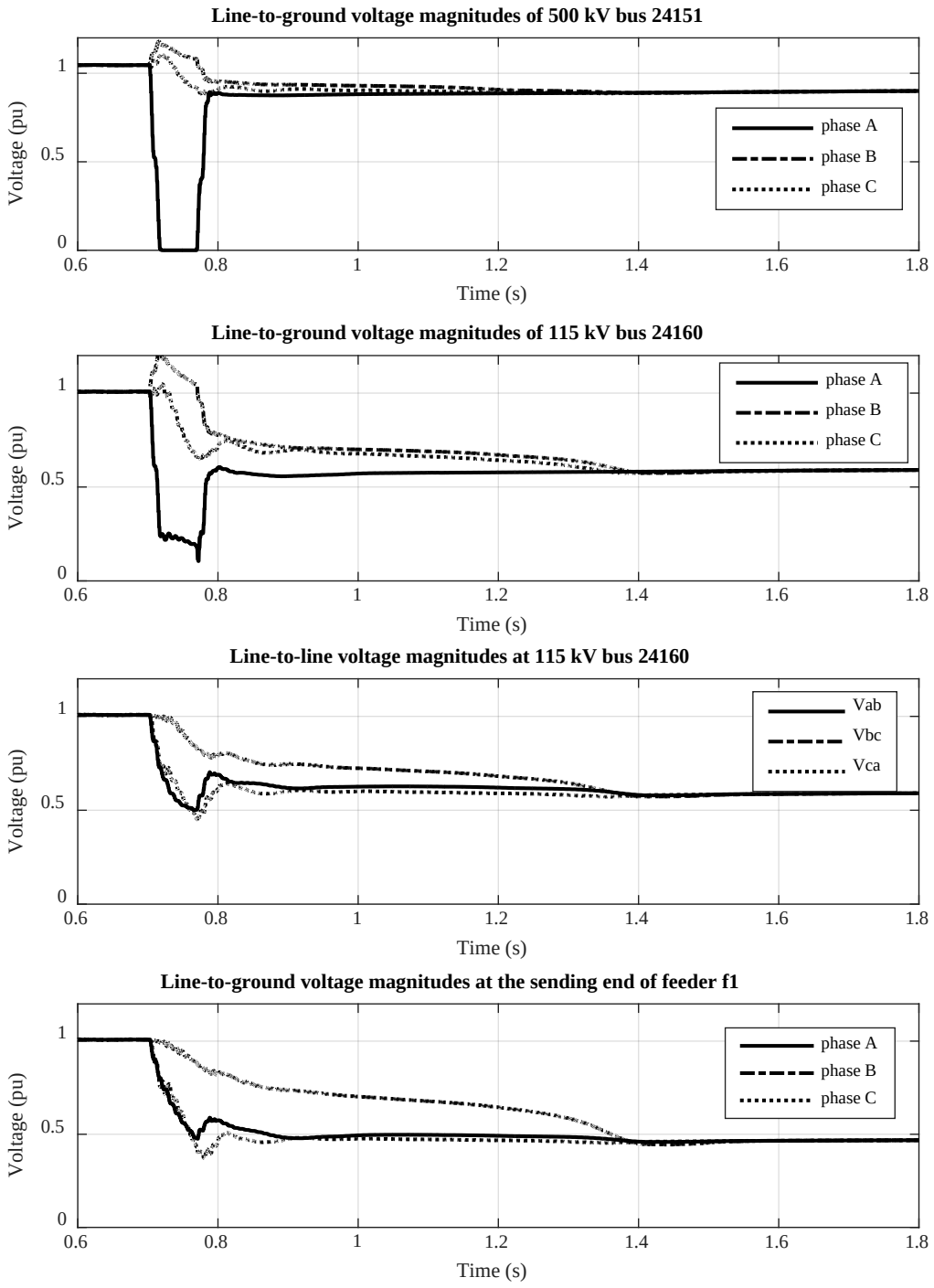

Fig. 1.2 Three phase voltage magnitudes of buses served by the substation of bus 24151

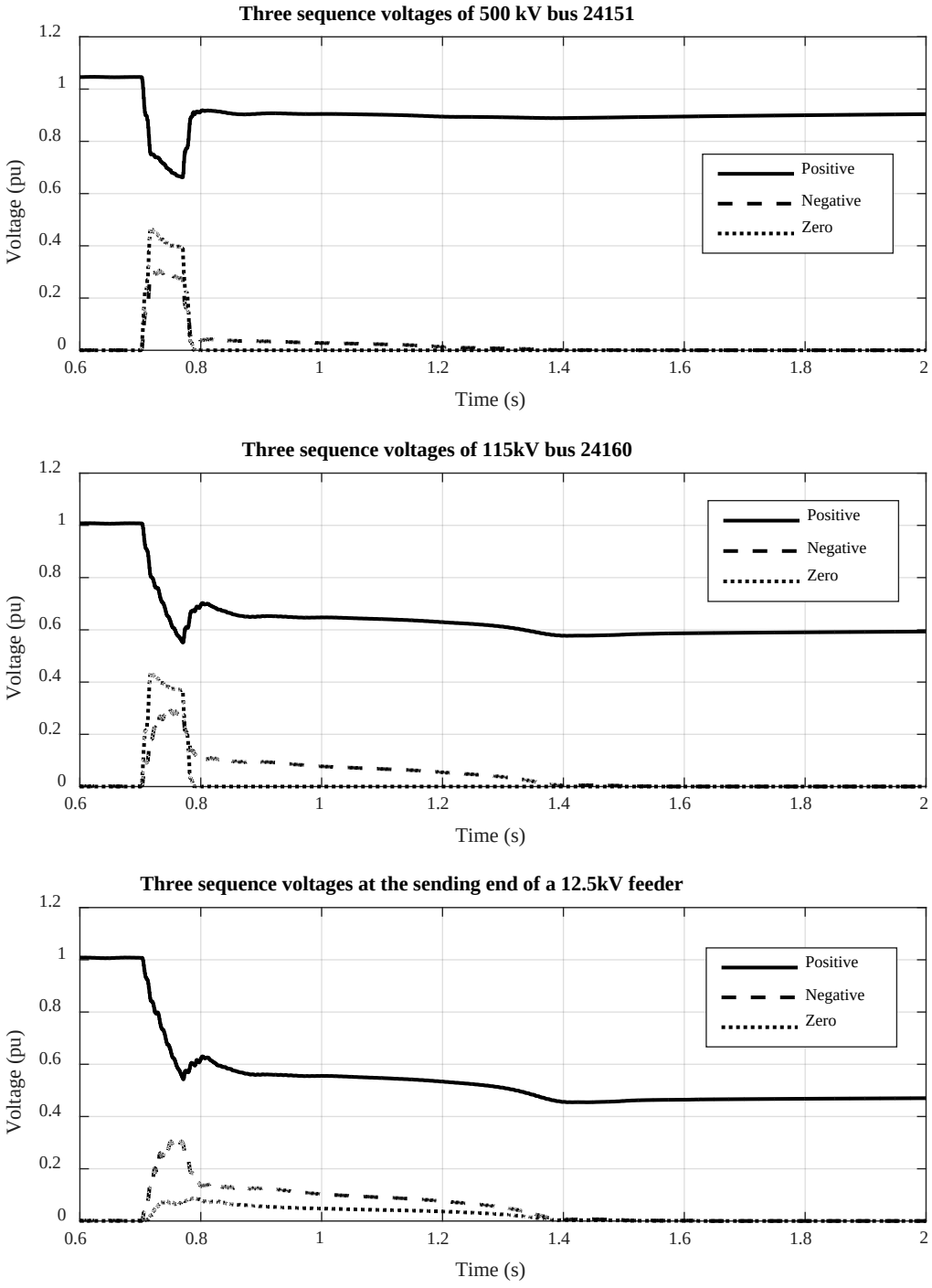

Fig. 1.3 Three-sequence voltage magnitudes of three buses served by bus 24151

1.4.5.3 Effects of load composition on A/C motor stalling

In this study, the effects of the load composition on A/C motor stalling and the occurrence of FIDVR events are simulated and analyzed. Five cases in total are examined as summarized in Table 1.4, with different percentages of single-phase A/C compressor motors, three-phase induction motors and constant impedance loads.

Table 1.4 Load composition data of the five study cases

Case #	Load composition (in terms of real power)
1	75% 1-Φ A/C compressor motor, 25% constant impedance
2	75% 1-Φ A/C compressor motor, 10% 3-Φ NEMA type B induction motor, 15% constant impedance
3	70% 1-Φ A/C compressor motor, 15% 3-Φ NEMA type B induction motor, 15% constant impedance
4	60% 1-Φ A/C compressor motor, 15% 3-Φ NEMA type B induction motor, 25% constant impedance
5	50% 1-Φ A/C compressor motor, 25% 3-Φ NEMA type B induction motor, 25% constant impedance

It is observed from Fig. 1.31 that the SLG fault at bus 24151 eventually causes A/Cs on all three phases within the footprint of bus 24151 to stall for all the five study

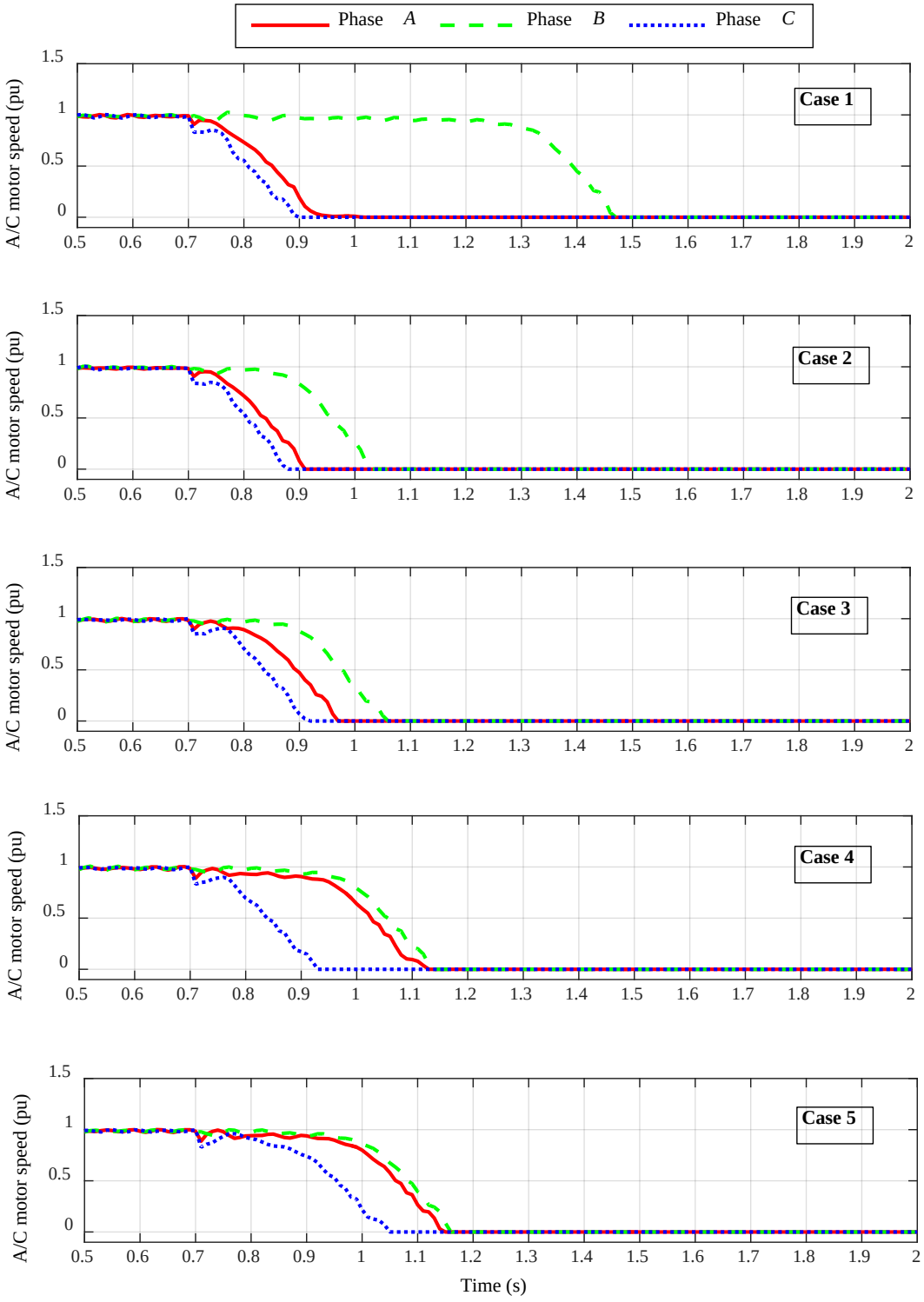

Fig. 1.4 The speeds of A/C compressor motors at the 1/4 length point of the feeder f-1 served by bus 24160 for all five cases.

cases. These results indicate that propagation of A/C motor stalling to unfaulted phase is consistent across a substantial range of load compositions. The study implies that the impacts of SLG faults close to certain regions of the system with high A/C penetration could be more severe than perceived, and more attentions should be paid to them.

The major difference among the results is the time at which A/C compressor motor stalling occurs. An obvious trend is that less the A/C loads, the longer it takes for A/C compressor motors to start stalling. In case 2, 75% of the load is single-phase A/C motors and 10% the load is three-phase induction motor. While in case 3, the corresponding percentages are 70% and 15%, respectively. Fig. 1.31 shows that it takes a longer time for A/Cs to stall in latter case than the former. The same trend is observed in the cases 4 and 5. These results confirm that three-phase induction motors are less onerous than the single-phase A/C compressor motor in terms of causing FIDVR problems. The reason is mainly twofold: first, less prone-to-stall A/C motors means less A/Cs will stall and less reactive power is drawn; second, during and immediately after the fault, three-phase induction motors actually support the system voltage by injecting VArs as they tend to keep their internal voltages constant during the fault period. This is apparent from the reactive power trace in Fig. 1.32.

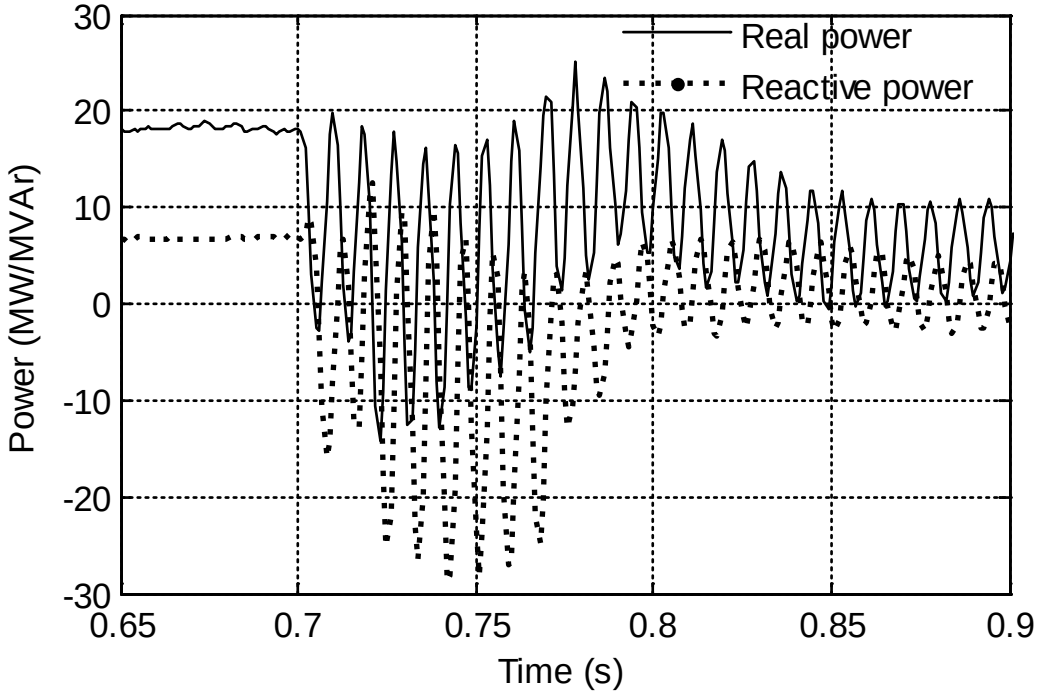

Fig. 1.5 Power consumption of the three-phase induction motors at the 1/4 length point of an equivalent feeder within bus 24229 substation for case 3

1.4.5.4 Effect of the point-on-wave (POW) characteristic of A/C compressor motor stalling

Previous research demonstrates that A/C compressor motor stalling is sensitive to the point on the voltage waveform when the fault is applied. How such a characteristic affects A/C motor stalling and the associated system dynamics with unsymmetrical faults in the transmission system is an

important question to be answered. This question is answered through a comparison study as follows:

The case 5 discussed before is used here as the base case, and a SLG fault is applied at phase *A* of 500 kV bus 24151 $t = 0.70$ s with POW = 0 degree. A comparison case with the same SLG fault being applied at POW of 90 degrees, referred to as case 5A hereafter, is considered for this study. The fault is cleared after 4 cycles in both cases. As shown in the previous Fig. 1.31, A/Cs on three phases all stall in case 5. The A/C stalling results in a FIDVR event and delays the voltage recovery of local transmission and distribution buses as shown in the plots on the left of Fig. 1.34.

The responses of the A/Cs at the quarter length point of a feeder in case 5A are shown in Figure 1.33. It can be seen from the A/C motor speed plots in Fig. 1.33 that no A/C stalls in case 5A. The real power drawn by the A/Cs on three phases changes slightly even during the fault period. A/C motors contribute VAr support to the system during the fault period, but their reactive power consumption recovers back to the pre-fault level within a very short period after the fault is cleared. The current they draw during the period between fault clearance and voltage full recovery (at about 1.5 s) are larger than their rated values. As a result, their terminal voltage recovery is to some extent delayed. It takes about 0.7 s after the fault clearance for the terminal voltages to recover back to the pre-fault level. The corresponding impacts on the local transmission and distribution bus voltages are shown in Fig. 1.34. The voltage recovery of these local buses is somehow delayed by the A/Cs.

The comparison results show that the POW effect leads to different results in terms of A/C stalling and the resulting system voltage recovery. Therefore, it is recommended that, for detailed FIDVR studies, the POW characteristic should be considered whenever possible, in order to obtain a clearer picture of potential outcomes as the POWs of actual faults in power systems are random.

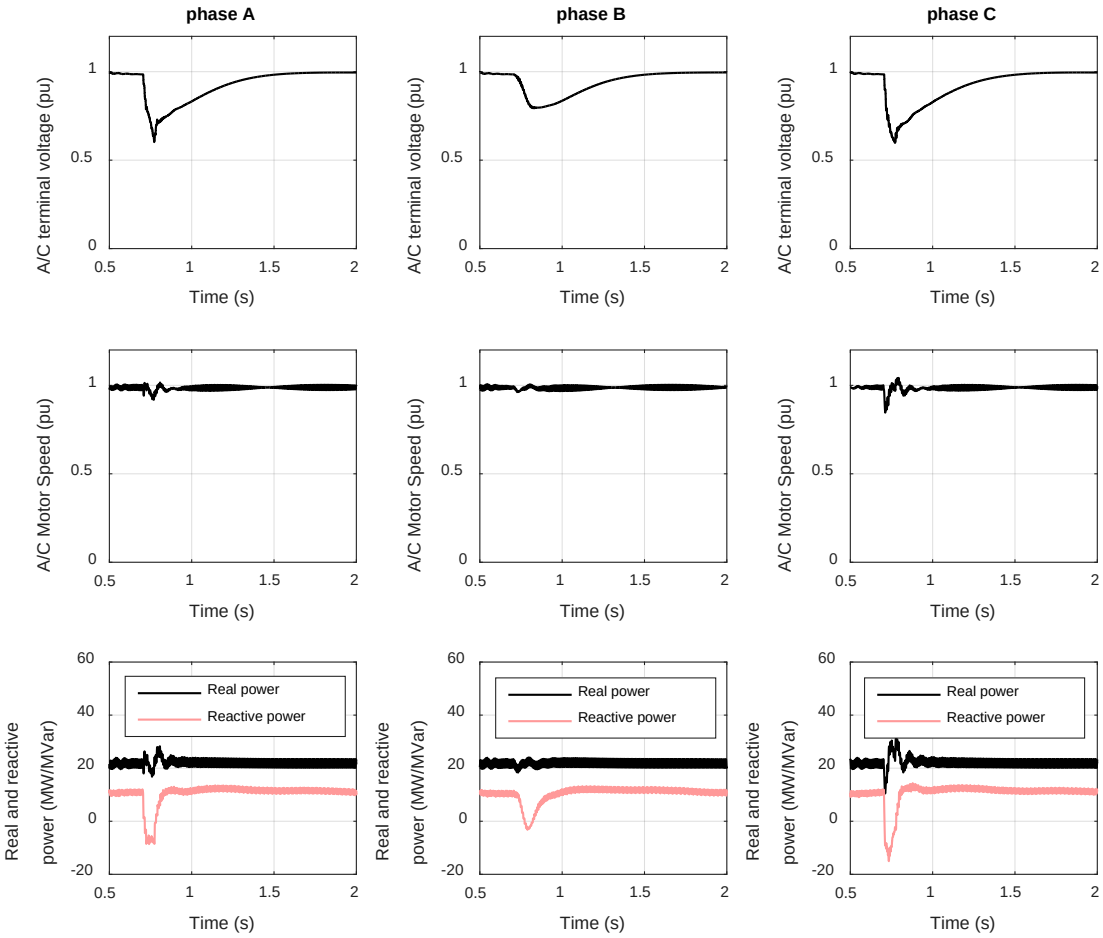

Fig. 1.6 The responses of the A/C motors at the quarter length point of a feeder with the fault POW as 90 degrees

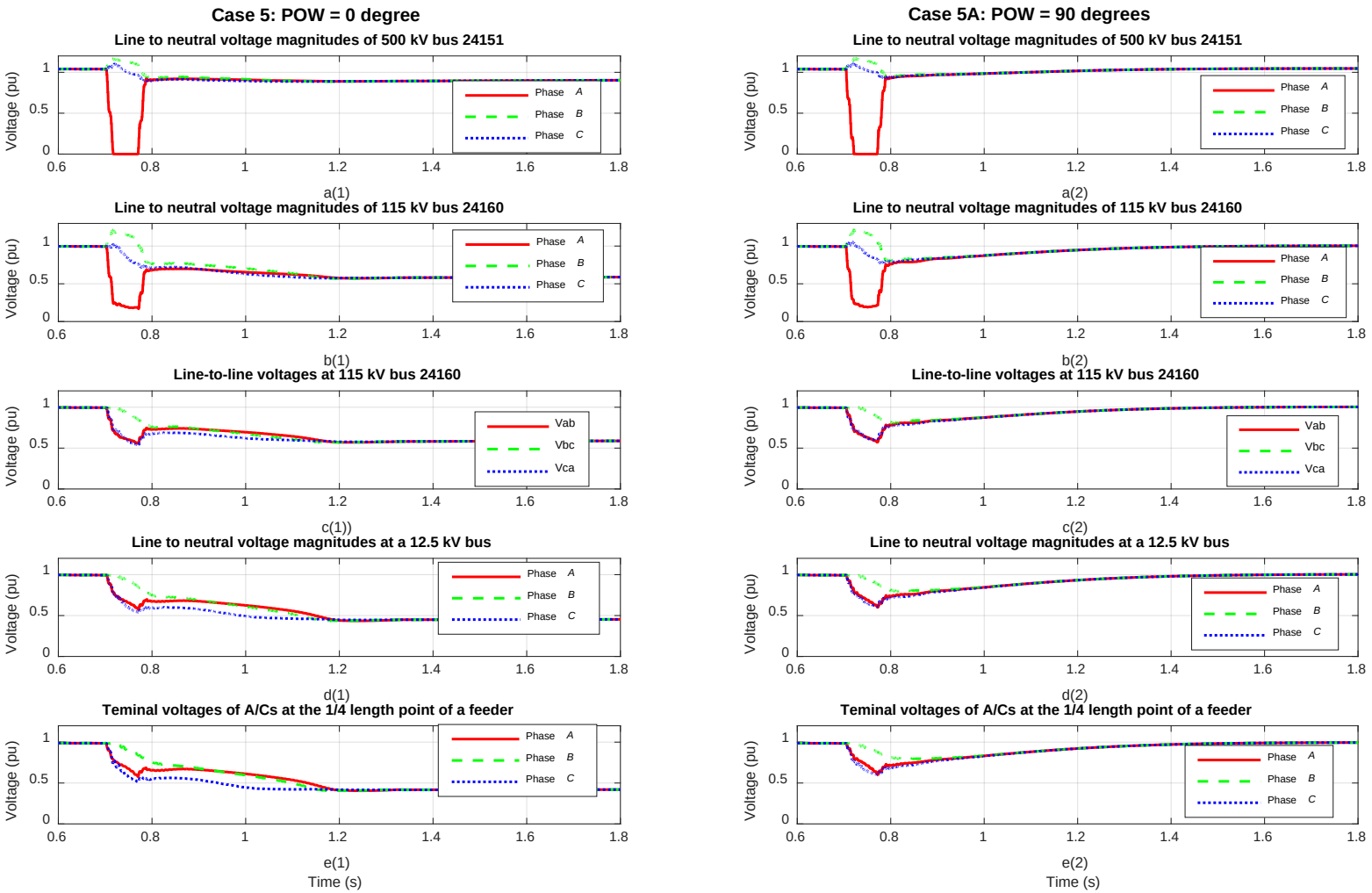

Fig. 1.7 Comparisons of the bus voltages for two different POW cases: (left) case 5; (right) case 5A

Computational performance

The experiment hybrid simulation platform set up in the laboratory consists of a desktop computer (processor: quad-core, 3.4 GHz, Intel Core i7-3770) and a laptop (processor: duo-core, 2.26 GHz, Intel Core P8400). Both are on the same LAN environment, connected via a wireless network with a speed of 250 Mb/s. PSCAD is installed and run on the desktop, while the developed three-sequence TS program is run on the laptop.

For a 3-second simulation of case 1, the computation times of different simulation approaches and interaction protocols are summarized in Table 1.5. The multi-core parallel computing capability of PSCAD (available since version 4.6) has been utilized in all the simulation methods. EMT-TS hybrid simulation results are reported in the first three rows. In the simulation done in the last row, the internal network is represented in detail but the external system is represented in a greatly simplified manned using a fixed Thévenin equivalent at the boundary buses. Correspondingly, the whole test case is simulated with PSCAD. Due to the large scale of the external system and utilization of multi-core parallel computing capability of PSCAD, the computational times used by the EMT and TS parts are comparable for this test case. In this context, compared to the serial protocol, the combined protocol reduces the computation time by 44%. The time difference between the combined and the serial protocols mainly corresponds to the time consumed by the TS part simulation and data exchange via the socket communication. Additionally, the computation time with the combined protocol is only marginally increased in comparison to that with the parallel protocol. Lastly, even compared with the pure EMT simulation of the detailed system, the computation time with the proposed hybrid simulation and the combined protocol is only moderately increased. However, more accurate simulation results of the detailed system and the external system can be achieved using the hybrid simulation approach.

It should be noted that the advantage of the combined protocol over the serial protocol would become less significant in cases where either the EMT or TS part of the hybrid simulation dominates the simulation in terms of computation time.

Table 1.5 Performances of the hybrid simulation with different protocols

Simulation method	Computation time /s
EMT-TS (parallel protocol)	371
EMT-TS (combined protocol)	387
EMT-TS (serial protocol)	692
EMT (the detailed system + a fixed equivalent of the external system)	264

1.5 Application of Hybrid Simulation To Power Systems Inter-Faced With HVDC Systems

1.5.1 Background

The power electronic converter and its control technology are the fundamental building blocks for model power electronic devices. Two prevailing converter technologies are the LCC and VSC. The LCC technology is mainly used in the classical HVDC transmission, where the thyristor valve is used. VSC is regarded as a new generation converter technology, and it has been increasingly adopted in VSC-HVDC transmission systems and advanced FACTS devices.

The proposed hybrid simulation mainly addresses the issues of 3-phase modeling, phase imbalance and detailed A/C motor modeling and simulation in Section 1.4. In this section, the hybrid simulation will be utilized to solve the problem related to modeling power electronic converter based devices in power system dynamic simulations, as discussed before. In the following two sections, the proposed hybrid simulation will be applied to two different study cases: (a) a power system with a classical LCC-HVDC infeed and (b) a power system embedded with a VSC-HVDC. The hybrid simulation is conducted using the combined interaction protocol introduced in Chapter 3, by default, unless otherwise specified. Through these tests, the applicability of the hybrid simulation tool will be comprehensively evaluated for the two mainstream converter technologies.

1.5.2 Application to Power Systems Interfaced with a Classic HVDC System

In this section, the developed hybrid simulation platform is tested on the IEEE 39 bus system [26] with a classical LCC-HVDC link connected to bus 39, as shown in Fig. 1.35. The HVDC link is based on the CIGRE HVDC benchmark model [27], rated at 230 kV, 1000 MW, and shown in Fig. 1.36. In the hybrid simulation mode, the HVDC link is modeled in PSCAD, with bus 39 as the boundary bus, while the remainder of the test system is simulated by the TS simulation. For benchmarking purpose, the whole test system is also modeled in PSCAD. The time step of the EMT simulation is 50 μs and the time step of the TS simulation is 5 ms.

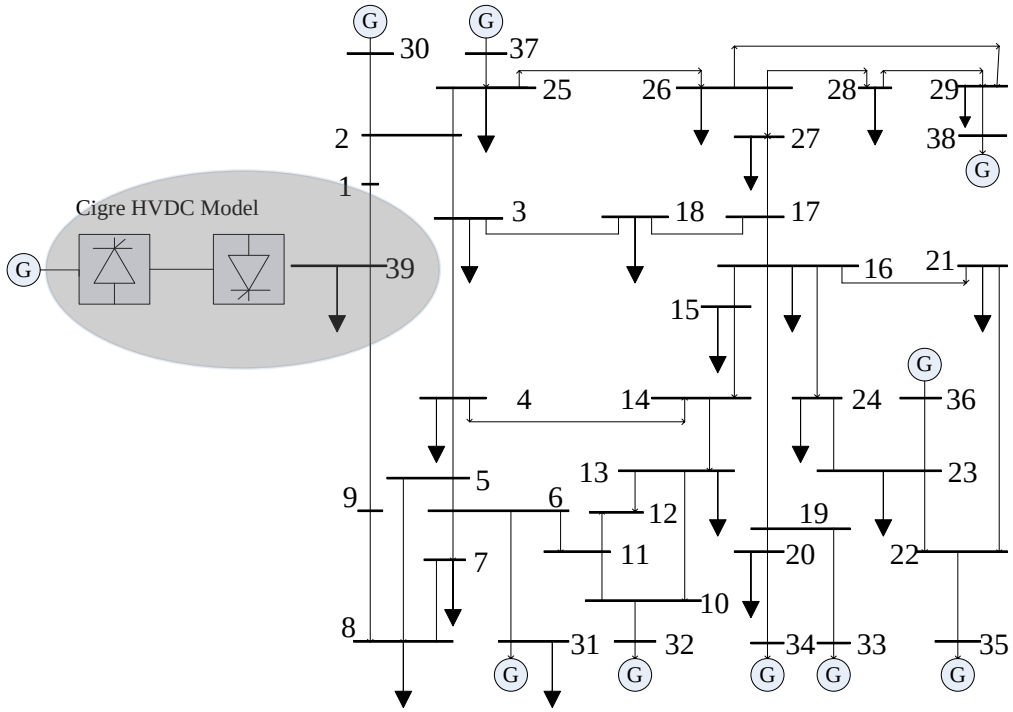

Fig. 1.8 A modified IEEE 39 bus system with an HVDC link connected to bus 39

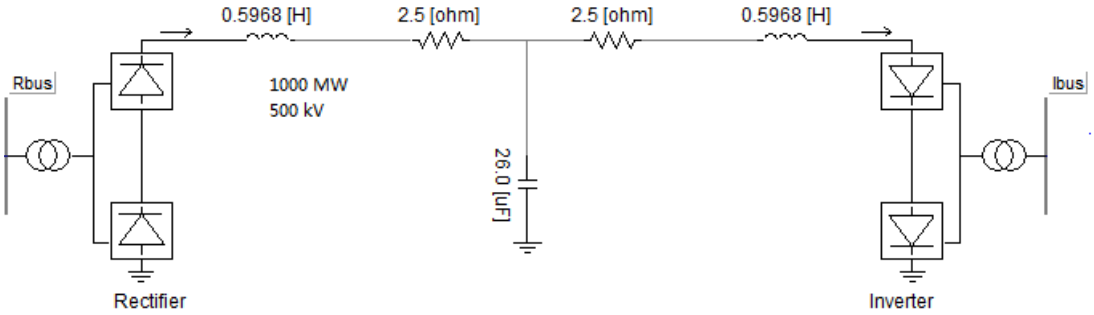

Fig. 1.9 The CIGRE HVDC benchmark model

The performance of the LCC-HVDC system is significantly influenced by the strength of the system at the point of interconnection. It is recommended that the short circuit ratio (SCR) should be at least 3.0 so that the HVDC system can achieve acceptable performance when subjected to severe disturbances [28]. In this test case, the SCR is 2.2. This means the connection point is weak for this HVDC infeed, which requires robustness of the hybrid simulation tool to handle such an unfavorable study case.

In this test case, a three-phase to ground fault is applied at bus 39, which is also the inverter AC bus, at 3.0 s and cleared in 4 cycles (0.0667 s). The benchmarking results are shown in Fig. 1.37 to Fig. 1.39. The results by both simulators overall are well matched, with a small discrepancy for a short period after the fault is cleared. The high frequency dynamics of the HVDC system over a short period after the fault is cleared is highlighted in Fig. 1.39(a). The results indicate that the hybrid simulation can adequately capture the high frequency behaviors of the HVDC model. It is

shown in Fig. 1.39 that the dc voltage becomes negative during the period between 3.01 s and 3.03 s, which will be prevented in actual HVDC systems by the converter controls and/or protections. The main reason is that control scheme and settings in the model are not sophisticatedly optimized [27]. Actually, a similar result was also observed with the CIGRE HVDC test system and documented in [27]. Considering that the main objective of this comparison study to verify the accuracy of the developed tool, rather than the performance of the HVDC system, this HVDC model is acceptable for this study.

The response of the external system is illustrated by the power of the generator at bus 30 shown in Fig. 1.40 and the positive sequence voltages at bus 1 and bus 9 shown in Fig. 1.41. The main discrepancy corresponds to the power oscillation during the fault period, which is mainly due to the difference in the modeling approaches between the two software packages. The other discrepancy corresponds to the oscillations observed in the real and reactive power output after the fault is cleared. The oscillation is of fundamental frequency, as shown in Fig. 1.42. It is found that the DC component in the stator current introduced by the fault clearing contributes to the oscillation. The DC component in the stator current is reflected as a fundamental frequency component in rotor, which results in fundamental frequency oscillation in the generator power output.

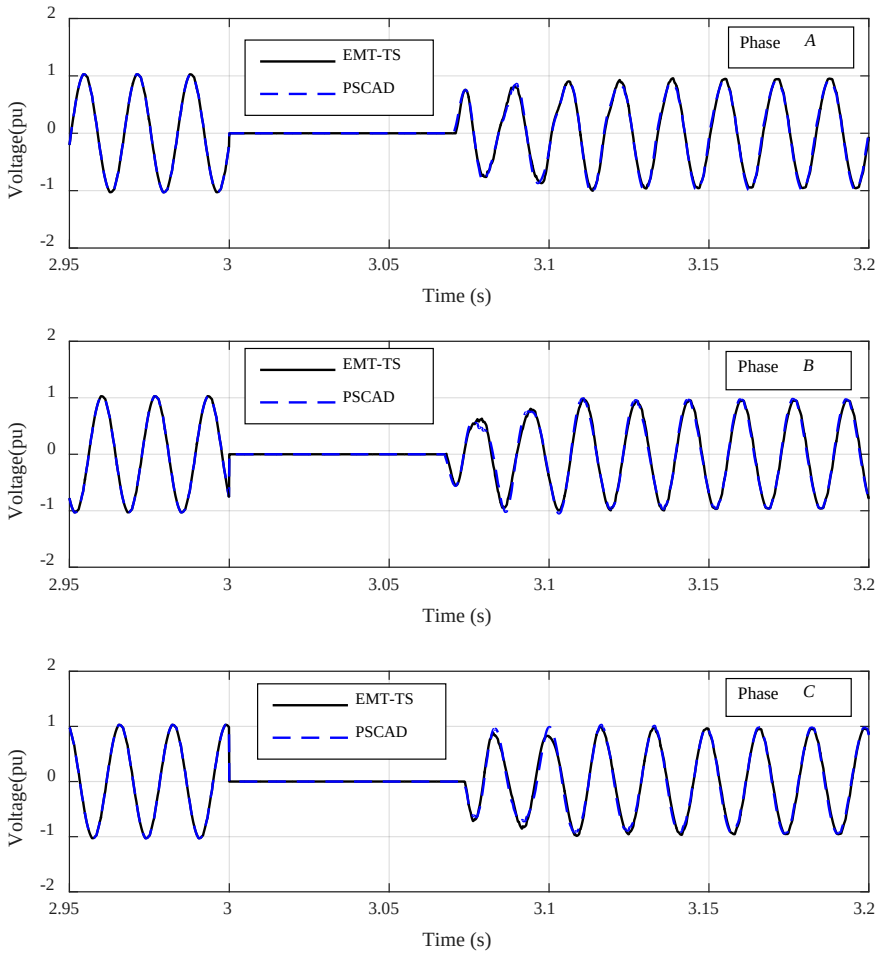

Fig. 1.10 Three-phase voltages of bus 39 (HVDC inverter AC bus)

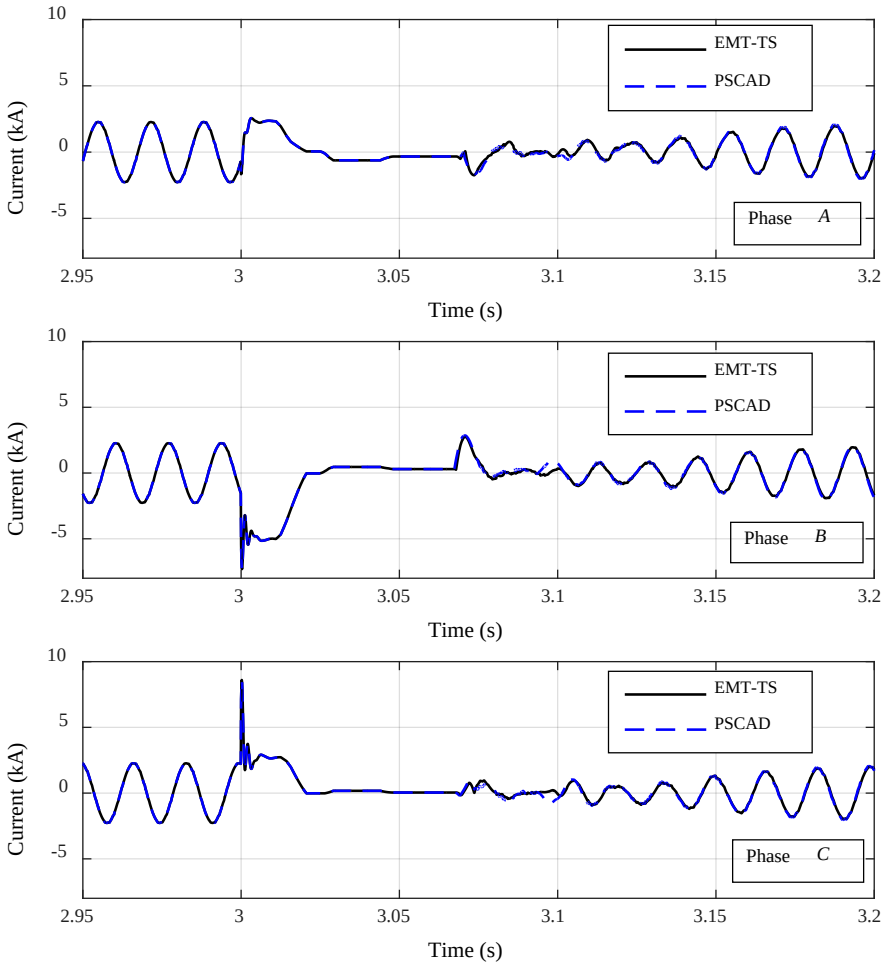

Fig. 1.11 Three-phase current injection into the bus 39 from the HVDC inverter

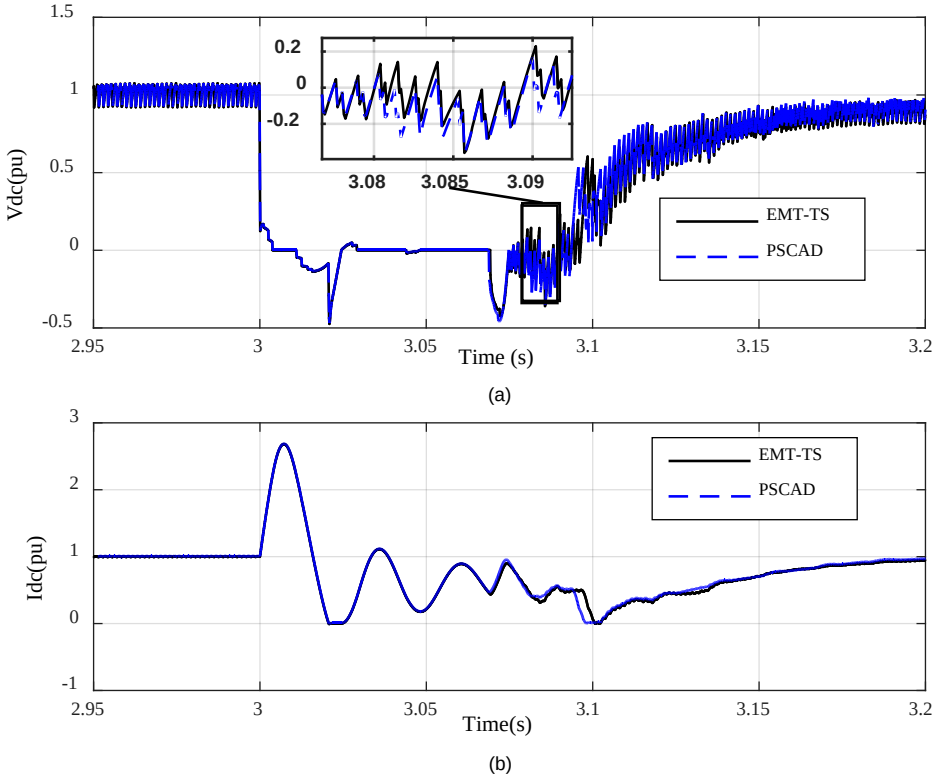

Fig. 1.12 DC voltage and current of the HVDC inverter: (a) DC voltage, (b) DC current

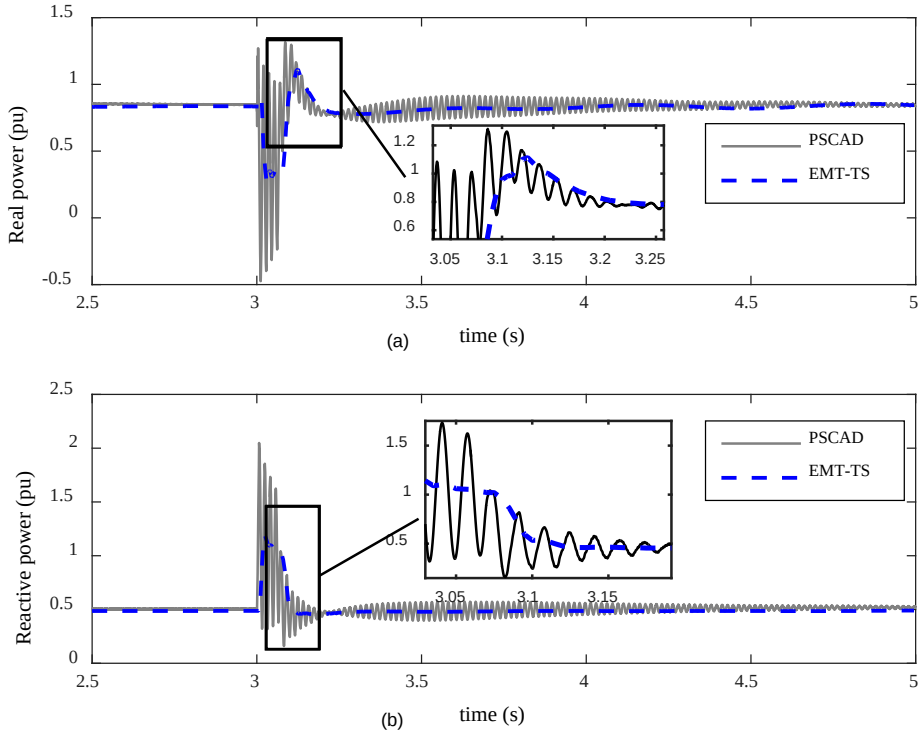

Fig. 1.13 Real and reactive power of the generator at bus 30

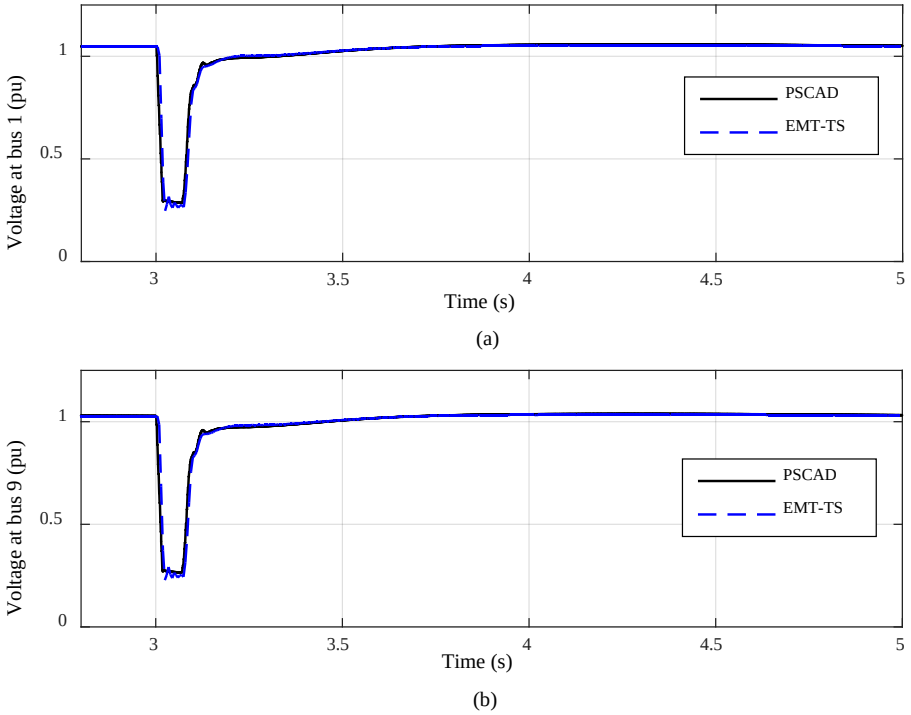

Fig. 1.14 Positive sequence bus voltages of the external system: (a) bus 1; (b) bus 9

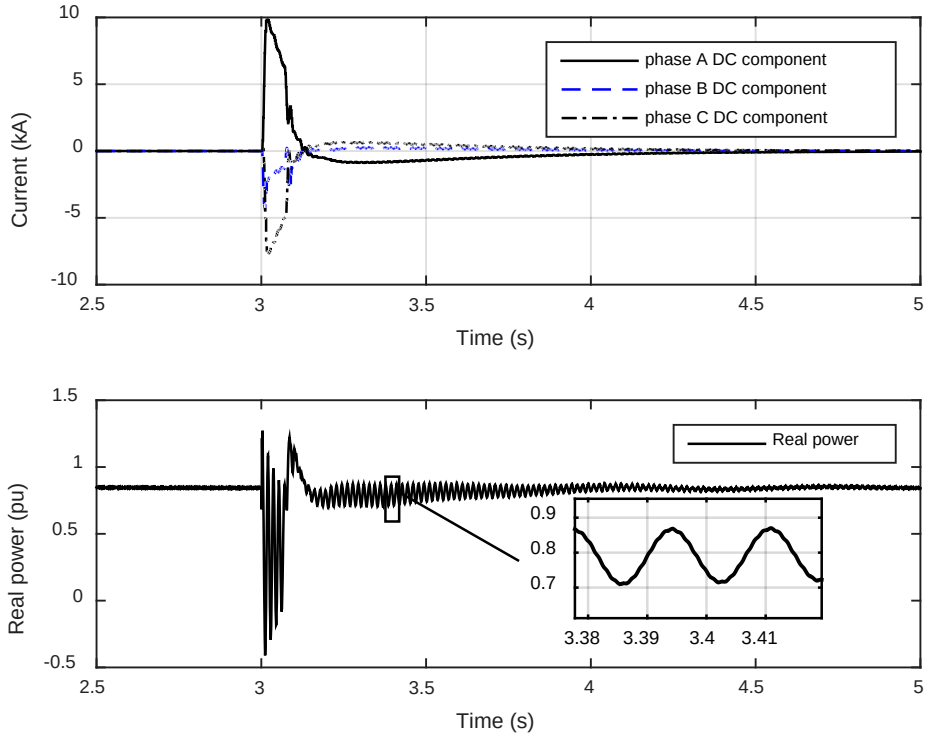

Fig. 1.15 The DC components of three-phase current injection and the real power of the generator at bus 30

In the hybrid simulation, bus 30 is represented in the external system, where the DC component of the generator stator current cannot be represented by the phasor modeling approach. Thus, the oscillation cannot be captured by hybrid simulation mode.

Except for these two discrepancies, the overall impacts of the fault on the external system are adequately captured by the hybrid simulation approach. Considering the low SCR and the severity of the fault in this test case, the robustness of the developed hybrid simulation tool is also verified.

1.5.3 Application to Power Systems Embedded with a VSC-HVDC System

There are two converter technologies for VSC-HVDC systems, i.e., high frequency pulse width modulation (PWM) control two-level or three-level type, and a more recent modular multilevel converter (MMC) type [29]. This research focuses on the PWM control two-level VSC-HVDC systems, as most of the commissioned VSC-HVDC projects use this type. The high switching frequency (in the range of 1000-2000 Hz) of the VSC-HVDC system poses a challenge to hybrid simulation, because a very small simulation time step has to be used in EMT simulation, and the resulting simulation time step ratio between EMT and TS become very large.

This test case is based on the IEEE 39 bus system, with a VSC-HVDC system added to connect the buses 8 and 29, as is shown in Fig. 1.43. The VSC-HVDC system is shown in Fig. 1.44. The constant active and reactive power controls are used in the rectifier, and a DC voltage control and an AC voltage control are employed in the inverter. The rated active power is 280 MW and the dc voltage is 400 kV.

The EMT simulation time step should be approximately one hundredth of the PWM carrier period to ensure good simulation precision. Hence, the EMT simulation time step is chosen as 5 μs, since the PWM carrier frequency of this VSC-HVDC system is 1980 Hz. The TS simulation time step is 5 ms.

The region encircled by the dashed line in Fig. 1.43 is the detailed system and modeled in PSCAD, with the rest of the AC system represented in three-sequence and simulated by the OpenHybridSim tool.

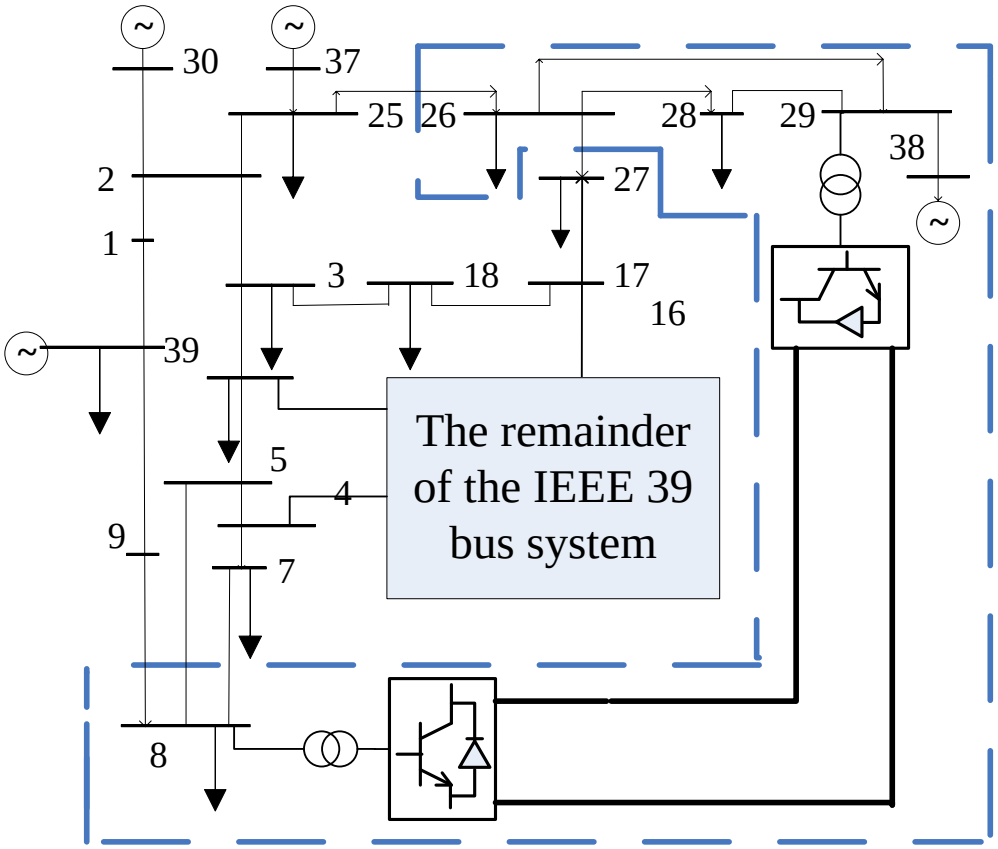

Fig. 1.16 IEEE 39 bus system interfaced with a VSC-HVDC connecting buses 8 and 29

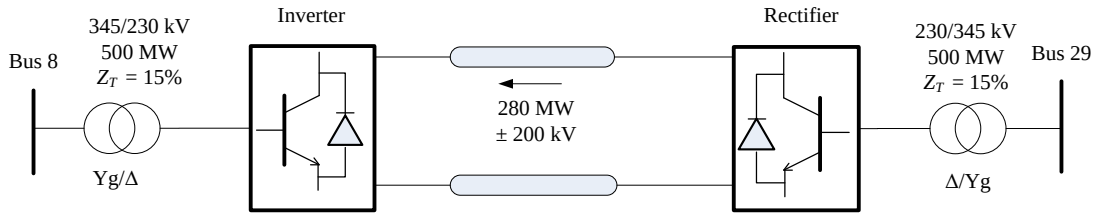

Fig. 1.17 A two-terminal VSC-HVDC system

A three-phase to ground fault is applied on bus 28 (one bus away from both the inverter AC bus and the boundary bus) at 1.0 s and it is cleared in 0.05 s (3 cycles). The responses of the VSC-HVDC system to the fault, including DC and AC voltages and currents of the VSC-HVDC system and power output of the generator at bus 38 are presented in Fig. 1.45 to Fig. 1.50. The simulation result differences with reference to the EMT simulation are summarized in Table 1.6.

First, the results show that the hybrid simulation results are close to the reference simulation results obtained by PSCAD. The average differences of some key parameters monitored are less than 0.05 pu, as shown in Table 1.6.

Second, the main discrepancies appear in the first 6 cycles after the fault is cleared. In addition, the discrepancies are generally more apparent in the variables of the VSC-HVDC system, e.g., the DC voltage V_{dc} and current I_{dc}, than those of the AC system. One factor contributing to the discrepancies is the harmonics and their impacts on the HVDC controls. The harmonics in the voltage and current at the inverter AC terminal are apparent during the fault period, as shown in the EMT simulation results in Fig. 1.45. However, high frequency characteristics of the external system are not adequately preserved in the equivalent used by the EMT-TS hybrid simulation. It is also observed that these discrepancies last for a very short period, thus they do not have a significant impact on the overall dynamics of the system. The simulation results obtained by the hybrid simulation and PSCAD simulation tend to "converge" again after 1.2 s.

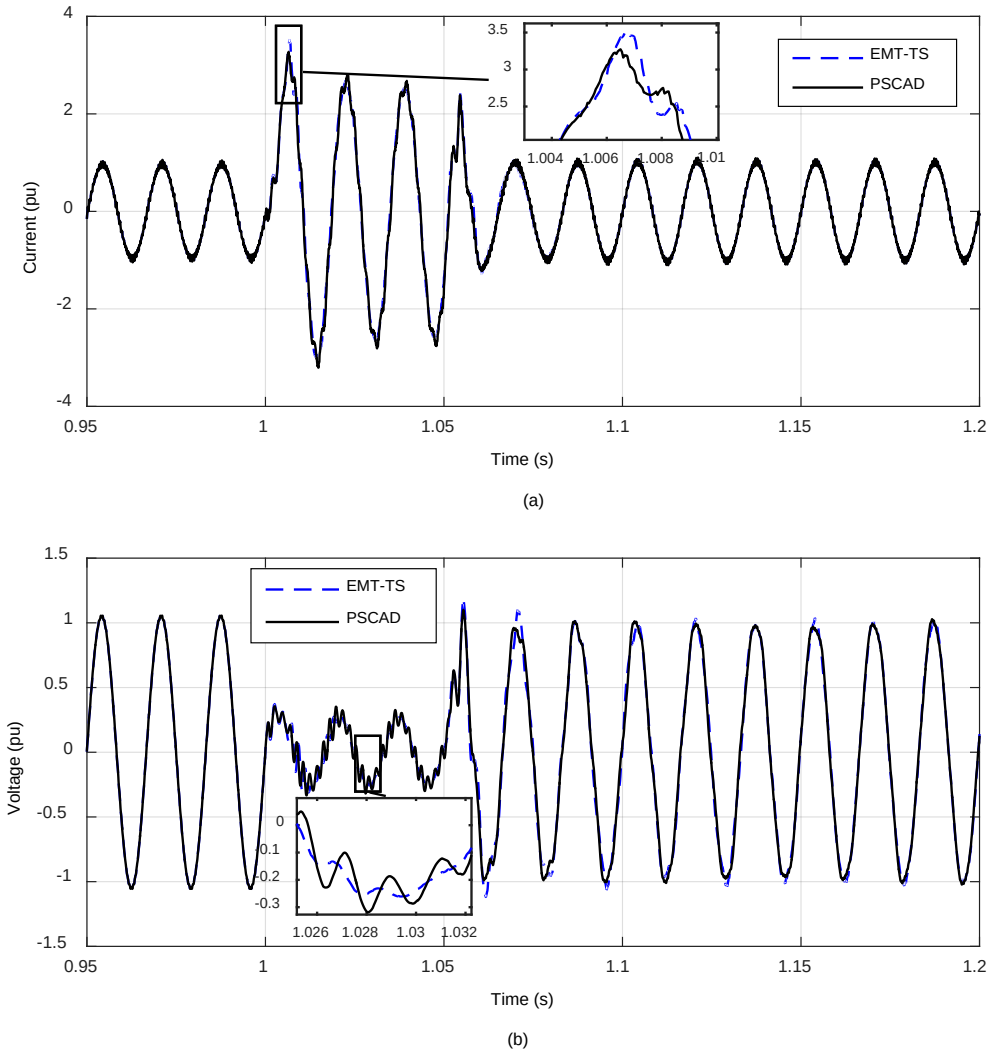

Fig. 1.18 (a) Phase A current flowing into the VSC-HVDC system at bus 29 and (b) phase A voltage of bus 29

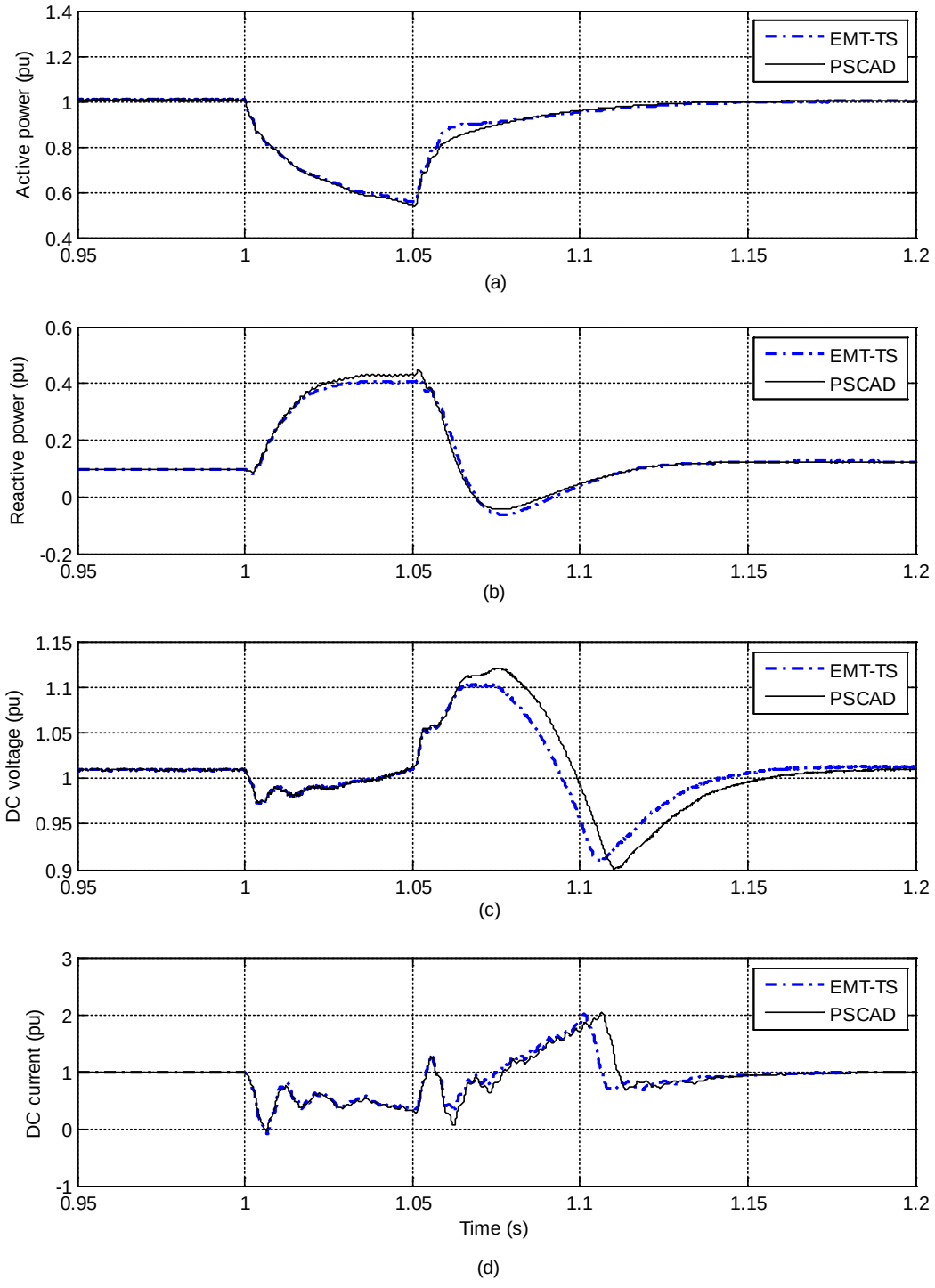

Fig. 1.19 Monitoring variables of VSC-HVDC rectifier: (a) real power, pu on VSC-HVDC system base; (b) reactive power flowing into the rectifier, pu on VSC-HVDC system base; (c) DC voltage; (d) DC current

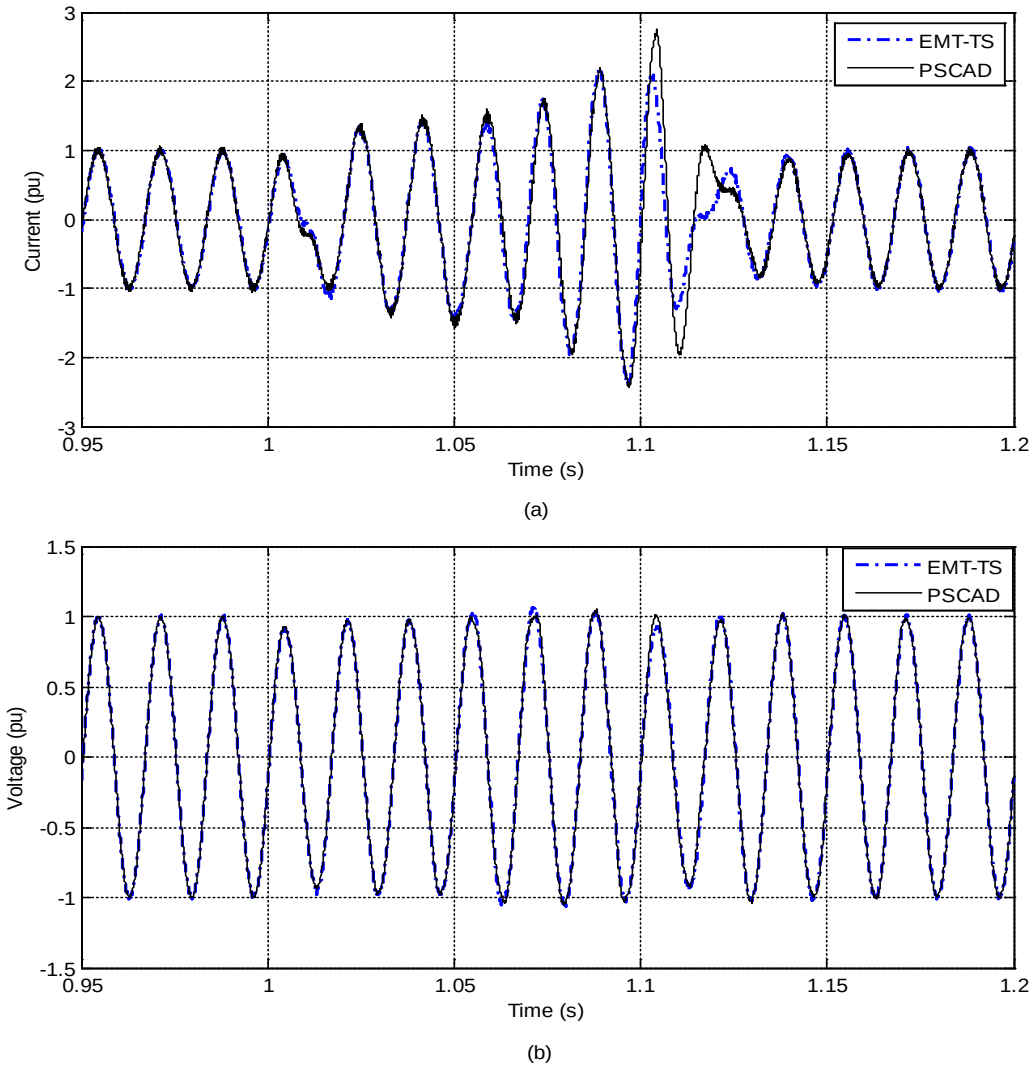

Fig. 1.20 (a) Phase A current from the VSC-HVDC inverter into bus 8 and (b) phase A voltage of bus 8

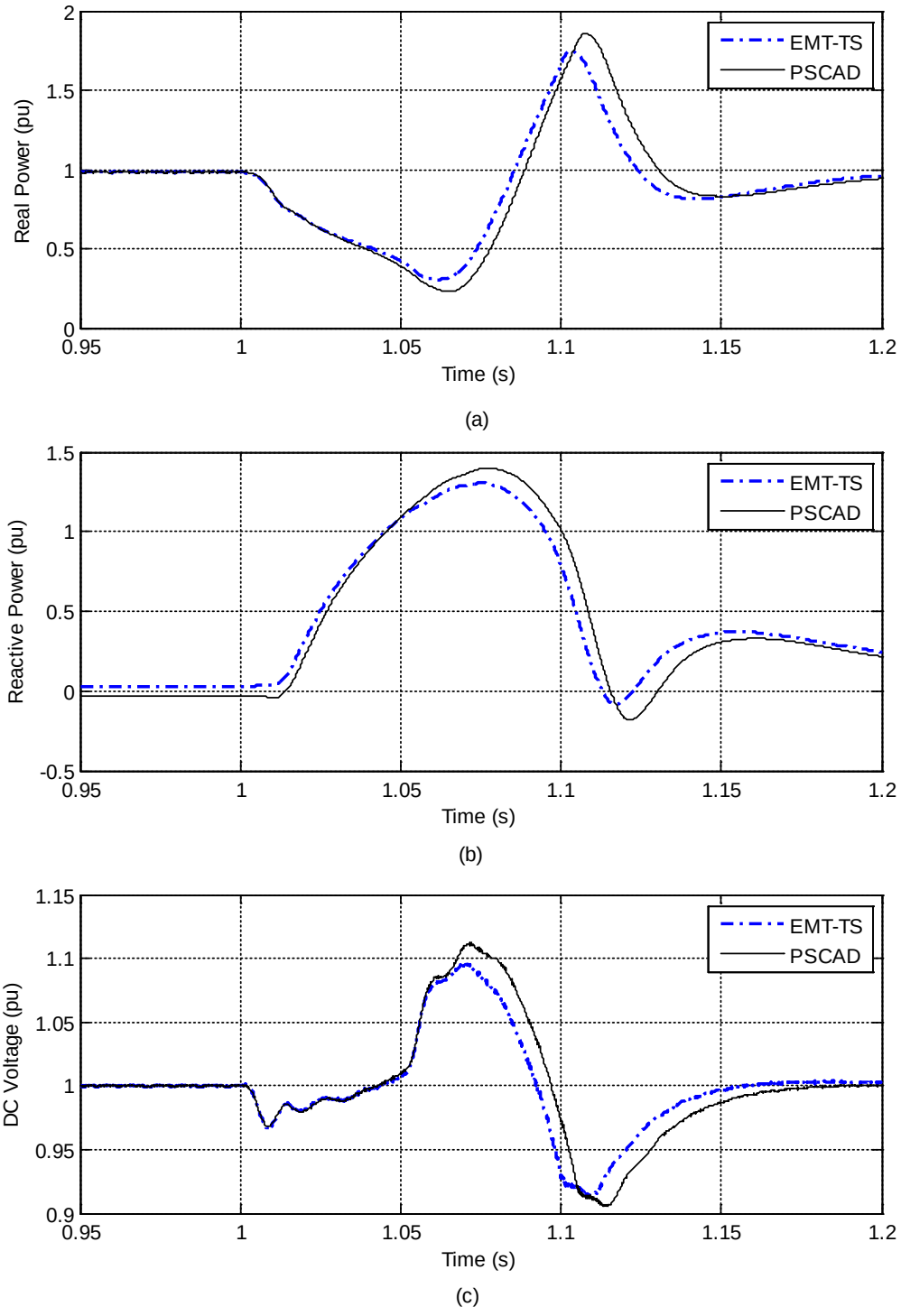

Fig. 1.21 Monitoring variables of VSC-HVDC inverter: (a) real power, pu on VSC-HVDC system base; (b) reactive power flowing into the rectifier, pu on VSC-HVDC system base; (c) DC voltage

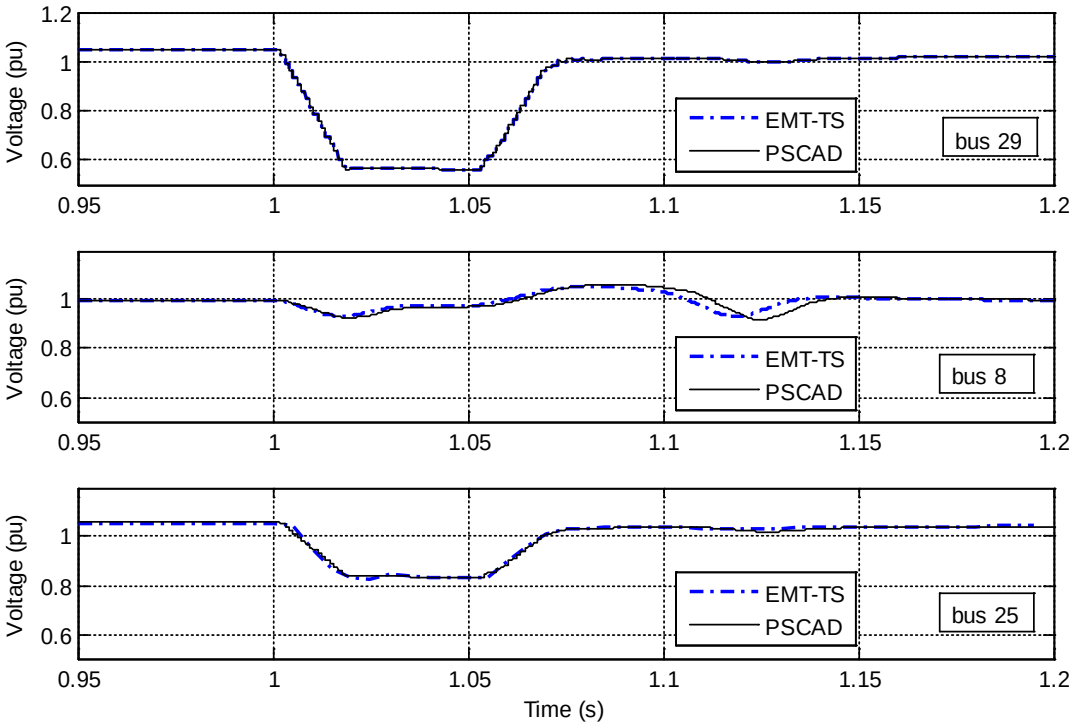

Fig. 1.22 Positive sequence voltage magnitudes of buses 29, 8 and 25

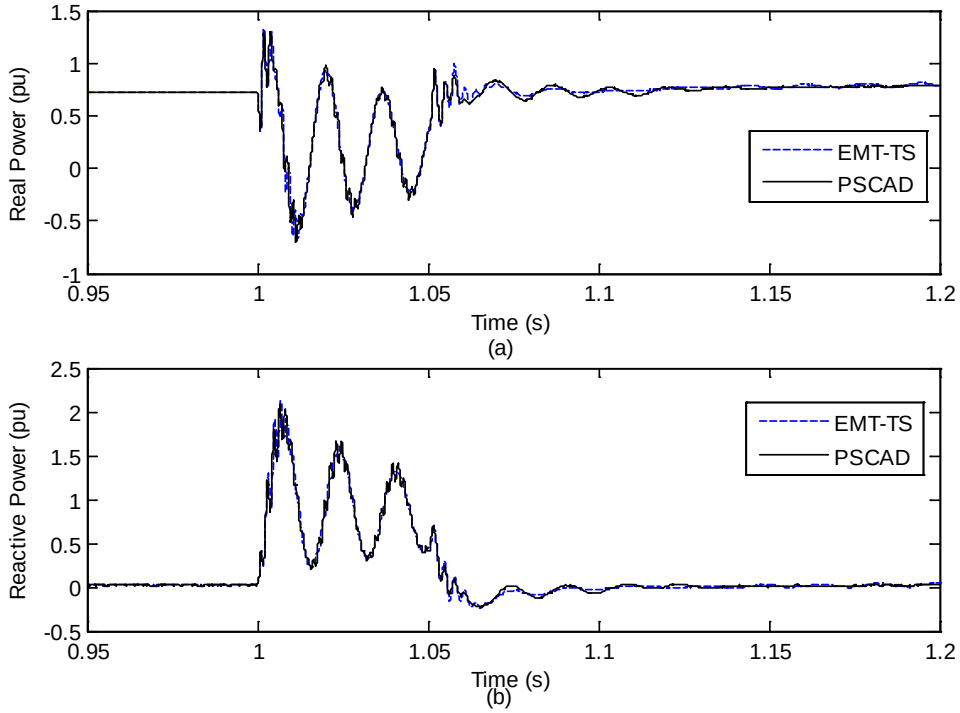

Fig. 1.23 Active and reactive power generation of the generator at bus 38

Table 1.6 The simulation result differences for the case of IEEE 39 bus system interfaced with a VSC-HVDC system (three-phase fault at bus 28)

	Average difference /pu	Maximum difference /pu
I_{dc} of Rectifier	0.046	1.075
V_{dc} of Rectifier	0.007	0.042
I_{abc} of Rectifier	0.029	0.412
V_{abc} of bus 29	0.030	0.203

With the simulation time step of EMT as 5 μs, and that of TS as 5 ms, the total simulation times of running the test system for a period of 2.0 s using PSCAD and the developed hybrid simulation tool, respectively, are summarized in Table 1.7. It shows that, for this study case, the performance of the developed EMT-TS hybrid simulation tool is approximately 7 times faster than the EMT simulation with PSCAD.

Table 1.7 Simulation performance comparison between hybrid simulation and EMT simulation for the case of IEEE 39 bus system embedded with a VSC-HVDC system

Simulation method	Time consumption (s)
EMT (with PSCAD)	1152
Hybrid simulation	164

1.6 Integrated Transmission and Distribution System Modeling and Simulation

Distribution systems increasingly influence the behavior of bulk power systems, as a result of nonlinear characteristics of the loads and distributed generation resources. The interactions between distribution and transmission systems have also increased. However, in traditional power system simulation tools, transmission and distribution systems are separately modeled and analyzed. Hence, it is difficult to analyze the impacts of distribution systems on transmission systems in detail and vice versa [30]-[34]. Admittedly, the hybrid simulation approach can be applied to analyze integrated transmission and distribution (T&D) systems, with the distribution systems being simulated by the EMT simulator. However, the hybrid simulation approach is not well suited for the cases with tens to hundreds of complex distribution systems interfaced with the transmission system.

A phasor modeling based integrated simulation approach is proposed to address the demand. An integrated modeling framework is first developed in this section, where the transmission system is modeled as one subsystem in three-sequence detail, while each distribution system is represented as a subsystem and modeled in three-phase detail. The integrated T&D power flow (TDPF) is solved by iteratively solving a three-sequence power flow for the transmission system and a three-phase power flow for each distribution system. For the integrated T&D dynamic simulation (TDDS), the main challenge is associated with different network representations in the transmission and the distribution systems. With the partitioned solution approach adopted in the

TDDS algorithm, the multi-area Thévenin equivalent (MATE) approach is utilized in the network solution step to address this challenge.

1.6.1 Integrated Transmission and Distribution System Modeling

In deciding an appropriate modeling approach for integrated transmission and distribution systems, the following two important factors have to be considered: (1) the physical features of transmission and distribution systems; (2) the common modeling assumptions that could be made for both power flow and dynamic simulation.

Firstly, distribution systems generally should be modeled in three-phase detail for both power flow and dynamic simulation, as distribution systems are inherently unbalanced. Secondly, the conditions at the boundary between the transmission and distribution systems are influenced by the unbalanced conditions of the distribution systems and the fault(s) considered in dynamic simulation. Therefore, although transmission systems can be assumed to be physically three-phase balanced, the typical assumption that the boundary conditions at the interfaces between transmission and distribution systems are reasonably balanced is not always valid, particularly in dynamic simulation. In this context, the transmission system should be represented in either three-sequence or three-phase detail. To avoid the modeling and computational complexity involved in three-phase representation and to effectively reuse the existing sequence component-based models and simulation algorithms, the transmission system is modeled in three-sequence in this research.

1.6.2 Power Flow Algorithm for Integrated Transmission and Distribution System

The proposed TDPF algorithm is formulated based on a master-slave approach [30], with the power flow of the transmission system as the master problem and the power flow of the distribution systems as the slave problem. The main differences from [30] include: 1) modeling the transmission system in three-sequence instead of positive sequence; 2) a three-sequence power flow algorithm is developed for the transmission system; 3) appropriate three-sequence representations of the distribution systems in the power flow formulation of the transmission system.

The boundary information exchanged between the transmission and the distribution systems during the integrated power flow solving process is illustrated in Fig. 1.51. At each iteration between the transmission and the distribution systems, the transmission system provides the three-phase voltages at the boundary buses, denoted by V_{Bi}^{abc}, to the corresponding distribution systems to update their boundary (source) bus voltages. Similarly, the results from the distribution systems are transformed to three sequence equivalents. The positive sequence component is represented by a constant power load $LoadPQ_i^{(1)}$ as in a conventional balance power flow. The negative- and zero-sequence components are represented by negative sequence current injection $Iinj_i^{(2)}$ and zero sequence current injection $Iinj_i^{(0)}$, respectively at the appropriate boundary buses.

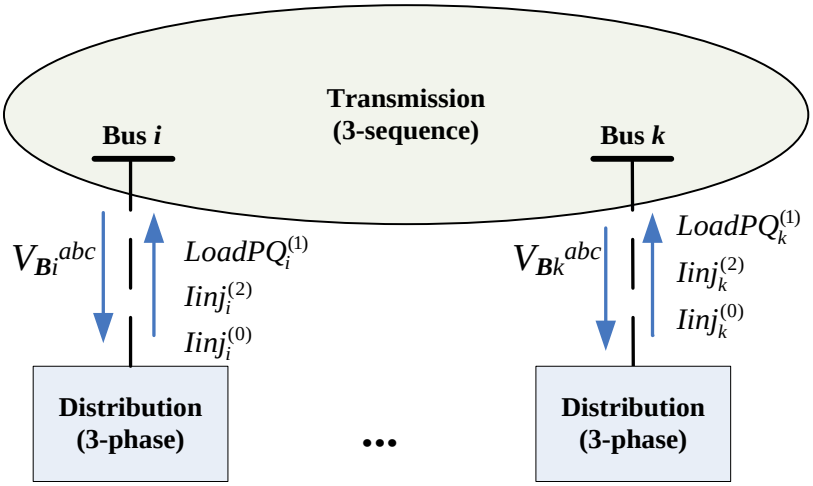

Fig. 1.24 Boundary data exchange between the transmission and the distribution systems in the integrated power flow

In the transmission system part, the three sequence networks are decoupled and solved independently. The positive sequence network is solved using existing positive sequence power flow algorithms. The negative- and zero-sequence networks are represented by (1.4) and (1.5).

$$\boldsymbol{I}^{(2)} = \boldsymbol{Y}^{(2)}\boldsymbol{V}^{(2)} \tag{1.4}$$

$$\boldsymbol{I}^{(0)} = \boldsymbol{Y}^{(0)}\boldsymbol{V}^{(0)} \tag{1.5}$$

Superscripts 2 and 0 denote negative- and zero- sequence components, respectively. The negative- and zero- sequence bus current injections in $\boldsymbol{I}^{(2)}$ and $\boldsymbol{I}^{(0)}$are zero except for the boundary buses when they are interfaced with unbalanced distribution systems. $\boldsymbol{V}^{(*)}$ is the sequence bus voltage vector**;** $\boldsymbol{Y}^{(*)}$ is the sequence admittance matrix of the network.

A sequence network solver for solving (1.4) and (1.5) has been developed based on the short circuit program in InterPSS. The sequence admittance matrices are fixed unless there is a network change. They are factorized at the initialization stage, and (1.4) and (1.5) are solved only once for each transmission system power flow. Thus, the computational burden due to the solution of (1.4) and (1.5) is marginal.

For the distribution systems, a three-phase power flow based on the backward/forward sweep (BFS) algorithm [25] has been developed. The flowchart of the integrated power flow algorithm is shown in Fig. 1.52.

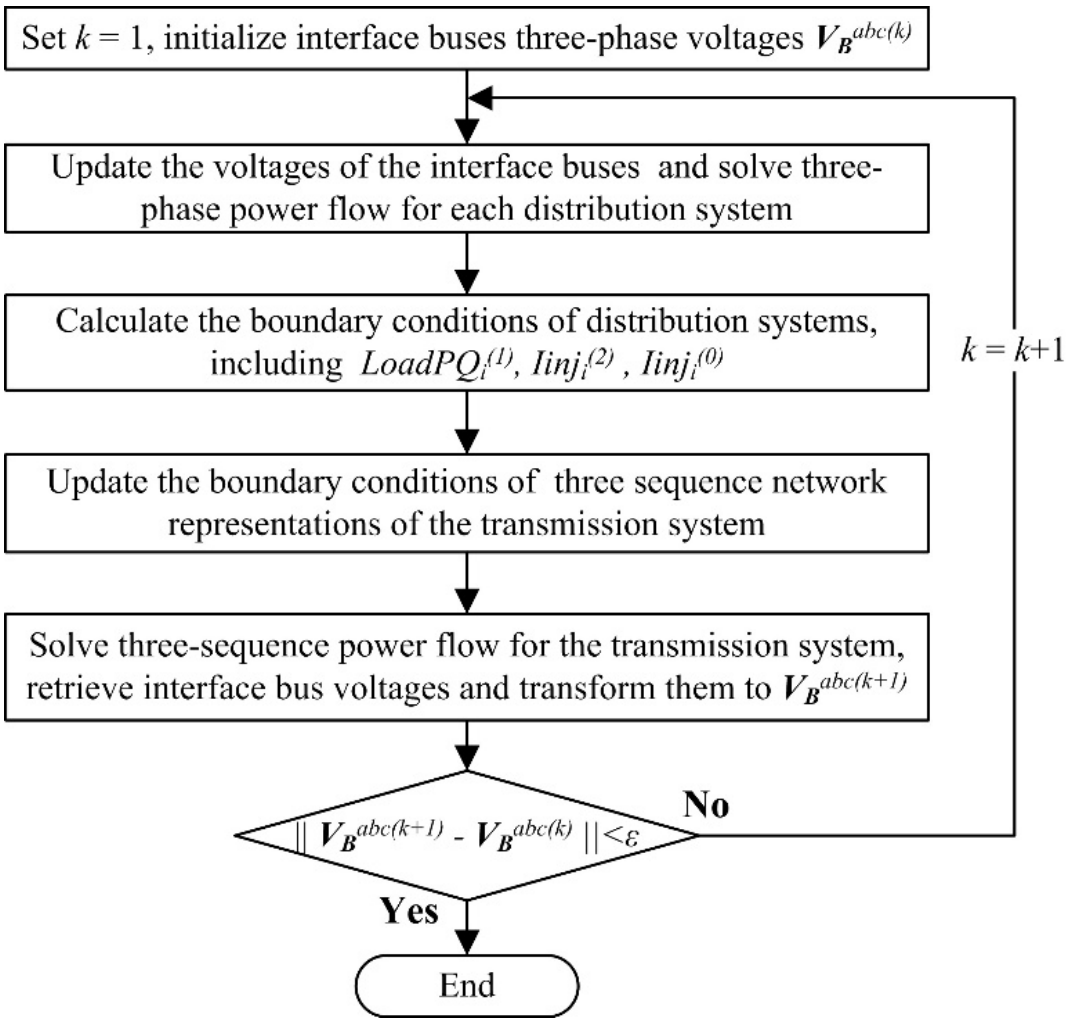

Fig. 1.25 The flowchart of the integrated T&D power flow

1.6.3 Dynamic Simulation for Integrated Transmission and Distribution System

1.6.3.1 Formulation and Solution of Dynamic Simulation

The dynamic simulation of power systems can be mathematically described as a solution to a set of differential-algebraic equations (DAEs) as follows [35]-[36]:

$$\dot{\boldsymbol{x}} = \boldsymbol{f}(\boldsymbol{x}, \boldsymbol{V}) \tag{1.6}$$

$$\boldsymbol{I}(\boldsymbol{x}, \boldsymbol{V}) = \boldsymbol{YV} \tag{1.7}$$

with a set of known initial conditions ($\boldsymbol{x_0}, \boldsymbol{V_0}$), where $\boldsymbol{x}$ is a vector of the state variables**;** $\boldsymbol{V}$ is the bus voltage vector**;** $\boldsymbol{I}$ is the bus current injection vector; $\boldsymbol{Y}$ is the nodal admittance matrix of the network. Conventionally $\boldsymbol{V}$, $\boldsymbol{I}$ and $\boldsymbol{Y}$ represent the positive sequence only. In the following sections, they will be extended to three-sequence and three-phase reference frameworks.

Based on the way in which (1.6) and (1.7) are interfaced with each other, there are basically two solution approaches for the above DAEs, i.e., a simultaneous approach and a partitioned approach [35]. In the simultaneous solution approach, (1.6) is first converted to a set of algebraic equations, which are lumped with (1.7) to form a single larger algebraic equation set. It is complicated to formulate the equation sets with different network representations for the transmission and the distribution systems. On the other hand, with the partitioned solution approach, the differential equation set (1.6) and the algebraic set (1.7) are solved separately**.** The corresponding solution processes are generally referred to as the integration step and the network solution step, respectively. Such a decoupling feature allows the integration method and the network solution method to be chosen independently and facilities the solution of integrated transmission and distribution systems.

Based on the discussions above, the partitioned solution approach is adopted for integrated transmission and distribution dynamic simulation. For the integration step, dynamic models basically require some local measurements (for example, bus voltage and frequency at the terminal or an associated remote control bus) to perform the integration. Furthermore, the transmission and the distribution systems are represented as individual subsystems based on the proposed modeling framework. Thus, appropriate integration algorithms can be reused or developed for the transmission and the distribution systems independently. Compared to existing dynamic simulation algorithms for bulk power systems [35]-[36], no special change is required in the integration step for the integrated transmission and distribution systems.

On the other hand, almost all the existing simulation programs require the same representation (either single-phase or three-phase) for the whole system to build the network admittance matrix for solving network solution. Considering the different representations in the proposed modeling approach, the single-network oriented network solution approach cannot be directly applied to the integrated transmission and distribution systems. Therefore, a special network solution approach, which is capable of accommodating multiple subsystems and distinct network representation of each subsystem, is needed at the network solution step. In this following section, a diakoptics [37] based network solution approach will be utilized to address this issue.

1.6.3.2 Diakoptics and Multi-area Thévenin Equivalent

One important benefit of the concept of diakoptics is that the individuality of the resulting subsystems is maintained, which allows these subsystems to be modeled and simulated distinctly. The original diakoptics based solution proposed by Happ [37], which was based on the concept of “open and closed path contours”, was difficult to visualize and formulate in a clear and straightforward manner [38]-[39]. In addition, the solution cannot be directly applied to the cases where the subsystems are not modeled at the same level of detail. The multi-area Thévenin equivalent (MATE) concept [38]-[39] reformulates and extends the diakoptics approach to make it easier to understand and program into an algorithm.

A detailed derivation and formulation of the MATE based algorithm can be found in the Appendix-B. The MATE approach based network solution for a system consisting of multiple subsystems includes four steps, as illustrated in Fig. 1.53:

1. Solve each subsystem network without current injections from the link branch(es) to obtain the bus voltages $\boldsymbol{V_{int,i}}$.

2. Retrieve boundary bus voltages from $\boldsymbol{V_{int,i}}$ and build the subsystem network Thévenin equivalents, as illustrated in the dashed rectangular part in Fig. 1.53(c)

3. Build the link subsystem by connecting the Thévenin equivalents with the link branches, and then solve it to obtain the currents of the link branches, as shown in Fig. 1.53(c)

4. Solve each subsystem network again considering only the link branch current injection(s) to obtain the solution $\boldsymbol{V_{ext,i}}$, as shown in Fig. 1.53(d). Based on the superposition theorem, the final bus voltages are obtained by

   $$\boldsymbol{V_{sub,i} = V_{int,i} + V_{ext,i}}.$$

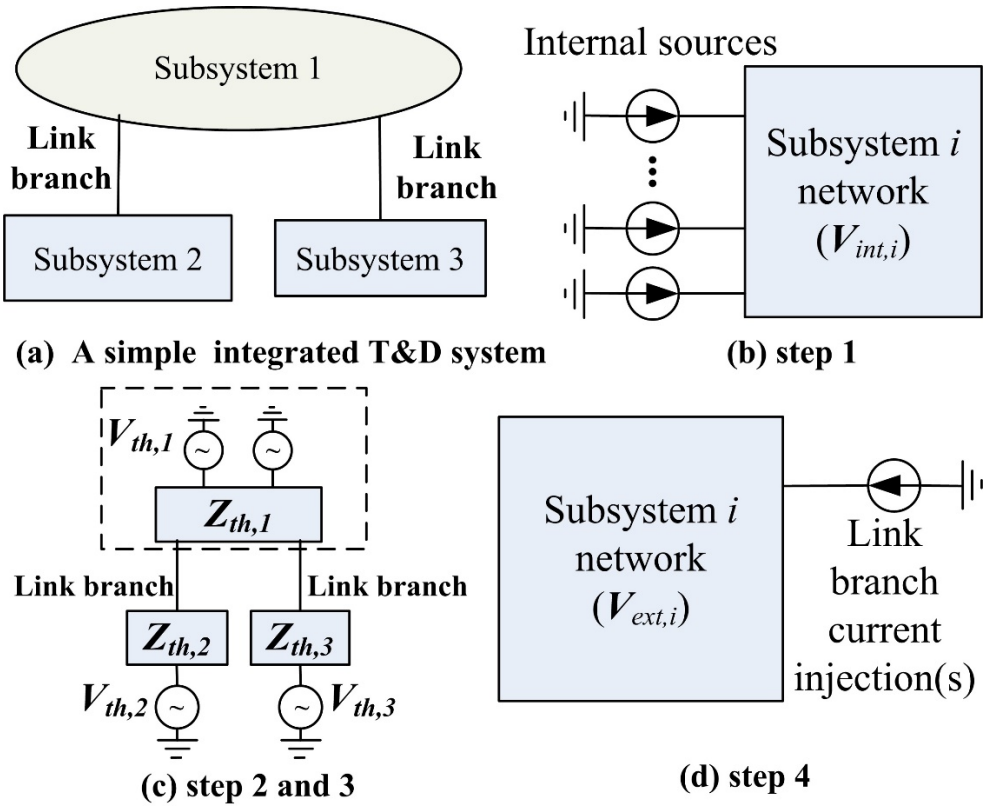

Fig. 1.26 A schematic illustration of the MATE approach

The MATE approach can be used to reconcile the individual solutions of subsystems into a full-system simultaneous solution at the network solution stage. When nonlinear models exist in the system, iterations of the solution process above are required. For integrated T&D systems, this

reconciliation process is illustrated in Fig. 1.54. The transmission system and the distribution systems can be first solved independently with their own representations and solution techniques. Then the interactions among them can be reconciled at the level of the link branches by sharing their Thévenin equivalents and solving the resulting link subsystem. Considering different representations, a reference coordinate system and necessary coordinate transformations are required at the coordination stage, which will be discussed in more detail in Section 1.6.3.4.

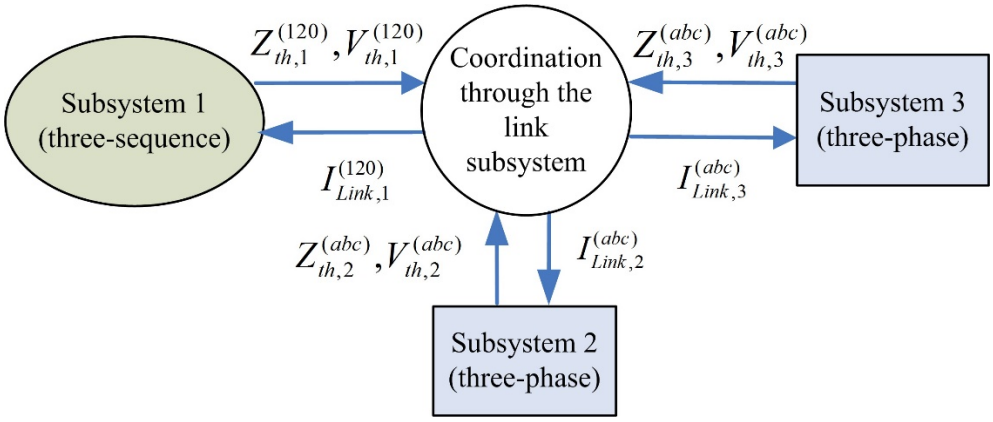

Fig. 1.27 Coordination of the subsystem simulation solutions through the link subsystem using the MATE approach

1.6.3.3 Development of Three-Phase Dynamic Simulation Algorithm

The three-sequence transient stability simulation algorithm developed in Section 1.3 can be used to simulate the transmission system. For the distribution systems, a three-phase dynamic simulation algorithm needs to be developed. The overall simulation procedure of three-phase dynamic simulation is similar to the existing positive sequence dynamic simulation. The main differences are associated with three-phase oriented network representation and dynamic modeling. One of the important objectives in this development process is that well-tested three-sequence based models are re-used and formidable re-programming efforts are avoided whenever possible. This objective is mainly achieved through applying the inheritance feature of object-oriented programming and the adapter design pattern [42] throughout the development.

(1) Modeling of three-phase components

The mapping relationship between three-sequence and three-phase modeling are shown in Fig. 1.55. Static components, such as transmission lines, transformers, static loads (impedances and admittances) can be directly transformed from three-sequence representations to three-phase representations. Existing three-sequence parameters can be used as input, and transformed to the corresponding three-phase values internally.

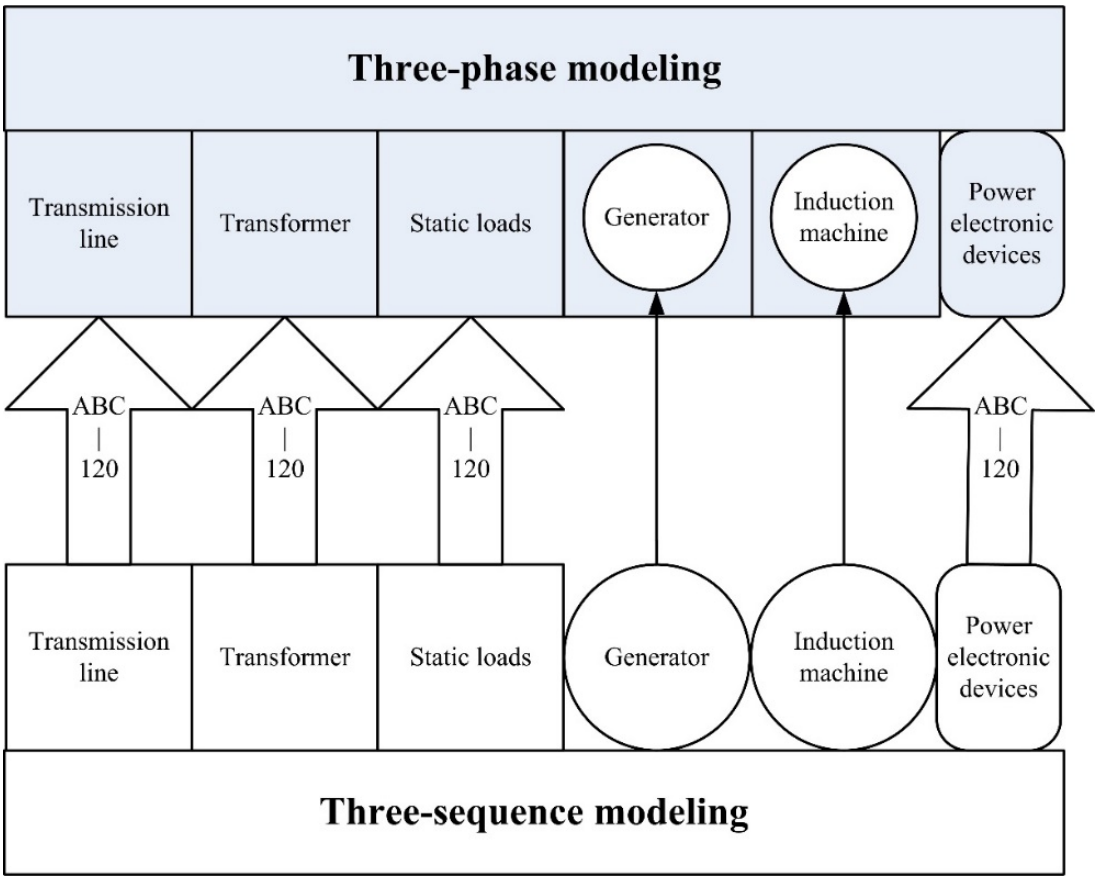

Fig. 1.28 Transformation from three-sequence modeling to three-phase modeling

For three-phase rotating machines, their structure and operation characteristics have been considered in developing their three-phase dynamic models. Firstly, their dynamics are mainly determined by the positive sequence components [36],[40],[41], due to the inherent symmetric structure of the rotating machines and the way they are connected to the system. Secondly, when interfaced with a three-phase network, they can be represented as a three-phase Norton equivalent as shown in Fig. 1.56. In addition, due to the internal symmetric structure of the machines, the internal three-phase current injection I_{gen}^{abc} shown in Fig. 1.56 is always balanced, and corresponds to the current injection in the positive sequence based model. I_{gen}^{abc} is dependent on the internal state variables and updated at each TS simulation time step, while the three-phase Norton admittance Y_{gen}^{abc} is transformed from the three-sequence machine admittances and kept constant during the simulation. With these features taken into account, the existing three-sequence based machine modeling of the three-phase rotating machines can be reused for three-phase TS simulation through the adapter design pattern, which is illustrated by the “wrapper” frame over the existing three-sequence based machine models in Fig. 1.56.

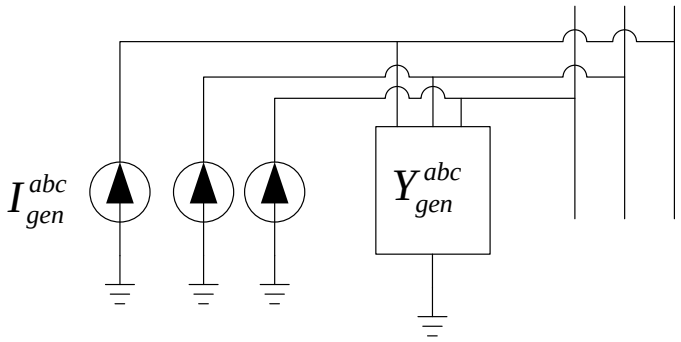

Fig. 1.29 A Norton equivalent model of the three-phase machine (both synchronous and induction machines) for three-phase TS simulation

The actual implementation of the three-phase machine model is illustrated in Fig. 1.57. The main function of the machine adapter is to invoke the functions of the existing positive sequence model to update the state variables through an integration step and then calculate the positive sequence current source, which is subsequently transformed to the three-phase current source I_{gen}^{abc} and used later in the three-phase oriented network solution.

(2) Modeling of single-phase components

Static single-phase components, such as single-phase secondary distribution feeder, impedances and admittances, can be modeled in a manner similar to the positive sequence modeling. In dynamic simulation, they are directly added to the network admittance matrix. As for single-phase dynamic components, such as single-phase residential air conditioners, a single-phase Norton equivalent model can be used to interface with the network. The equivalent current source should be updated at each step based on the dynamic response of the component to the boundary bus condition, while the equivalent admittance should be fixed during the simulation. A dynamic model of single-phase air-conditioner has been developed with this modeling approach. The dynamic performance of this model is based on the A/C performance model proposed by WECC [5], which has two operating states, i.e., run and stall, and the corresponding characteristics are shown in Fig. 1.58. In this research, this model is developed in a single-phase oriented framework, instead of the original positive-sequence representation. This model will be used in the test cases in this section and next section.

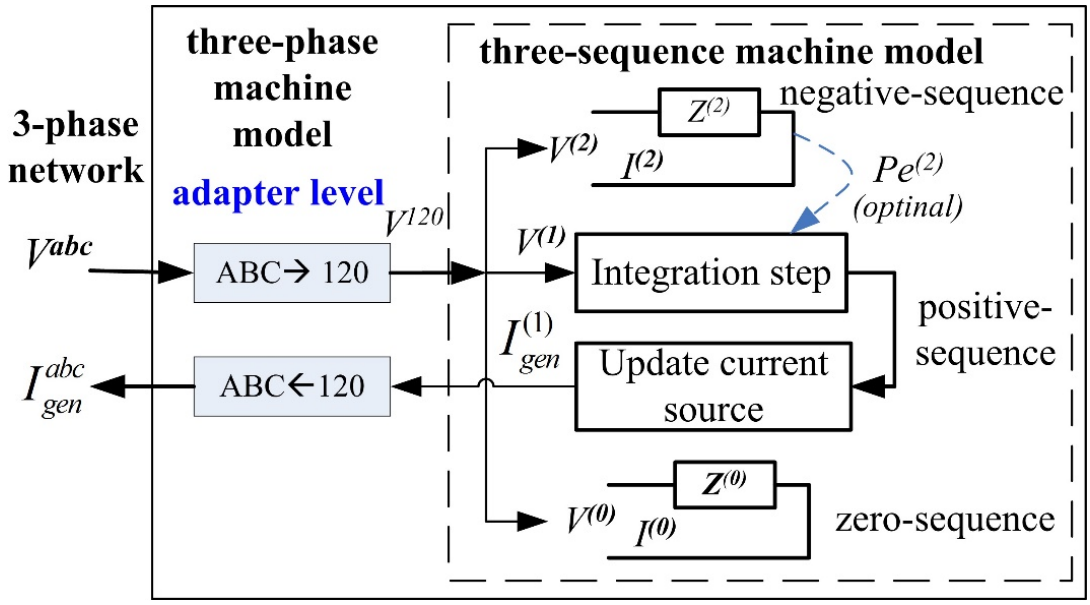

Fig. 1.30 Implementation of three-phase machine model based on the corresponding three-sequence model using adapter pattern

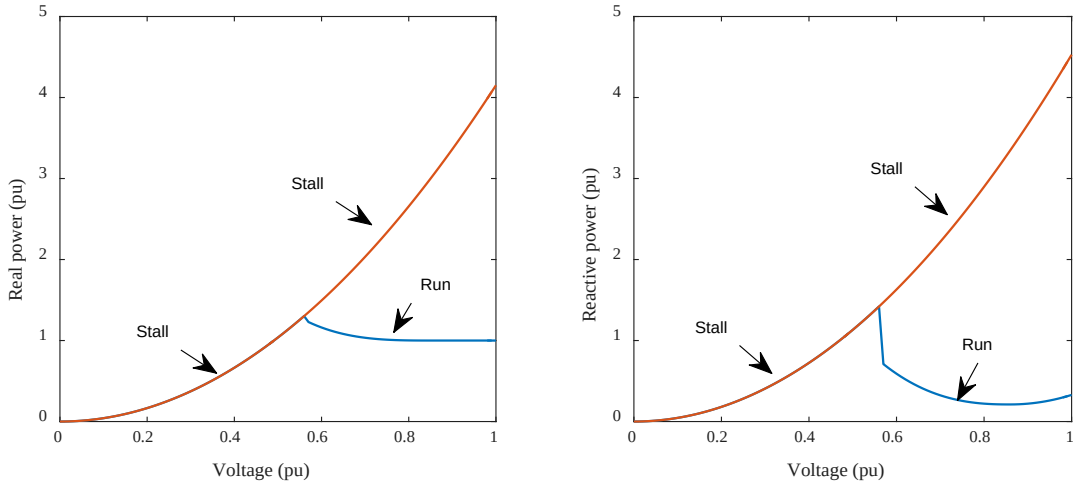

(a) (b)

Fig. 1.31 The power consumption versus terminal voltage characterisitcs of the A/C compressor motor under the “run” and “stall” operation conditions [80]

1.6.3.4 MATE-based Three-Phase/Three-Sequence Dynamic Simulation Algorithm

The three sequence TS simulation, the three-phase dynamic simulation combined with the MATE approach together form the TDDS algorithm. The key steps of the TDDS algorithm are shown in Fig. 1.59. During the implementation, several key issues have been identified and addressed:

1) For the proposed power flow algorithm, a common boundary bus shared by the transmission system and a distribution system is required. On the other hand, for the dynamic simulation, the subsystems should be connected through branches, as illustrated in Fig. 1.53(a), in order to comply with the formulation of the MATE approach. To facilitate the same subsystem model being used for both power flow and dynamic simulation, the subsystems are split based on the bus splitting concept and connected by "virtual" breakers. For each boundary bus, a dummy bus is created during the network partition stage. Subsequently, a "virtual breaker" (represented by a branch with a small impedance, i.e., 0.0001 pu) is introduced to connect them. At the simulation stage, the virtual breakers connecting the transmission and the distribution subsystems are "switched off" and not used in power flow, but "switched on" for the integrated dynamic simulation. The virtual breakers become the link branches in MATE based dynamic co-simulation.

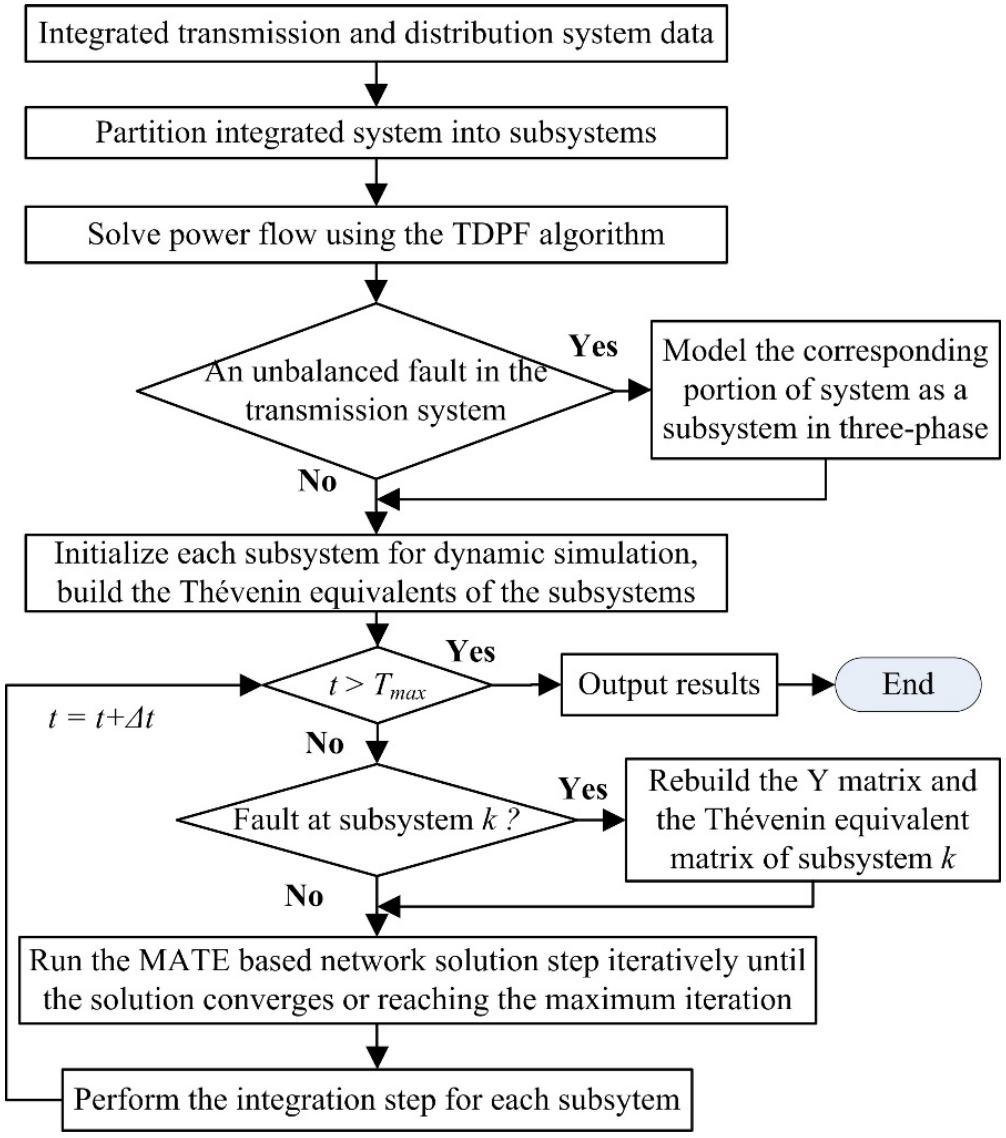

Fig. 1.32 The flowchart of the proposed TDDS algorithm

2) While the transmission system is modeled and solved as one subsystem in power flow, it is not necessarily represented as one subsystem for dynamic simulation. It can also be further split into subsystems and the resulting subsystems can be represented either in three-sequence or three-phase, depending on the application requirements. Such splitting is useful for analyzing unbalanced faults in the transmission system and realizing parallel dynamic simulation.

3) A common (reference) coordinate system should be predefined and used for coordinating different representations of transmission and distribution systems. In the present implementation, the three-sequence coordinate is chosen as the default common coordinate. For the subsystem(s) modeled in three-phase detail, the following data processing is required: (a) the three-phase Thévenin equivalent is built first, and transformed to the three-sequence Thévenin equivalent; (b) after the three-sequence currents of the link branches are obtained from the link subsystem solution results, they need to be converted to three-phase.

4) Unbalanced faults are processed in a special manner. A basic requirement of building a three-sequence Thévenin impedance matrix for a subsystem modeled in three-sequence representation is that three sequence networks of the subsystem are decoupled. If an unbalanced fault were applied to a subsystem modeled in three-sequence representation, the three sequence networks would become coupled at the fault point, which violates the requirement. Therefore, if an unbalanced fault is applied in the transmission system, the corresponding portion of the transmission system should be represented as one subsystem modeled in three-phase detail. However, it should be emphasized that the size of this three-phase modeling portion can be as small as only including the faulted bus. Therefore, the advantage of three-sequence modeling can be preserved.

5) Both the coordinate systems (three-phase or three-sequence) and network (transmission or distribution) attributes are added to the subsystems. As the solution methods for three-phase and three-sequence coordinates are different, so also are the solution methods for transmission and distribution systems. The coordinate and network attributes added to the subsystems can help identify an appropriate simulation algorithm for each subsystem during simulation.

1.6.4 Test Cases

A simple 8-bus distribution feeder shown in Fig. 1.60 is used to build the distribution systems. The total load on the feeder is 8 MW. The feeder consists of 7 sections of non-perfectly transposed overhead lines. The line codes and parameters are based on the IEEE 13-bus test feeder [43]. There are 7 equivalent loads, and their parameters are shown in Fig. 1.60. The loads are wye-connected and are identical on the three phases, unless otherwise specified in the test cases.

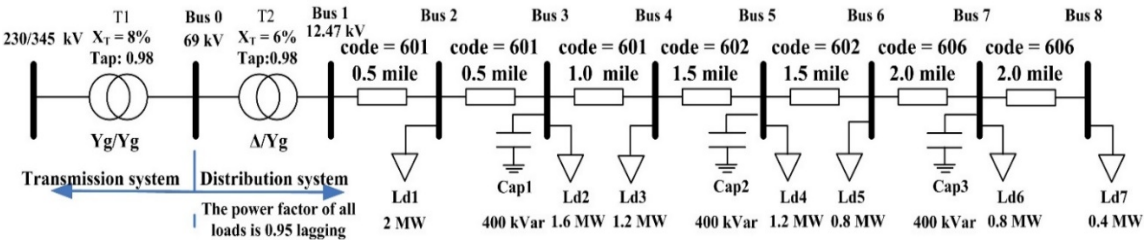

Fig. 1.33 A simple 8-bus distribution feeder

In the following test cases, the IEEE 9 bus and 39 bus test systems are used to represent the transmission system. In creating the integrated T&D systems, the distributed system shown in Fig. 1.60 is used to replace the original aggregated loads connected at the transmission buses. In addition, the feeder model and loads are scaled to match the original load seen by the transmission system. In the test case involving the IEEE 9 bus system, the loads served by buses 5, 6 and 8 are replaced by the distribution systems. The resulting integrated system is referred to as T9D3. In the test case involving the IEEE 39 bus system, the loads served by buses 15, 16, 18, 26, 27 and 28 are replaced by the distribution systems, and the resulting integrated system is referred to as T39D6 hereafter. The corresponding portion of the system is shown in Fig. 1.61.

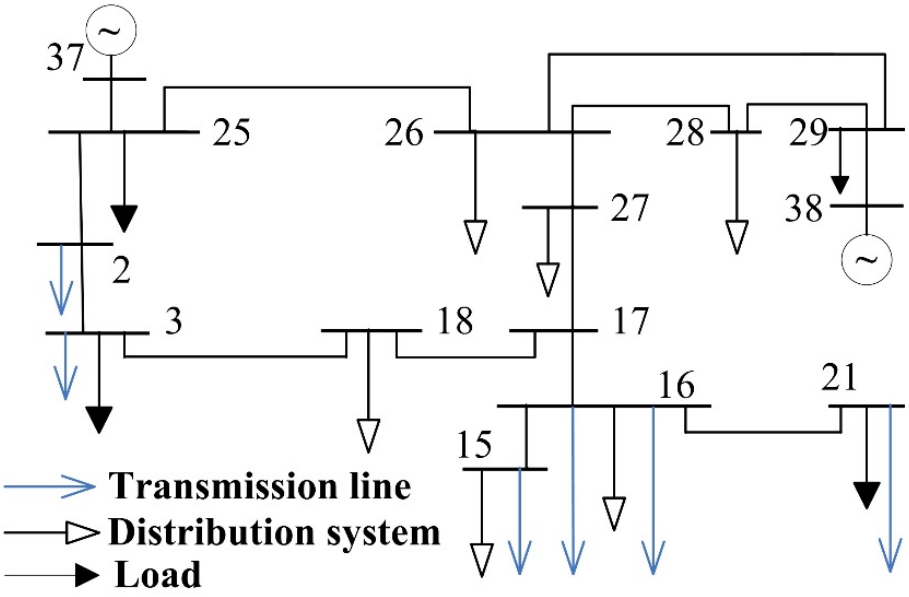

Fig. 1.34 A portion of the IEEE 39 bus system

The 69 kV subtransmission buses (corresponding to the Bus 0 in Fig. 1.60) are selected as the interface between the transmission and the distribution systems. The number of a distribution bus in the integrated system is defined based on (1.8):

$$N_{dist,i}^{new} = 10N_{tran,i} + N_{dist,i}^{old} \tag{1.8}$$

$N_{dist,i}^{new}$ denotes the new bus number of distribution bus i ; $N_{tran,i}$ is the number of the transmission bus to which the associated distribution system of bus i is connected; $N_{dist,i}^{old}$ is the original bus number of distribution bus i used in Fig. 1.60.

To consider load unbalance condition, a loading unbalance factor β is defined. Loads on the three phases are defined as:

$$P_{L,i}^{A} = \frac{1}{3} P_{Total,i}, P_{L,i}^{B} = \frac{1-\beta}{3} P_{Total,i}, P_{L,i}^{C} = \frac{1+\beta}{3} P_{Total,i} \quad (1.9)$$

where $P_{L,i}^{A}$, $P_{L,i}^{B}$ and $P_{L,i}^{C}$ are the real part of load on phase *A*, *B* and *C* of bus *i*, respectively, and $P_{Total,i}$ is the sum of them.

1.6.4.1 Test The Integrated T&D Power Flow Algorithm

(1) Verification by Comparing with PSCAD

There is no publically available phasor domain simulation program capable of modeling and simulating integrated T&D systems that can be used for comparison. Electromagnetic transient simulation programs support modeling and simulating integrated T&D systems in three-phase, point-on-wave detail. Hence, the proposed integrated T&D power flow algorithm is benchmarked against PSCAD. The T9D3 test case is used for benchmarking purposes. The comparison results are shown in Table 1.8 and Table 1.9. The positive sequence bus voltages are extracted from their corresponding voltage waveforms using the FFT component in PSCAD. It can be observed that the both the transmission and distribution power flow results obtained from the proposed TDPF algorithm closely match with those of PSCAD.

Table 1.8 Positive sequence voltages of the buses in the transmission system

	magnitude (pu)		**angle (degree)**	
bus	**TDPF**	**PSCAD**	**TDPF**	**PSCAD**
4	1.028	1.028	-2.23	-2.24
5	1.002	1.001	-3.98	-4.02
6	1.014	1.013	-3.81	-3.82
7	1.028	1.027	3.56	3.52
8	1.018	1.017	0.51	0.49
9	1.033	1.033	1.78	1.79

Table 1.9 Three phase voltages of some selected buses in the distribution system served by bus 5

bus	phase	magnitude (pu)		angle (degree)	
		TDPF	**PSCAD**	**TDPF**	**PSCAD**
51	*A*	1.007	1.009	-40.52	-40.56
	B	1.009	1.011	-160.41	-160.46
	C	1.007	1.010	79.50	79.46
55	*A*	0.967	0.967	-43.61	-43.54
	B	0.981	0.984	-163.86	-163.69
	C	0.964	0.967	76.00	75.82
58	*A*	0.947	0.945	-44.86	-44.79
	B	0.960	0.963	-165.10	-165.26
	C	0.935	0.940	74.65	74.48

(2) Robustness of the proposed algorithm under different levels of load unbalance

As shown in Table 1.10, the integrated T&D power flow iteration counts for both test cases are insensitive to the load unbalance conditions in the distribution systems, which indicates the robustness of the proposed algorithm.

Table 1.10 Number of iterations in the integrated T&D power flow under different load unbalance conditions

Test case	Scenario	Number of iterations (*k* in Fig. 7.2)
T9D3 (IEEE 9 bus system interfaced with 3 distribution systems)	Base case	3
	5% load unbalance	3
	10 % load unbalance	3
T39D6 (IEEE 39 bus system interfaced with	Base case	3
	5% load unbalance	3

6 distribution systems)	10 % load unbalance	3

1.6.4.2 The Integrated T&D Dynamic Simulation Algorithm

The proposed TDDS algorithm has been tested on the T9D3 system. In dynamic simulation, all loads are represented by constant impedances. The whole system has also been modeled and simulated in PSCAD. At 1.0 s, a single-line-to-ground (SLG) fault is applied at the 69 kV bus 50 of the distribution system served by bus 5, and cleared after 0.07 s. The three-phase voltages of bus 52 in the distribution system is shown in Fig. 1.62, and the three-sequence voltages of bus 5 is shown in Fig. 1.63. It can be seen from both results that, other than the 1-cycle time delay introduced in extracting the fundamental frequency components using the FFT component in PSCAD, the simulation results of TDDS match well with those of PSCAD.

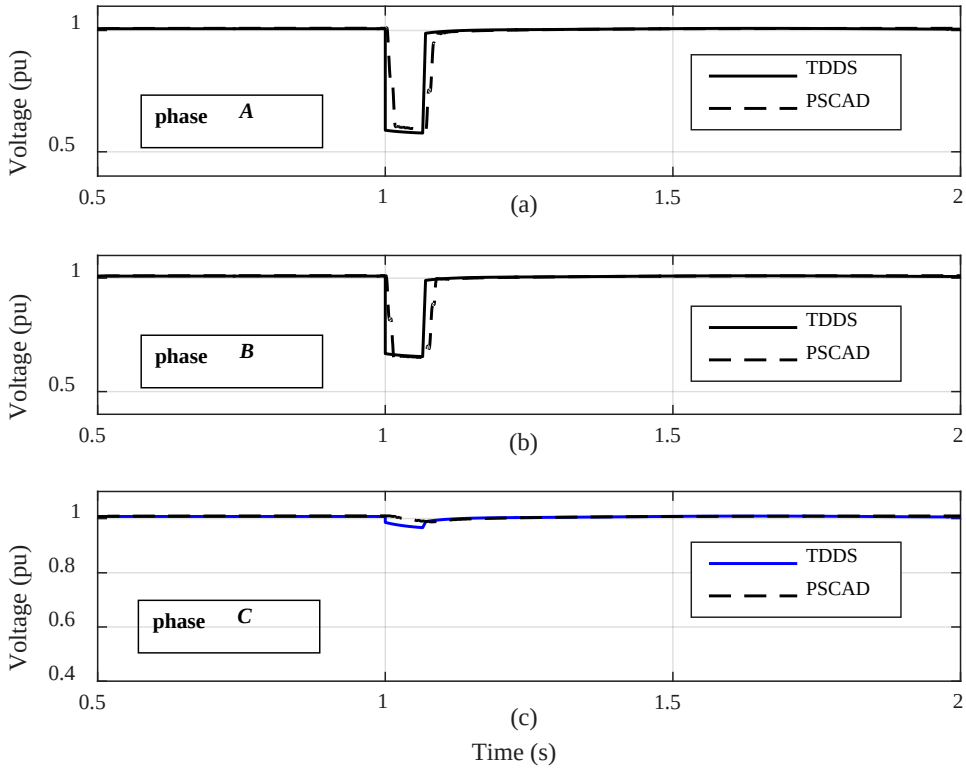

Fig. 1.35 Three phase voltages of bus 52 in the distribution system served by bus 5

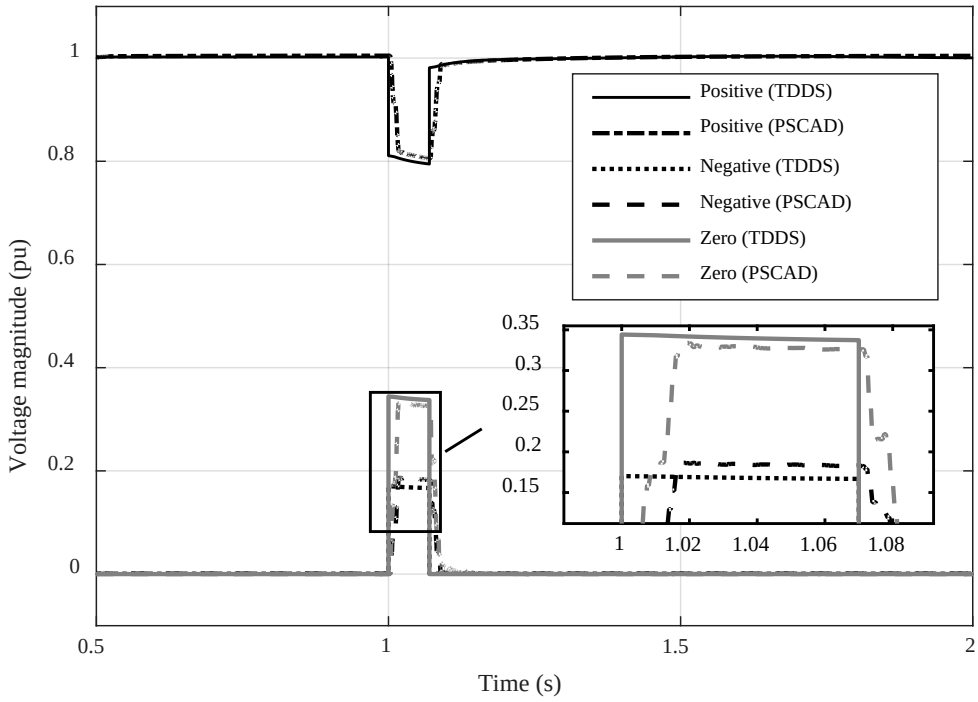

Fig. 1.36 Three-sequence voltages of bus 5 in the transmission system

1.6.5 Application to FIDVR Study Under Unbalanced Conditions

The FIDVR problem has been mainly studied using the composite load model and positive-sequence TS simulation programs [5]. It is pointed out in [5] this modeling and simulation approach is not applicable to unbalanced fault conditions. In addition, an aggregation approach has been used to build the composite load model. All motors in a feeder are assumed to have the same running and stall characteristics, and they stall at the same time. Considering their location differences as well as the resulting A/C stall time and trip time differences, the assumption could result in simulation results significantly different from their actual responses. These issues can be addressed by the proposed integrated T&D modeling and simulation approach. The following two study cases are conducted on the T39D6 system. In the base case, the three-phase loads are assumed to be balanced. The load composition is 50% single-phase residential A/C motor combined with 50% constant impedances. The default parameters of the A/C performance model provided in PSLF user manual are used in the studies, except that the stalling voltage threshold is set to 0.65 pu. The stalling time is 0.033 s

(1) A FIDVR Event Triggered by a SLG Fault in The Transmission System

In this test case, bus 17 and the connected branches in the transmission system are modeled as a subsystem in three-phase detail during dynamic simulation to accommodate an unbalanced fault. A SLG fault is applied on phase *A* of bus 17 at 1.0 s and cleared after 0.07 s. Due to the delta-wye connection of the distribution transformers, phases *A* and *B* at the distribution systems are directly

affected by the fault. The phase *A* voltages of the buses at the end of the feeders are shown in Fig. 1.64.

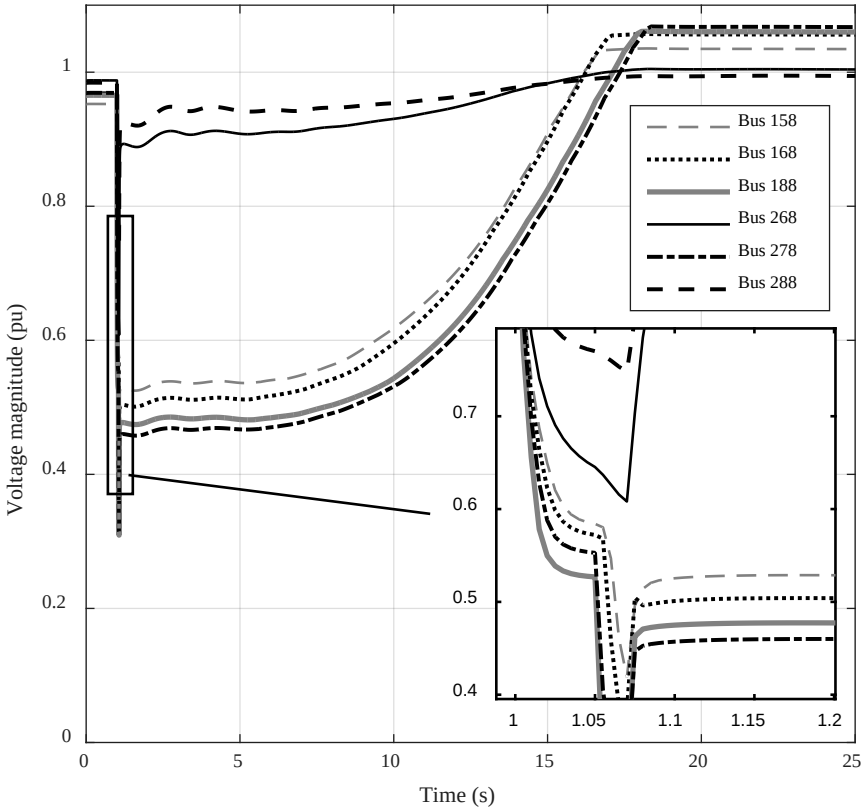

Fig. 1.37 Phase A voltages of the buses at the end of the feeders

It can be observed that the SLG fault causes stalling of A/Cs on phase A in the distribution systems served by buses 15, 16, 18 and 27, but there is no A/C stalling within the distribution systems served by buses 26 and 28, as both are relatively far away from the fault. Phase *A* voltages start to recover at around 5 s as A/C motors are gradually tripped off by their thermal protections.

The phase *A* voltages of the distribution feeder buses served by bus 15 are shown in Fig. 1.65. The voltage profiles of the buses at different locations within one distribution system are significantly different. As shown in the Fig. 1.65, in this FIDVR event, only the A/Cs connected at bus 154 and the buses downstream of bus 154 stall, while those connected to the upstream buses (i.e., buses 152 and 153) do not stall. Such diverse responses of A/Cs in the same distribution system have not been properly represented in the existing composite load model [5], where all A/Cs served by the same substation are provide valuable references to further improve the composite load models, particularly the aggregation of A/Cs considering the different responses.

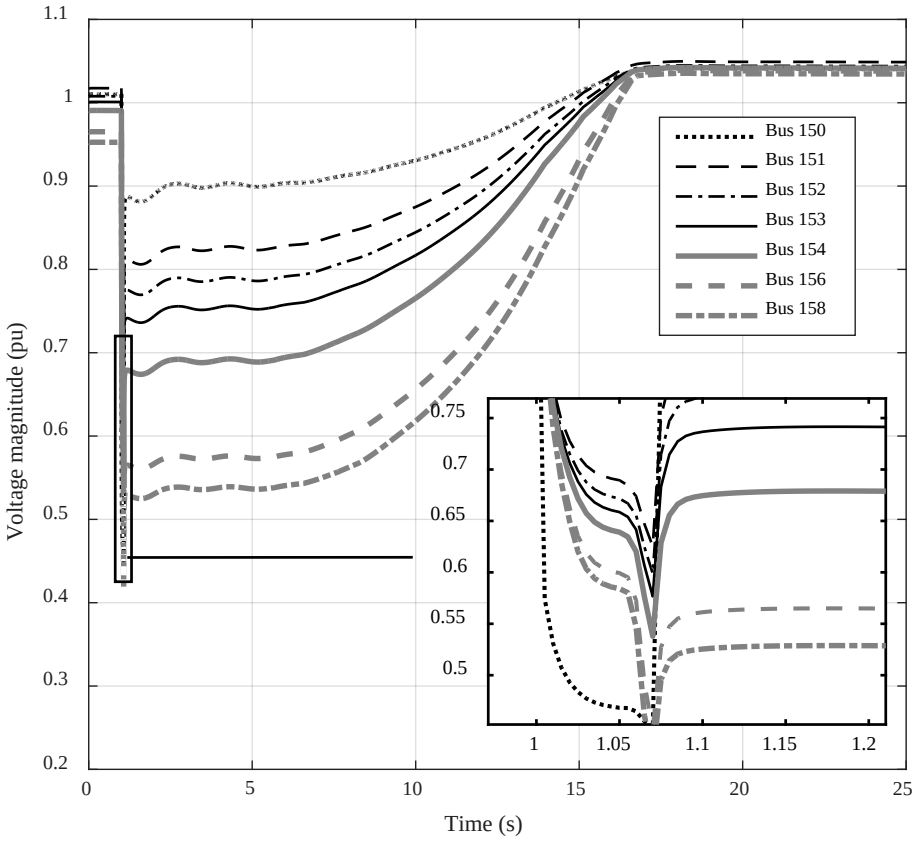

Fig. 1.38 Phase A voltage of feeder buses served by bus 15

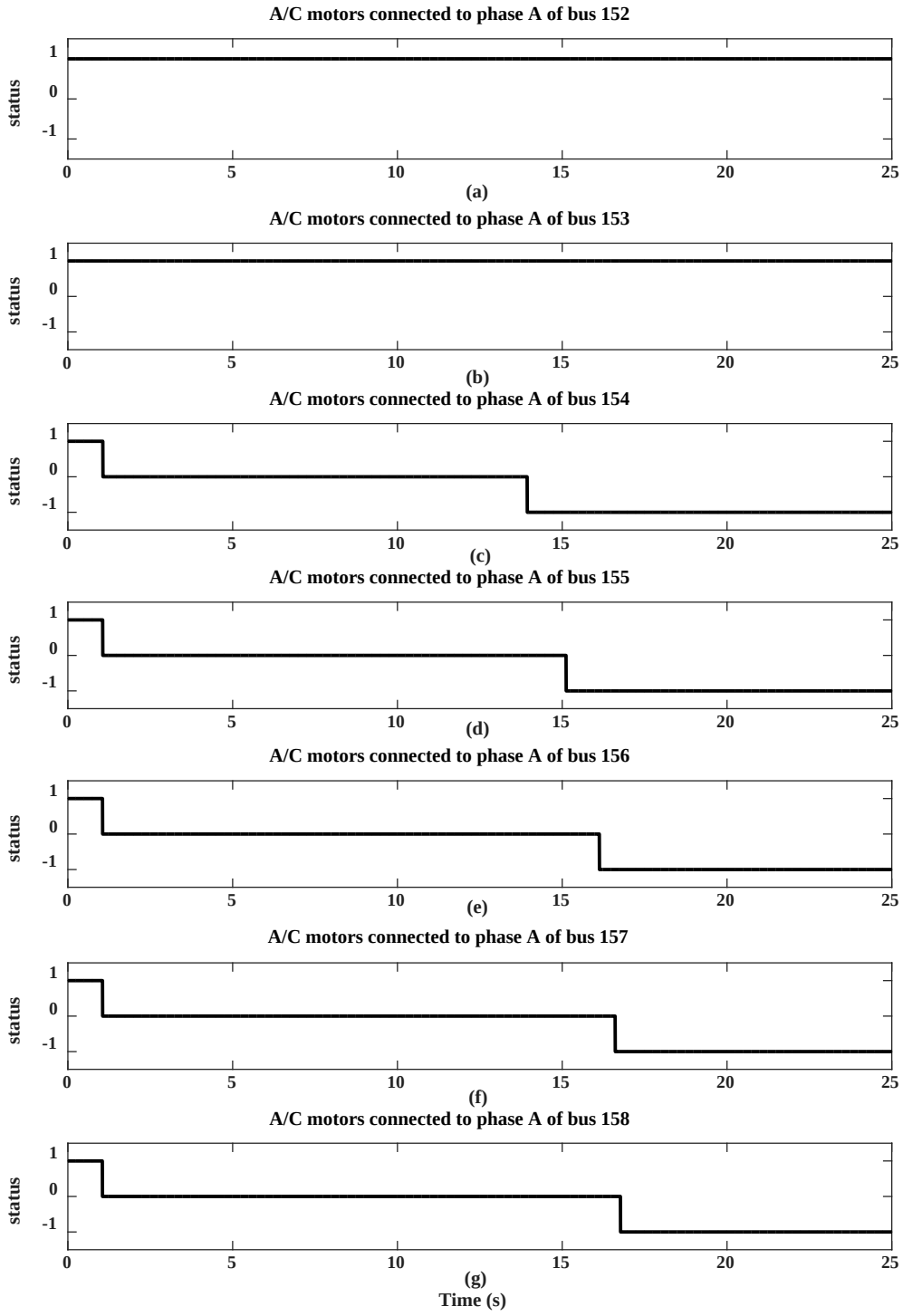

Fig. 1.39 The operation status of the A/C motors connected to phase A of the buses along a feeder served by bus 15 (status = 1 means running, status = 0 means stall and status = -1 means being tripped off)

On phase *B*, only the A/Cs connected to the bus at the end of the feeder served by bus 18 stall, the A/Cs on phase *B* of the upper stream buses of the same distribution system and within other distribution systems do not stall. Although phase *C* is not directly affected by the fault, the impacts of the FIDVR event on phase *C* of buses within each distribution system are obvious, as illustrated in Fig. 1.67. The impacts are mainly due to the three-phase interactions through the delta-wye connection of the distribution transformers.

The impact of the FIDVR event on the transmission system is shown in Fig. 1.68, which are the positive and negative sequence voltages of buses 15, 27 and 28. The results show that the load unbalance in the distribution systems during the event results in noticeable voltage unbalance in the transmission system, indicated by the negative sequence voltages. Zero sequence voltages only appear in transmission system during the fault period, thus they are not included in Fig. 1.68.

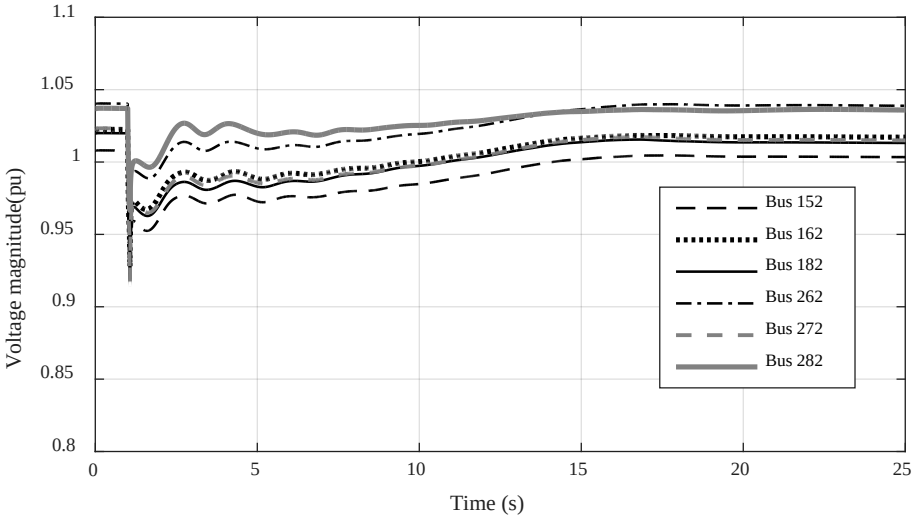

Fig. 1.40 Phase C voltages of buses in the distribution systems

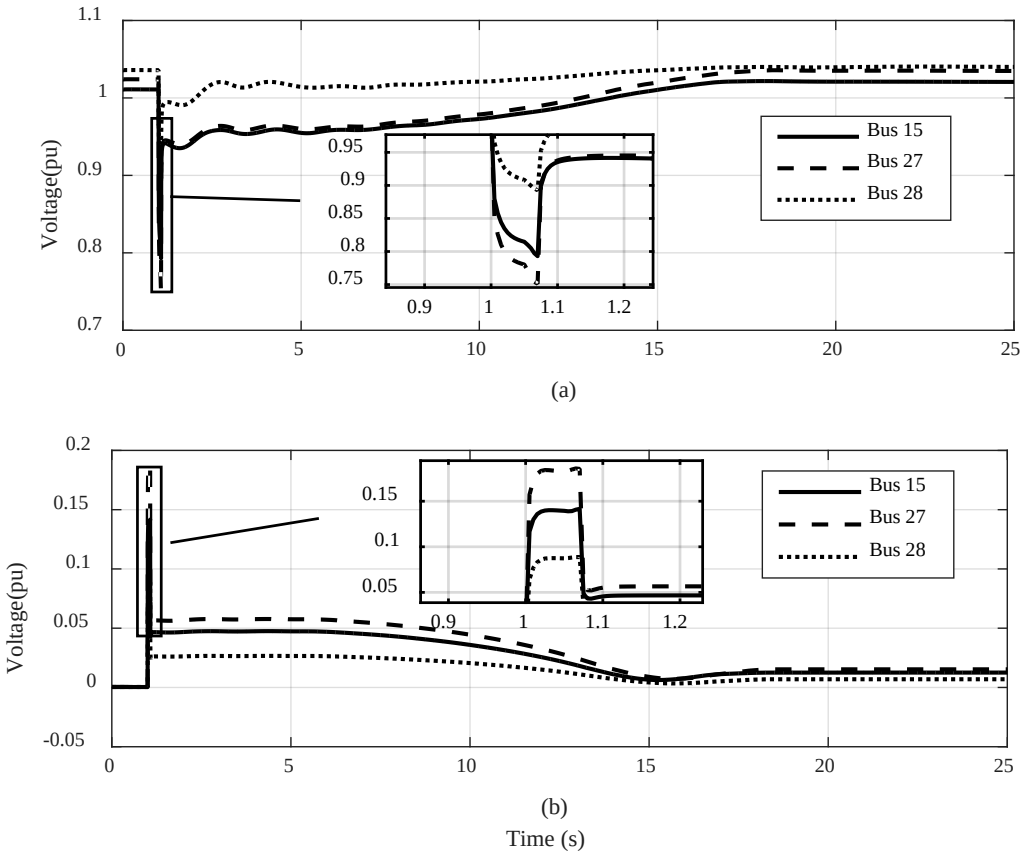

Fig. 1.41 Sequence voltages of transmission buses 15, 27 and 28: (a) positive sequence; (b) negative sequence

(2) Impacts of load unbalance and composition unbalance

In the following study, the load unbalance factor β is set to be 5%. The load composition unbalance is considered by changing the A/C load composition on phases *A* and *C* by 5%, namely, the percentages of single-phase A/C motors on phases *A*, *B* and *C* become 45%, 50% and 55%, respectively. Correspondingly, the percentages of impedance loads on three phases are changed to 55%, 50% and 45%, respectively. Two scenarios have been studied: 1) only load unbalance; 2) both load unbalance and composition unbalance.

A three-phase fault is applied at bus 3 at 1.0 s and cleared after 0.07 s. The three-phase voltages of bus 158 (at the end of a feeder) are shown in Fig. 1.69. The three phase voltages of bus 150 (an interface bus between transmission and distribution) are shown in Fig. 1.70. Although the fault is a three-phase fault, the load unbalance and load composition unbalance result in different voltage recovery rates on each phase, thus causing three-phase voltage unbalance. The results show that combined effects of a small unbalance (5%) in three-phase loads and load composition can be significant. The unbalanced conditions at the interface bus 150 suggests that single-phase representation of transmission system is not adequate for a system with similar load unbalance and/or load composition unbalance conditions.

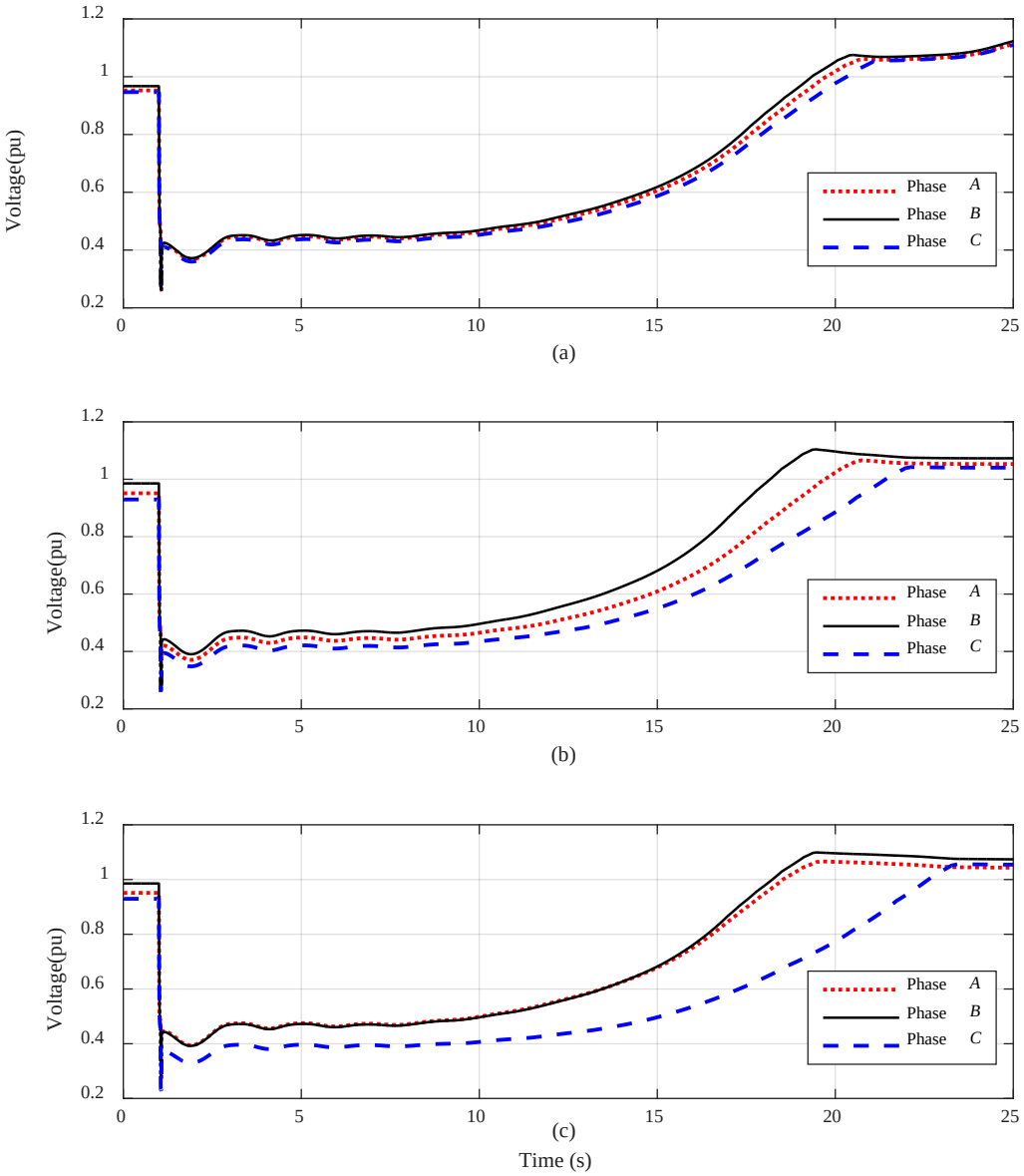

Fig. 1.42 Three-phase line-to-ground voltages of bus 158: (a) base case; (b) 5% load unbalance; (c) 5% load unbalance and 5% load composition unbalance

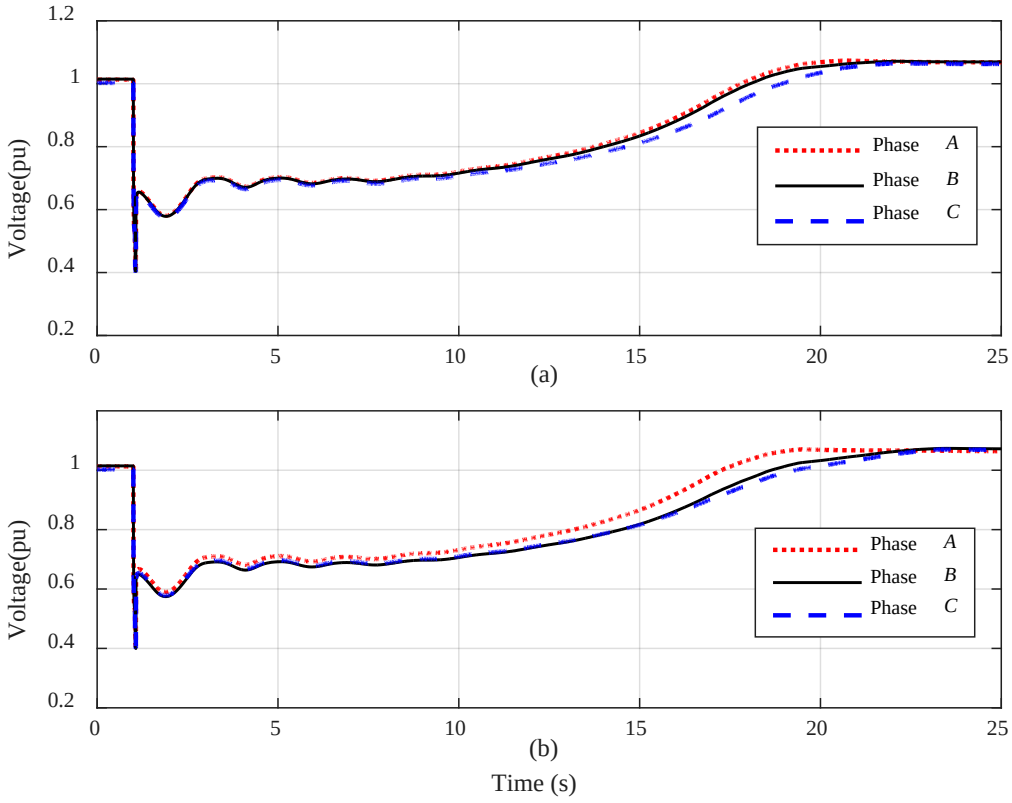

Fig. 1.43 Three-phase line-to-ground voltages of bus 150: (a) 5% load unbalance (b) 5% load unbalance and 5% load composition unbalance

1.7 Advanced EMT-TS Hybrid Simulation with Capability of Switching Back to TS Simulation

1.7.1 Background

Compared to TS simulation, EMT simulation is, in general, better suited for modeling and simulating power electronic devices (e.g., HVDC and FACTS) and/or some single-phase devices (e.g., single-phase A/C motors) in detail and capturing their non-linear, fast dynamic responses. Thus, the primary motivation behind switching from TS simulation to EMT-TS hybrid simulation is to take advantage of these capabilities of EMT simulation. Fast dynamics in power system usually settle in a short time-period after the fault is cleared or the disturbance disappears. When the dominant dynamics in the system are in the low frequency range (e.g., below 5 Hz), these components represented in the EMT simulator can be well represented by their corresponding quasi-steady-state (QSS) models [36]. Therefore, it is theoretically feasible to switch from EMT-TS hybrid simulation back to pure TS simulation after the fast dynamics settle down without significantly compromising the simulation accuracy.

Further, in the cases where a relative large-scale (e.g., more than 100 buses) subsystem or a subsystem with several converters is modeled in detail in the EMT simulator, the EMT part of the simulation is usually much slower than the TS part, even when a large-scale subsystem is simulated

by TS simulation. Therefore, using the developed EMT-TS hybrid simulation only for a short period after the fault application and removal and switching back to TS simulation for the remainder of the simulation, instead of running EMT-TS hybrid simulation for the whole simulation period, could significantly reduce the simulation time. Thus, from the simulation efficiency perspective, the option of switching back to TS simulation is attractive.

Switching from pure TS simulation to EMT-TS hybrid simulation provides the "zoom-in" capability to capture the fast dynamic details, while switching from EMT-TS hybrid simulation back to TS simulation allows users to "zoom-out" from the detailed models, as the details have been adequately captured during "zoom-in" period. Such a "zoom-in/zoom-out" capability provides more flexibility to the users in terms of modeling and simulation. The question that remains to be answered is how to realize the proposed switch between the two simulation algorithms automatically during simulation?

Switching from TS to EMT-TS is relatively easy to achieve since it is completed under the pre-fault, normal operating condition. In contrast, switching from EMT-TS simulation to TS simulation is performed when the system is operating under a non-equilibrium condition. A direct approach proposed in [18] is to initialize a phasor modeling representation of the detailed system before switching to the TS simulation. To accomplish such an initialization task, all information to initialize the bus voltages and state variables must be available to the TS simulator and the TS simulator must support initialization under a non-steady-state condition. Thus, this approach is feasible only when both the EMT and the TS simulators are under the users' control and can be modified to fulfill the initialization process discussed above. Such a strict requirement cannot be satisfied by most of the existing EMT and TS simulators. In fact, in [18], switching from hybrid simulation to pure TS simulation using such an initialization approach is demonstrated using in-house EMT and TS simulators and the test case is rather simple with only one thyristor controlled series capacitor (TCSC) system modeled in the detailed subsystem.

Another approach of performing the simulation mode switching is proposed in [8], where the main idea is as follows: a phasor model representation of the detailed system is simulated using TS simulation in parallel while EMT-TS hybrid simulation is running. The TS simulation of the detailed system actually serves to replace the aforementioned initialization process. To realize the switching, simulation results of both the phasor representation and the point-on-wave representation of the detailed system are tracked. The switching operation is performed when the simulation results of both representations are within a predefined tolerance and over a set time-period. The detailed and external systems represented using a phasor model are re-connected to form a complete system (same as the original full system) and the remainder of the simulation is conducted using TS simulation with this complete system. Compared to the first approach, this approach requires minor modification to the existing EMT-TS hybrid simulation and the TS simulation algorithms.

However, the second approach also suffers from two significant drawbacks. The first drawback lies in the implicit assumption that simulation results of the two representations of the detailed system will converge at some point after the fast dynamics settle down. However, the convergence is not guaranteed due to the inherent differences between the models used in the EMT and the TS simulations. Secondly, the two subsystems are reconnected to form a full network to continue the TS simulation. This means that both portions of the system must be modeled with the same

representation. In other words, this approach limits the modeling flexibility and is not suitable for integrated transmission and distribution systems. In addition, with the aforementioned approach, the simulation object is in fact changed after switching back to TS simulation. Hence, the TS simulation algorithm has to be augmented to handle the situation of two separate models merged into one, which further complicates the implementation. Besides these two major issues, the details of the implementation are not provided and the choice of the key parameters is not discussed in [8]

1.7.2 Implementation by Combining Hybrid Simulation and Dynamic Co-simulation

1.7.2.1 Overview of the Proposed Method

The solution proposed in this research for switching from the EMT-TS hybrid simulation to the TS simulation follows the basic idea of the second approach discussed in the last section. In the proposed approach, the EMT-TS hybrid simulation developed in section 1.3 and the MATE-based dynamic co-simulation algorithm developed in Section 1.6 are combined. Significant improvements have been made to address the two drawbacks discussed above. The simulation result discrepancy issue between the EMT and TS simulation of the detailed system is addressed from both the modeling and simulation result coordination perspectives:

Firstly, from the modeling perspective, the three-phase phasor modeling is naturally more closely relates to the three-phase point-on-wave models used in the EMT simulation than the three-sequence phasor modeling. The proposed approach supports the three-phase phasor modeling approach developed in Section 1.6. This feature is particularly useful when there are some models (for example, single-phase induction motors), which are better modeled in phase-oriented representation, in the detailed system portion.

Secondly, it is observed from past simulation experiences that major simulation result discrepancies at the post-disturbance stage between the EMT and the TS simulation are usually related to control actions and operation state changes of the critical components modeled in the detailed system. The main reason is that these actions and/or state changes may not be correctly represented by the phasor representation or captured by the TS simulation. Therefore, in the proposed approach, critical discrete event or control signals obtained from EMT simulation results can be fed back to the TS simulation of the detailed system. These signals are used as external control inputs to override the corresponding control or stage change signals in the TS simulation. These important signals can be, for example, a converter blocking signal when an HVDC inverter is undergoing commutation failure or a signal of an A/C motor state change during a FIDVR event.

In addition, re-connecting the two subsystems into a full network becomes unnecessary with the use of the MATE based dynamic simulation. After switching back to the TS simulation mode, the detailed and the external systems are still two individual subsystems under the MATE based simulation framework.

With the proposed simulation algorithm, the full system is split into two parts, i.e., the detailed system and the external system, using the bus splitting method as shown in Fig. 1.71. The detailed system is not only represented in the 3-phase point-on-wave modeling in the chosen EMT simulator, but also modeled in the three-phase phasor representation. The external system is

modeled in the three-sequence phasor representation. The whole simulation is divided into three stages, i.e., pre-fault TS simulation stage, EMT-TS hybrid simulation stage, post-disturbance TS simulation stage, as illustrated in Fig. 1.72. The multi-area dynamic simulation approach is employed at the first and the last simulation stages. The interactions between the detailed system and the external system for the three stages are shown in Fig. 1.73.

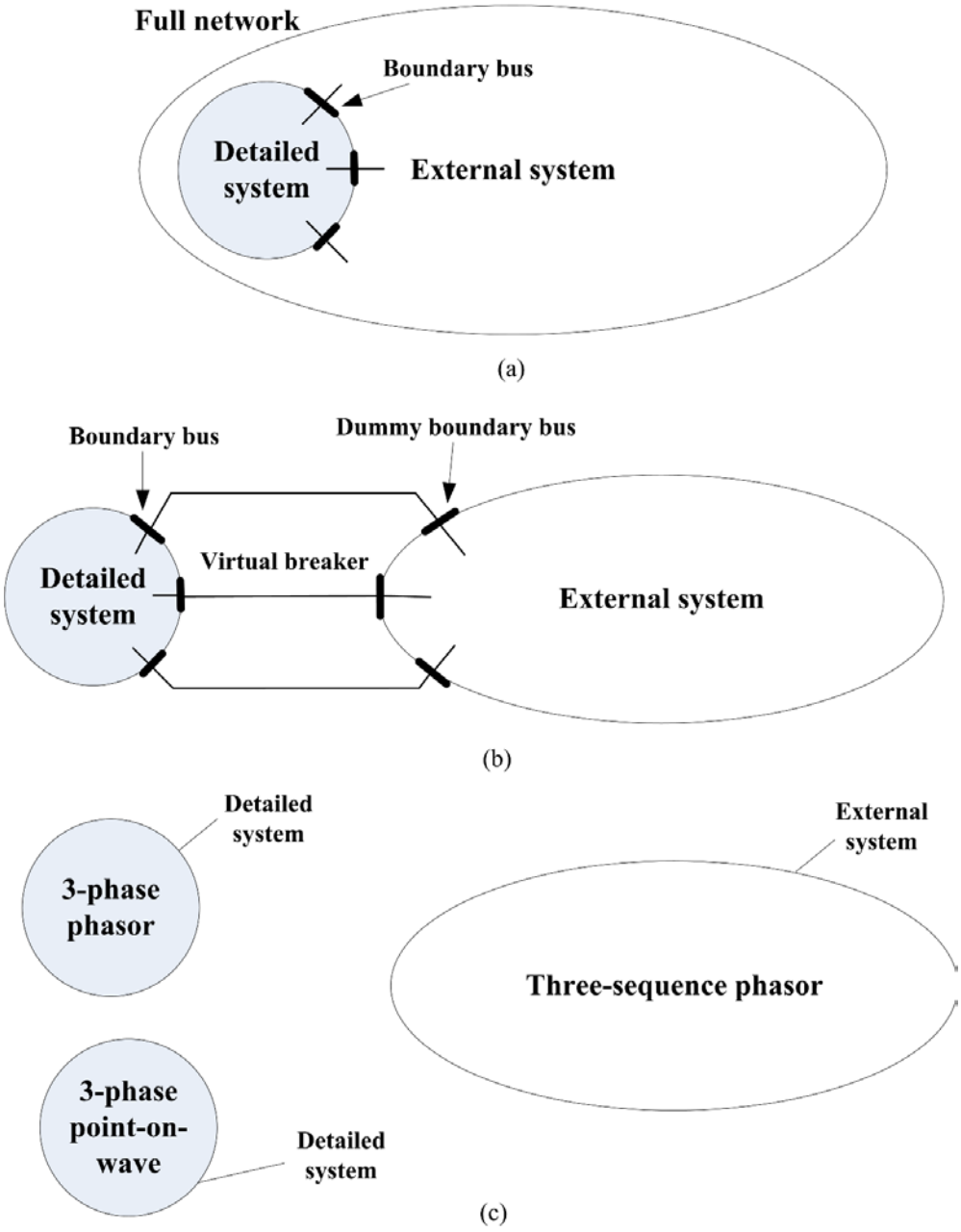

Fig. 1.44 (a) the full network (b) the full network is split into the detailed system and the external system connected by virtual breakers; (c) representations of the detailed system and the external system used in the proposed method

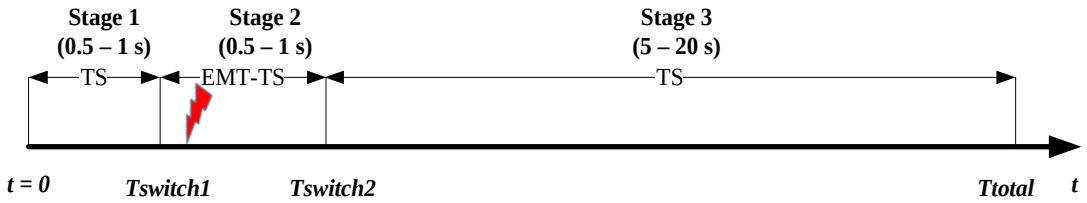

Fig. 1.45 Schematic diagram for illustrating the proposed 3-stage simulation

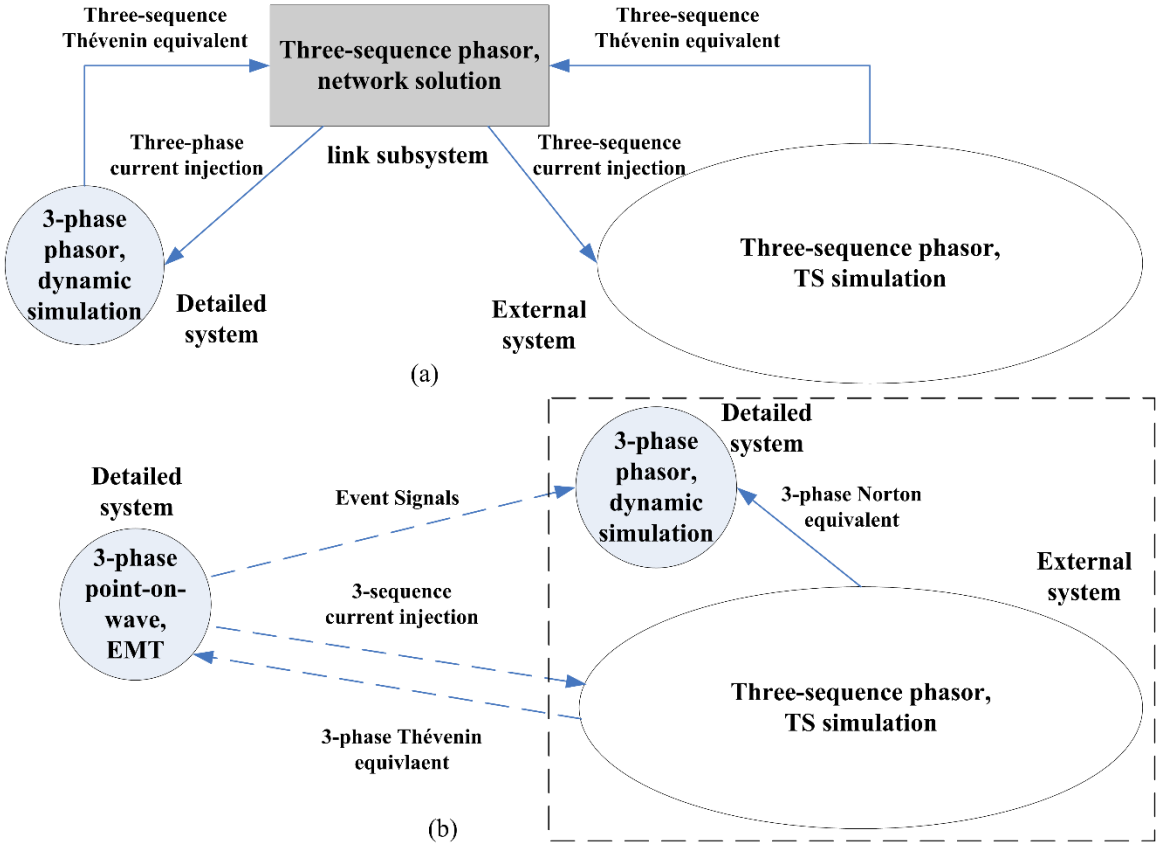

Fig. 1.46 Interactions between the detailed and the external systems: (a) for both stages 1 and 3; (b) for stage 2

For the second stage, the EMT-TS hybrid simulation algorithm developed in Chapter 4 has been augmented. The hybrid simulation is augmented by running the dynamic simulation of the detailed system and the switch controller in parallel to the existing hybrid simulation algorithm, as shown in Fig. 1.73. The actual implementation of the augmented algorithm is shown in Fig. 1.74. A three-phase Norton equivalent is used as the external system equivalent in the dynamic simulation (DS) of the detailed system. The three-phase Norton equivalent can be easily obtained for this implementation, as it is a byproduct of the calculation of the three-phase Thévenin equivalent, which is presented in section 1.2.1. The admittance matrix of the three-phase Norton equivalent is added to admittance matrix of the detailed system after switching from the stage 1 to stage 2. The

three-phase current source of the Norton equivalent is directly used in the network solution step. When switching from stage 2 to stage 3, the admittance matrix of the detailed system has to be rebuilt to remove the admittance matrix of the three-phase Norton equivalent.

To address the modeling discrepancy and the simulation convergence issue, key discrete event signal(s) obtained from the EMT simulation results can also be used as external control inputs to replace their corresponding control signals in the dynamic simulation of the detailed system, which is also demonstrated in Fig. 1.74. After the effect of the disturbance disappears, boundary conditions obtained from the three-phase dynamic simulation results of the detailed system and the three-sequence TS simulation results of the external system are used as inputs to the simulation switching controller block to identify whether at the next step it is appropriate to switch back to the TS simulation. Details of the simulation switching controller design will be discussed in the next section.

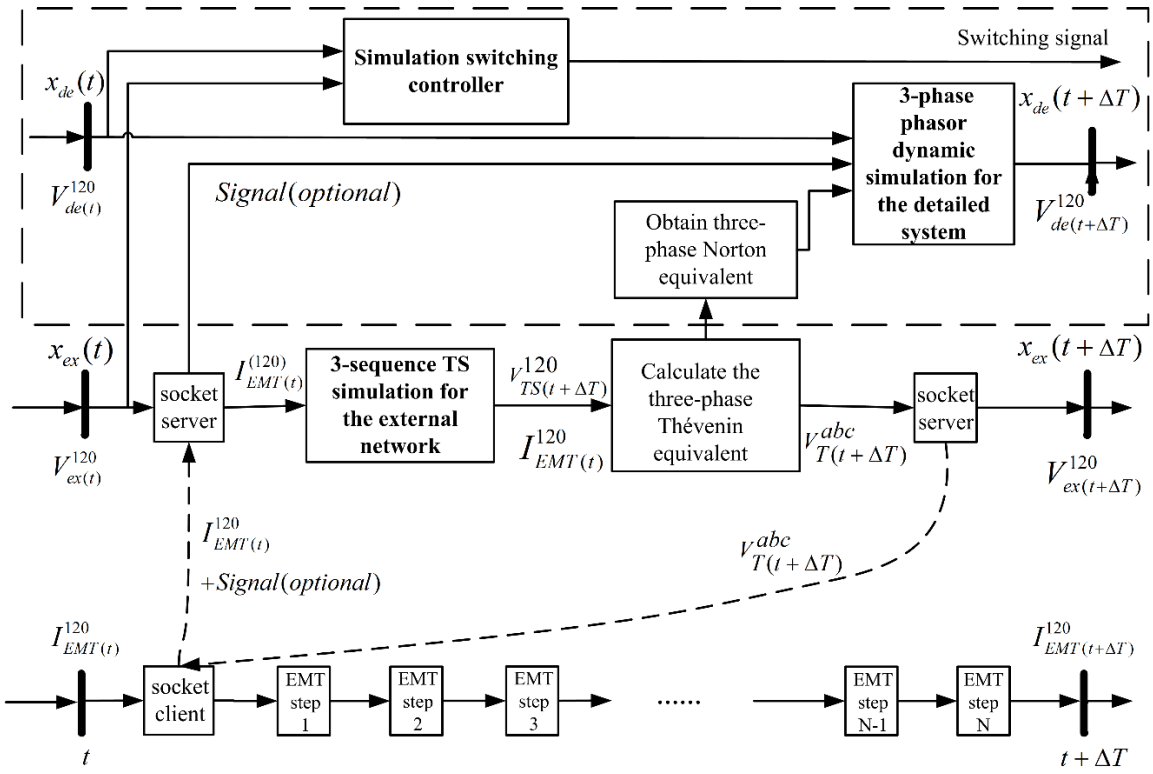

Fig. 1.47 Implementations of the augmented hybrid simulation at the stage-2

1.7.2.2 Implementation Details

(1) Network Splitting using the Bus-Splitting Concept

Considering that the EMT-TS hybrid simulation requires common boundary buses shared by the detailed and external systems, bus splitting based network splitting is used for dividing the full system into two parts. For each boundary bus, a dummy bus is created during the network splitting stage. The original boundary bus and the dummy bus are assigned to the detailed system and the external system, respectively, as shown in Fig. 1.71(b). In order to make the splitting scheme

compatible with the MATE-based TS co-simulation algorithm, a “virtual breaker” is introduced to link the original boundary bus and the dummy bus.

(2) Simulation switching controller and the switching criteria

After the disturbance or fault is isolated, it generally takes 0.1 - 0.5 s for the system to transit from a fast dynamic state to a slow dynamic state where the system can be adequately represented by phasor models. Thus, a time delay can be used to account for this transition period before switching from EMT simulation to TS simulation. Some a priori knowledge of the simulated system and phenomenon involved can help in choosing an appropriate value for this delay setting. Based on the simulation experiences, the default delay setting is chosen to be 0.2 s.

Once the time delay criterion is met after a fault is cleared, the switching controller begins to compare the boundary conditions obtained from the dynamic simulation of the detailed system and the TS simulation of the external system. Similar to reconnecting a generator to the grid, one primary requirement of reconnecting the detailed and external systems as an integrated system is that boundary conditions of the detailed and external systems should be very close. The key parameters that can represent the boundary bus conditions include the bus voltage (both magnitude and angle), the current through the boundary and the power exchange through the boundary. Given that the Norton equivalent of the external system is used in the dynamic simulation of the detailed system, if the boundary bus voltages obtained by the dynamic simulation of the detailed system and the TS simulation of the external system are the same, the currents and powers through the boundary in both simulations must be the same. Therefore, the voltage is selected as the monitored parameter in this implementation.

The maximum difference of the boundary bus voltages between the detailed system and the external system is used as the indicator for simulation switching. At each step, this indicator is calculated and compared with a preset tolerance (for example 0.005 pu). Furthermore, in order to make sure the boundary conditions of the detailed and external systems truly converge, the maximum voltage difference must be within the preset tolerance for a reasonably long period (for example, several cycles). Once these two criteria are satisfied, the simulation switch controller outputs a signal to indicate that the simulation can be switched to the TS simulation starting from the following time step.

(3) Discrete event signals obtained from the EMT simulation are utilized to enhance the accuracy of the dynamic simulation of the detailed system

One necessary condition for the simulation results obtained from the EMT simulation and the dynamic simulation to converge after the fast transients settle down is that the critical discrete events (such as control actions and operation mode changes), if any, are adequately represented by the dynamic simulation (assuming that these events are accurately captured by the EMT simulation). Based on past experiences, such a condition cannot be satisfied in some cases due to the inherent modeling limitations of the dynamic simulation as well as the modeling differences between the EMT and the dynamic simulations.

The approach employed in the simulation design shown in Fig. 1.72 is straightforward. The critical discrete event signals obtained from the simulation results of the EMT simulation are transferred

to the dynamic simulation of the detailed system and used as external control signals either to override the corresponding internal control signals or to directly control the corresponding devices. It should be noted that since only critical discrete event signals, such as A/C motor operation state change and inverter blocking signal due to commutation failure, are considered, the additional communication overhead is negligible. In addition, this function is optional, and it is recommended to be used based on the requirement of the study system.

1.7.3 Test case

The proposed advanced EMT-TS hybrid simulation with the capability of switching back to TS simulation has been tested with a modified IEEE 9 bus system. Originally, the loads served by bus 5 are represented as an aggregated load and directly connected to the 230 kV bus. In this test case, the aggregated load at bus 5 is replaced by an equivalent subtransmission and distribution system, as shown in Fig. 1.75. Modeling of the sub-transmission and distribution system is shown in Fig. 1.75.

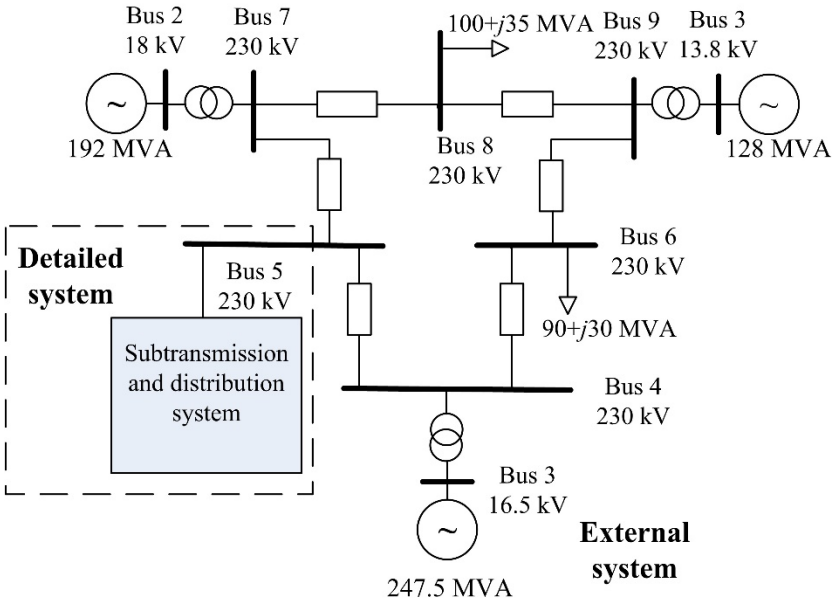

Fig. 1.48 One-line diagram of a modified IEEE 9 bus system

The loads are connected to an equivalent feeder. As for the load composition, 50% of the total load in terms of active power is represented by single-phase residential A/C motors, while the remainder is modeled as constant impedances in the TS simulation. When the detailed system is simulated by EMT simulation, the POW detailed A/C model is used. On the other hand, when the detailed system is simulated by three-phase dynamic simulation, the A/C performance model developed in section 1.6.3.3 is used to represent the A/Cs. In the test cases, the TS simulation time step is set at 0.005 s and the EMT simulation time step is chosen to be 20 μs.

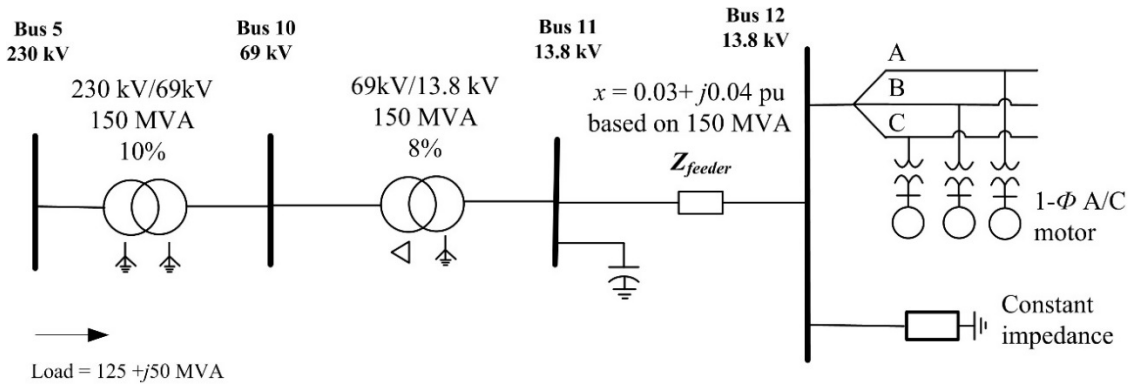

Fig. 1.49 Modeling of the sub-transmission and distribution system served by bus 5

1.7.3.1 Use of Discrete Event Signals to Reconcile the Two Detailed System Simulations

A SLG fault is applied to bus 10 at 0.5 s and cleared after 0.07 s. In order to better study the effects of using discrete event signals from the EMT side to enhance the accuracy of TS simulation, the simulation switching function is disabled. The simulation results without and with sending the A/C motor operation status signals from the EMT side to 3-phase dynamic simulation are shown in Fig. 1.77 and Fig. 1.78, respectively.

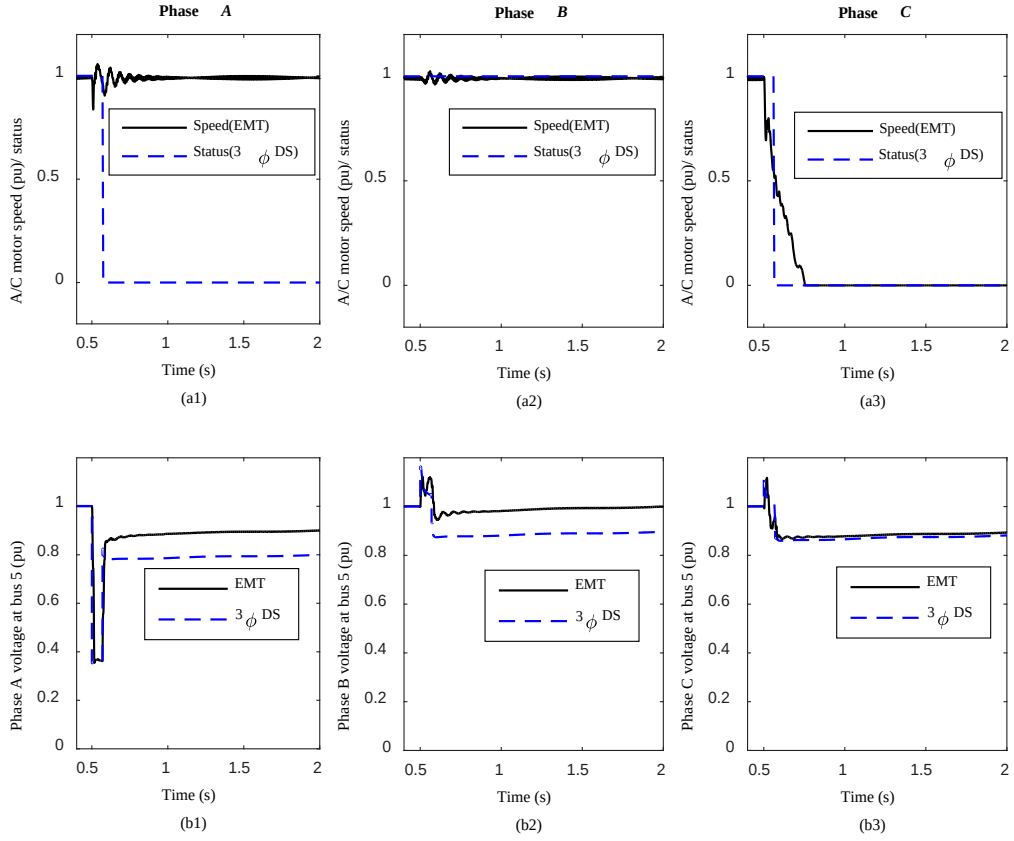

Fig. 1.50 Simulation results of the detailed system without sending the A/C motor status signals obtained from the EMT simulation to the 3-phase dynamic simulation.

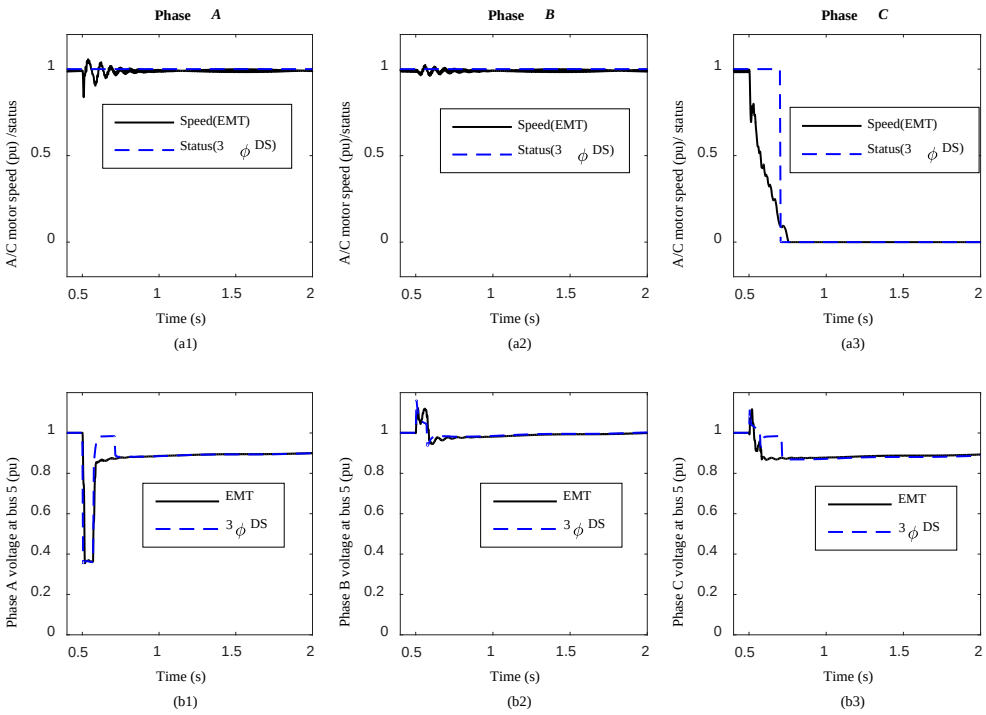

Fig. 1.51 Simulation results of the detailed system with sending the A/C motor status signals obtained from the EMT simulation to the 3-phase dynamic simulation

In the scenario without sending the A/C motor operation status signals from the EMT side to three-phase dynamic simulation, simulation results of the EMT and the dynamic simulation are significantly different in terms of A/C motor stalling. A/C motors on two phases stalled in the detailed system simulated by the 3-phase dynamic simulation. In contrast, the EMT simulation results show that only the A/C motor on phase *C* stalled. This difference results in significant differences between the two simulation results in the three-phase voltages of the boundary bus (bus 5 in this case.) the proposed simulation switching criteria are not satisfied and the simulation keeps running in the hybrid simulation mode till the end of the whole simulation.

In the scenario with sending the A/C motor operation status signals from the EMT side to 3-phase dynamic simulation, the A/C stalling results are coordinated to make sure A/C motors in the dynamic simulation are in the same status as those simulated by the EMT simulation during stage 2. While there are some discrepancies observed in the three-phase boundary bus voltages after the fault is cleared, the discrepancies last only a short time period (approximately 0.15 s) and disappear after the A/C motor on phase *C* effectively stalls in both the EMT simulation and the three-phase dynamic simulation.

The discrepancies discussed above is related to the A/C motor stalling process, which is simulated in the EMT simulator, but cannot be represented by the performance model of the A/C motor in the dynamic simulation. During the A/C motor stalling process, the reactive power drawn by the A/C motor on phase *C* increases significantly when the A/C motor speed decreases to lower than 0.5 pu, as shown in Fig. 1.79. The increased reactive power consumption depresses the voltages of both phase A and C of bus 5 after the fault is cleared, as shown in Fig. 1.77 (b1)-(b3). On the other hand, before receiving the A/C motor stalling signals from the EMT side, all three A/C

motors operate in the running mode in the detailed system simulated by the three-phase dynamic simulation. After the fault is cleared, the bus voltages recover to the levels close to their pre-fault values. These different responses of the A/C motors in the two detailed system simulations contribute to the discrepancies shown in Fig. 1.77(b1)-(b3).

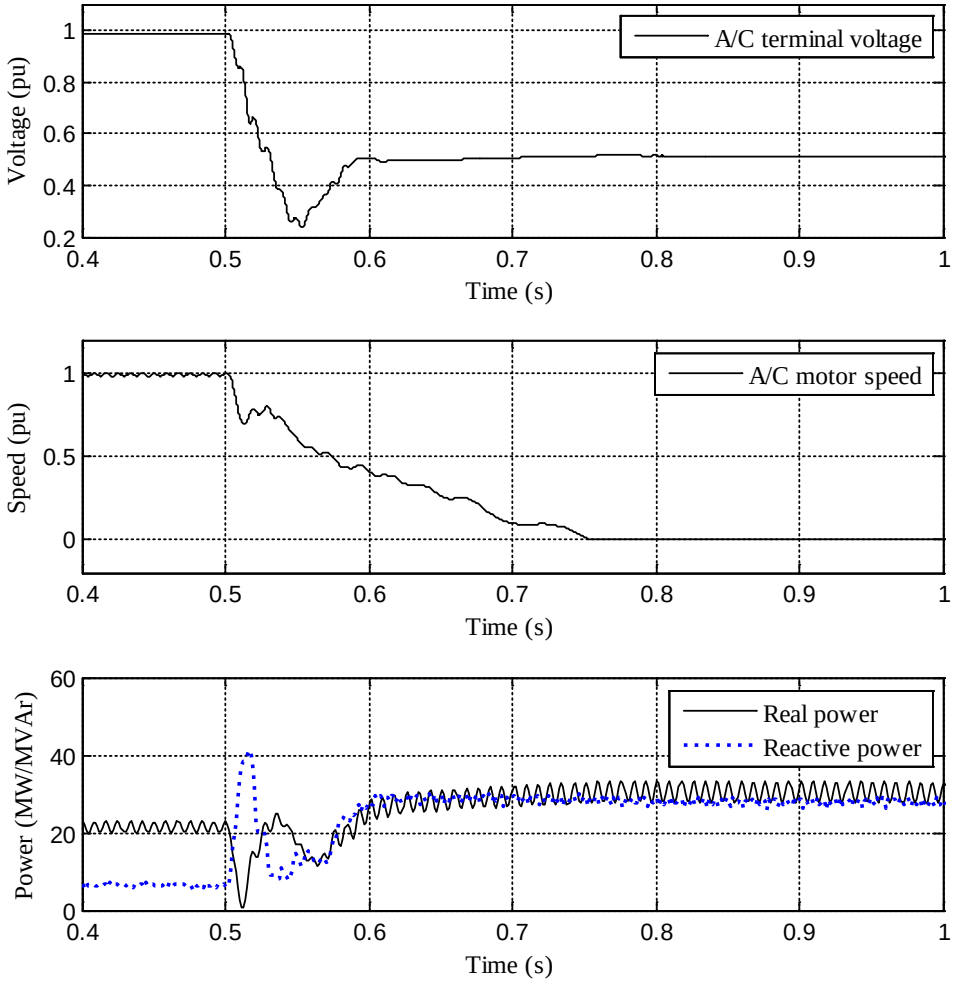

Fig. 1.52 EMT simulation results of the A/C motor on phase C

1.7.3.2 Simulation Switching Criterion

Based on the discussions in Section 1.8.2.2, the proposed switching criterion is as follows: starting at 0.2 s after the fault is cleared, if the maximum difference of boundary bus voltages ($max\Delta V$) obtained by the dynamic simulation of the detailed and the external systems is less than 0.005 pu for more than 2 cycles, simulation will be switched from the EMT-TS hybrid simulation mode to the pure TS simulation mode.

The results in the last section show that the proposed approach can significantly reduce the simulation result discrepancy caused by the modeling difference of some components in the EMT and the TS simulation by coordinating the critical discrete events in the EMT simulation with the

TS simulation. With this approach applied to the test case, the monitored maximum bus voltage difference during stage 2 is shown in Fig. 1.80. The simulation is switched from the EMT-TS hybrid simulation to the pure TS simulation at 0.805 s, which is 0.235 s after the fault is cleared. It should be noted that the switching is performed under an unbalanced system condition. The simulation results are compared with that simulated by the hybrid simulation approach without switching back to TS simulation, which are shown in Fig. 1.81 and Fig. 1.82. The results of both approaches match closely, demonstrating the effectiveness of the proposed approach.

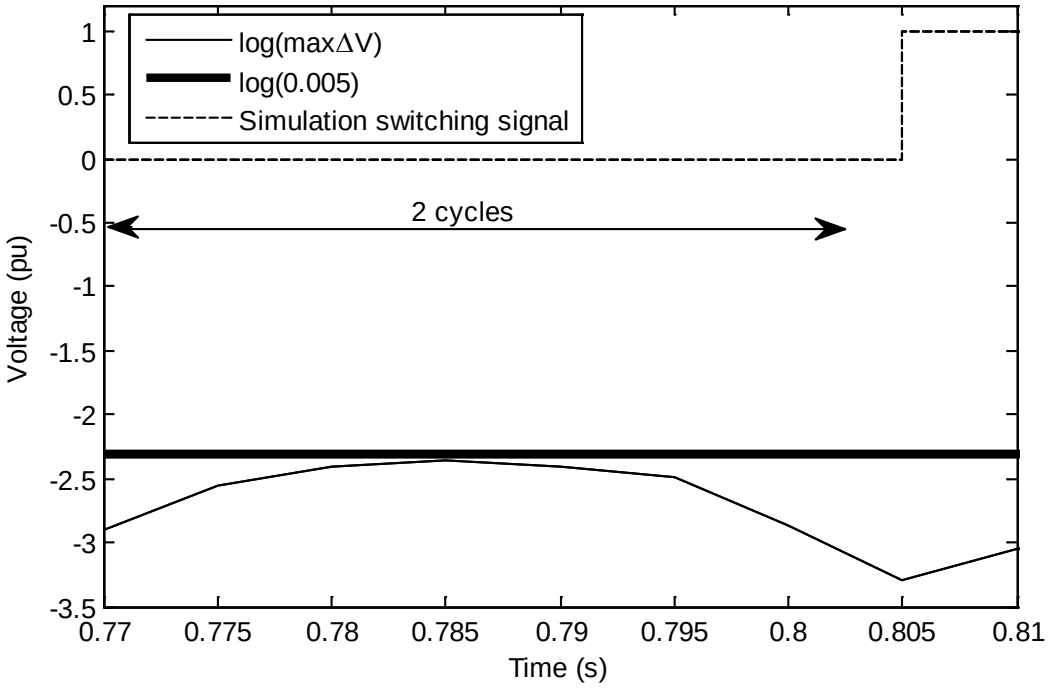

Fig. 1.53 The maximum difference of boundary buses and the switching signal

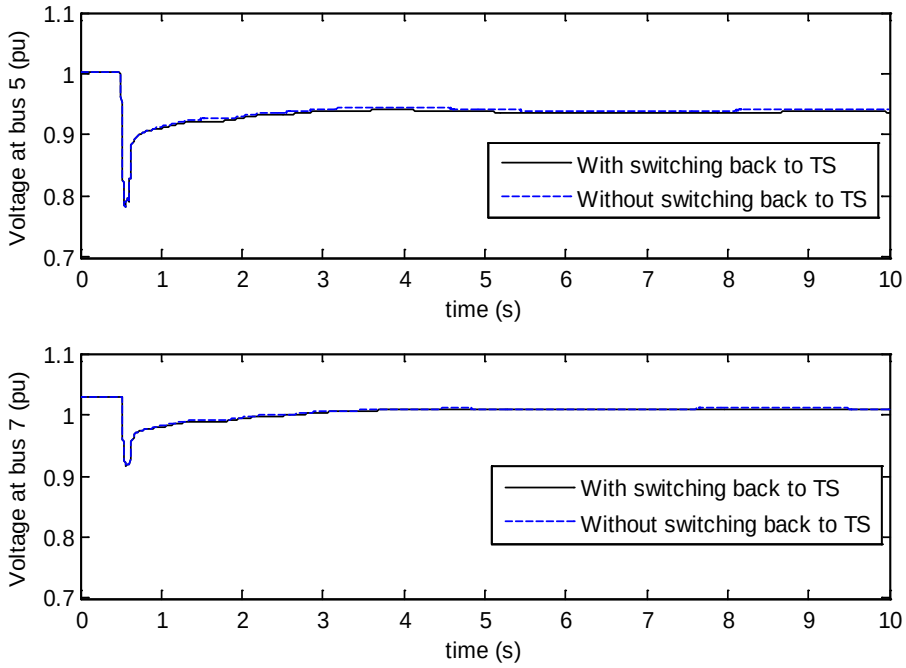

Fig. 1.54 Positive sequence voltages of bus 5 and bus 7

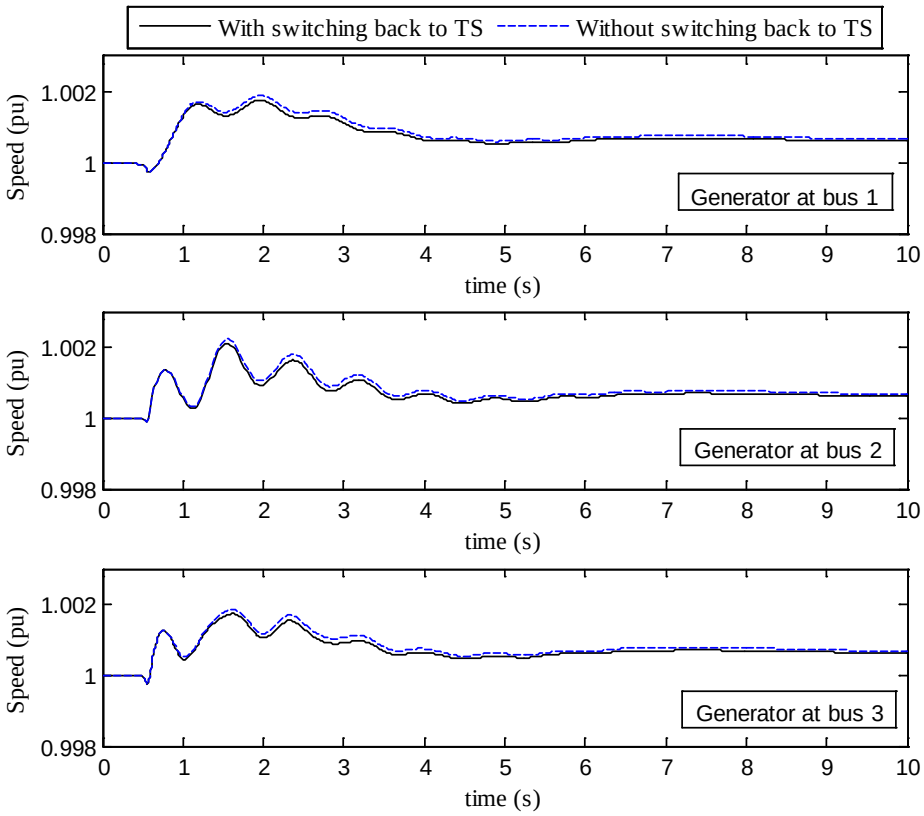

Fig. 1.55 Speeds of the generators at buses 1, 2 and 3

1.7.3.3 Computational Performance

The computational times of a 10 s simulation of the test system with different methods are shown in Table 1.11. Compared to the hybrid simulation without switching back to TS simulation, the proposed approach achieves a 91.86 % saving of computational time. In other words, for this specific case, the proposed approach is, on average, twelve times faster than the EMT-TS hybrid simulation without the capability of switching back to TS simulation.

Table 1.11 The computational times of different methods

Simulation method	**Computational time /s**
EMT-TS hybrid simulation without switching back to TS simulation	189.2
EMT-TS hybrid simulation with switching back to TS simulation	15.4
Three-phase TS simulation	1.2

1.8 Conclusions

Electromagnetic transient and electro-mechanical transient stability hybrid simulation has been investigated in this research. With the hybrid simulation approach, both the fast transients and slow dynamics can be adequately captured by the EMT and TS simulator, respectively, while simultaneously addressing the dilemma of handling both the detailed modeling and the large scale of the system being examined. The proposed approach and the developed simulation tool together provide necessary simulation capabilities to adequately investigate the interactions between the transmission and distribution systems, such as the FIDVR problem, as well as the dynamic performance of power systems interfaced with power electronic devices, such as HVDC systems.

The main contributions of this research are summarized as follows:

1. In Section 1.2, a three-phase Thévenin equivalent and a three-sequence current source equivalent for representing the external system and the detailed system, respectively, are proposed for hybrid simulation. Correspondingly, a three-sequence TS simulation algorithm is developed. These analytical developments facilitate the simulation of unsymmetrical faults inside the detailed system without extensively extending the boundary and the extent of the detailed system.
2. A new interaction protocol design combining both the serial and parallel interaction protocols in a flexible manner is developed to achieve good simulation performance without comprising the accuracy.
3. An open source tool for hybrid simulation has been developed in Section 1.3. A generic interface is designed for integrating with different EMT simulators.
4. The proposed hybrid simulation approach has been applied to a detailed FIDVR study on the WECC system in Section 1.4. Some significant insights on the evolution of a FIDVR event triggered by a normally cleared SLG fault are uncovered. With a typical

delta-wye grounded connection for step down transformers, the event begins with A/Cs stalling on two directly impacted phases, followed by A/C stalling propagating to the unfaulted phase. Further, the effects of the load composition and the point-on-wave of fault inception are also investigated.

5. A common modeling framework for integrated T&D system power flow and dynamic simulation is proposed. Then an integrated T&D power flow algorithm is solved by iteratively solving a three-sequence power flow for the transmission system and a three-phase power flow for each distribution system. For integrated T&D dynamic simulation, the multi-area Thévenin equivalent approach is employed to solve the integrated T&D networks. The integrated T&D simulation provides the capability to simulate the effects of persistent unbalanced loads and voltages in the distribution systems. This capability has been applied to study FIDVR events under unbalanced fault and unbalanced loads conditions.
6. An advanced EMT-TS hybrid simulation with the capability to switch back to the TS simulation has been developed in Section 1.7. The new simulation algorithm is developed by combining the EMT-TS hybrid simulation algorithm and the MATE-based dynamic simulation algorithm. The proposed algorithm effectively addresses the simulation efficiency issue of the original EMT-TS simulation for a long dynamic simulation.

References

[1] M. D. Heffernan, K. S. Turner, J. Arrillaga, and C. P. Arnold, "Computation of A.C.-D.C. System Disturbances - Part I, II and III," IEEE Transactions on Power Apparatus and Systems, vol. PAS-100, pp. 4341-4348, 1981.

[2] G. D. Irwin, C. Amarasinghe, N. Kroeker, and D. Woodford, "Parallel processing and hybrid simulation for HVDC/VSC PSCAD studies," in 10th IET International Conference on AC and DC Power Transmission, 2012, pp. 1-6.

[3] NERC Transmission Issues Subcommittee and System Protection and Control Subcommittee, "A Technical Reference Paper Fault-Induced Delayed Voltage Recovery," 2009.

[4] B. R. Williams, W. R. Schmus, and D. C. Dawson, "Transmission voltage recovery delayed by stalled air conditioner compressors," IEEE Transactions on Power Systems, vol. 7, pp. 1173-1181, 1992

[5] D. N. Kosterev and A. Meklin, "Load Modeling in WECC," in Proc. 2006 Power Systems Conference and Exposition, pp. 576-581.

[6] D. N. Kosterev, A. Meklin, J. Undrill, B. Lesieutre, W. Price, D. Chassin, et al., "Load modeling in power system studies: WECC progress update," in Proc. IEEE Power and Energy Society General Meeting, 2008, pp. 1-8

[7] Y. Liu, V. Vittal, J. Undrill, and J. H. Eto, "Transient Model of Air-Conditioner Compressor Single Phase Induction Motor," IEEE Transactions on Power Systems, vol. 28, pp. 4528-4536, 2013.

[8] G. W. J. Anderson, N. R. Watson, C. P. Arnold, and J. Arrillaga, "A new hybrid algorithm for analysis of HVDC and FACTS systems," in Proceedings of International Conference on Energy Management and Power Delivery,1995, vol.2, pp. 462-467.

[9] H. Su, K. Chan, L. A. Snider, and T. Chung. "A parallel implementation of electromagnetic electromechanical hybrid simulation protocol." In Proceedings of the 2004 IEEE International Conference on Electric Utility Deregulation, Restructuring and Power Technologies, vol. 1, pp. 151-155. 2004.

[10] F. Tian, C. Yue, Z. Wu, and X. Zhou, “Realization of electromechanical transient and electromagnetic transient real time hybrid simulation in power system,” in Proc. IEEE Power Eng. Soc. Transmission and Distribution Conf. Exhibit.: Asia and Pacific, 2005

[11] V. Jalili-Marandi, V. Dinavahi, K. Strunz, J. A. Martinez, and A. Ramirez, "Interfacing Techniques for Transient Stability and Electromagnetic Transient Programs," IEEE Transactions on Power Delivery, vol. 24, pp. 2385-2395, 2009.

[12] W. Liu, J. Hou, Y. Tang, L. Wan, X. Song, and S. Fan, "An electromechanical/electromagnetic transient hybrid simulation method that considers asymmetric faults in an electromechanical network," in 2011 IEEE/PES Power Systems Conference and Exposition, 2011, pp. 1-7.

[13] Y. Zhang, W. Wang., B. Zhang, and A. M. Gole, "A decoupled interface method for electromagnetic and electromechanical simulation," in 2011 IEEE Electrical Power and Energy Conference, 2011, pp. 187-191.

[14] X. Wang, P. Wilson, and D. Woodford, "Interfacing transient stability program to EMTDC program," in Proc. 2002 International Conference on Power System Technology, 2002. pp. 1264-1269 vol.2.

[15] Y. Zhang, A. M. Gole, W.Wu, B. Zhang and H. Sun, "Development and Analysis of Applicability of a Hybrid Transient Simulation Platform Combining TSA and EMT Elements," IEEE Transactions on Power Systems, vol. 28, pp. 357-366, 2013.
[16] A. M. Stankovic and T. Aydin, “Analysis of asymmetrical faults in power systems using dynamic phasors," IEEE Transactions on Power Systems, vol. 15, pp. 1062-1068, 2000.
[17] F. Gao and K. Strunz,“Frequency-adaptive power system modeling for multiscale simulation of transients”, IEEE Transactions on Power Systems, vol. 24, pp. 561-571, 2009.
[18] M. Sultan, J. Reeve, R. Adapa, "Combined transient and dynamic analysis of HVDC and FACTS systems," IEEE Transactions on Power Delivery, vol.13, no.4, pp.1271-1277,1998
[19] F. Plumier, P. Aristidou, C. Geuzaine, T. Van Cutsem, “A Relaxation Scheme to Combine Phasor-Mode and Electromagnetic Transients Simulations,” In Proceedings of Power Systems Computation Conference (PSCC), Wroclaw, Poland, Aug 18-22, 2014.
[20] A.A van der Meer; M. Gibescu, M.A.M.M.van der Meijden; W.L. Kling; J.A. Ferreira, "Advanced Hybrid Transient Stability and EMT Simulation for VSC-HVDC Systems," IEEE Transactions on Power Delivery. vol.30, no.3, pp.1057,1066, June 2015
[21] Manitoba HVDC Research Centre, PSCAD/EMTDC. Available from https://hvdc.ca/pscad/
[22] M. Zhou and S. Zhang, "Internet, Open-source and Power System Simulation," in IEEE PES General Meeting, 2007. pp. 1-5
[23] FREEDM distributed grid intelligence (DGI) Project. Available from https://github.com/FREEDM-DGI/FREEDM
[24] P. M. Anderson and A. A. Fouad, Power System Control and Stability (2nd Edition). Wiley-IEEE Press, 2002.
[25] William H. Kersting, Distribution System Modeling and Analysis (Second Edition), CRC Press, 2006, p.52-54
[26] M. A. Pai, Energy function analysis for power system stability: Springer Science & Business Media, 1989.
[27] M. Szechtman; T. Wess; C.V. Thio, "A benchmark model for HVDC system studies," International Conference on AC and DC Power Transmission, pp.374-378, 1991
[28] IEEE guide for planning dc links terminating at ac system locations having low short-circuit capacities, IEEE Std. 1204–1997, IEEE, Piscataway, NJ, 1997
[29] J. Peralta, H. Saad, S. Dennetière, J. Mahseredjian, and S. Nguefeu, "Detailed and averaged models for a 401-level MMC–HVDC system," IEEE Transactions on Power Delivery, vol. 27, pp. 1501-1508, 2012.
[30] H. Sun, Q. Guo, B. Zhang, Y. Guo, Z. Li, and J. Wang, "Master–slave-splitting based distributed global power flow method for integrated transmission and distribution analysis," IEEE Transactions on Smart Grid, vol.6, no. 3, pp. 1484-1492, 2015.
[31] Z. Li, J. Wang, H. Sun, and Q. Guo, "Transmission contingency analysis based on integrated transmission and distribution power flow in smart Grid," IEEE Transactions on Power Systems, vol. 30, no. 6, pp. 3356-3367, 2015.
[32] K. Kalsi, J. Fuller, et al. “Integrated transmission and distribution control,” [Online]. Available:http://www.pnnl.gov/main/publications/external/technical_reports/PNNL-22157.pdf

[33] B. Palmintier, E. Hale, et al. Integrated distribution transmission analysis for very high penetration solar pv. 2016, [Online]. Available: http://www.nrel.gov/docs/fy16osti/65550.pdf
[34] Petros Aristidou, and Thierry Van Cutsem. "A parallel processing approach to dynamic simulations of combined transmission and distribution systems," International Journal of Electrical Power & Energy Systems, vol.72, pp.58-65, 2015
[35] B. Stott, “Power system dynamic response calculations,” Proceedings of the IEEE, vol.67, no.2, pp.219-241, 1979
[36] P. Kundur, Power system stability and control. New York: McGraw-Hill, 1994
[37] Happ, Harvey H. "Diakoptics—the solution of system problems by tearing," Proceedings of the IEEE, vol. 62, no. 7, pp.930-940, 1974
[38] Marti, J. R., L. R. Linares, J. Calvino, H. W. Dommel, and J. Lin. "OVNI: an object approach to real-time power system simulators," in Proceedings of International Conference on Power System Technology, vol. 2, pp. 977-981. 1998.
[39] Martí, José R., Luis R. Linares, Jorge A. Hollman, and Fernando A. Moreira. "OVNI: Integrated software/hardware solution for real-time simulation of large power systems," In Proceedings of the Power System Computation Conference (PSCC), vol. 2, pp.1-6, 2002.
[40] Ehsan Nasr-Azadani, Claudio Canizares, Daniel E. Olivares, and Kankar Bhattacharya. "Stability analysis of unbalanced distribution systems with synchronous machine and dfig based distributed generators," IEEE Transactions on Smart Grid, vol.5, no. 5, pp.2326-2338, 2014
[41] Marcelo Elizondo, Francis K. Tuffner, and Kevin P. Schneider. "Three-phase unbalanced transient dynamics and powerflow for modeling distribution systems with synchronous machines," IEEE Transactions on Power Systems, vol. 31, no. 1, pp. 105-115, Jan. 2016.
[42] Erich Gamma, Richard Helm, Ralph Johnson, John Vlissides. Design patterns: elements of reusable object-oriented software. Pearson Education, 1994
[43] IEEE PES Distribution System Analysis Subcommittee, Distribution test feeders. [Online]. Available from: http://ewh.ieee.org/soc/pes/dsacom/testfeeders/

Part II

Hybrid Simulation Method

Sakis Meliopoulos
Jiahao Xie
Rohit Jinsiwale

Georgia Institute of Technology

For information about this project, contact:

Sakis A.P. Meliopoulos
Georgia Institute of Technology
School of Electrical and Computer Engineering
Atlanta, Georgia 30332-0250
Phone: 404-894-2926
E-mail: sakis.m@gatech.edu

Power Systems Engineering Research Center

The Power Systems Engineering Research Center (PSERC) is a multi-university Center conducting research on challenges facing the electric power industry and educating the next generation of power engineers. More information about PSERC can be found at the Center's website: http://www.pserc.org.

For additional information, contact:

Power Systems Engineering Research Center
Arizona State University
527 Engineering Research Center
Tempe, Arizona 85287-5706
Phone: 480-965-1643
Fax: 480-727-2052

Notice Concerning Copyright Material

Table of Contents

List of Figures

List of Tables

1. Introduction

1.1 Background

The proposed study is primarily motivated by the demand of better simulation tools for phenomena such as (a) FIDVR, (b) Geomagnetically Induced Currents, (c) HV ACDC systems, (d) inverter interfaced generation, etc. and associated studies in large power systems under unsymmetrical fault conditions. The computations are study of these phenomena requires time domain simulations. For large scale systems, such as a utility system, time domain simulation of the entire system is a practical impossibility. The objective of this project is to develop a hybrid method that will allow time domain analysis of selected parts of the system where subsystems of wind farms, FACTS devices, etc. while the rest of the system can be simultaneously modeled and analyzed with standard quasi-dynamic models.

The quasi-dynamic domain analysis is based on sequence components electromechanical models considering network unbalance and harmonic distortion. This enables the platform to simulate unbalance conditions to the subsystem modeled in this domain and to derive an equivalent at the interface that can be used for a simultaneous solution with the subsystem that is modeled in time domain. Although there is an additional computational effort in handling the three sequence networks in the quasi-dynamic simulation, the computational increase is only several times higher than the usual per phase based dynamic analysis and therefore still practical for large scale systems. The additional modeling, however, is required for a higher accuracy solution at the interface between the quasi-dynamic domain model and the time domain model.

Methods for quasi-dynamic domain analysis as well as time domain analysis have been well developed as independent methods. For a particular study, one can select one method or the other. The information obtained from these analyses is well understood, i.e. the ability of each approach to capture specific phenomena is well understood. The hybrid method aims at capturing effects of waveform distortion and power electronic control system on the time domain subsystem while capturing the electromechanical oscillations in the subsystem modeled in the quasi-dynamic domain. In order to accurately capture the interaction of the two models, it is necessary to obtain an accurate solution at the interface between the two subsystems. The report describes the overall approach and the implementation details for doing just that. A small scale example illustrates the feasibility of the method.

We have also investigated the implementation of the proposed method in an object-oriented approach. Specifically, the object orientation is achieved by expressing each component of the system into the SCAQCF standard. SCAQCF stands for State and Control Algebraic Quadratic Companion Form. It is derived by first using the standard model of a component in terms of linear and nonlinear, algebraic and differential equations in terms of state and control variables as well as inequalities imposed on controls and functions. These equations may be quasi dynamic for the use in electromechanical transient analysis or could be full dynamic for use in electromagnetic transient analysis. The model is quadratized by the introduction of additional variables, if necessary, and subsequently integrated with the quadratic integration method to yield the SCAQCF. This approach enables the expression of electromechanical models and electromagnetic

transient models to be expressed with the same syntax mathematical objects. These objects enable an object oriented implementation of the hybrid method.

1.2 Motivation and Objectives

The main motivation behind developing the hybrid approach stems from the general inadequacies of the transient stability programs to capture the dynamics created from new resources in the power system, such as wind farms, PV plants and in general power grid connected power electronics systems. As it has been mentioned it is a practical impossibility to use transient solvers for large scale power systems with wind farms and PV plants. The approach presented in this report it will make possible to use the same platform for Time domain, Phasor domain or hybrid scheme approaches. The developed platform could be used to analyze phenomena such as Fault Induced Delayed Voltage Recovery, simulation of AC-DC hybrid systems, simulation of large system under geomagnetically induced currents, etc.

The hybrid method significantly reduces computation burden compared to traditional transient simulation packages. A large influx of inverter interfaced generation can be observed in current power systems. Nonlinear and switching phenomena in such systems can be analyzed using the hybrid method.

A major problem with interfacing the two domains lies in the assumptions made while simulating systems in the Phasor Domain. Models in the phasor domain are designed to evolve at 60 Hz. Because the models do not account for harmonic content which is ever present in systems with power electronic subsystems, these models are not directly interfacable with time domain analysis models. We propose new schemes to account of harmonic propagation into the quasi-dynamic models. The interfacing protocol is largely designed by obtaining reduced equivalents for each domain at the interface boundary. Reduced equivalents of quasi-dynamic domain models at the interface are computed by linearizing the quasi dynamic models. The simulation fidelity remains high because of the slow dynamics of these systems. Numerical experiments show reasonable accuracy of the approach.

1.3 Organization of the Report

The report is structured so as to provide an overview of the proposed hybrid simulation method. The standard SCAQCF (State and Control Algebraic Quadratic Form) is illustrated below. The format is developed by using the Quadratic Integration Approach. This involves converting the algebraic and differential equation to equations that are quadratic at most. The equations are then discretized using a second order polynomial basis. The method results in the illustrated SCAQCF format. As long as each model is arranged in this format the approach illustrated below holds.

The QD-QACF approach is then illustrated. Here an approach is proposed to reduce the SCAQCF model for the Quasi-Dynamic subsystem to obtain an equivalent at the interface. The method to handle harmonics at the interface for the Quasi-Dynamic domain model is also introduced. The report then describes TD-QACF approach, which connects QD-QACF system to the Time domain part. Finally, the method for simultaneous simulation of two domains is presented.

In appendix, there are illustrative cases explaining the hybrid method. First, a test system is chosen and models are designed in the Quasi-Dynamic domain. These models are then tested to verify their accuracy. Some transient phenomenon can be observed in the simulation performed. Using the standard SCAQCF format an approach called QD-QACF reduction is then presented. This approach is implemented on the test system. The obtained reduced model can then be used to test the proposed Hybrid simulation scheme. Then, a demonstration case is presented to compare the performance of time domain and phasor domain. Comparison is performed by simulating entire system in time domain and then in phasor domain.

2. Literature Review

Increased adoption of Distributed Energy Resources (DERs) has necessitated incorporation of inverter interfaced generation in conventional power systems. Fast switching devices are thus introduced into the system. In addition to increasing computational burden, the harmonic footprint introduced by these components has increased as well. Analysis of such components necessitates the use of Time-Domain analysis. However, owing to the size of the system, this process becomes inefficient. Traditional Quasi-Dynamic approaches exist for simulating large scale systems. These approaches incorporate information from the sequence components for the system and couple them with the dynamics of the electromechanical systems. Typical of this approach are the traditional transient stability programs. We refer top these methods as the Quasi-Dynamic domain analysis.

The main disadvantage with using Quasi-Dynamic methods for simulating these systems is that they are unable to maintain accuracy while simulating systems with wind farms, PV plants, etc. Some methods have been devised in previous literature to solve this dilemma. The scale of the system can be reduced by modeling a large portion of the system as a Norton or Thevenin equivalent [6], [7]. The main drawback of this approach is that the dynamic response of the subsystem cannot be accurately captured. Another alternative method that has been used is the dynamic phasor approach [1]. This approach involves decomposing the signals from the subsystem to obtain time-varying Fourier components. These components can be encoded into device models so as to simulate the subsystem while preserving the harmonic content. Another approach involves using a frequency adaptive modeling approach [2]. This approach involves creating models by shifting the Fourier spectrum of the signals from the subsystem around a different frequency range to obtain multi-frequency models. Although these approaches maintain a good level of accuracy and are stable, they necessitate an algorithm to decompose the system heavily which significantly increases the computational burden.

Another method [4] involves modeling the subsystems independently in Phasor and Time domain and using an interface protocol to bridge the two. The method is similar to previous approaches in that a current source is created to serve as an equivalent for the Phasor network and a voltage source is created for the Time domain network. However, the approach in this reference involves dynamic modulation and demodulation of the equivalents to reduce the error. The current equation at the Time domain interface is demodulated to develop an equivalent for the phasor network. Conversely, the voltage term at the Phasor domain port modulates an ideal voltage source connected to the Time domain port. In order to estimate the current phasor from the time domain port phase locked loops and Goetzel DFT filter have been proposed. The caveat to using this approach is that the DFT algorithm requires a certain amount of past history to estimate the phasor equivalent for the time domain current thereby not making it *real time*. Also, the filter in this approach is efficient when it comes to isolating one frequency but fails to capture harmonic data at the interface. Another method illustrated by *Meyer, Dommel* [9] shows a technique to converge to adequate Fourier components using each network model and using these Fourier components to achieve equivalents. Although, this approach captures the harmonic data efficiently, it tends to be computationally intensive for large systems.

A similar method [10] has been developed to perform the equivalent operations on the Quasi-dynamic Domain side of the system. Here, the DFT algorithm extracts positive, negative and zero sequence equivalents from the Time domain subsystem. Thus, dynamic models are generated on

the Phasor/Quasi-dynamic domain side instead of switching to the traditional Time-Domain equivalent technique. Although the approach accelerates the speed of simulating a particular time frame, the accuracy by simulating in the Quasi-dynamic Domain side is seriously compromised. The harmonic content is mostly lost. This approach is not as accurate for subsystems with nonlinear switching devices due to the same reason.

A method proposed in [5] involves constructing the system matrix for the phasor domain side of the system and reducing it to achieve symmetry along the diagonal so as to convert it to a traditional impedance network. An equivalent for this impedance network is then created to interface with the time domain network and achieve convergence. However, it is possible to see that the slow varying dynamics are almost ignored and the approach does not take into account the transient stability paradigm.

One of the approaches towards developing accurate equivalents has been highlighted in [8]. Here an approach is developed towards generating an equivalent lumped impedance network. The network is modeled so as to achieve the exact transient response of the Quasi-Domain model. A lumped network with RLC components is created to replicate the dynamic response of the network. This network can then be used to reduce system size and achieve simultaneous simulations.

Regarding numerical integration methods, the trapezoidal integration method or higher order Runge-Kutta methods for simulating large systems are popular. These methods are extensively used for the traditional transient stability analysis. Our research team has been successfully using the Quadratic Integration method to simulate complex systems. It has been shown that the Quadratic Integration method exhibits greater accuracy and stability properties compared to traditional method [3]. Quadratic Integration method also performs well in simulating switching devices owing to its ability to naturally suppress fictitious oscillations observed when using trapezoidal integration method. For this reason the proposed hybrid simulation method is based on the quadratic integration method.

3. Overview of Hybrid Method

The objective of this project is to develop an accurate, robust, and efficient simulation method while maintaining the ability to capture nonlinearities and switching actions of power electronic subsystems and reduce computational burden. Increased adoption of renewable resources has made switching devices a necessity. To capture nonlinearities and switching actions of these devices, a time domain method is required. A promising approach is to model these subsystems in the time domain, while the remaining (the legacy power system) in the frequency domain. Some approaches use a sequential solution between the two domains. Sequential solutions in general may generate substantial discrepancy errors at the interface, especially when the waveform distortion is ignored at the interfaces. In addition, convergence is in general not linear. To avoid these problems, we propose an approach that achieves simultaneous solution at the interface between the two domains. Our approach involves generating three phase asymmetrical models for system components and discretizing them using the Quadratic Integration approach. These models can be developed in the frequency (quasi-dynamic) domain (QD-QACF) or in the time domain (TD-QACF). The time domain approach captures nonlinearities and switching adequately and generates a highly accurate model. The frequency (quasi-dynamic) domain approach, models electrical quantities with phasors and the slow dynamics (electromechanical oscillations and control actions) with differential equations, as a result electrical transients are ignored. In summary, our approach allows separation of a large power system into two subsystems, one modeled in the frequency (quasi-dynamic) domain and the other in the time domain. At the interface of the two subsystems the two models are matched and solved simultaneously. Description of the method is provided next, including the formulation and experimentation of the proposed method.

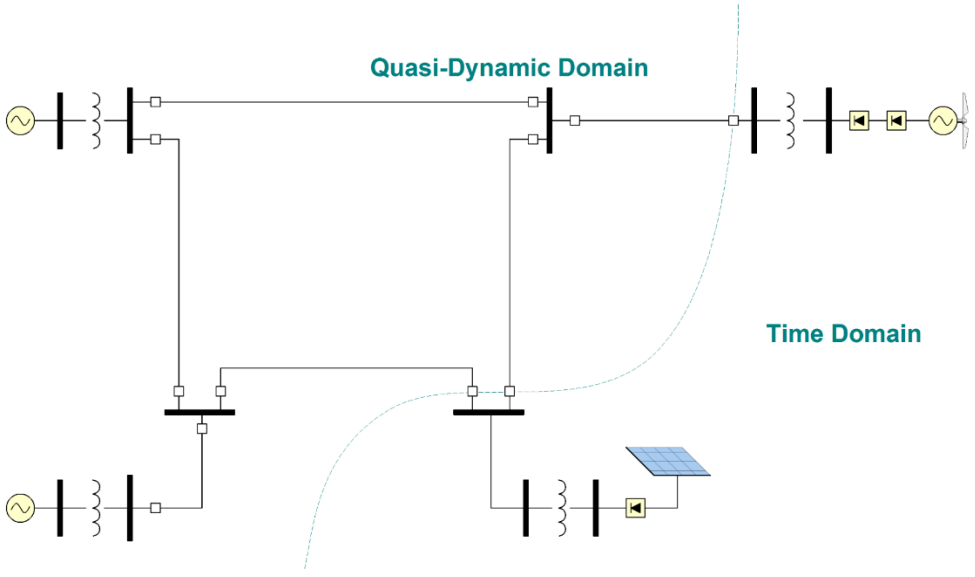

Figure 2.1: Arbitrary Separation of a Large System into Two Subsystems

The separation of the bulk power system into two subsystems is arbitrary as shown in Figure 2.1. The separation defines the interface between the two subsystems. One subsystem is modeled in

the frequency domain (model QD-QACF) and the other subsystem is modeled in the time domain (TD- QACF). The first model is in terms of phasor voltages and currents (as well as generator speed, phase angle, etc.) and the second model is in terms of time domain values of voltages and currents. At the interface, a simultaneous solution must be obtained by converting one of the models to the other domain. Specifically, the QD-QACF model is converted into an equivalent time domain model at the interface. This equivalent is combined with the TD- QACF model to provide the simultaneous solution.

Consider the QD-QACF model of the subsystem that has been modeled in the frequency domain. Linearization and Kron reduction provides the equivalent QD-QACF model at the interface of the two subsystems. The result below shows the equations expressed in term of real and imaginary parts of currents and states of the subsystem.

$$\begin{bmatrix} I_{r,\text{int}}(t) \\ I_{i,\text{int}}(t) \\ 0 \\ I_{r,\text{int}}(t_{mq}) \\ I_{\text{i,int}}(t_{mq}) \\ 0 \end{bmatrix} = Y_{eqqd}\begin{bmatrix} x(t) \\ x(t_{m_q}) \end{bmatrix} + \left\langle \begin{bmatrix} x(t) \\ x(t_{mq}) \end{bmatrix}^T F_{eqqd}\begin{bmatrix} x(t) \\ x(t_{mq}) \end{bmatrix} \right\rangle - b_{eqqd}$$

Upon application of linearization and Kron reduction, we obtain:

$$\begin{bmatrix} I_{r,\text{int}}(t) \\ I_{i,\text{int}}(t) \\ I_{r,\text{int}}(t_{mq}) \\ I_{\text{i,int}}(t_{mq}) \end{bmatrix} = Y_{Keqqd}\begin{bmatrix} x_{\text{int}}(t) \\ x_{\text{int}}(t_{mq}) \end{bmatrix} + \left\langle \begin{bmatrix} x_{\text{int}}(t) \\ x_{\text{int}}(t_{mq}) \end{bmatrix}^T F_{Keqqd}\begin{bmatrix} x_{\text{int}}(t) \\ x_{\text{int}}(t_{mq}) \end{bmatrix} \right\rangle - b_{Keqqd}$$

Next these equations are converted into time domain equations at instances coinciding with the time step of the time domain model. The time domain equivalent equations are given below. Derivation of these equations is provided in the next sections.

$$i_{\text{int}}(t) = I_{r,\text{int}}(t) = QF_t\left(x_{\text{int}}(t), x_{\text{int}}(t_{mq})\right)$$

$$i_{\text{int}}\left(t - h_q / N\right) = i\left(t - h_q\right) + b\left(t - h_q / N\right) + c\left(t - h_q / N\right)^2$$

$$i_{\text{int}}\left(t - 2h_q / N\right) = i\left(t - h_q\right) + b\left(t - 2h_q / N\right) + c\left(t - 2h_q / N\right)^2$$

$$i_{\text{int}}\left(t_{mq}\right) = I_{r,\text{int}}\left(t_{mq}\right) = QF_{t_{mq}}\left(x_{\text{int}}(t), x_{\text{int}}\left(t_{mq}\right)\right)$$

The overall approach is shown in Figure 2.2 and Figure 3.3. Note that the frequency domain model is integrated with time step, h_q, while the time domain model is integrated with time step h. For

practical reasons, our approach requires that h_q is a multiple integer of h. Note that the above computational procedure to achieve simultaneous solution is repeated each $h_q/2$ time step.

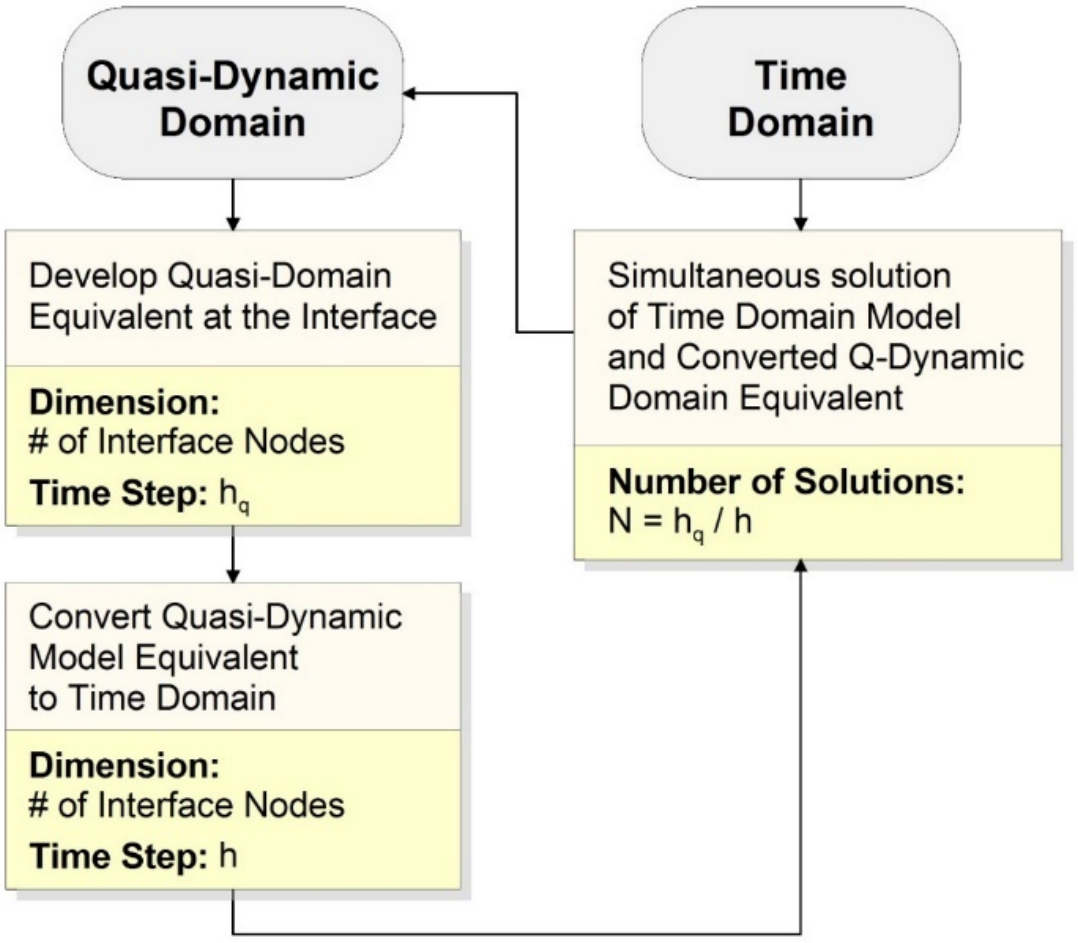

Figure 2.2: Proposed Approach for Simultaneous Solution at the Interface

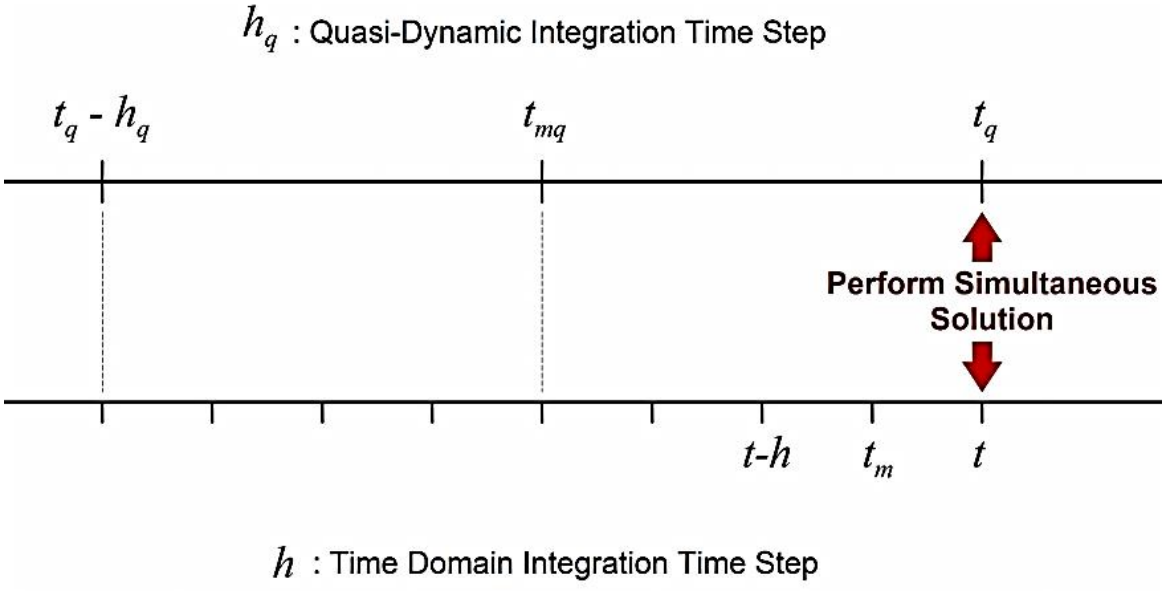

Figure 2.3: Simulation Steps in Time Sequence

Another issue is waveform distortion at the interface of the two subsystems. Specifically, the subsystem that contains power electronics and nonlinear devices may generate distortion (harmonics) that may be injected into the other subsystem via the interface. The level will depend on the harmonic impedances of the subsystem. For this reason, the QD-QACF model is computed at various frequencies over a user selected frequency range of interest. Then harmonic equivalent QD-QACF models are computed at the interface. The overall approach is shown in Figure 2.4. Note that we propose to use models up to the 11^{th} harmonic.

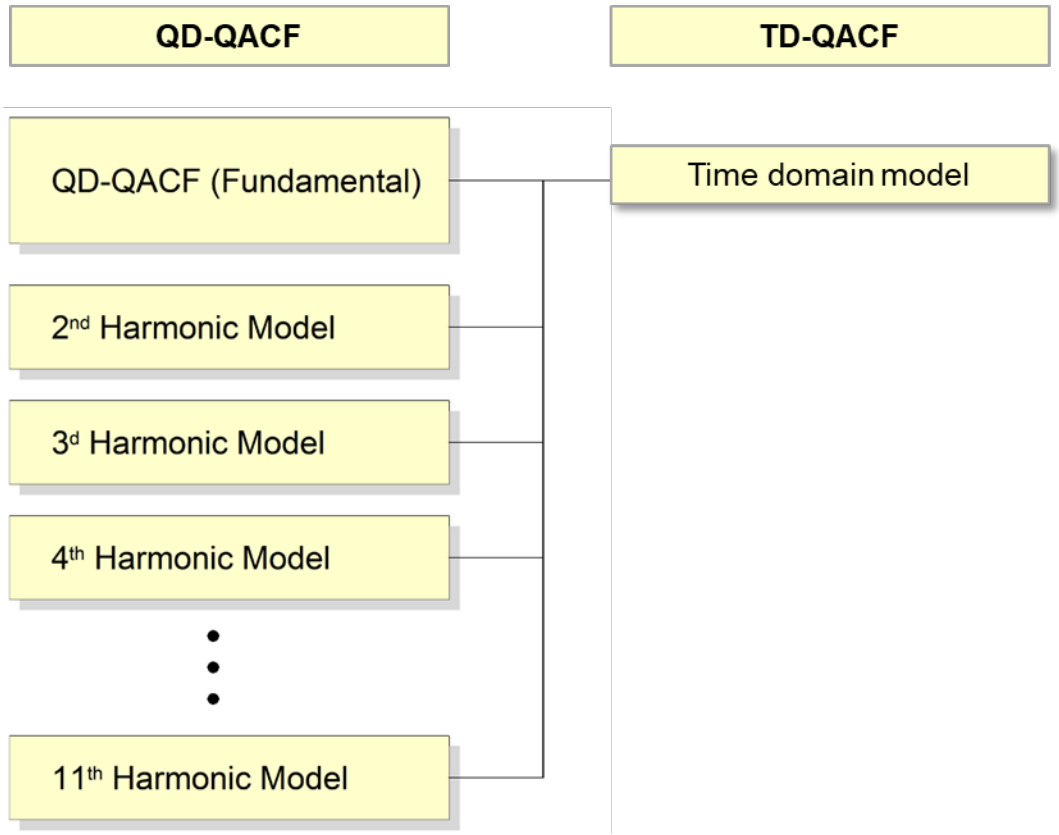

Figure 2.4: Modeling Waveform Distortion at the QD/TD Interface

4. The QD-QACF Approach

In order to reduce computational burden, we split a given topology arbitrarily into two domains – Time domain and Quasi-dynamic domain. Given the fact that the Quasi-dynamic domain operates on a much larger time step a scheme has been proposed to achieve simultaneous solutions with the Time domain component of the system. The scheme involves reducing the Quasi-dynamic domain system so that the set of equations only depends on the interface nodes. Since the equations are derived using the Quadratic Integration Approach a suitable quadratic polynomial is derived for each of the Quasi-dynamic domain subsystem equations. This polynomial is used with the Time domain model to achieve simultaneous solutions at the interface. The approach summarized above is presented in more detail below.

4.1 Quasi-Dynamic Domain Device Model

A Quasi-dynamic domain AQCF model has the mathematical form presented below. The ACQF model is obtained from the Quadratized Device Model (QDM).

$$\begin{Bmatrix} \tilde{I}(t_q) \\ 0 \\ 0 \\ \tilde{I}(t_{mq}) \\ 0 \\ 0 \end{Bmatrix} = Y_{eqx}\tilde{\mathbf{x}} + \begin{Bmatrix} \vdots \\ \tilde{\mathbf{x}}^T \left\langle F^i_{eqx} \right\rangle \tilde{\mathbf{x}} \\ \vdots \end{Bmatrix} + Y_{QDequ}\tilde{\mathbf{u}} + \begin{Bmatrix} \vdots \\ \tilde{\mathbf{u}}^T \left\langle F^i_{equ} \right\rangle \tilde{\mathbf{u}} \\ \vdots \end{Bmatrix} + \begin{Bmatrix} \vdots \\ \tilde{\mathbf{u}}^T \left\langle F^i_{equx} \right\rangle \tilde{\mathbf{x}} \\ \vdots \end{Bmatrix} - B_{eq}$$

$$B_{eq} = -N_{eq,x}\tilde{\mathbf{x}}(t_q - h_q) - N_{eq,u}\tilde{\mathbf{u}}(t_q - h_q) - M_{eq}\tilde{I}(t_q - h_q) - K_{eq}$$

Where,

Y_{eqx} : matrix defining the linear part for state variables,

F_{eqx} : matrices defining the quadratic part for state variables,

Y_{equ} : matrix defining the linear part for control variables,

F_{equ} : matrices defining the quadratic part for control variables,

F_{equx} : matrices defining the quadratic part for the product of state and control variables,

B_{eq} : history dependent vector of the device model,

$N_{eq,x}$: matrix defining the last integration step state variables part,

$N_{eq,u}$: matrix defining the last integration step control variables part,

M_{eq} : matrix defining the last integration step through variables part,

K_{eq} : constant vector of the device model,

Here, the first set of equations corresponds to the through variables (i.e. the currents entering the device), the second set consists of the linear internal equations and the third set consists of the nonlinear (quadratic) equations. This model has been derived by integration of the quasi-dynamic model using the quadratic integration method with a time step h_q. In order to interface this to the time domain system it needs to be converted into an equivalent at the interface nodes and in time domain. The process used involves linearization, Kron reduction and conversion of phasor equations into time domain equations.

4.2 Quasi-Dynamic Domain Network Model

The AQCF models for each component in a system are presented in the form illustrated in the previous section. Given various models conforming to the SCAQCF format, it is possible to construct the model for a whole system.

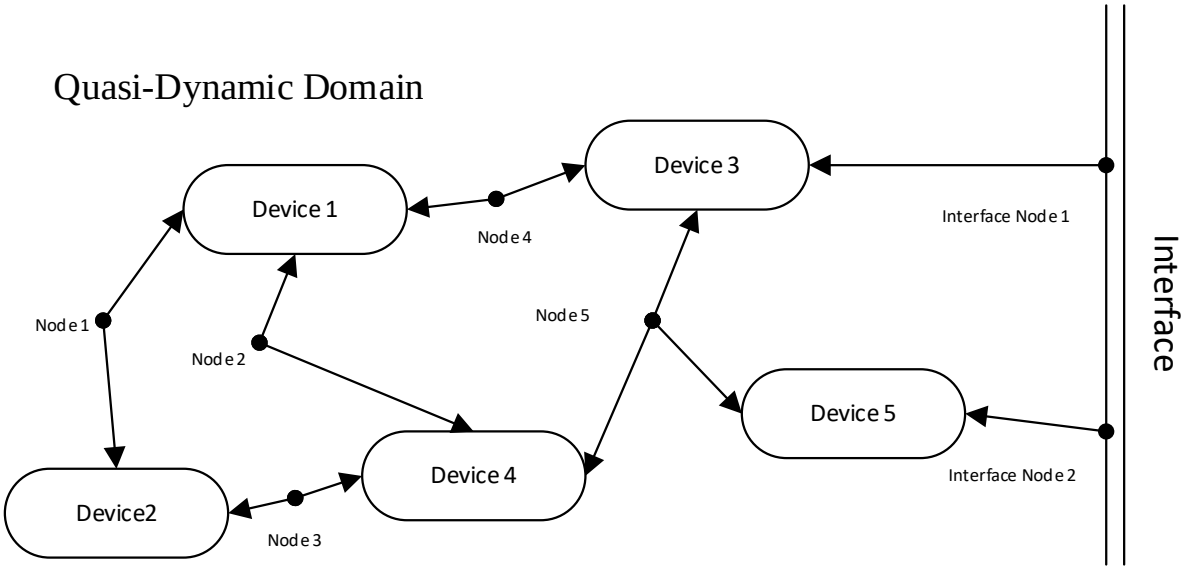

Figure 3.1: A Network of Devices in QD domain

Consider the network of devices in Figure 4.1. This system consists of multiple devices connected at different nodes. Each device in the above topology has a set of equations conforming to the SCAQCF format. The SCAQCF format consists of a series of equations a subset of which consists of the through current entering each device. Now by applying Kirchhoff's Current Law (KCL) at the nodes the through variables (currents) are eliminated. By appending the internal equations of all devices to the resulting equations, the network model is obtained.

For example, consider **Node 1**. The Devices 1 and 2 are connected at Node1. Consider the SCAQCF models for each of these devices.

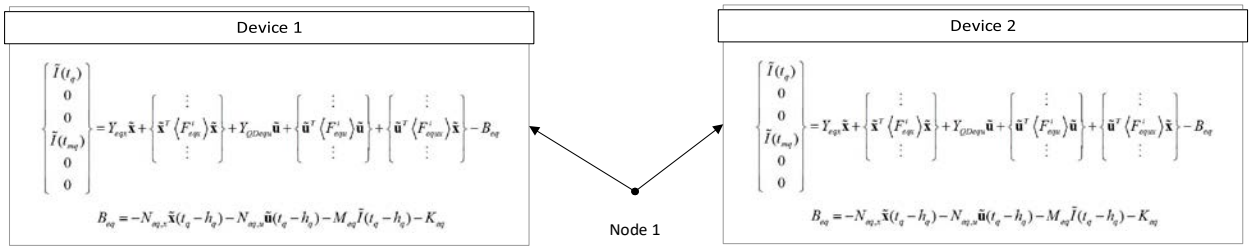

Figure 3.2 Interface at Node1

At Node 1

$$0 = \tilde{I}(t_q)_{Device1} + \tilde{I}(t_q)_{Device2}$$

$$0 = \tilde{I}(t_{mq})_{Device1} + \tilde{I}(t_{mq})_{Device2}$$

The rest of the internal equations can be appended to the system of equations obtained above. Hence, provided that the models for each of the components are modeled in the standard SCAQCF format, the same approach can be applied to each node to develop a model for the whole system.

This object-oriented approach enables construction of the full system model. Since, the interface nodes are open circuited, the model for the full system will look exactly similar to the standard SCAQCF model for each component.

$$\begin{Bmatrix} \tilde{I}(t_q) \\ 0 \\ 0 \\ \tilde{I}(t_{mq}) \\ 0 \\ 0 \end{Bmatrix} = Y_{eqx}\tilde{\mathbf{x}} + \begin{Bmatrix} \vdots \\ \tilde{\mathbf{x}}^T \left\langle F^i_{eqx} \right\rangle \tilde{\mathbf{x}} \\ \vdots \end{Bmatrix} + Y_{QDequ}\tilde{\mathbf{u}} + \begin{Bmatrix} \vdots \\ \tilde{\mathbf{u}}^T \left\langle F^i_{equ} \right\rangle \tilde{\mathbf{u}} \\ \vdots \end{Bmatrix} + \begin{Bmatrix} \vdots \\ \tilde{\mathbf{u}}^T \left\langle F^i_{equx} \right\rangle \tilde{\mathbf{x}} \\ \vdots \end{Bmatrix} - B_{eq}$$

$$B_{eq} = -N_{eq,x}\tilde{\mathbf{x}}(t_q - h_q) - N_{eq,u}\tilde{\mathbf{u}}(t_q - h_q) - M_{eq}\tilde{I}(t_q - h_q) - K_{eq}$$

Where,

$\tilde{I}(t_q)$ = Currents flowing into subsystem interface terminal at time t_q

$\tilde{I}(t_{mq})$ = Currents flowing into subsystem interface terminal at time t_{mq}

4.3 QD-QACF Model Formation

The model in the above format needs to be converted to an equivalent in order to achieve a simultaneous solution with the Time domain system. Since, the time domain system operates on a smaller time step, an equivalent for the Quasi-domain system needs to be constructed to achieve simultaneous solutions at each time step. The first step on this process is reducing the system equations to those associated with the interface nodes. The model is reduced sequentially first by linearizing the quadratic equations and then eliminating non-interface variables. The procedure is illustrated below. The objective is to obtain a set of equations which depend only on the interface variables (related to nodes where the system is connected to the time domain system).

4.4 Model Reduction at the QD-TD Interface

The interface for the Hybrid simulation scheme corresponds to the boundary between the Quasi-dynamic domain subsystem and Time domain subsystem. The terminal quantities at the interface nodes will be refereed as the interface variables. Once, the interface is identified, the system of equations is reordered so that the equations associated with the interface nodes are on top of the system of equations. Model reduction is carried out via Kron's elimination to reduce the system of equations to those associated with the interface nodes.

The Quasi-Dynamic domain model for the QD subsystem has been shown in the previous section and it is repeated here:

$$\begin{Bmatrix} \tilde{I}(t_q) \\ 0 \\ 0 \\ \tilde{I}(t_{mq}) \\ 0 \\ 0 \end{Bmatrix} = Y_{eqx}\tilde{\mathbf{x}} + \begin{Bmatrix} \vdots \\ \tilde{\mathbf{x}}^T \left\langle F^i_{eqx} \right\rangle \tilde{\mathbf{x}} \\ \vdots \end{Bmatrix} + Y_{QDequ}\tilde{\mathbf{u}} + \begin{Bmatrix} \vdots \\ \tilde{\mathbf{u}}^T \left\langle F^i_{equ} \right\rangle \tilde{\mathbf{u}} \\ \vdots \end{Bmatrix} + \begin{Bmatrix} \vdots \\ \tilde{\mathbf{u}}^T \left\langle F^i_{equx} \right\rangle \tilde{\mathbf{x}} \\ \vdots \end{Bmatrix} - B_{eq} \quad \textbf{(1)}$$

$$B_{eq} = -N_{eq,x}\tilde{\mathbf{x}}(t_q - h_q) - N_{eq,u}\tilde{\mathbf{u}}(t_q - h_q) - M_{eq}\tilde{I}(t_q - h_q) - K_{eq}$$

The following steps result in an equivalent at the interface.

<u>Step I: Linearization of Quadratic terms</u>

The system in the form presented above contains Quadratic nonlinear terms in some of its equations. The model is linearized using the <u>Maclaurin series expansion</u>.

For a given nonlinear function $f(x)$ where $f(0)$ is known the *Maclaurin series expansion* is given by:

$$f(x) = f(0) + f'(0)x + f''(0)\frac{x^2}{2} + ...$$

For linearization the first two terms are retained and higher order terms are discarded.

Now consider a single nonlinear equation from the SCAQCF form:

$$0 = Y_{eqx}\tilde{\mathbf{x}} + \tilde{\mathbf{x}}^T \left\langle F^i_{eqx} \right\rangle \tilde{\mathbf{x}} + Y_{QDequ}\tilde{\mathbf{u}} + \tilde{\mathbf{u}}^T \left\langle F^i_{equ} \right\rangle \tilde{\mathbf{u}} + \tilde{\mathbf{u}}^T \left\langle F^i_{equx} \right\rangle \tilde{\mathbf{x}} - B_{eq}$$

$$B_{eq} = -N_{eq,x}\tilde{\mathbf{x}}(t_q - h_q) - N_{eq,u}\tilde{\mathbf{u}}(t_q - h_q) - M_{eq}\tilde{I}(t_q - h_q) - K_{eq}$$

In order to linearize this equation it is first necessary to evaluate the equation as well as its first derivative at '$\tilde{\mathbf{x}}_0, \tilde{\mathbf{u}}_0$ 'where $\tilde{\mathbf{x}}_0$ and $\tilde{\mathbf{u}}_0$ are the state vector and control variable vector corresponding to the last time step $(t_q - h_q)$ respectively.

(a) Evaluation of nonlinear equations at $(\tilde{\mathbf{x}}_0, \tilde{\mathbf{u}}_0)$

$$f(\tilde{\mathbf{x}}_0, \tilde{\mathbf{u}}_0) = Y_{eqx}\tilde{\mathbf{x}}_0 + \tilde{\mathbf{x}}_0{}^T \left\langle F^i_{eqx} \right\rangle \tilde{\mathbf{x}}_0 + Y_{QDequ}\tilde{\mathbf{u}}_0 + \tilde{\mathbf{u}}_0{}^T \left\langle F^i_{equ} \right\rangle \tilde{\mathbf{u}}_0 + \tilde{\mathbf{u}}_0{}^T \left\langle F^i_{equx} \right\rangle \tilde{\mathbf{x}}_0 - B_{eq} \quad \textbf{(2)}$$

$$B_{eq} = -N_{eq,x}\tilde{\mathbf{x}}(t_q - h_q) - N_{eq,u}\tilde{\mathbf{u}}(t_q - h_q) - M_{eq}\tilde{I}(t_q - h_q) - K_{eq}$$

$\tilde{\mathbf{x}}_0$ = State vector evaluated at $(t_q - h_q)$ [$\tilde{\mathbf{x}}(t_q - h_q)$]

$\tilde{\mathbf{u}}_0$ = Control vector evaluated at $(t_q - h_q)$ [$\tilde{\mathbf{u}}(t_q - h_q)$]

(b) Evaluation of the Jacobian:

$$\left[\frac{df}{d\tilde{\mathbf{x}}}\right]_{(\tilde{\mathbf{x}}=\tilde{\mathbf{x}}_0, \tilde{\mathbf{u}}=\tilde{\mathbf{u}}_0)} = \left[Y_{eqx} + \left\{\tilde{\mathbf{x}}^T \left\langle F^i_{eqx} \right\rangle + \left\langle F^i_{eqx} \right\rangle \tilde{\mathbf{x}}\right\} + \left\{\tilde{\mathbf{u}}^T \left\langle F^i_{equx} \right\rangle\right\}\right]_{(\tilde{\mathbf{x}}=\tilde{\mathbf{x}}_0, \tilde{\mathbf{u}}=\tilde{\mathbf{u}}_0)} \quad \textbf{(3)}$$

$$\left[\frac{df}{d\tilde{\mathbf{u}}}\right]_{(\tilde{\mathbf{x}}=\tilde{\mathbf{x}}_0, \tilde{\mathbf{u}}=\tilde{\mathbf{u}}_0)} = \left[Y_{QDequ} + \left\{\left\langle F^i_{equ} \right\rangle \tilde{\mathbf{u}} + \tilde{\mathbf{u}}^T \left\langle F^i_{equ} \right\rangle\right\} + \left\{\left\langle F^i_{equx} \right\rangle \tilde{\mathbf{x}}\right\}\right]_{(\tilde{\mathbf{x}}=\tilde{\mathbf{x}}_0, \tilde{\mathbf{u}}=\tilde{\mathbf{u}}_0)} \quad \textbf{(4)}$$

(c) Linearized Equation

The linearized versions of the above nonlinear equations look as follows:

$$0 = f(\tilde{\mathbf{x}}_0, \tilde{\mathbf{u}}_0) + \left[\frac{df}{d\tilde{\mathbf{x}}}\right]_{(\tilde{\mathbf{x}}=\tilde{\mathbf{x}}, \tilde{\mathbf{u}}=\tilde{\mathbf{u}}_0)} (\tilde{\mathbf{x}} - \tilde{\mathbf{x}}_0) + \left[\frac{df}{d\tilde{\mathbf{u}}}\right]_{(\tilde{\mathbf{x}}=\tilde{\mathbf{x}}_0, \tilde{\mathbf{u}}=\tilde{\mathbf{u}}_0)} (\tilde{\mathbf{u}} - \tilde{\mathbf{u}}_0) \quad \textbf{(5)}$$

The linearized equations (5) replace the original nonlinear (quadratic) equations. It is however, critical to conform to the QD-SCAQCF standard specified in (1). Hence, the equations are rearranged so as to conform to the SCAQCF format.

$$\begin{Bmatrix} \tilde{I}(t_q) \\ 0 \\ 0 \\ \tilde{I}(t_{mq}) \\ 0 \\ 0 \end{Bmatrix} = Y_{eqx}\tilde{\mathbf{x}} + Y_{QDequ}\tilde{\mathbf{u}} - B_{eq} \quad \textbf{(6)}$$

$$B_{eq} = -N_{eq,x}\tilde{\mathbf{x}}(t_q - h_q) - N_{eq,u}\tilde{\mathbf{u}}(t_q - h_q) - M_{eq}\tilde{I}(t_q - h_q) - K_{eq}$$

Where,

Y_{eqx} - consists of the original components from the linear equations as well as components from the Jacobian added in from (3).

Y_{QDequ} - consists of original components from the linear equations as well as components from the Jacobian added in from (4)

K_{eq} - consists of the original components corresponding to the linear equations as well as

$$\left[f(\tilde{\mathbf{x}}_0, \tilde{\mathbf{u}}_0) + \left[\frac{df}{d\tilde{\mathbf{x}}}\right]_{(\tilde{\mathbf{x}}=\tilde{\mathbf{x}}_0, \tilde{\mathbf{u}}=\tilde{\mathbf{u}}_0)} \tilde{\mathbf{x}}_0 + \left[\frac{df}{d\tilde{\mathbf{u}}}\right]_{(\tilde{\mathbf{x}}=\tilde{\mathbf{x}}_0, \tilde{\mathbf{u}}=\tilde{\mathbf{u}}_0)} \tilde{\mathbf{u}}_0 \right]$$

The rest of the matrices remain the same.

Step II: Kron Reduction

In order to eliminate all variables except the interface terminal voltages, we perform Kron reduction. Kron reduction involves eliminating a set of variables by substituting them in terms of variables that we wish to retain.

Consider the following equations where the number of equations equals the number of unknowns:

$$i(t) = ax_1 + bx_2 + cx_3 + \dots$$
$$0 = cx_1 + dx_2 \dots$$
$$\vdots$$

It can be seen that $x_2 \dots x_n$ can be eliminated quite easily by substituting them in terms of x_1 .

Consider the Linearized SCAQCF form presented in (6) which is repeated here for convenience.

$$\begin{Bmatrix} \tilde{I}(t_q) \\ 0 \\ 0 \\ \tilde{I}(t_{mq}) \\ 0 \\ 0 \end{Bmatrix} = Y_{eqx}\tilde{\mathbf{x}} + Y_{QDequ}\tilde{\mathbf{u}} - B_{eq}$$

$$B_{eq} = -N_{eq,x}\tilde{\mathbf{x}}(t_q - h_q) - N_{eq,u}\tilde{\mathbf{u}}(t_q - h_q) - M_{eq}\tilde{I}(t_q - h_q) - K_{eq}$$

Now these equations are written in terms of states which primarily belong to two categories for the purposes of our reduction which are the interface quantities (Voltages at the interface boundary) $\tilde{\mathbf{x}}_{\text{int}}$ and non-interface quantities $\tilde{\mathbf{x}}_{non-\text{int}}$. For the purposes of representation, the above equation (after ignoring the input variables) can be considered as follows:

$$\begin{Bmatrix} \tilde{I}(t_q) \\ 0 \\ 0 \\ \tilde{I}(t_{mq}) \\ 0 \\ 0 \end{Bmatrix} = \begin{bmatrix} Y_{eqx\_11} & Y_{eqx\_12} \\ Y_{eqx\_21} & Y_{eqx\_22} \end{bmatrix} \begin{bmatrix} \tilde{\mathbf{x}}_{\text{int}} \\ \tilde{\mathbf{x}}_{non-\text{int}} \end{bmatrix} - \begin{bmatrix} B_{eq\_11} \\ B_{eq\_22} \end{bmatrix}$$

It can be seen that:

$$0 = Y_{eqx\_21}\tilde{\mathbf{x}}_{\text{int}} + Y_{eqx\_22}\tilde{\mathbf{x}}_{non-\text{int}} - B_{eq\_22}$$
$$\therefore \tilde{\mathbf{x}}_{non-\text{int}} = -(Y_{eqx\_22})^{-1}\left\{Y_{eqx\_21}\tilde{\mathbf{x}}_{\text{int}} - B_{eq\_22}\right\} \quad (8)$$

Now that the non-interface variables can be expressed in terms of the interface variables, they are substituted into the though equations so as to obtain a compact form. Hence, the above linearized SCAQCF form is reduced to

$$\left\{\begin{matrix}\tilde{I}_{\text{int}}(t_q)\\ \tilde{I}_{\text{int}}(t_{mq})\end{matrix}\right\} = Y_{eqx}\tilde{\mathbf{x}}_{\text{int}} - B_{eq} \quad (7)$$

$$B_{eq} = -N_{eq,x}\tilde{\mathbf{x}}(t_q - h_q) - N_{eq,u}\tilde{\mathbf{u}}(t_q - h_q) - M_{eq}\tilde{I}(t_q - h_q) - K_{eq}$$

$$Y_{eqx} = Y_{eqx\_11} - Y_{eqx\_12}(Y_{eqx\_22})^{-1}Y_{eqx\_21}$$

$$B_{eq} = B_{eq\_11} - Y_{eqx\_12}(Y_{eqx\_22})^{-1}B_{eq\_22}$$

Where,

$\tilde{I}_{\text{int}}(t_q)$ = Currents flowing into subsystem interface terminal at time t_q

$\tilde{I}_{\text{int}}(t_{mq})$ = Currents flowing into subsystem interface terminal at time t_{mq}

$\tilde{\mathbf{x}}_{\text{int}}$ = Terminal Voltages at interface for Quasi Dynamic Domain subsystem

This reduced form gives the equivalent of the Quasi-Dynamic domain subsystem as seen at the interface between the two subsystems.

In summary, the flowchart for computing the equivalent model at the interface nodes is shown in Figure 4.3.

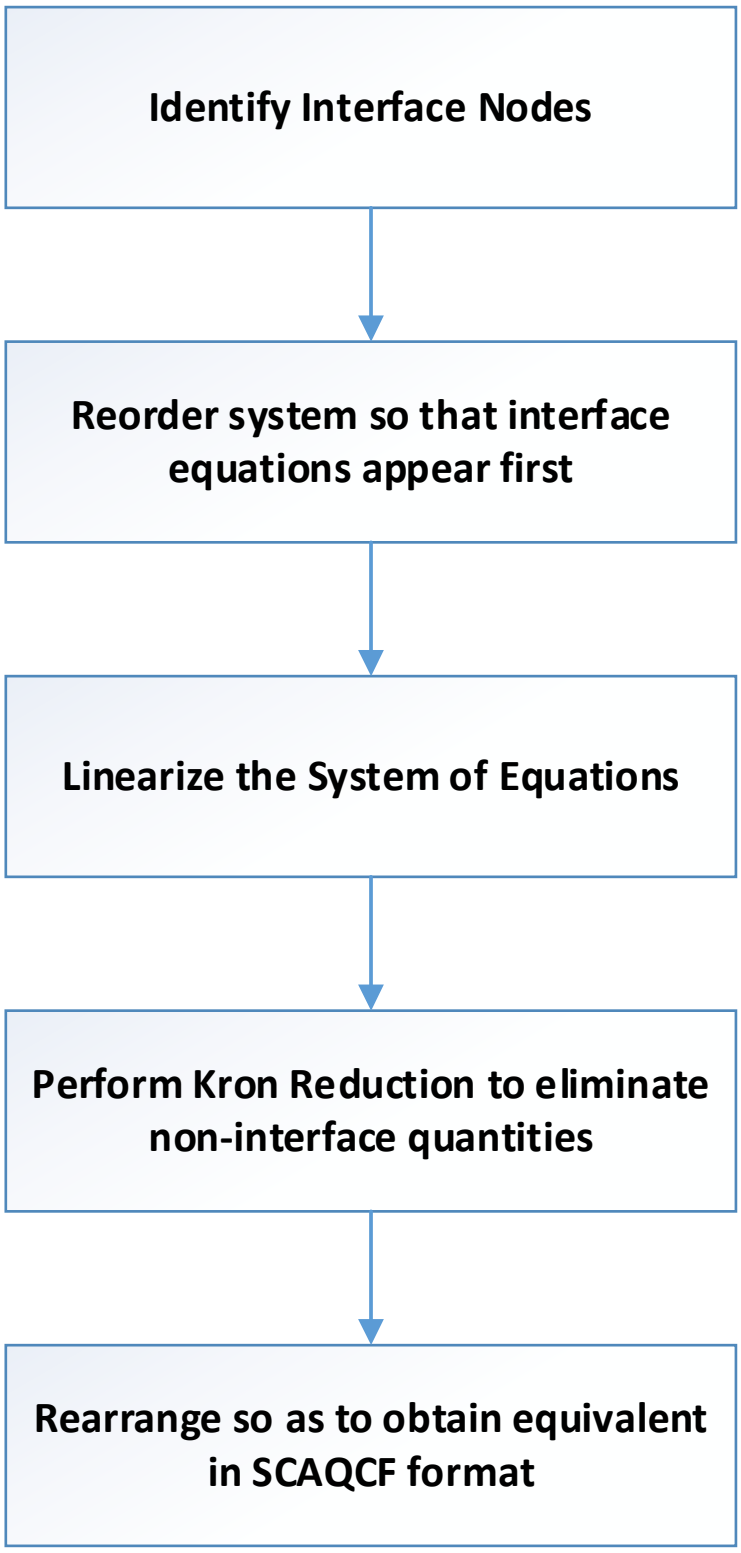

Figure 3.3: Algorithmic Flowchart for Computing the QD-QACF Equivalent

The reduced model at the QD-TD interface has the same syntax as the SCAQCF. A visualization of this model is shown in Figure 4-4.

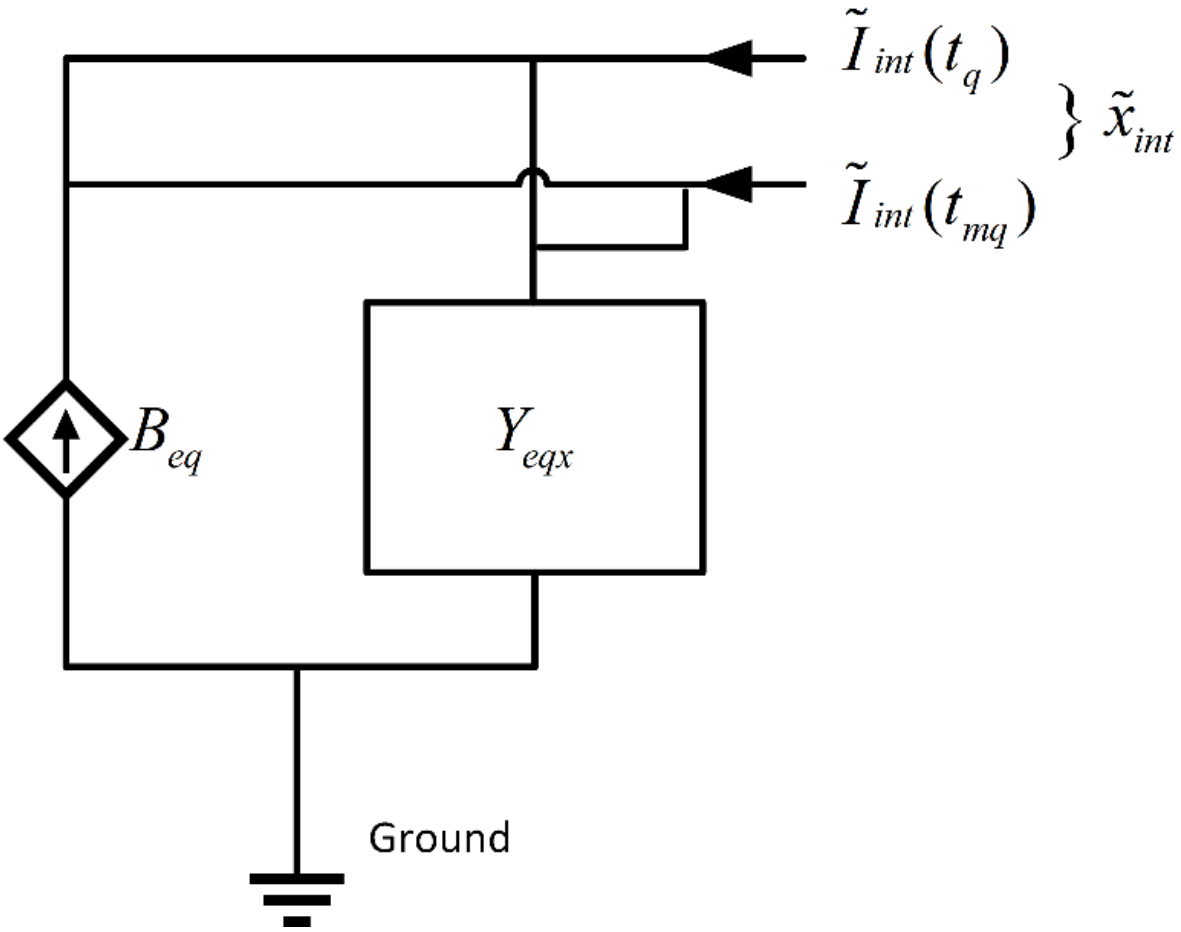

Figure 3.4: Visualization of Reduced Model at the QD-TD Interface

Note that above equivalent is in phasor domain. Subsequently the process is repeated for the harmonic components of this system and then converted into time domain.

4.5 Inclusion of Harmonic Components in the Equivalent

A harmonic equivalent for any subsystem can be developed. This is done by calculating equivalent impedances seen from the interface for each harmonic. This equivalent is added in parallel to the developed equivalent for fundamental frequency. A plot for the harmonic impedance for each frequency can be obtained.

Our approach limits harmonic equivalents for harmonics till the order 11. A sample plot for the test system proposed later is illustrated below.

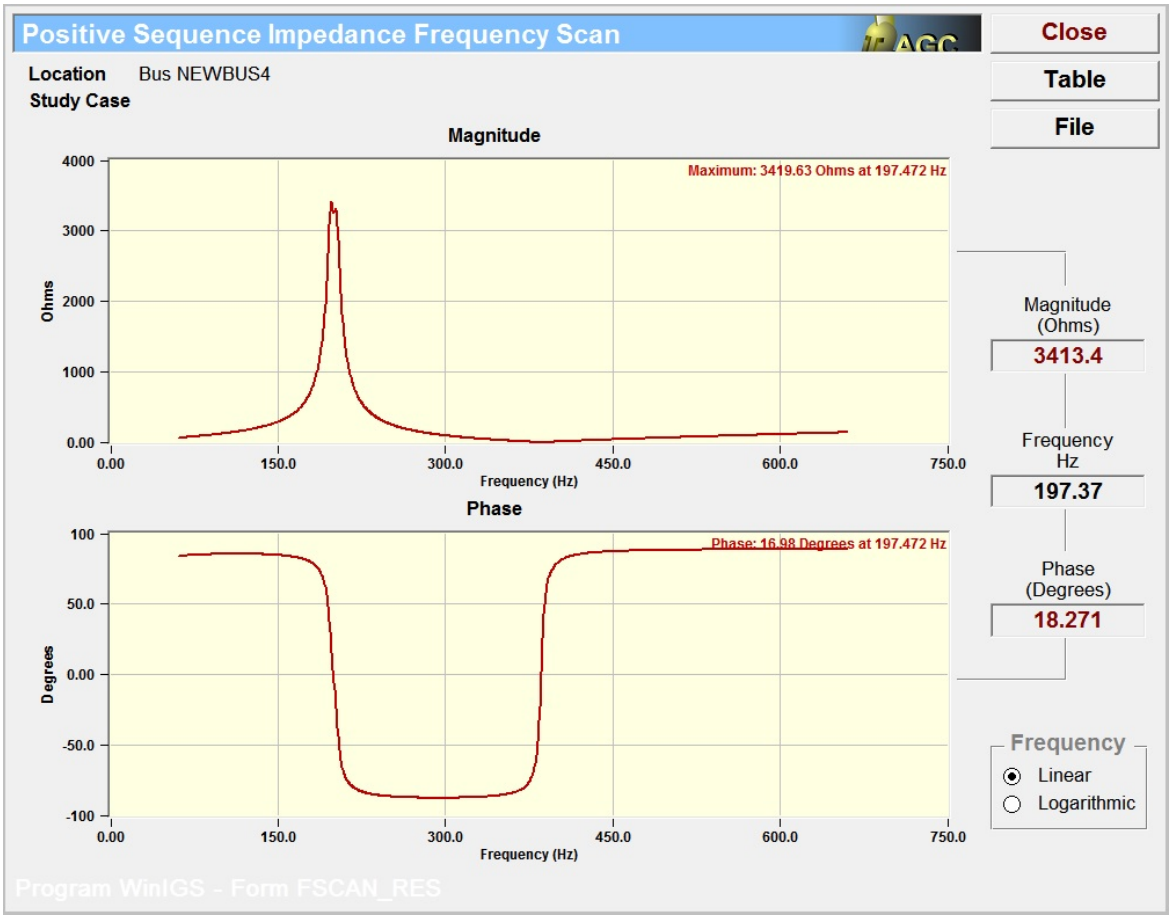

Figure 3.5 Example of Driving Point Impedance at a QD-TD Interface

Given the Kron reduction in frequency domain and the equivalent impedance from harmonic model, we can develop a series of equations for the desirable frequency range. In the following equations, the number on the upper-right position of the variable denotes the corresponding harmonic order. For example, I^{11} is the current in 11th order harmonic.

$$I^2 = Y_{eqx}^2 \tilde{\mathbf{x}}_{\text{int}}^2$$

$$I^3 = Y_{eqx}^3 \tilde{\mathbf{x}}_{\text{int}}^3$$

...

$$I^k = Y_{eqx}^k \tilde{\mathbf{x}}_{\text{int}}^k$$

$$I^{11} = Y_{eqx}^{11} \tilde{\mathbf{x}}_{\text{int}}^{11}$$

It is worth noting that there are not B_{eq} in the harmonic model, because sources are assumed to be at fundamental frequency only. The above model combines the harmonic models with fundamental frequency.

4.6 Equivalent QD-QACF model to Time Domain Conversion

In the previous sections, the QD-QACF reduction scheme was discussed. This involves reducing the model by linearizing and eliminating non-interface equations. The obtained reduced model looks as follows:

$$\begin{bmatrix} I(t_q) \\ I(t_{mq}) \end{bmatrix} = Y_{eq} \begin{bmatrix} X(t_q) \\ X(t_{mq}) \end{bmatrix} + Y_{QDequ}\tilde{\mathbf{u}} + \begin{Bmatrix} \vdots \\ \tilde{\mathbf{u}}^T \left\langle F^i_{equ} \right\rangle \tilde{\mathbf{u}} \\ \vdots \end{Bmatrix} + \begin{Bmatrix} \vdots \\ \tilde{\mathbf{u}}^T \left\langle F^i_{equx} \right\rangle \tilde{\mathbf{x}} \\ \vdots \end{Bmatrix} - B_{eq}$$

$$B_{eq} = -N_{eq,x}\tilde{\mathbf{x}}(t_q - h_q) - N_{eq,u}\tilde{\mathbf{u}}(t_q - h_q) - M_{eq}\tilde{I}(t_q - h_q) - K_{eq}$$

Where,

$$I(t_q) = \begin{bmatrix} I_r(t_q) & I_i(t_q) \end{bmatrix} \qquad X(t_q) = \begin{bmatrix} V_r(t_q) & V_i(t_q) \end{bmatrix}$$
$$I(t_{mq}) = \begin{bmatrix} I_r(t_{mq}) & I_i(t_{mq}) \end{bmatrix} \qquad X(t_{mq}) = \begin{bmatrix} V_r(t_{mq}) & V_i(t_{mq}) \end{bmatrix}$$

And the harmonic equivalents at the interface.

$$I^2 = Y^2_{eqx}\tilde{\mathbf{x}}^2_{\text{int}}$$

$$I^3 = Y^3_{eqx}\tilde{\mathbf{x}}^3_{\text{int}}$$

...

$$I^k = Y^k_{eqx}\tilde{\mathbf{x}}^k_{\text{int}}$$

$$I^{11} = Y^{11}_{eqx}\tilde{\mathbf{x}}^{11}_{\text{int}}$$

Above model is in phasor domain. Subsequently is converted into time domain.

4.7 Phasor to Time Domain conversion

The QD-QACF conversion is obtained in terms of rectangular components, $V_r(t_q)\ V_i(t_q)\ V_r(t_{mq})\ V_i(t_{mq})$. In order to interface these quantities to the Time domain instantaneous states $V(t_q)$ and $V(t+(n)(h/2))$ from the TD-AQCF form, the QD-QACF variables are converted to time domain via the following equations.

$V_r(t_q) + jV_i(t_q) \rightarrow Mag\angle\cos(\omega t_q + \varphi) \rightarrow V(t_q)$

Where,

$$Mag = \sqrt{V_r^{\,2} + V_i^{\,2}} \text{ and } \varphi = \tan^{-1}\left(\frac{V_i(t_q)}{V_r(t_q)}\right)$$

By expanding the $\cos(\omega t_q + \varphi) = \cos(\omega t_q)\cos(\varphi) - \sin(\omega t_q)\sin(\varphi)$ term it can be seen that:

$$V(t_q) = V_r(t_q)\cos(\omega t_q) - V_i(t_q)\sin(\omega t_q)$$

Using the result just shown it is possible to change the QDQACF structure:

Consider the following QD-QACF form:

$$\begin{bmatrix} I_r(t_q) \\ I_i(t_q) \\ I_r(t_{mq}) \\ I_i(t_{mq}) \end{bmatrix} = \begin{bmatrix} Y_{eqx} \end{bmatrix} \begin{bmatrix} V_r(t_q) \\ V_i(t_q) \\ V_r(t_{mq}) \\ V_i(t_{mq}) \end{bmatrix} + K_{eq}$$

The above form can be modified by conducting row and column transforms proposed in the previous section so that:

$$\begin{aligned} V(t_q) &= V_r(t_q)\cos(\omega t_q) - V_i(t_q)\sin(\omega t_q) \\ V(t_{mq}) &= V_r(t_{mq})\cos(\omega t_{mq}) - V_i(t_{mq})\sin(\omega t_{mq}) \\ I(t_q) &= I_r(t_q)\cos(\omega t_q) - I_i(t_q)\sin(\omega t_q) \\ I(t_{mq}) &= I_r(t_{mq})\cos(\omega t_{mq}) - I_i(t_{mq})\sin(\omega t_{mq}) \end{aligned} \rightarrow (t_q \text{ and } t_{mq} \text{ derived from program time counter})$$

This makes the reduced QD system:

$$\begin{bmatrix} I(t_q) \\ I(t_{mq}) \end{bmatrix} = [Y_{eqx-\text{modified}}] \begin{bmatrix} V(t_q) \\ V(t_{mq}) \end{bmatrix} + K_{eq-\text{modified}}$$

Similarly, this procedure applies for harmonic equivalents, the only modification is ω. Therefore, the network considering all harmonics can be represented as:

$$\begin{bmatrix} I(t_q) \\ I(t_{mq}) \end{bmatrix} = \sum_{k=1}^{11} Y_{eqx-\text{modified}}^{k} \begin{bmatrix} V(t_q) \\ V(t_{mq}) \end{bmatrix} + K_{eq-\text{modified}}$$

In which, k represents the harmonic order, not exponent.

For the time instants between $t - h_q$ and t_q, the current equivalents can be derived using the fact that a quadratic variation is used for the above equations. The approach is discussed in the following section.

The above form of the equivalent at the interface is compatible with the time domain model.

4.8 Full QD equivalent

The objective of the reduction above is to have a system of equation which are only expressed in terms of the interface states. Once this is done, the system of equations can be expressed in time-domain. The phasor equivalents can be used to interpolate the current equations at intermediate time steps. In other words, we should calculate the approximate value of through quantities at instances corresponding to the time domain system time steps within the interval **[t_q-h_q, t_q]**, and thereby enabling the simultaneous solution of QD and TD.

Let us consider the equation for $I(t)$. This quantity has equations at t_q *and* t_{mq}. Knowing the equations at these two points and past history, the basic principle of Quadratic Integration states that a time dependent equation can be constructed as follows:

The polynomial is $I(t) = a + bt + ct^2$ where,

$$a = I\left(t_q - h_q\right)$$

$$b = \frac{4}{h_q}\left[I\left(t_{mq}\right) - \frac{1}{4} I\left(t_q\right) - \frac{3}{4} I\left(t_q - h_q\right) \right]$$

$$c = \frac{1}{h_q^{\,2}}\left[2I\left(t_q\right) + 2I\left(t_q - h_q\right) - 4I\left(t_{mq}\right) \right]$$

Where equations for $I(t_q)$ and $I(t_{mq})$ are known and can be substituted to find the polynomial. This polynomial describes the variation of *I(t)* over the time step h_q. By substituting h into these equations, the equivalent for each interface through quantity can be evaluated at each time domain time step. Hence, an equivalent can be created for each time step '*h*' from the Time domain simulation.

Now, if $h_q = n.h$ where, h is the time step used for the t-domain equations, then a corresponding system of equations for the Q-domain side can be generated from the reduced system which has the following mathematical form:

$$I(t_q - h_q) = a + b(t_q - h_q) + c(t_q - h_q)^2$$

$$I(t_q - h_q + h) = a + b(t_q - h_q + h) + c(t_q - h_q + h)^2$$

$$I(t_q - h_q + 2h) = a + b(t_q - h_q + 2h) + c(t_q - h_q + 2h)^2$$

.

.

.

$$I(t_q - h_q + (n-1)h) = a + b(t_q - h_q + (n-1)h) + c(t_q - h_q + (n-1)h)^2$$

$$I(t_q) = a + b(t_q) + c(t_q)^2$$

5. The TD-QACF Approach

The TD-QACF Approach is applied to the subsystem to be simulated with a time domain algorithm. The TD-QACF model is obtained by modeling each component of this subsystem with a quadratized model and subsequent integration using the quadratic integration. The time step for this integration is h. Note that the procedure is similar to that for the QD-QACF model, except here all dynamics are modeled.

The resulting model in time domain is in the SCAQCF format and has the following mathematical form:

$$\begin{Bmatrix} i(t) \\ 0 \\ 0 \\ i(t_m) \\ 0 \\ 0 \end{Bmatrix} = Y_{eqx}\mathbf{x} + Y_{equ}\mathbf{u} + \begin{Bmatrix} \vdots \\ \mathbf{x}^T \left\langle F^i_{eqx} \right\rangle \mathbf{x} \\ \vdots \end{Bmatrix} + \begin{Bmatrix} \vdots \\ \mathbf{u}^T \left\langle F^i_{equ} \right\rangle \mathbf{u} \\ \vdots \end{Bmatrix} + \begin{Bmatrix} \vdots \\ \mathbf{u}^T \left\langle F^i_{equx} \right\rangle \mathbf{x} \\ \vdots \end{Bmatrix} - B_{eq}$$

$$B_{eq} = -N_{eqx}\mathbf{x}(t-h) - N_{equ}\mathbf{u}(t-h) - M_{eq}i(t-h) - K_{eq}$$

where:

$i(t)$ *and* $i(t_m)$: the through variables of the device model

$\mathbf{x}$: external and internal state variables of the device model, $\mathbf{x} = [\mathbf{x}(t), \mathbf{x}(t_m)]$

$\mathbf{u}$: control variables of the device model, i.e. transformer tap, etc. $\mathbf{u} = [\mathbf{u}(t), \mathbf{u}(t_m)]$

$t_m = t - h/2$

Above model is quadratic and it is compatible to the time domain equivalent of the subsystem that is modeled in the QD domain presented in the previous section. It can be modified to align in time with the compatible model for the quasi-dynamic domain presented in the previous section.

Consider the simple time domain system model:

$$\begin{Bmatrix} i(t) \\ 0 \\ 0 \\ i(t_m) \\ 0 \\ 0 \end{Bmatrix} = Y_{eqx}\mathbf{x} + \begin{Bmatrix} \vdots \\ \mathbf{x}^T \left\langle F^i_{eqx} \right\rangle \mathbf{x} \\ \vdots \end{Bmatrix} + N_{eqx}\mathbf{x}(t-h) + K_{eq}$$

This discrete time domain model can be aligned with the time t_q and stacked with several time instances to provide the following family of equations.

$$\begin{Bmatrix} i(t_q) \\ 0 \\ 0 \\ i(t_q - h/2) \\ 0 \\ 0 \\ \vdots \\ i(2h) \\ 0 \\ 0 \\ i(3h/2) \\ 0 \\ 0 \\ i(h) \\ 0 \\ 0 \\ i(h/2) \\ 0 \\ 0 \end{Bmatrix} = \hat{Y}_{eqx} \begin{bmatrix} \mathbf{x}(t_q) \\ \mathbf{x}(t_q - h/2) \\ \vdots \\ \mathbf{x}(2h) \\ \mathbf{x}(3h/2) \\ \mathbf{x}(h) \\ \mathbf{x}(h/2) \end{bmatrix} + \hat{N}_{eqx} \begin{bmatrix} \mathbf{x}(t_q - h) \\ \vdots \\ \mathbf{x}(h) \\ \mathbf{x}(0) \end{bmatrix} + \hat{K}_{eq}$$

Here, the augmented matrices $\hat{Y}_{eqx}, \hat{N}_{eqx}, \hat{K}_{eq}$ are as follows:

$$\hat{Y}_{eqx} = \begin{bmatrix} Y_{eqx} & N_{eqx} & 0 & \cdots & \cdots \\ 0 & \ddots & 0 & 0 & \\ \vdots & 0 & Y_{eqx} & N_{eqx} & 0 \\ \vdots & 0 & 0 & Y_{eqx} & \end{bmatrix}$$

$$\hat{N}_{eqx} = \begin{bmatrix} 0 & 0 & 0 & 0 & 0 \\ 0 & 0 & 0 & 0 & \\ 0 & 0 & 0 & 0 & \\ 0 & 0 & 0 & N_{eqx} & \end{bmatrix}$$

$$\hat{K}_{eq} = \begin{bmatrix} K_{eq} \\ \vdots \\ K_{eq} \end{bmatrix}$$

Thus, a stacked system of Time domain can be achieved from time $(t_q - h_q)$ to t_q. These equations are used to obtain a simultaneous solution at the interface as explained in the next section.

6. Simultaneous Solution

The simultaneous solution at the interface is obtained by combining the equivalent representations of the two subsystems at the interface. In the previous two sections, these equivalents were derived. They are summarized below.

Equivalent at the interface form the QD-AQCF subsystem:

$$I(t_q - h_q) = a + b(t_q - h_q) + c(t_q - h_q)^2$$
$$I(t_q - h_q + h) = a + b(t_q - h_q + h) + c(t_q - h_q + h)^2$$
$$I(t_q - h_q + 2h) = a + b(t_q - h_q + 2h) + c(t_q - h_q + 2h)^2$$

.

.

.

$$I(t_q - h_q + (n-1)h) = a + b(t_q - h_q + (n-1)h) + c(t_q - h_q + (n-1)h)^2$$
$$I(t_q) = a + b(t_q) + c(t_q)^2$$

Equivalent at the interface form the TD-AQCF subsystem:

$$\begin{Bmatrix} i(t_q) \\ 0 \\ 0 \\ i(t_q - h/2) \\ 0 \\ 0 \\ \vdots \\ i(2h) \\ 0 \\ 0 \\ i(3h/2) \\ 0 \\ 0 \\ i(h) \\ 0 \\ 0 \\ i(h/2) \\ 0 \\ 0 \end{Bmatrix} = \hat{Y}_{eqx} \begin{bmatrix} \mathbf{x}(t_q) \\ \mathbf{x}(t_q - h/2) \\ \vdots \\ \mathbf{x}(2h) \\ \mathbf{x}(3h/2) \\ \mathbf{x}(h) \\ \mathbf{x}(h/2) \end{bmatrix} + \hat{N}_{eqx} \begin{bmatrix} \mathbf{x}(t_q - h) \\ \vdots \\ \mathbf{x}(h) \\ \mathbf{x}(0) \end{bmatrix} + \hat{K}_{eq}$$

Since, an equivalent current equation exists for both models at every time step, KCL is applied so as to obtain a system of equations which can be solved for the interface variables.

Once the simultaneous solution has been achieved, the interface states are sent back to the Full Quasi-Domain model to analyze the slow moving dynamics as well as the full time domain model. This way the simulation proceeds and the simultaneous solution at the interface is repeated each $h_q / 2$ interval.

The overall algorithm is shown in 6.1.

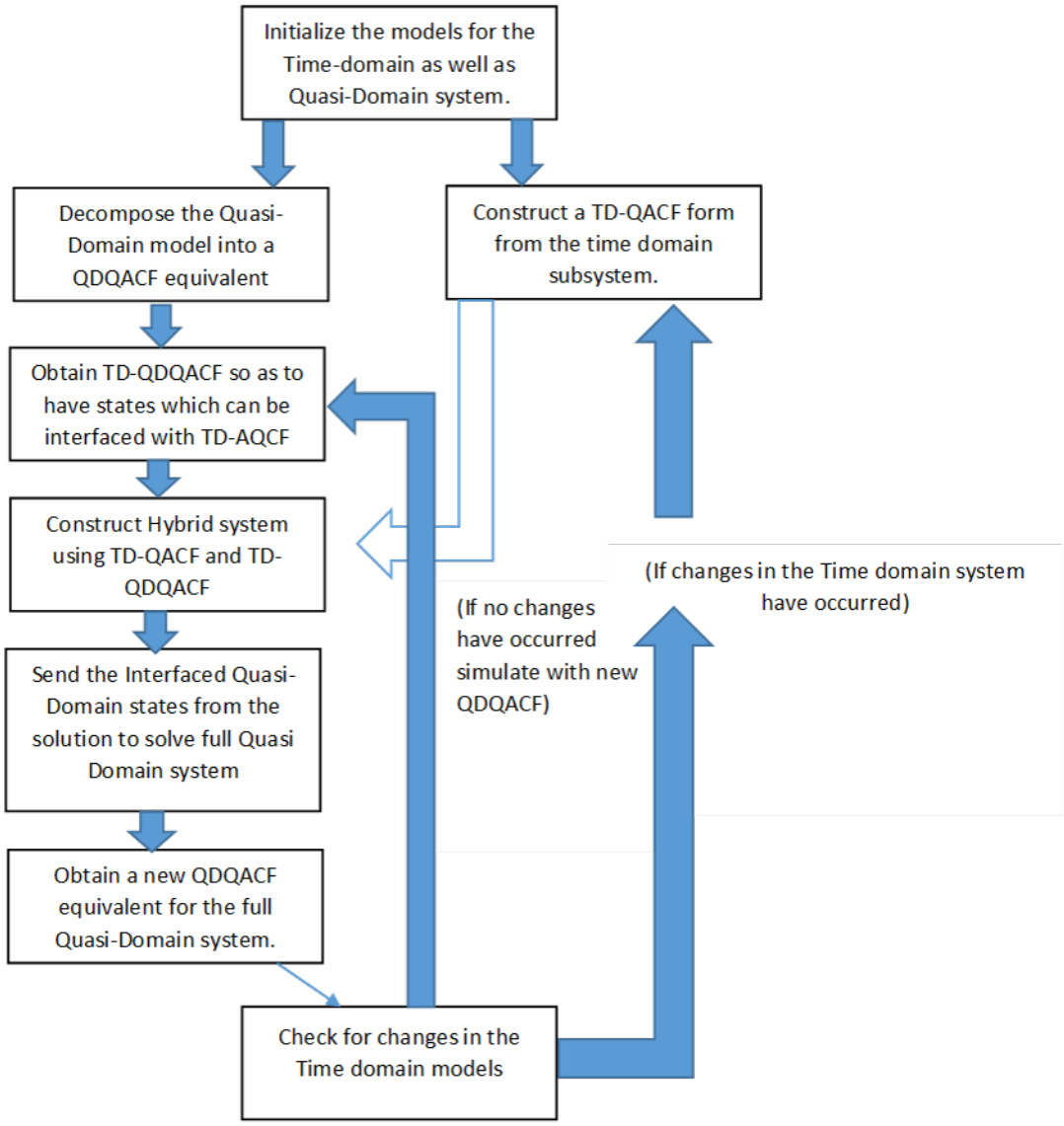

Figure 5.1: Hybrid Simulation Scheme

7. Conclusions and Future Work

A new hybrid simulation method has been developed using a new general modeling approach that has the same syntax in the Quasi-Dynamic Domain and the Time-Domain. The modeling approach is based on the Quadratized-Model, Quadratic Integration Method (QMQI). The developed method provides a simultaneous solution of the two domains at the interface enabling accurate representation of the interaction of the two subsystems.

The method is applicable to many problems: (a) simulating inrush currents in selected parts of a system, (b) simulating the operation of power electronics systems in time domain while the rest of the system is simulated in QD, (c) simulating FIDVR events in parts of the system while the reaming system is simulated in QD, and others.

It is desirable to develop the method into a commercial product.

Appendix: Illustrative Example

This section illustrates the comparison between time domain and quasi-dynamic domain simulation of a multi-event case. The configuration of the system is shown in **Error! Reference source not found.**. This system contains generators, which have slow electromechanical transients. Also, there are inverters in the system, which need fast simulation in time domain to capture electromagnetic transient. Therefore, a reasonable division between time domain and quasi-dynamic domain is the blue line in **Error! Reference source not found.**.

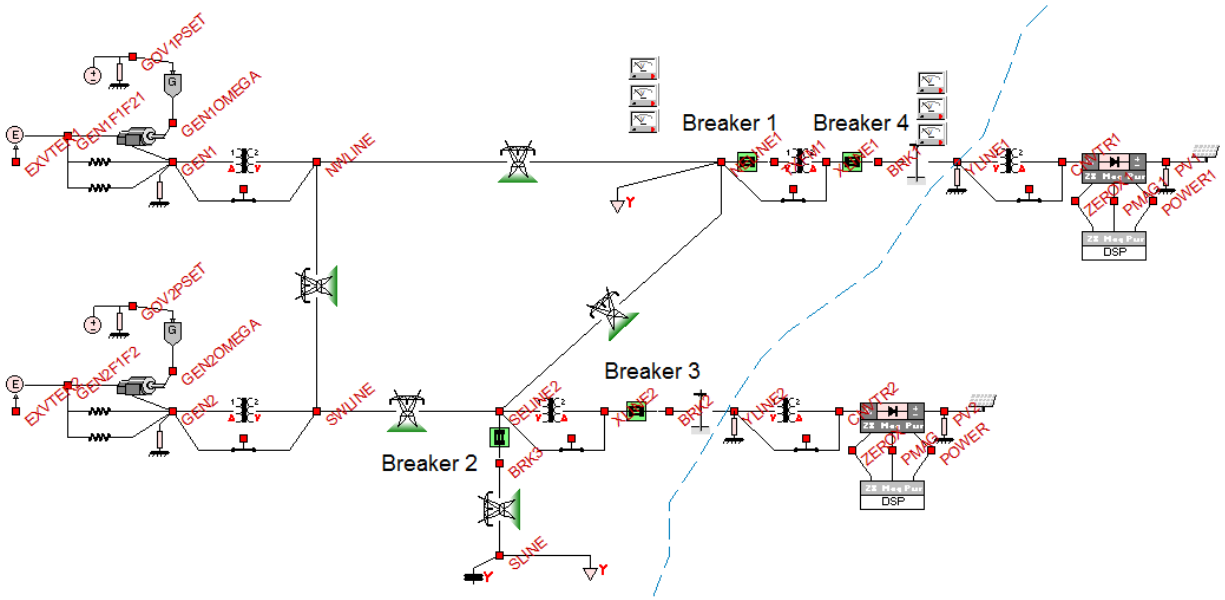

Figure A.1: System single line diagram for illustrative case

There are two generators in the system, both are modeled as 2-axes synchronous generator with governor and exciter. Details of the parameters are available in Table A.1, Figure A.2 and Figure A.3. There are two step-up transformers corresponding to the generators. Their parameters follow the data in Table A.2.

Table A.1: Parameters for the Two Generators

	Generator 1 (GEN1)	Generator 2 (GEN2)
Rated Power	250MVA	160MVA
Rated Voltage	15kV	18kV
Per Unit Inertia H	2.8	2.8
Control Mode	slack bus	PV bus 120.00MW 106.00MVar

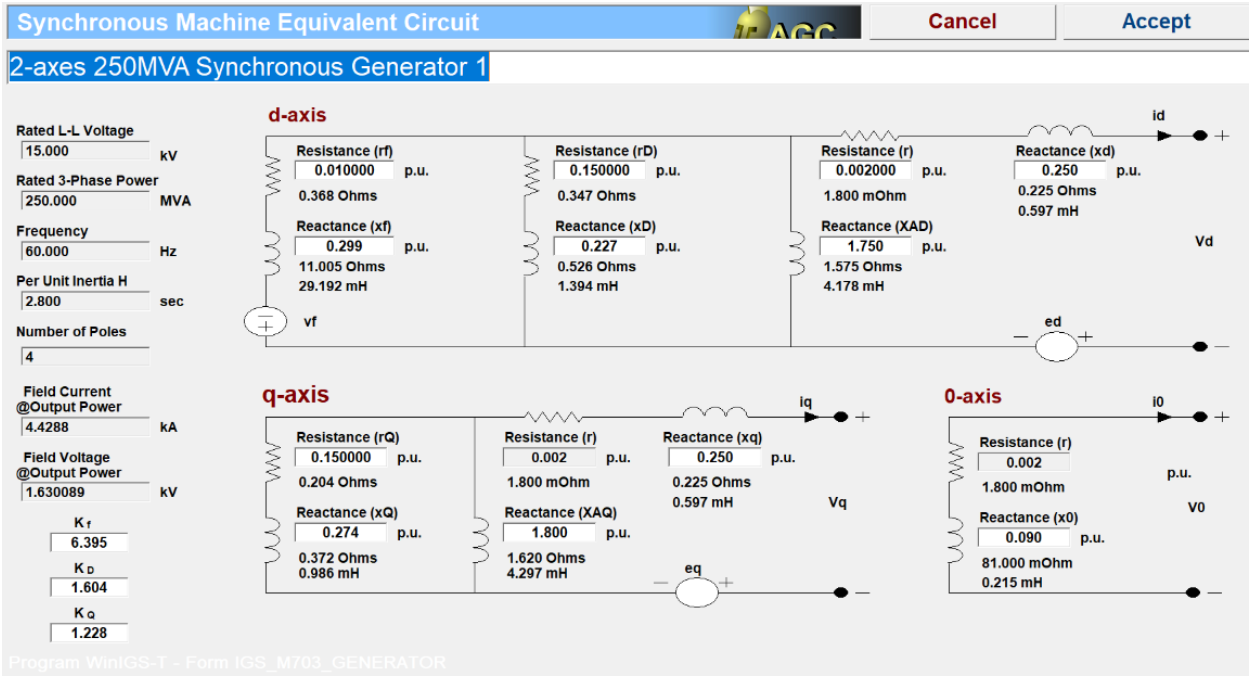

Figure A.2: d-q parameters for generator 1

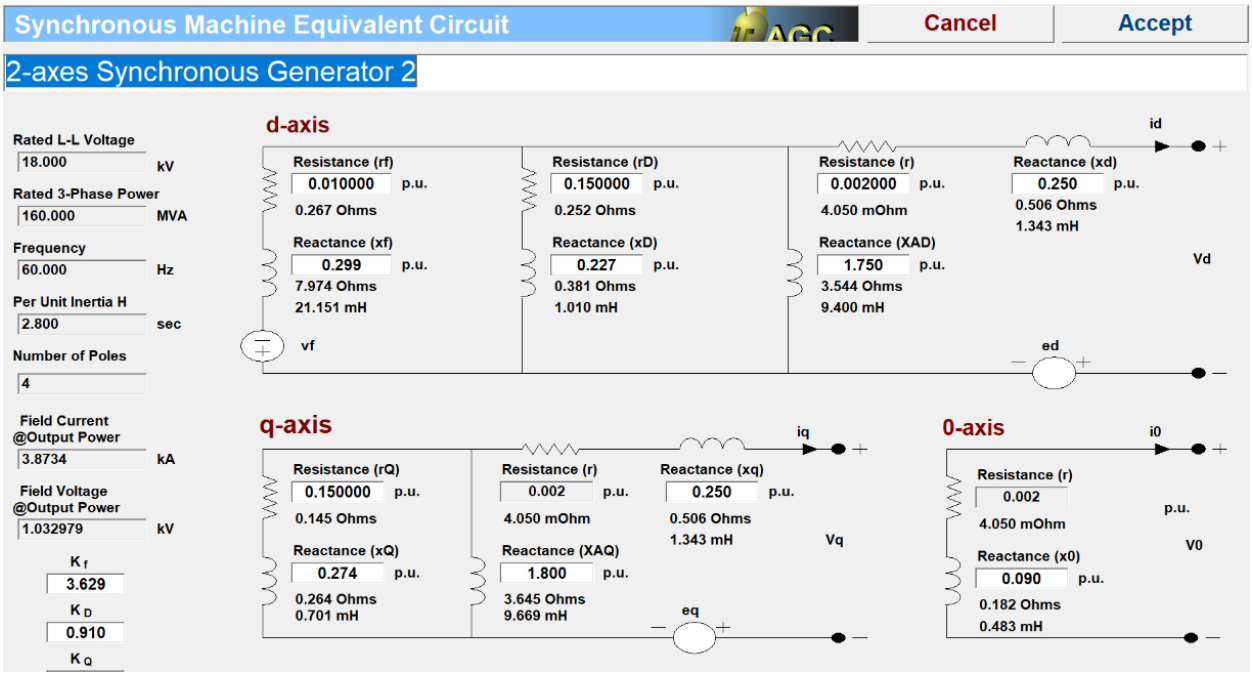

Figure A.3: d-q parameters for generator 2

Table A.2: Parameters for Transformers

	Transformer1	Transformer2
Rated Power	300MVA	200MVA
Rated Voltage	15kV /115kV $\Delta - Y$	18kV/115kV $\Delta - Y$
Winding Resistance	0.01 pu	0.01 pu
Leakage Reactance	0.1 pu	0.1 pu

In addition, there are five transmission lines in the system, all of them have the same configuration as shown in Table A.3. The length of each line is available in Table A.4.

Table A.3: Parameters of Transmission Lines

Phase Conductors	ACSR DRAKE
Shields/Neutral	HS 5/16HS
Tower	101A
Operating Voltage	115kV

Table A.4: Length of Transmission Lines

Name	miles
NW-SW	18
NW-NE	37.5
SW-SE	15
SE-NE	20
SE-South	3.5

There are two equivalent loads in the 115kV system, their parameters are presented in Table A.5.

Table A.5: Parameters for Loads

Bus Name	NELINE1	SELINE2
Rated Voltage	115kV	115kV
Real Power	240MW	110MW
Reactive Power	30MVar	12MVar

A capacitor bank used for reactive power compensation is installed at bus SLINE. It provides 42 MVAr reactive power at rated voltage (115kV). The details for the distribution transformers and the distribution line are provided in Table A.6 and Table A.7.

Table A.6: Parameters for Distribution Transformers

	Transformer1	Transformer2
Rated Power	10MVA	12MVA
Rated Voltage	115kV/34.5kV $\Delta - Y$	115kV/13.8kV $\Delta - Y$
Winding Resistance	0.01 pu	0.01 pu
Leakage Reactance	0.1 pu	0.1 pu

Table A.7: Parameters for Distribution Line

	D-Yline1	D-Yline2
Phase Conductors	ACSR SWIFT	ACSR HAWK/SD
Shields/Neutral	ACSR OSTRICH	ACSR JUNCO
Tower	AGC-DP-35	AGC-DP-35
Operating Voltage	34.5kV	13.8kV
Length	5.5 miles	1.5 miles

To achieve simultaneous simulation between time domain and quasi-dynamic domain, the equivalent impedance at the interface node is calculated, and result is presented in Figures A.4 to A.11.

During the simulation, the following events occur chronologically:

- At t = 2.0 s, Breaker 1 closes (energization of circuit at YLINE1)
- At t = 2.5 s, Breaker 2 opens (load loss)
- At t = 3.0 s, Breaker 3 closes (energization of transformer at YLINE2)
- At t = 3.5 s, Breaker 2 closes (load reconnection)
- At t= 4.0 s, Breaker 4 closes (energization of transformer at YLINE1)

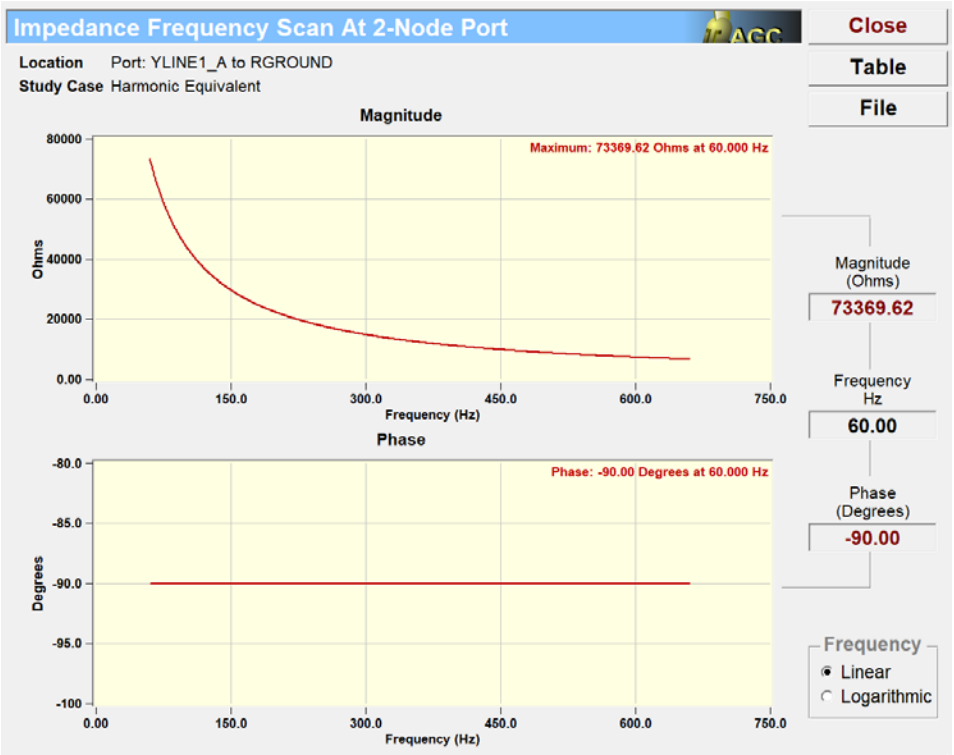

Figure A.4: equivalent impedance for Phase A at bus YLINE1

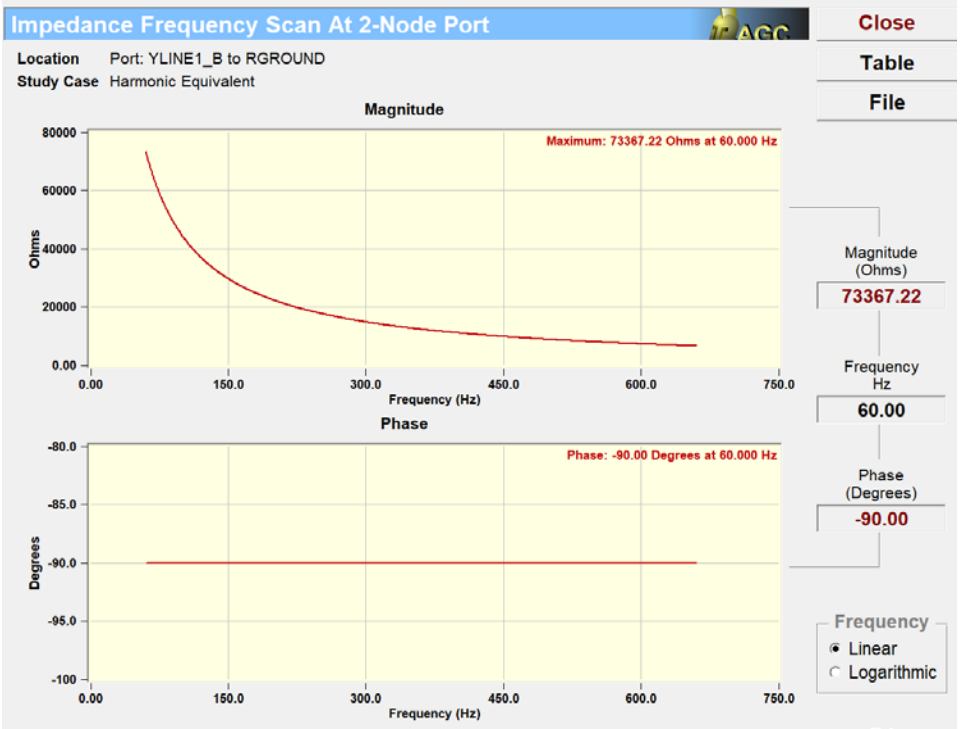

Figure A.5: equivalent impedance for Phase B at bus YLINE1

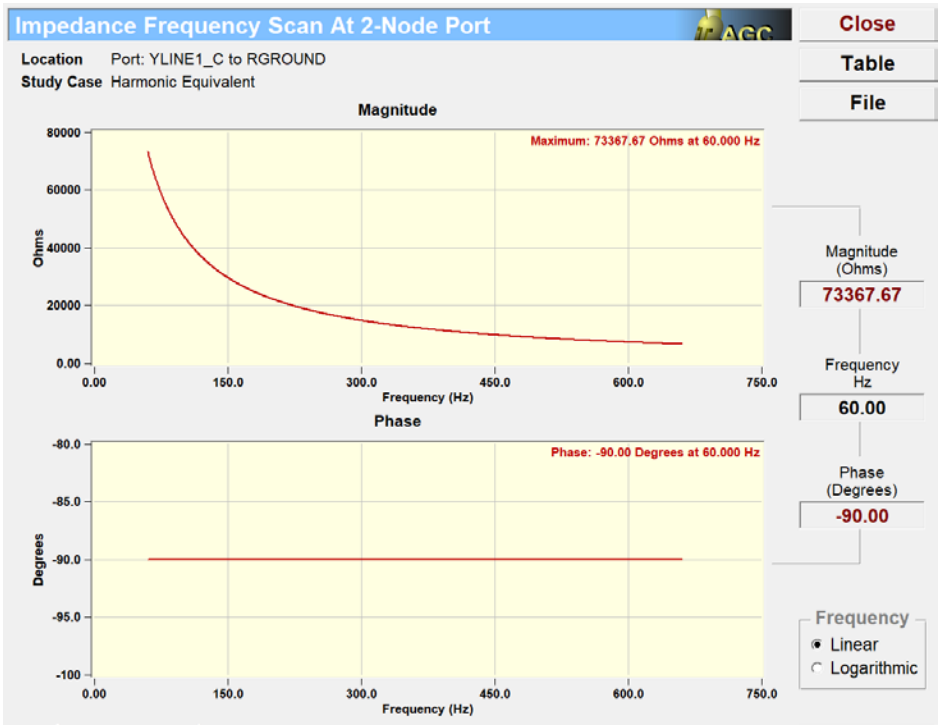

Figure A.6: equivalent impedance for Phase C at bus YLINE1

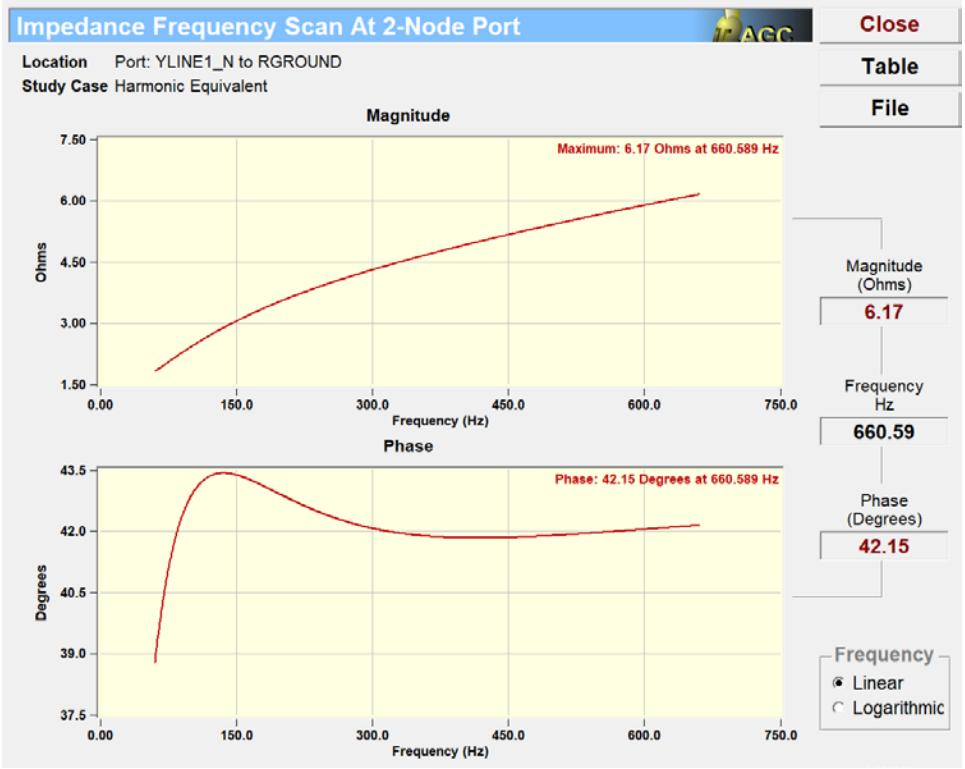

Figure A.7: equivalent impedance for Phase N at bus YLINE1

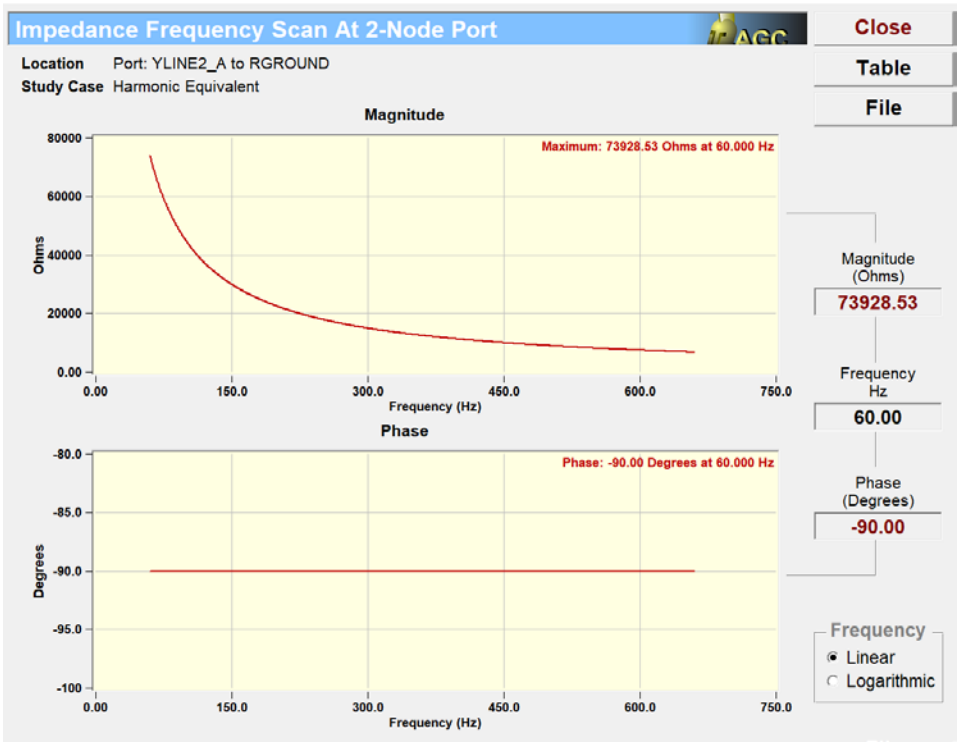

Figure A.8: equivalent impedance for Phase A at bus YLINE2

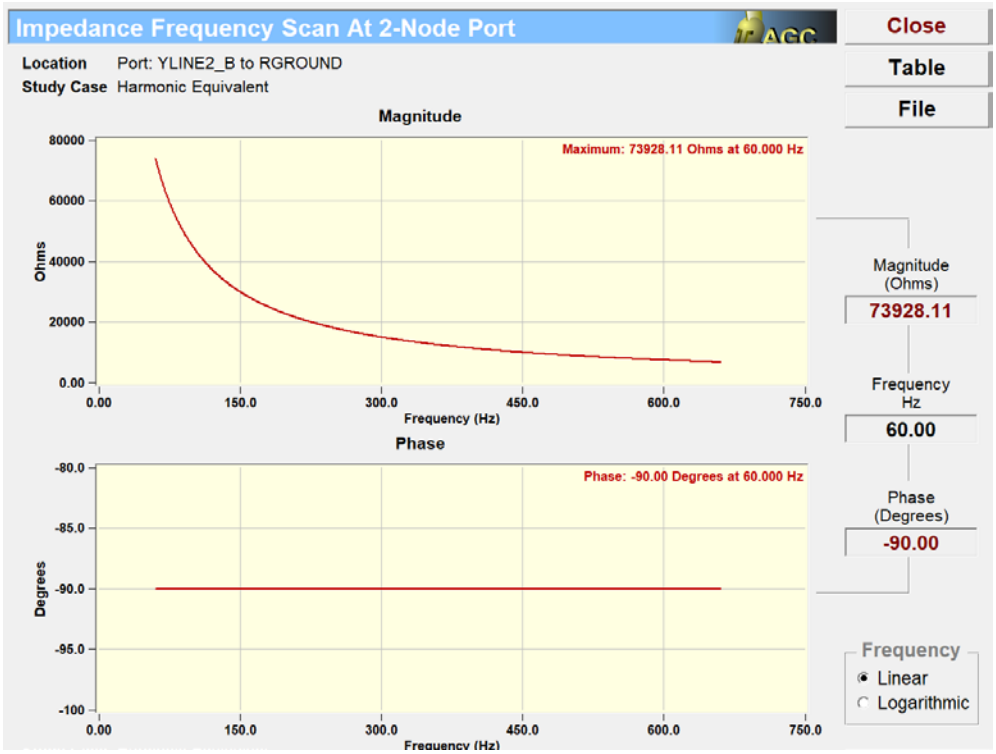

Figure A.9: equivalent impedance for Phase B at bus YLINE2

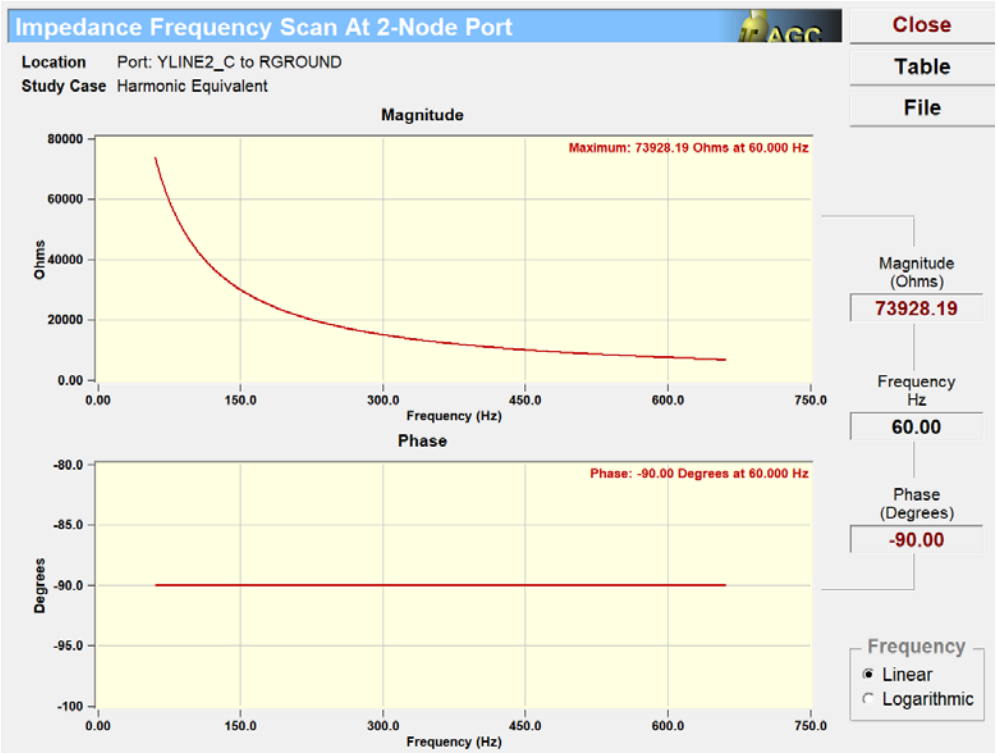

Figure A.10: equivalent impedance for Phase C at bus YLINE2

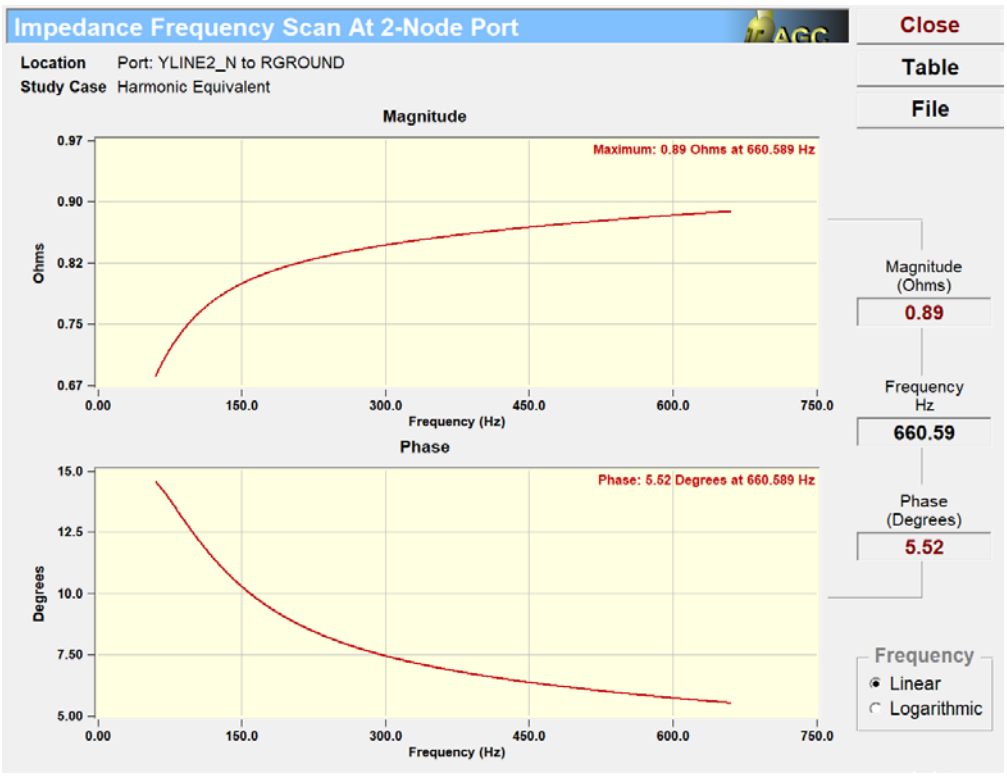

Figure A.11: equivalent impedance for Phase N at bus YLINE2

Next, several comparative results from time domain and quasi-dynamic domain are presented. Figure A.12 shows waveforms (V and I) at the interface of the QD and TD models. Figure A.13 to Figure A.16 show the comparison results.

Comparison is performed by simulating entire system in TD (first trace) and in QD (second trace). Results are compared by forming the difference TD-QD (third trace). The results show that the proposed hybrid simulation method accurately captures the waveform distortion at the interface between the two systems while the QD-QACF simulation alone misses the waveform distortion. Note that the missed distortion is quite significant. This means that methods that ignore the interaction between the two subsystems are laced with large errors.

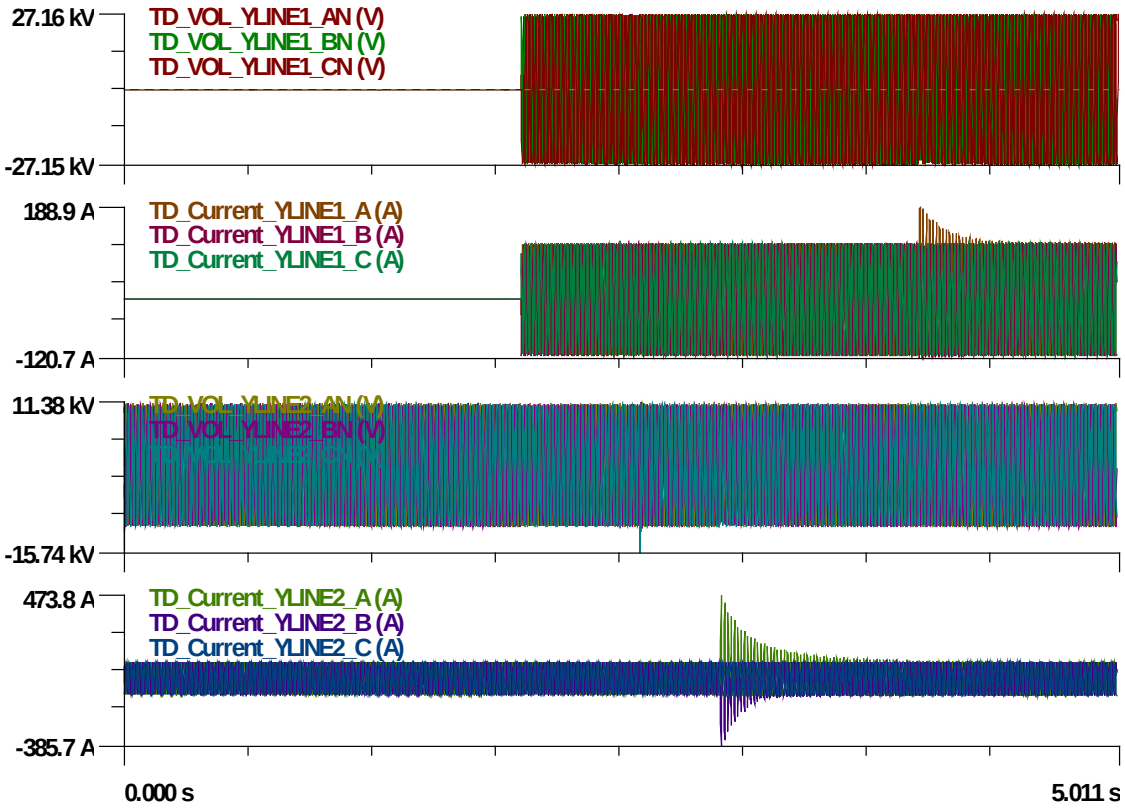

Figure A.12: waveforms (V and I) at the interface of the QD and TD models

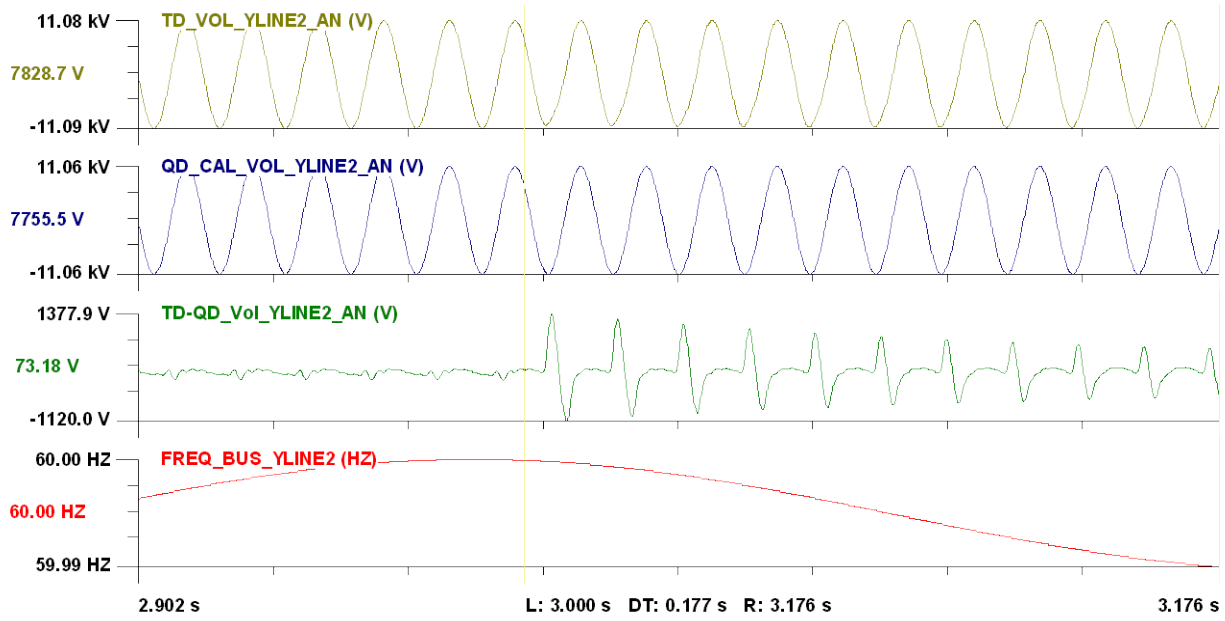

Figure A.13: Comparison around t=3.0 seconds (Interface 1)

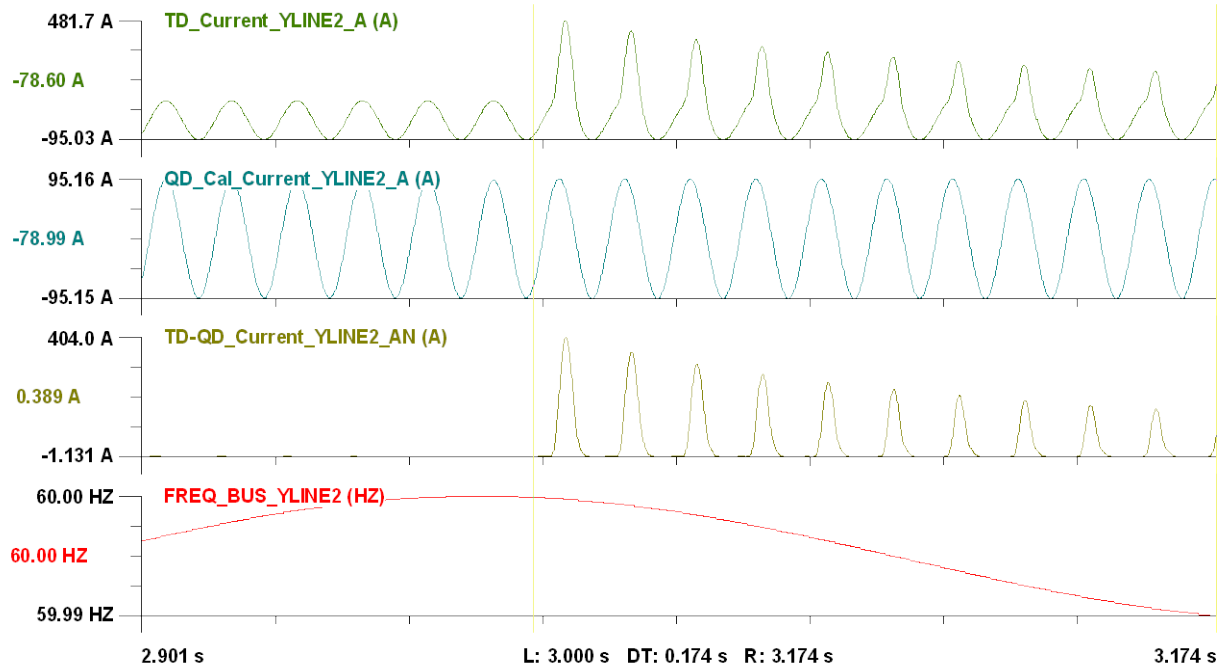

Figure A.14: Comparison around t=3.0 seconds (Interface 1)

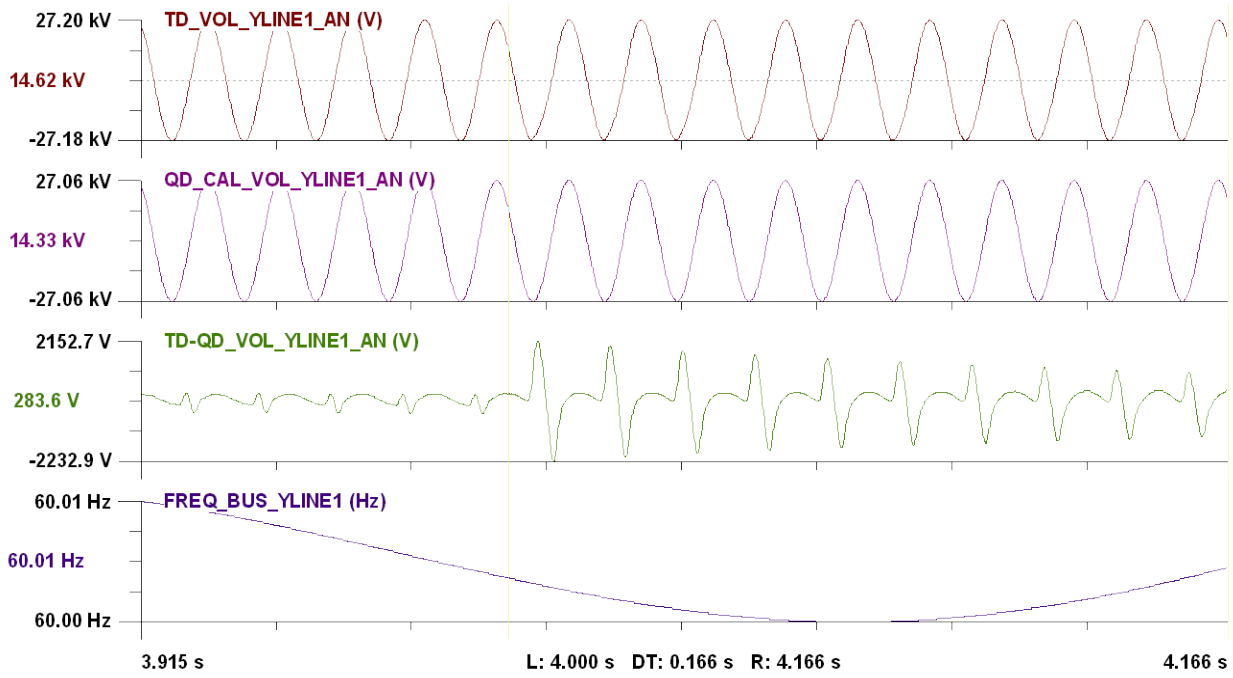

Figure A.15: Comparison around t=4.0 seconds (Interface 2)

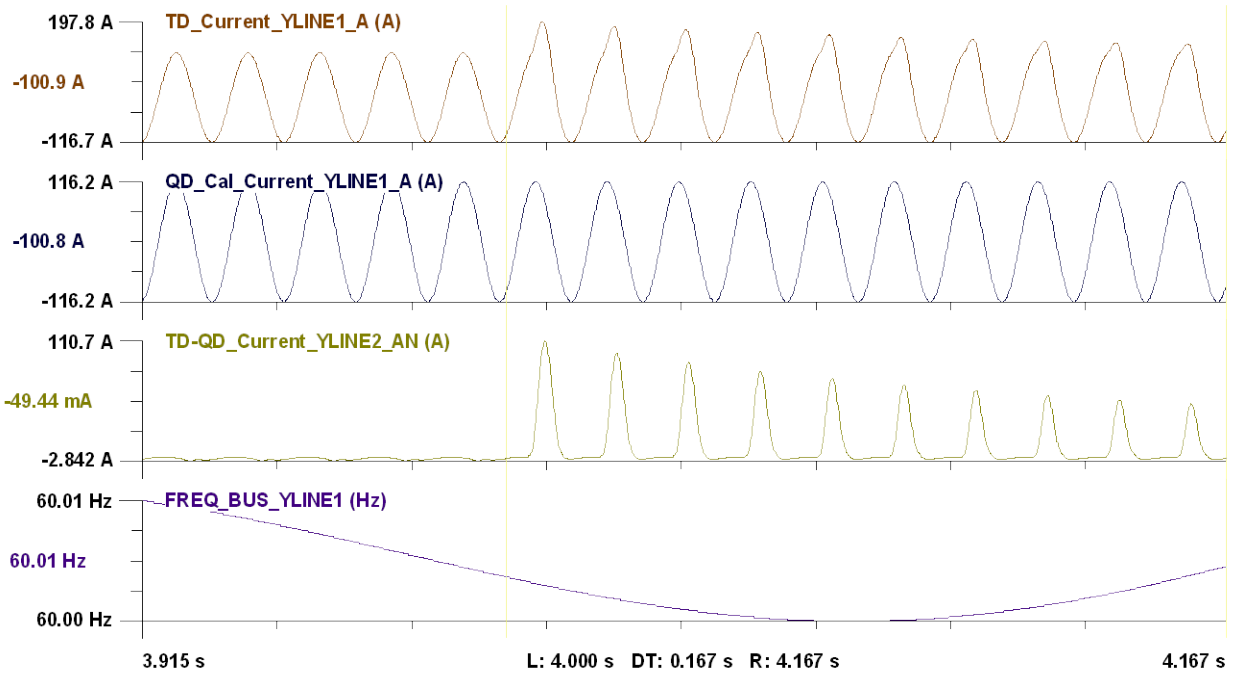

Figure A.16: Comparison around t=4.0 seconds (Interface 2)

The actual quantitative error of the proposed hybrid method is shown in Figures A.17 through A.20. Note that the hybrid method captures the waveform distortion quite well and the errors between the full time domain simulation and the hybrid method are in the range 0.44% to 1.08% for voltages and in the range 1.3% to 2.29% for the currents. It should be noted that this errors occur at transitions with high waveform distortion. During normal operating conditions and mild transients the error is very small.

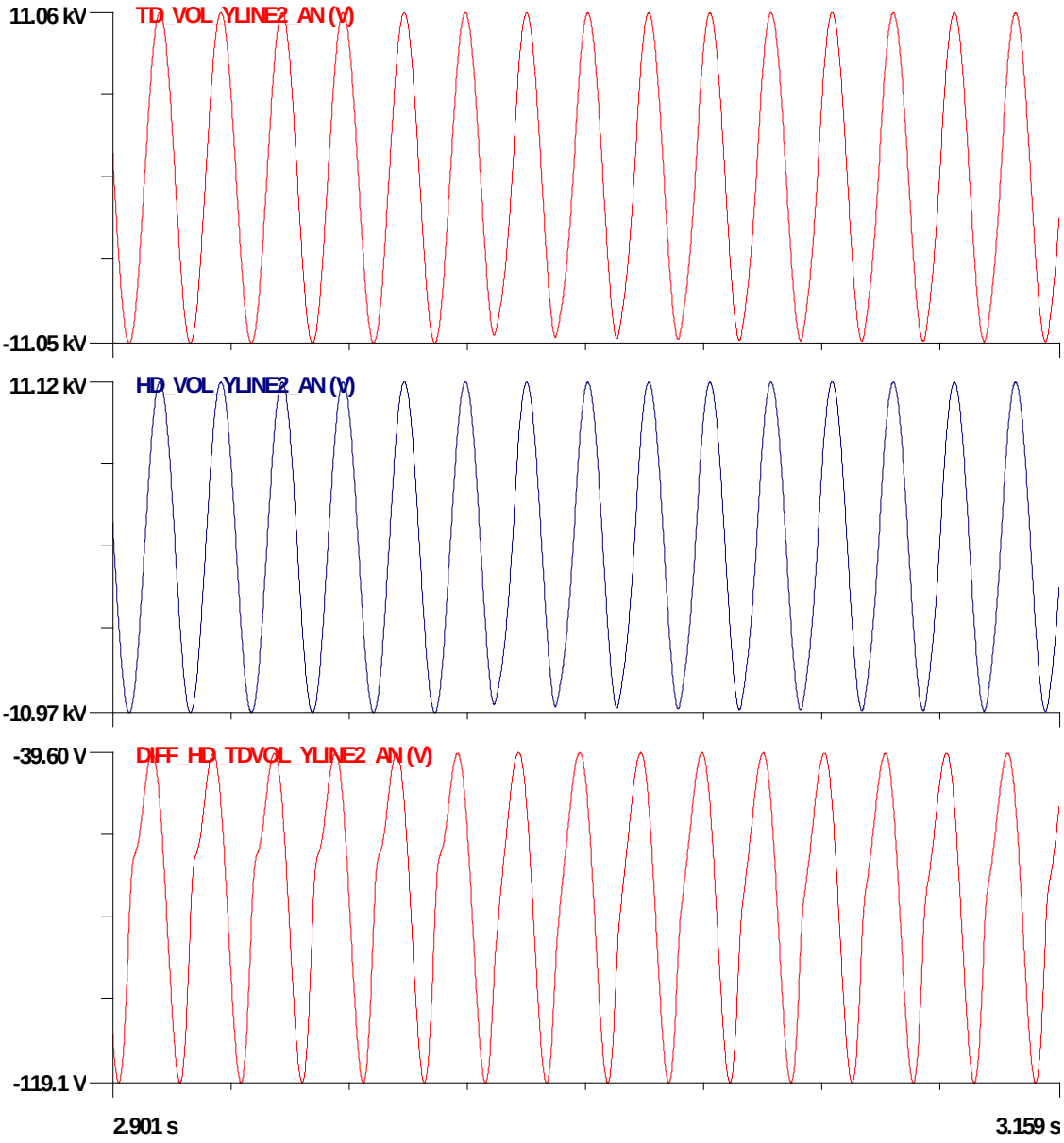

Figure A.17: Comparison of voltages around t=3.0 seconds (Interface 1)

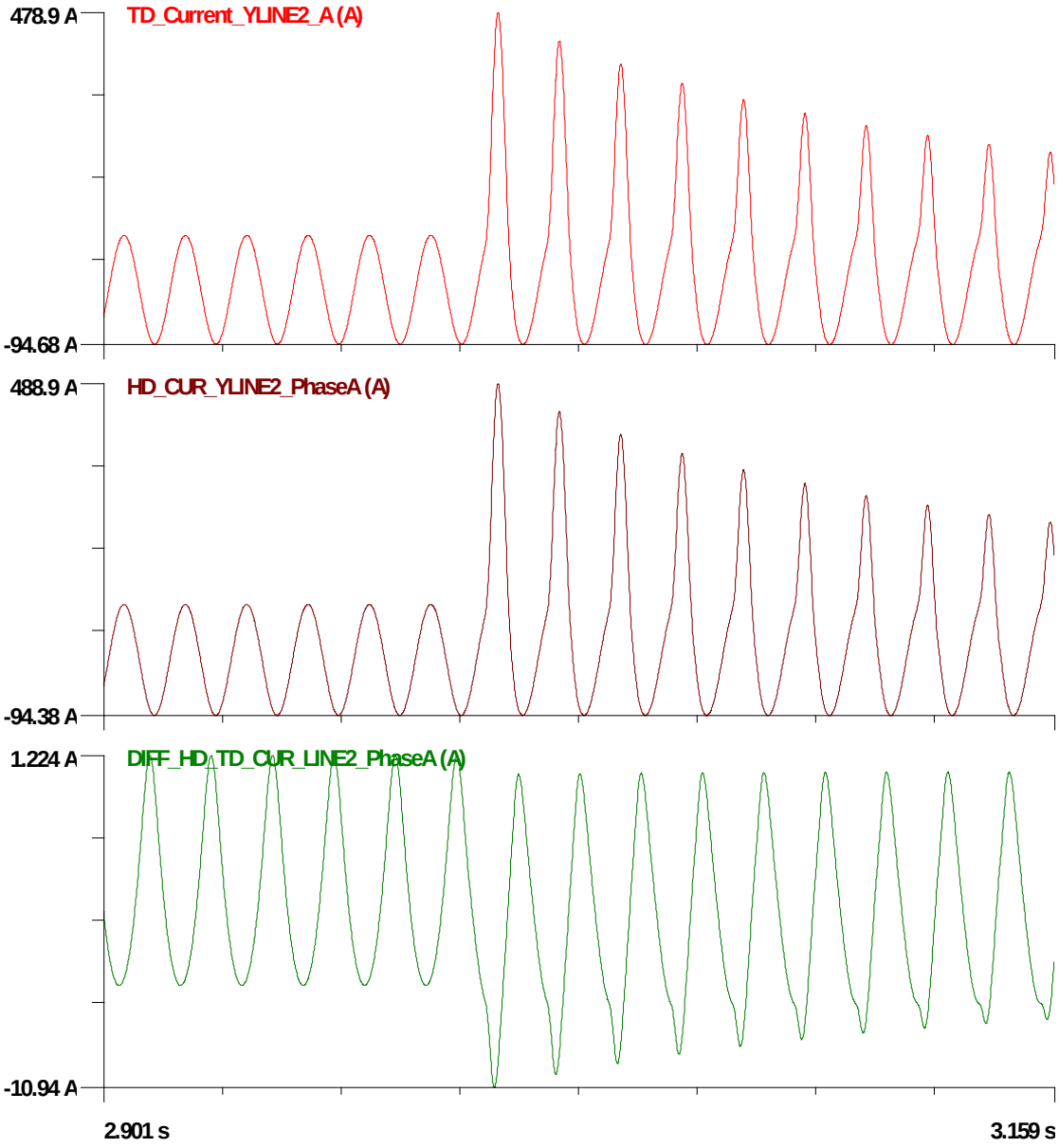

Figure A.18: Comparison of currents around t=3.0 seconds (Interface 1)

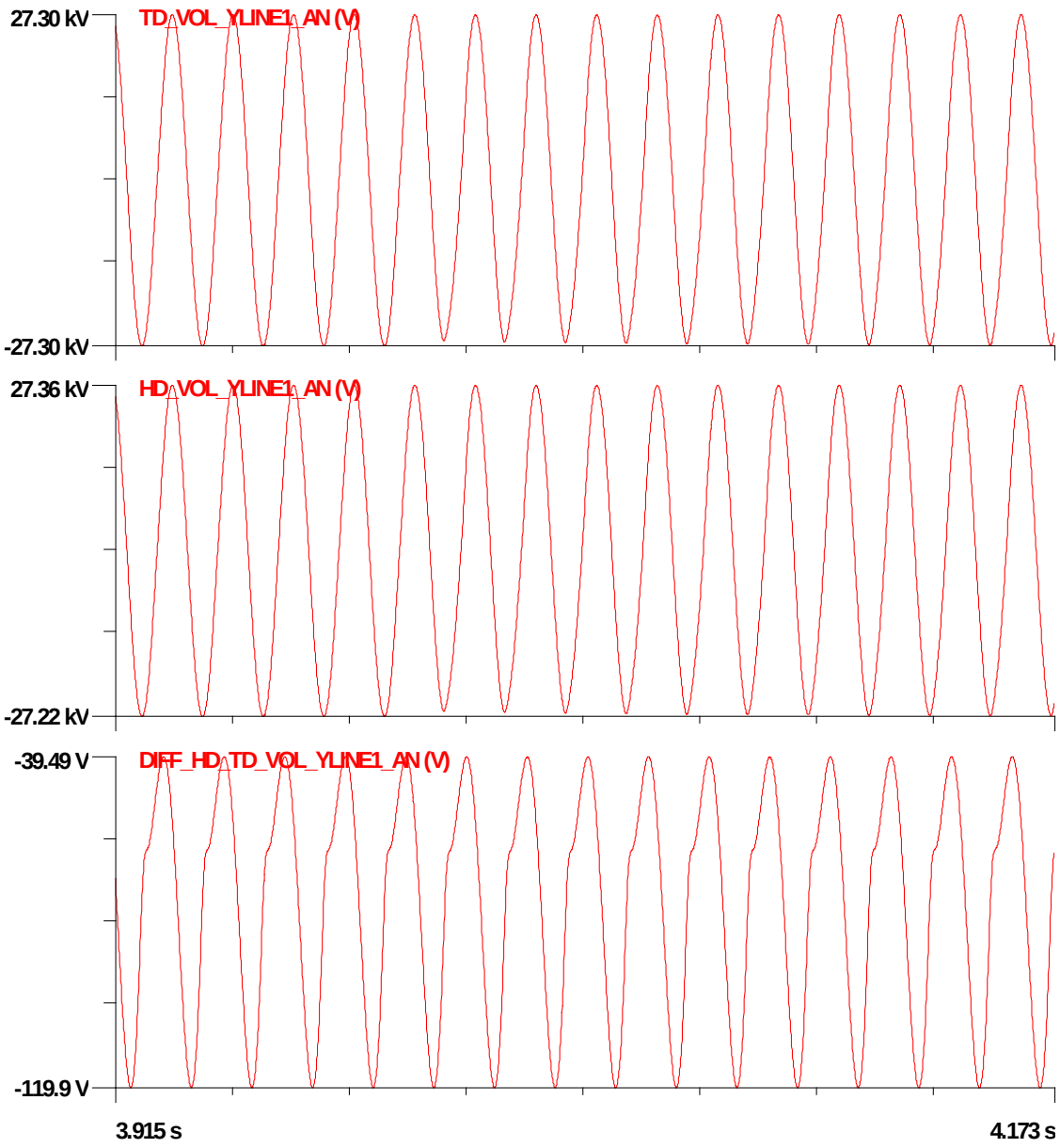

Figure A.19: Comparison of voltages around t=4.0 seconds (Interface 2)

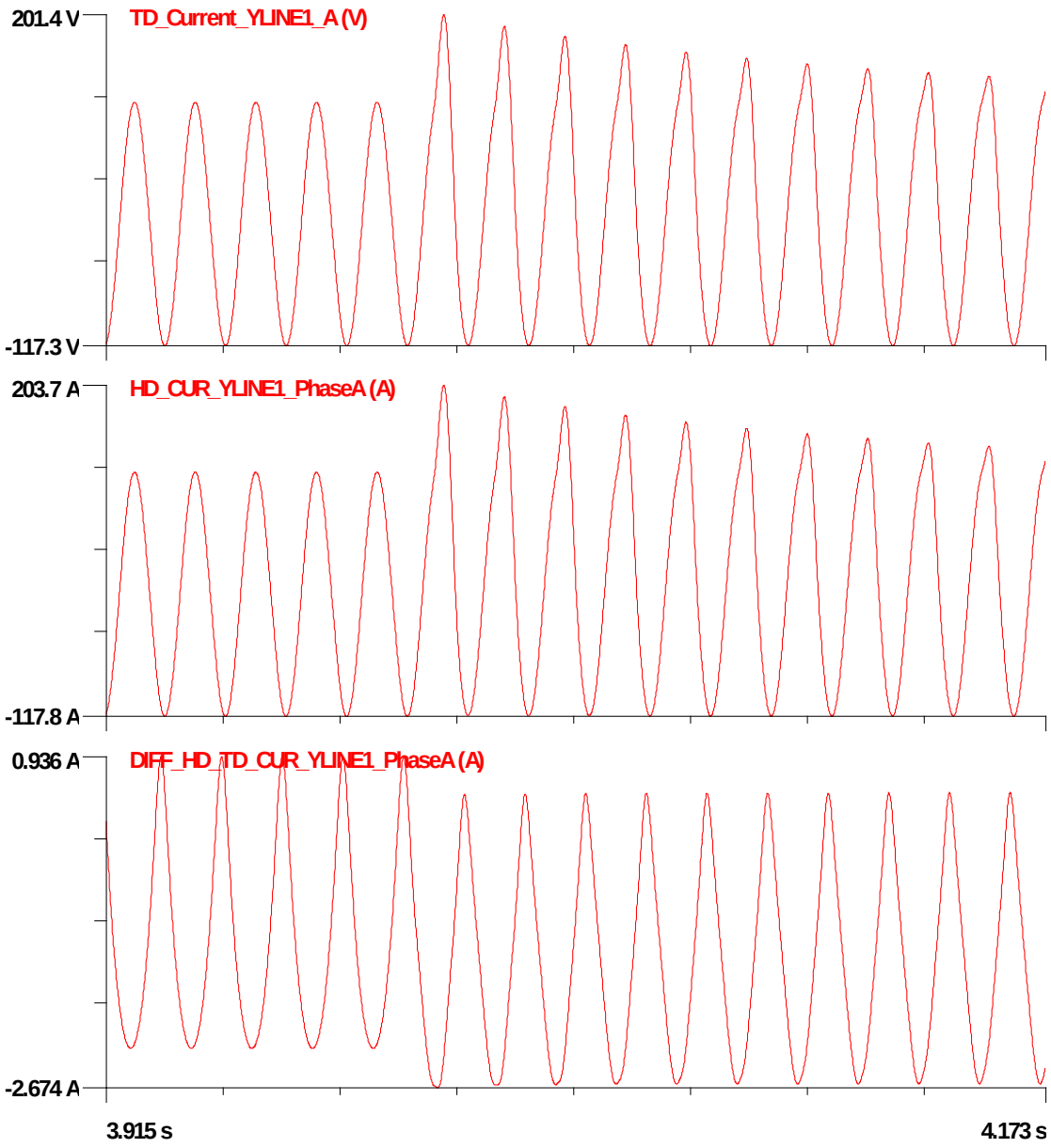

Figure A.20: Comparison of current around t=4.0 seconds (Interface 2)

References

[1] Analysis of Asymmetrical Faults in Power Systems Using Dynamic Phasors. *Aleksandar M. Stankovic, Timur Aydin.*

[2] Frequency-Adaptive Power System Modeling for Multiscale Simulation of Transients. *Feng Gao, Kai Strunz*

[3] Quadratic Integration Method. *A.P. Meliopoulos, George J. Cokkinides, George K. Stefopoulos*

[4] A Method for Coupling Phasor and Time Domain Networks. *Joseph M. Hood, Roger A. Dougal*

[5] Computation of the Periodic Steady State in Systems with Nonlinear Components Using A Hybrid Time and Frequency Domain Methodology. *Adam Semlien, Aurelio Medina*

[6] Combined Transient and Dynamic Analysis of HVDC and FACTS Systems. *M.Sultan, J.Reeve, R.Adapa*

[7] Realization of Electromechanical Transient and Electromagnetic Transient Real Time Hybrid Simulation in Power System. *Tian Fang, Yue Chenyang, Wu Zhongxi, Zhou Xiaoxin.*

[8] Transmission Network Equivalents for Electromagnetic Transient Studies. *A.S. Morched, V. Brandwajn*

[9] Numerical Modeling of Frequency-Dependent Transmission-Line Parameters in an Electromagnetic Transients Program. *W.Scott Meyer, Hermann W. Dommel*

[10] Parallel Processing and Hybrid Simulation for HVDCNSC PSCAD Studies. *G.D. Irwin, C.Amarasinghe, N.Kroeker, D.Woodford*